



# **Regulation of the Brain Acetylome by Sirtuin-2 and During Ageing**

A thesis presented to Department of Biomedical Science in the School of  
Biosciences in the Faculty of Science at the University of Sheffield

In partial fulfilment of the requirements  
of a degree of  
Doctor of Philosophy

By Hatoon Musead Alamri  
Registration Number: 170119953

February 2022

## ***Acknowledgements***

First and foremost, praises and thanks the God, the Almighty, for His blessings throughout my research work to complete this dissertation.

I want to express my deep and sincere gratitude to my research supervisor. Dr Mark Collins, for giving me the opportunity to conduct this research and providing invaluable guidance throughout this research. I am grateful for his vision, sincerity, support, patience, and motivation that has deeply inspired me. I am extremely grateful for what he has offered me. I would also like to thank him for his friendship, which made my journey in the UK much easier.

I want to express my sincere gratitude to the King Abdullah Medical City (KAMC) for offering me this great opportunity to be part of their optimistic plan.

I would also like to thank my advisors Dr Elizabeth Seward, Professor Steve Winder, and Professor Carl Smythe, for their advice throughout the project.

I would like to thank Collin's lab colleagues, Dr Keith, Dr Maria, Dr Khoa, and Weronika, for their encouragement and support throughout my study.

My appreciation also goes out to the people outside the lab, Amani, Dr Mohammed, Dr Alaa, Haifa, Salma, and Nadia, for listening to my endless complaining about lab experiments; I thank them for sharing their stories with me and being great friends, especially during the pandemic. I thank all members of the E floor office for making the place a suitable environment for work and friendship.

A special word of thanks goes over to my friends (my own support team), who have always been a huge source of motivation when things get pretty difficult. Thank you for your endless love.

I am extremely grateful to my family for their love, prayers, caring, sacrifices and everything they have done for me throughout my life, especially to my great father, Mr Musead Alamri who I dedicate this work to his soul, as well as my late brother Abdulrazak who had supported and inspired me by his love and advice.

I would like to thank my mother, Fatimah, for being an excellent example of a great, loving and strong woman. Without her tremendous understanding and encouragement in the past few years, it would be impossible for me to complete my study. I would like to extend my sincere thanks to my brothers and sisters for their unending support. To my nephews and nieces, thank you for the video calls that always cheer me up. Soon we will be spending lots of time together.

## **Abstract**

Non-histone lysine acetylation was recently recognised as a highly enriched post-translational modification in the brain. Lysine acetylation regulates the stability of important synaptic proteins such as the AMPA receptor and Arc protein. Sirt2 is a NAD-dependent enzyme, expressed highly in the brain and is associated with neurodegenerative diseases and ageing. Sirt2<sup>-/-</sup> mice exhibit impaired synaptic plasticity, including altered LTP and LTD, as well as significant impairments in spatial and contextual memory. To fully understand how Sirt2 regulates brain function, it is necessary to characterise the range of substrates that it deacetylates and regulates in vivo.

To date, only a limited number of Sirt2 substrates have been characterised, and the regulatory role of Sirt2 is poorly understood in the brain. The role of acetylation has been recognised in the physiology and pathology of ageing, mostly in relation to Sirtuin enzymes. However, few studies have investigated the changes in non-histone acetylation during ageing and none in a global manner.

Here we have sought to identify putative Sirt2 substrates through comparative acetylome analysis of Sirt2 knockout and wild type mouse brain tissue. To understand how acetylation changes during ageing, a comparative analysis of acetylation in old and young mouse brain tissue was performed. These datasets were generated by the analysis of immuno-enriched acetylated peptides from tissue samples using quantitative mass spectrometry.

Using this strategy, we identified 2,054 unique acetylation sites on 818 acetylated proteins in a Sirt2 knockout versus wild type brain tissue dataset. 226 sites had significantly higher acetylation levels in Sirt2 knockout mice and represent putative Sirt2 substrate sites. Acetylome analysis of aged mouse brain tissues identified 2,496 unique acetylation sites on

1,091 different proteins, 60 of which exhibited a significant change in acetylation in aged (old) brain tissues. We found that acetylation increased in 24 sites and decreased in 36 sites.

Our data identify novel putative Sirt2 substrates in the brain and characterise changes in lysine acetylation during ageing. This work will advance the understanding of the role of lysine acetylation and Sirt2 in the brain and how they contribute to neurodegenerative diseases.

<b>Table of Contents</b>	
<b>Acknowledgements</b>	2
<b>Abstract</b>	4
Table of Contents	6
List of Tables	10
List of Figures	11
<b>Declaration</b>	14
<b>Abbreviations</b>	15
<b><u>CHAPTER 1</u></b>	21
1.1 <i>Lysine acetylation as major post-translation modification</i>	22
1.1.1 <i>Post-translational modifications of proteins</i>	22
1.1.2 <i>Lysine acetylation</i>	22
1.1.3 <i>Generation of mitochondrial and cytosolic acetyl coenzyme A</i>	24
1.1.4 <i>Enzymatic control of lysine acetylation</i>	25
1.1.5 <i>non-enzymatic acetylation</i>	28
1.1.6 <i>Detection of lysine acetylation.</i>	29
1.1.7 <i>Functions of lysine acetylation</i>	33
1.1.8 <i>The role of acetylation in disease</i>	39
1.1.9 <i>Lysine acetylation and neurodegenerative diseases</i>	39
1.1.10 <i>Lysine acetylation and synaptic proteins</i>	41
1.2 <i>Sirt2</i>	45
1.2.1 <i>Structure and expression</i>	45
1.2.2 <i>Sirt2 subcellular localisation</i>	49
1.2.3 <i>Sirt2 protein expression</i>	50
1.2.4 <i>PTMs of Sirt2</i>	51
1.2.5 <i>Known Sirt2 substrates and protein interactions</i>	52
1.2.6 <i>Sirt2 role in cells</i>	58
1.2.7 <i>The phenotype of Sirt2 knockout mice</i>	60
1.2.8 <i>Sirt2 in diseases</i>	62
1.2.9 <i>Sirt2 and neurodegenerative disease.</i>	63
1.2.10 <i>Sirt2 in ageing</i>	65
1.2.11 <i>KDAC Inhibitors</i>	67
1.3 <i>Hypothesis</i>	69
1.4 <i>Objectives</i>	69
<b><u>CHAPTER 2</u></b>	70
2.1 <i>Cell lines and tissue culture</i>	71

2.1.1 Culture of immortalised cell lines	71
2.1.2 Mouse Brain Tissue	71
2.2 Acetylome analysis of mice brain tissue	72
2.2.1 Filter-Aided Sample Preparation (FASP)	72
2.2.2 Acetone precipitation of proteins	73
2.2.3 S-TRAP sample preparation for brain tissue	74
2.2.4 Peptide desalting	75
2.2.5 Offline high pH reversed-phase peptide fractionation	76
2.2.6 Immuno-affinity purification of acetyl-lysine containing peptides (IAP)	77
2.2.7 Desalting peptides with stage tips	77
2.2.9 Mass spectrometry data analysis	78
2.2.10 Proteomics data analysis	80
2.3 Protein expression analysis	81
2.3.1 Protein extraction and quantification	81
2.4 Immunoblotting	81
2.4.1 Imaging and Analysis	82
2.4.2 Immunofluorescence	82
2.4.3 Imaging and Analysis	83
2.5 Immunoprecipitation (IP)	84
2.5.1 Pulldowns of tagged proteins from cell lines:	84
2.5.2 IP of endogenous proteins from mouse brain tissue	85
2.5.3 IP of endogenous proteins from a cell line	86
2.6 Antibodies	87
2.7 Plasmid preparation	88
2.7.1 Agar plate preparation	88
2.7.2 Cell transformation and DNA isolation	88
2.8 Transfection	89
2.9 siRNA	90
2.10 Drug treatments	91
<b><u>CHAPTER 3</u></b>	92
3.1 Introduction	93
3.1.1 Sirt2 substrates	93
3.2 Aims	97
3.3 Results	98
3.3.1 Lysine acetylation is a major PTM of synaptic proteins	98
3.3.2 Acetylome analysis of Sirt2 knockout versus wild type mouse brain tissue	101

3.3.2.1	<i>Optimisation of brain tissue acetylome analysis</i>	101
3.3.2.2	<i>Mouse brain acetylome profile</i>	105
3.3.2.3	<i>Characterisation and bioinformatics analysis of Sirt2 putative substrates</i>	124
3.3.3	<i>Proteome profiling of Sirt2 knockout versus wild type mouse brain tissue</i>	137
3.4	<i>Discussion</i>	142
3.4.1	<i>Mouse brain acetylome</i>	142
3.4.2	<i>Characterisation of the Sirt2-regulated mouse brain acetylome</i>	143
3.4.3	<i>Sirt2 KO versus WT proteome profile</i>	146
3.4.4	<i>Acetylome analysis technical points</i>	147
	<b><u>CHAPTER 4</u></b>	148
4.1	<i>Introduction</i>	149
4.2	<i>Aims</i>	153
4.3	<i>Results</i>	154
4.3.1	<i>Acetylome analysis of Old (24 months) versus Young (2 months) mouse brain tissue</i>	154
4.3.1.1	<i>Optimisation of brain tissue acetylome using S-trap digestion column</i>	154
4.3.1.2	<i>Quantitative acetylome analysis of old versus young mouse brain tissue</i>	156
4.3.1.3	<i>Characterisation of acetylation sites changes in the aged brain</i>	163
4.3.2	<i>Proteome profile of old brain tissue versus young brain tissue</i>	175
4.3.3	<i>Understanding the relationship between Sirt2 substrates and changes in acetylation during ageing.</i>	182
4.3.3.1	<i>Sirt2 KO versus old/young acetylome profiles.</i>	182
4.4	<i>Discussion</i>	186
4.4.1	<i>aged mouse brain acetylome</i>	186
4.4.2	<i>acetylation sites level changes during ageing</i>	186
4.4.3	<i>Old versus young proteome profile</i>	188
	<b><u>CHAPTER 5</u></b>	189
5.1	<i>Introduction</i>	190
5.2	<i>Aims</i>	191
5.3	<i>Results</i>	192
5.3.1	<i>Challenges in the detection of non-histone acetylation</i>	192
5.3.2	<i>Manipulation of Sirt2 activity in cells and detection of acetylation</i>	193
5.3.3	<i>Testing VAMP2/3 deacetylation by Sirt2</i>	208
5.3.4	<i>Identification of VAMP2/3 acetylation sites with AP-MS</i>	216
5.3.5	<i>Testing VAMP2 deacetylation by Sirt2</i>	218
5.3.6	<i>Testing known substrates of Sirt2</i>	228
5.3.7	<i>Acetylation stoichiometry</i>	240

5.3.8 <i>Sirt2 interactome</i>	243
5.3.9 <i>BioPlex data analysis</i>	256
5.3.10 <i>Does protein interaction are required for Sirt2 deacetylase functions</i>	259
5.4 <i>Discussion</i>	260
5.4.1 <i>VAMP2/3 acetylation</i>	260
5.4.2 <i>Sirt2 interactors from HEK239 cells</i>	262
<b><u>CHAPTER 6</u></b>	265
6.1 <i>Summary of significant findings and discussion</i>	266
6.1.1 <i>Chapter 3 - Characterisation of the Sirt2-regulated mouse brain acetylome</i>	266
6.1.2 <i>Chapter 4 - Acetylome profiling of young versus old mouse brain tissue</i>	269
6.1.3 <i>Chapter 5 - Validation of putative Sirt2 substrates</i>	271
6.2 <i>Overview and future work</i>	274
6.2.1 <i>Synaptic proteins are regulated by acetylation and Sirt2 deacetylase enzyme</i>	274
6.2.2 <i>Non-enzymatic and enzymatic acetylation of brain proteins</i>	275
6.2.3 <i>Ubiquitination and acetylation crosstalk</i>	276
6.3 <i>Clinical implications of Sirt2 and acetylation in the brain</i>	277
6.3.1 <i>Parkinson's disease</i>	277
6.3.2 <i>Alzheimer's disease</i>	278
6.3.3 <i>Myelination</i>	279
6.4 <i>Do low stoichiometry acetylation sites have a biological function?</i>	280
6.5 <i>Future prospects</i>	283
6.7 <i>Conclusion</i>	287
<b><i>Bibliography</i></b>	288

## List of Tables

Table 1.1 Examples of known Sirt2 substrates .....	56
Table 2.1 - Datasets used for bioinformatics analysis. ....	80
Table 3.1 – Selection of characterised Sirt2 substrates. ....	96
Table 3.2 – Correlation values of Sirt2 WT and KO replicate datasets. ....	110
Table 3.3 Summary of proteins and peptides identified in brain tissue from Sirt2 KO versus WT mice. .....	110
Table 3.4 – Acetylated proteins grouped into Panther pathways. ....	119
Table 3.5 – Acetylated proteins grouped into protein classes. ....	120
Table 3.6 known ac(K) sites found in Sirt2 knockout brain tissues. ....	126
Table 3.7 Panther pathway enrichment analysis of the putative Sirt2 substrates. ....	134
Table 3.8 – Multi-scatter plots of Sirt2 WT and KO proteome profiling samples. ....	139
Table 4.1 – Summary of proteins and peptides identified in an acetylome analysis of brain tissue from old versus young mice. ....	156
Table 4.2- correlation values of old and young replicate datasets. ....	158
Table 4.3 – Cellular distribution of acetylated proteins regulated by ageing. ....	165
Table 4.4 – Panther pathway enrichment analysis of the acetylated proteins regulated by aging. ....	171
Table 4.5 – Correlation values of old and young proteome profile replicate datasets. ....	176
Table 4.6 – List of significantly changed proteins in acetylated and protein abundance levels in old versus young brain tissue. ....	178
Table 4.7 – Example of some significantly enriched proteins grouped into panther pathways. ....	180
Table 4.8 – a comparison of Sirt2 KO acetylome dataset to old versus young acetylome. ....	184
Table 4.9 – Overlap of regulated acetylated proteins from old and young acetylome and Sirt2 putative substrates. ....	185
Table 5.1 – Bait peptides identified by LC-MS/MS of VAMP3-HA pulldown. ....	217
5.3.5 Testing VAMP2 deacetylation by Sirt2 .....	218
Table 5.2 – VAMP2 peptides identified by LC-MS/MS of VAMP2_GFP pulldowns. ....	223
Table 5.3 – Bait peptides identified by LC-MS/MS of FLAG_NRF2 and CDK9_FLAG pulldowns. ....	235
Table 5.4 – Identified peptides by LC-MS/MS of GLUA1_GFP and CDK9_FLAG pulldowns. ....	239
Table 5.5 – Acetylation stoichiometry levels of some putative Sirt2 substrates. ....	242
Table 5.6 – Correlation values of Sirt2 and control replicate datasets. ....	246
Table 5.7 – Panther pathways significantly enriched in Sirt2 interactors. ....	254
Table 5.8 – Putative Sirt2 interactors grouped into protein classes. ....	255
Table 5.9 – List of significantly enriched protein in Sirt2 pulldowns and those previously identified from the BioPlex dataset. ....	258

## List of Figures

Figure 1.1 – Enzymatic regulation of acetylation by KATs and KDACs/Sirtuins. ....	23
Figure 1.2 – Sub-cellular localisation of Sirtuins. ....	27
Figure 1.3 – Timeline of acetylome datasets reported in the past decade. ....	32
Figure 1.4 – Acetylation regulates many cellular processes and is implicated in ageing and disease. ....	33
Figure 1.5 – Functional networks of KDACs -regulated non-histone proteins. ....	35
Figure 1.6 – Functional networks of KATs-regulated non-histone proteins. ....	36
Figure 1.7 – IBAQ intensity of KDAC enzymes found in mouse synaptic proteome. ....	43
Figure 1.8 – Sirt2 domain structure. ....	46
Figure 1.9 – Alignment of Sirt2 isoform protein sequences. ....	47
Figure 1.10 – Human Sirt2 3D structure. ....	48
Figure 1.11 – Sirt2 subcellular localisation in the U-251 cell line. ....	49
Figure 1.12 – Distribution of Sirt2 expression across human tissues. ....	51
Figure 1.13 – PTM sites of Sirt2; ....	52
Figure 1.14 – Sirt2 protein interactions. ....	58
Figure 1.15 – Phenotypes of Sirt2 <sup>-/-</sup> mice. ....	61
Figure 1.16 – Immunohistochemistry staining for Sirt2 in the adult mouse brain. ....	62
Figure 3.1 – The majority of synaptic proteins are acetylated. ....	99
Figure 3.2 – PTM Cross-talk of acetylation and ubiquitination. ....	100
Figure 3.3 Initial workflow for acetylome analysis of mouse brain tissue. ....	102
Figure 3.4 – Optimisation of sample preparation for acetylome profiling. ....	105
Figure 3.5 – Workflow used for the acetylome analysis of wild-type and Sirt2 knockout brain tissue .....	106
Figure 3.6 – Volcano plot showing Sirt2 significantly expressed in wild type tissue. ....	107
Figure 3.7 – Histogram of LFQ intensity columns for replicates of Sirt2 KO versus Sirt2 WT. ....	109
Figure 3.8 – Identified acetylated proteins are enriched in synaptosomes and PSDs. ....	111
Figure 3.9 – Number of acetylated sites per acetylated proteins. ....	112
Figure 3.10 – Venn diagram of known and novel acetylated sites; ....	114
Figure 3.11 – Ac(K) sites were previously identified in rat brain tissue. ....	115
Figure 3.12 – Cellular distribution of ac(K) proteins. ....	116
Figure 3.13 – Significantly enriched proteins grouped into cellular component molecular pathways and biological processes. ....	117
Figure 3.14 – Significantly enriched proteins grouped into cellular component molecular pathways and biological processes. ....	118
Figure 3.15 – Sequence logo plots represent normalised amino acid frequencies for -/+7 amino acids from the lysine-acetylated site. ....	121
Figure 3.16 – CBP/Ep300 acetyltransferase enzymes may regulate acetylation in brain tissue. ....	122
Figure 3.17 – KAT2B and KATA2 are predicted to be the significant KATs regulating the brain acetylome. ....	123
Figure 3.18 – Volcano plot showing acetylation sites regulated by Sirt2; ....	125
Figure 3.19 – Identified putative Sirt2 are enriched in synaptosomes and PSDs. ....	127
Figure 3.20 – Heat map of highly acetylated peptides within the putative Sirt2 regulated dataset. ....	129
Figure 3.21 – Cellular distribution of putative Sirt2 substrates. ....	130
Figure 3.22 – Gene ontology enrichment analysis of putative Sirt2 substrates compared to the mouse genome. ....	132
Figure 3.23 – Gene ontology enrichment analysis of putative Sirt2 substrates compared to the brain proteome. ....	133

Figure 3.24 – Sequence logo plots of normalised amino acid frequencies for -/+7 amino acids from putative Sirt2 substrate acetylation sites compared to the mouse genome. ....	135
Figure 3.25 – KAT2B and KATA2 are predicted to be the major KATs responsible for acetylation of putative Sirt2 substrates in the brain. ....	136
Figure 3.26– Histogram of imputed LFQ intensity values for Sirt2 KO versus Sirt2 WT samples. ....	138
Figure 3.27 – Volcano plot of differential protein abundance in Sirt2 KO versus WT brain tissue. ....	141
Figure 4.1 – NAD <sup>+</sup> biosynthetic enzyme (NAMPT) and sirtuin responses to dietary and environmental changes control ageing and longevity. ....	151
Figure 4.2 – Life phase equivalences of mouse and human. ....	152
Figure 4.3 – Optimisation of protein extraction from brain tissue samples for S-trap digestion. ....	155
Figure 4.4 – Histogram of ac(K) site intensity values for replicates of old versus young acetylomes	157
Figure 4.5 – Known acetylated and ubiquitinated sites .....	159
Figure 4.6 – Cellular distribution of ac(K) proteins and sites identified from old versus young mouse brain tissue. ....	160
Figure 4.7 – Identified acetylated proteins are enriched in synaptosomes, and PSDs .....	161
Figure 4.8 – ac(K) sites previously identified in rat brain tissue .....	162
Figure 4.9 – Volcano plot showing acetylation sites significantly regulated by ageing .....	164
Figure 4.10 – Heat map of identified acetylated peptides within the putative ageing regulated dataset. ....	167
Figure 4.11 – Gene ontology enrichment analysis of acetylated proteins regulated by ageing compared to the mouse genome. ....	169
Figure 4.12 – Gene ontology enrichment analysis of acetylated proteins regulated by ageing compared to the brain proteome .....	170
Figure 4.13 – KAT2B is predicted to be the major KAT regulating the old versus young brain acetylomes. ....	173
Figure 4.14 – Sequence logo plots of normalised amino acid frequencies for -/+7 amino acids of acetylated sites regulated during ageing from old versus young acetylome profile compared to the mouse genome. ....	174
Figure 4.15 – Histogram of LFQ intensity values for replicates of old versus young samples, .....	176
Figure 4.16 – Volcano plot showing the results of statistical analysis of old versus young brain proteomes. Data were filtered to retain proteins .....	177
Figure 4.17 – Sirt2 protein expression difference between old and young mouse brain tissue. ....	181
Figure 4.18 – Venn diagram represents Ac(K) sites between Sirt2KO/WT and old/young mouse brain acetylome profile .....	183
Figure 5.1 – Flowchart summarised optimisation of detection acetylation to validate Sirt2 putative substrates. ....	193
Figure 5.2 – Optimisation of KDAC inhibitor concentrations .....	195
Figure 5.3 – Sirt2 (KDAC) inhibitors increase ac tubulin levels. ....	196
Figure 5.4 – Overexpression of FLAG-tagged-Sirt2. ....	197
Figure 5.5 – Optimisation of overexpression and inhibition of Sirt2. ....	198
Figure 5.7 – Overexpression of Sirt2 significantly reduces acetylation levels. ....	200
Figure 5.8 – Immunoprecipitation of Sirt2-FLAG. ....	202
Figure 5.9 – Optimisation of Sirt2 knockdown in HeLa cells. ....	204
Figure 5.10 – Optimisation of Sirt2 knockdown and measurement of acetylation levels in HeLa cells .....	206
Figure 5.11 – Detection of a change in ubiquitination levels in response to Sirt2 overexpression in HeLa cells. ....	207
Figure 5.12 – Multiple sequence alignment of VAMP 1,2,3 protein sequences. ....	208

Figure 5.13 – The tertiary structure of SNARE complex. ....	210
Figure 5.14 – Domain structure and PTM sites of human VAMP3. ....	211
Figure 5.15 – Immunoblotting of HA-tagged VAMP3 pulldowns ....	212
Figure 5.16 – VAMP3-HA pulldown with inhibition of KDAC deacetylase activity. ....	214
Figure 5.17 – Detection of VAMP3 in VAMP3_ HA pulldowns ....	215
Figure 5.18 – VAMP2 is expressed in NSC34 cells. ....	218
Figure 5.19 – Endogenous IP of VAMP2 and IP of acetylated proteins in NSC34 cells ....	220
Figure 5.20 – Endogenous IP of VAMP2 from HEK cells ....	221
Figure 5.21 – Testing the performance of a pan anti-acetyl-lysine antibody using chemically acetylated BSA ....	224
Figure 5.22 – Detection of acetylation in AGK2 treated HEK293 cells ....	225
Figure 5.23 – Inducing acetylation level by KDAC inhibitors ....	228
Figure 5.24 – Immunoprecipitation of CDK9_FLAG. ....	230
Figure 5.25 – Anti-acetyl-lysine immunoblot of CDK9 pulldowns. ....	232
Figure 5.26 Inhibition of KDAC deacetylase activity to detect GLUa1 and SNCA acetylation; ....	233
Figure 5.27 – Venn diagram of the total number of proteins found in AP-MS from each tagged version, ....	244
Figure 5.28 Histogram of LFQ intensity values for replicates of Sirt2-FLAG versus control pulldowns. ....	245
Figure 5.29 – Volcano plot of AP-MS data for FLAG-Sirt2 versus control pulldowns. ....	247
Figure 5.30 – Overlap between Sirt2 interactors in HEK239 and HeLa cells; ....	249
Figure 5.31 – Cellular localisation of putative Sirt2 interactors ....	250
Figure 5.32 – Significantly enriched proteins grouped into cellular component molecular pathways and biological processes ....	252
Figure 6.1 – Acetylation site stoichiometry. ....	280

**Declaration**

*I, the author, confirm that the Thesis is my work. I am aware of the University's Guidance on the Use of Unfair Means ([www.sheffield.ac.uk/ssid/unfair-means](http://www.sheffield.ac.uk/ssid/unfair-means)). This work has not previously been presented for an award at this, or any other, university.*

## **Abbreviations**

ABCD3 - ATP-binding cassette sub-family D member 3

Ac(K) - Acetylated-Lysine

ACLY - ATP-citrate synthase

ACSS1 - Acetyl-coenzyme A synthetase 2-like, mitochondrial

ACSS2 - Acetyl-coenzyme A synthetase, cytoplasmic

AD - Alzheimer's disease

AGK2 - Acylglycerol kinase, mitochondrial

AIFM1 - Apoptosis-inducing factor 1

AK-7 - Adenylate kinase 7

ALDH1A1 - Aldehyde dehydrogenase 1A1

ALDH1I1 - Cytosolic 10-formyltetrahydrofolate dehydrogenase

Aldh7a1 - Alpha-aminoadipic semialdehyde dehydrogenase

ALS - Amyotrophic lateral sclerosis

AMPAR - Glutamate receptor

AP-MS - affinity purification mass spectrometry

Arc (Arg3.1) - Activity-regulated cytoskeleton-associated protein

ASD - Autism spectrum disorder

ASPSCR1 - Tether containing UBX domain for GLUT4

ATG5 - Autophagy protein 5

ATP/ADP - Adenosine tri-phosphate/Adenosine di-phosphate

ATP1A1 - Sodium/potassium-transporting ATPase subunit alpha-1

ATP2A2 - Sarcoplasmic/endoplasmic reticulum calcium ATPase 2

ATRIP - ATR-interacting protein

BSA - Bovine Serum Albumin

BSG - Basigin

BubR1 - Mitotic checkpoint serine/threonine-protein kinase BUB1 beta

C1QBP - Complement component 1 Q subcomponent-binding protein

Ca2 - Carbonic anhydrase 2

CamK2a - Calcium/calmodulin-dependent protein kinase type II subunit alpha

CaMKII $\alpha$  - Calcium/calmodulin-dependent protein kinase

CANX - Calnexin

CCT3 - T-complex protein 1 subunit gamma

CDK5 - Cyclin-dependent-like kinase 5

CDK9 - Cyclin-dependent kinase 9

CID - Collision-induced dissociation

c-Myc - Myc proto-oncogene protein

CNK1 - Connector enhancer of kinase

CNS - Central nervous system

COPA - Coatamer subunit alpha

COPB1 - Coatamer subunit beta

CREBBP - CREB-binding protein

CtBP2 - C-terminal-binding protein 2

DDOST - Dolichyl-diphosphooligosaccharide--protein glycosyltransferase

DMSO - Dimethylsulfoxide

DNAJA1- DnaJ homolog subfamily A member 1

DPM1 - Dolichol-phosphate mannosyltransferase subunit 1

DYC1h1 - Cytoplasmic dynein 1 heavy chain 1

Ep300 - Histone acetyltransferase p300

FAR1 - Fatty acyl-CoA reductase 1

FASN - Fatty acid synthase

FASP - Filter aided sample preparation

FDR - false discovery rate

FOXO1 - Forkhead box protein O1

FOXO3a - Forkhead box protein O3

G6PD - Glucose-6-phosphate 1-dehydrogenase

GABA - B-Gamma-aminobutyric acid type B receptor subunit 1

GCN5 (KAT2A) - Histone acetyltransferase KAT2A

GKRP - Glucokinase regulatory protein

GltP - Glycolipid transfer protein

GluA1 - Glutamate receptor 1

GLUL - Glutamine synthetase  
GSK3 - Glycogen synthase kinase-3  
GSK3 $\beta$  - Glycogen synthase kinase-3 beta  
H1-5 - Histone H1.5  
Hapln2 - Hyaluronan and proteoglycan link protein 2  
HAT1 - Histone acetyltransferase type B catalytic subunit  
HAT - Histone Acetyltransferase  
HAX1 - HCLS1-associated protein X-1  
HDAC11 - Histone deacetylase 11  
HDAC6 - Histone deacetylase 6  
HDAC - Histone deacetylase  
HD - Huntington's disease  
HEK239 - Human embryonic kidney 293 cells  
HIF-1 $\alpha$  - Hypoxia-inducible factor 1-alpha  
HIST1H2BB - Histone H2B type 1-B  
HNF4 - Hepatocyte nuclear factor 4-alpha  
HSD17B12 - Very-long-chain 3-oxoacyl-CoA reductase  
HSP90AB1 - Heat shock protein HSP 90-beta  
HSP90 - Heat shock protein 90  
HSPA1B - Heat shock 70 kDa protein 1B  
HSPA4 - Heat shock 70 kDa protein 4  
HSPA6 - Heat shock 70 kDa protein 6  
HSPA8 - Heat shock cognate 71 kDa protein  
HSPB1 - Heat shock protein beta-1  
HSPD1 - 60 kDa heat shock protein  
IBAQ - Intensity Based Absolute Quantification  
IB- Immunoblotting  
IDH1 - Isocitrate dehydrogenase [NADP] cytoplasmic  
IMMT - MICOS complex subunit MIC60  
IP - Immunoprecipitation  
IPO7 - Importin-7

IPO9 - Importin-9  
IRS4 - Insulin receptor substrate 4  
JNKs - Mitogen-activated protein kinase 8  
KAT - Acetyltransferase enzymes  
KAT2A - Histone acetyltransferase KAT2A  
KAT2B - Histone acetyltransferase KAT2B  
KAT5 - Histone acetyltransferase KAT5  
KAT8-Histone acetyltransferase KAT8  
KDAC - Protein lysine deacetylases  
KO - Knockout (-/-)  
KPNA2 - Importin subunit alpha-1  
KPNB1 - Importin subunit beta-1  
KRAS - GTPase KRas  
KRT8 - Keratin, type II cytoskeletal 8  
LC-MS/MS - Liquid Chromatography with tandem mass spectrometry  
LDH-A- L-lactate dehydrogenase A chain  
LFQ - Label-free quantification  
LKB1 - Serine/threonine-protein kinase STK11  
LTD - Long-term depression  
LTP - Long-term potentiation  
MAPT-Microtubule-associated protein tau  
MEFs - Mouse Embryonic Fibroblasts  
MEK1 - Dual specificity mitogen-activated protein kinase kinase 1  
MKP-1 - MAP kinase phosphatase 1  
MSH6 - DNA mismatch repair protein Msh6  
MS - Mass spectrometry  
NAD+ - Nicotinamide adenine dinucleotide  
NAM - Nicotinamide  
NFAT - Nuclear factor of activated T-cells  
NF-Kb - Nuclear factor kappa B  
NRF2 - Nuclear factor erythroid 2-related factor 2

NSC34 - Neuroblastoma × Spinal Cord

NUP93 - Nuclear pore complex protein Nup93

p53 - Cellular tumor antigen p53

P65 - Nuclear factor NF-kappa-B p65

PCAF (KAT2B) - Histone acetyltransferase KAT2B

PCBP2 - Poly(rC)-binding protein 2

PCLO - Protein piccolo

PCNA - Proliferating cell nuclear antigen

PD - Parkinson's disease

PEPCK1 - Phosphoenolpyruvate carboxykinase (ATP)

PGAM2 - Phosphoglycerate mutase 2

PgK1 - Phosphoglycerate kinase 1

PHB - Prohibitin

PHGDH - D-3-phosphoglycerate dehydrogenase

PKM2 - Pyruvate kinase 2

PLP1 - Myelin proteolipid protein

PRKDC - DNA-dependent protein kinase catalytic subunit

PTM - Post translation modification

Q8IXJ6 - NAD-dependent protein deacetylase sirtuin-2

RAB3GAP1 - Rab3 GTPase-activating protein catalytic subunit

RAB3GAP2 - Rab3 GTPase-activating protein non-catalytic subunit

RIPA - Radioimmunoprecipitation Assay

RUNX3 - Runt-related transcription factor 3

SDS - Sodium Dodecyl Sulfate

SirReal2 - potent and selective Sirt2 inhibitor

SKP2 - S-phase kinase-associated protein 2

SNAI2 - Slug-Zinc finger protein

Snap25 - Synaptosomal-associated protein 25

SNCA - Alpha-synuclein

SOD1 - Superoxide dismutase [Cu-Zn]

SOX2 - Transcription factor SOX-2

SREBP - 2-Sterol regulatory element-binding protein 2  
SRPRB - Signal recognition particle receptor subunit beta  
SSR1 - Translocon-associated protein subunit alpha  
SSR4 - Translocon-associated protein subunit delta  
STAT5 - Signal transducer and activator of transcription 5A  
STX1A - Syntaxin-1A  
Taldo1 - Transaldolase  
TCP1 - T-complex protein 1 subunit alpha  
TDP-43 - TAR DNA-binding protein 43  
TFA - Trifluoroacetic acid  
TIMM50 - Mitochondrial import inner membrane translocase subunit TIM50  
TRIP13 - Pachytene checkpoint protein 2 homolog  
TUBA1a - Tubulin alpha chain  
TUBB - Tubulin beta chain  
VAMP2 - Vesicle-associated membrane protein 2  
VAMP3 - Vesicle-associated membrane protein 3  
WT - Wild-type (+/+)  
XPO5 - Exportin-5  
XPO7 - Exportin-7  
zDHC5 - Zinc Finger DHHC-Type Palmitoyltransferase 5

# **CHAPTER 1**

## ***Introduction***

## **1.1 Lysine acetylation as major post-translation modification**

### **1.1.1 Post-translational modifications of proteins**

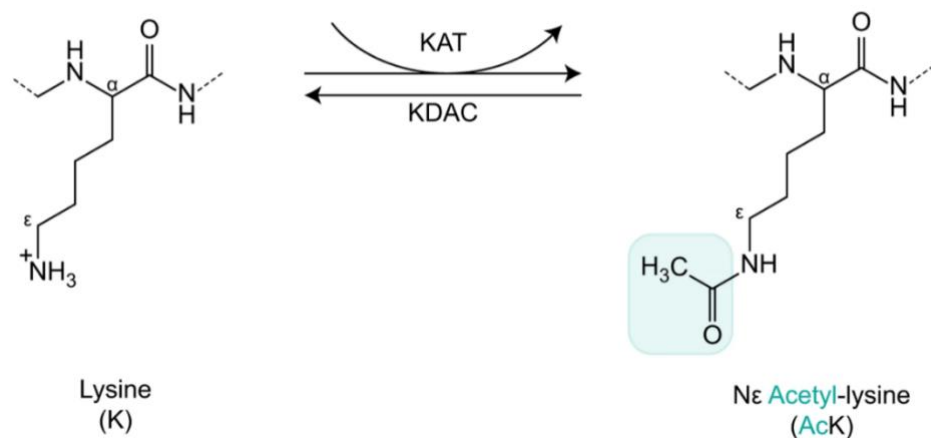
Proteins are modulated by adding and removing a range of post-translation modifications (PTMs) that can regulate protein activity, structure, stability, and localisation (Choudhary et al., 2014, Seo and Lee, 2004, Wang et al., 2017a). There are over two hundred different types of PTMs known, including phosphorylation, methylation, ubiquitination, and acetylation. Phosphorylation, for example, has been studied intensively compared to other PTMs because of its prominent role in regulating enzyme activity and cell signalling pathways. Many PTMs are reversible where some enzymes modify proteins, and others remove the modification to return the protein to its unmodified form, e.g. phosphorylation and de-phosphorylation and acetylation and deacetylation. The reversible nature of these PTMs allows them to regulate protein function dynamically (Drazic et al., 2016, Zhou et al., 2016a).

### **1.1.2 Lysine acetylation**

Protein acetylation is a PTM that can occur in two different ways N-terminal (Nt) acetylation and acetylation of  $\epsilon$ -amino acid of lysine(K) (Choudhary et al., 2009b). N-terminal acetylation is an irreversible abundant co- post-translation modification, occur at a high-frequency level in almost all organisms (Soppa, 2010, Drazic et al., 2016). Proteins are N-terminally-acetylated by N-terminal acetyltransferases (NATs), which attach an acetyl group from acetyl-CoA to  $\alpha$ -amino group of the polypeptide N-terminus (Helsens et al., 2011, Xiao et al., 2010). This modification occurs on newly synthesised proteins; when the acetyl group is attached, it prevents other modifications by neutralising the charge of the amino group (Drazic et al., 2016). Around 80-90% of human soluble proteins are acetylated on their N-

terminus. This acetylation can occur partially, which means the same protein can exist in both acetylated and unacetylated forms (Arnesen et al., 2009, Drazic et al., 2016).

The second type of acetylation is called lysine acetylation; in this type of acetylation, the acetyl groups are attached to the  $\epsilon$ -amino acid of lysine (K) residues in proteins enzymatically or non-enzymatically (Glozak et al., 2005, Choudhary et al., 2014) (Figure 1.1). It is a reversible process that is regulated by lysine acetyltransferases (KATs) and lysine deacetylases (KDACs) to control many complex cellular and biological processes involved in important cellular pathways. The acetyl group has a molar mass of (43.045 g·mol<sup>-1</sup>) and it contains a methyl group single-bonded to a carbonyl group (CH<sub>3</sub>CO). The carbonyl has one nonbonded electron with which it forms a chemical bond to the remainder R of the molecule such as (acetyl-CoA) (Nakao et al., 2000).



---

**Figure 1.1 – Enzymatic regulation of acetylation by KATs and KDACs/Sirtuins.** The transfer of an acetyl group (CH<sub>3</sub>CO, turquoise) to the free -amino group of protein to the -amino group of lysine (K) side chains is catalysed by KATs. The positive charge (+) of the amino group is removed by covalent attachment of an acetyl group, affecting local electrostatic properties. KDACs can remove the acetyl moiety from lysine acetylation, making it a reversible protein modification.

Lysine acetylation was discovered in the early 1960s, shortly after the discovery of acetyl-CoA and its role in acetylation. At that time, this discovery allowed Allfrey and his colleagues (Allfrey et al., 1964, Ali et al., 2018) to hypothesise and investigate the role of acetylation in gene expression, which led them to identify that histone proteins are acetylated on lysine residues and that this process regulates gene expression. Acetylation of histones changes chromatin architecture and activates gene transcription, and is, therefore, a critical regulator of gene expression (Allfrey et al., 1964, Verdin and Ott, 2015).

In recent years through developments in mass spectrometry-based proteomics, we now know that lysine acetylation is not limited to histone proteins; studies have indicated that acetylation could be the most abundant PTM after phosphorylation (Choudhary et al., 2014, Lundby et al., 2012b, Yang and Seto, 2008, Lundby et al., 2012a). Unfortunately, the study of lysine acetylation has been delayed more than 30 years after its first identification in the 1960s. Many reasons caused this issue, but the main one is that it is technically challenging to measure or identify acetylation sites in the proteins (Verdin and Ott, 2015).

### ***1.1.3 Generation of mitochondrial and cytosolic acetyl coenzyme A***

Protein acetylation depends on the availability of the acetyl group donor in different cellular compartments. Acetylation occurs in the nucleus, mitochondria, and cytoplasm. The abundance of acetyl-CoA in a cell compartment can influence the rate of protein acetylation, which will affect gene expression, signal transduction, and metabolism (Wellen and Thompson, 2012). Acetyl-CoA is a molecule with a crucial position as an intermediate metabolic mediator involved in many cellular processes. It works as a fuel for anabolic and catabolic reactions and is the central molecule in lipid synthesis and the tricarboxylic acid

(TCA) cycle (Choudhary et al., 2014, Pietrocola et al., 2015). In addition, it is the only donor of the acetyl group; thus, it is essential for the whole process of protein acetylation by KATs.

In mammalian cells, acetyl-CoA is generated by many different metabolic pathways and found in both mitochondrial and non-mitochondrial pools (Pietrocola et al., 2015), the levels of which depend on the nutrient status of cells. For example, during fasting or in a calorie-restricted diet, the production of acetyl-CoA is sensitive to the availability of glucose (Pougovkina et al., 2014, Wellen and Thompson, 2012).

In mitochondria, acetyl-CoA is produced from many metabolic pathways such as glycolysis, pyruvate oxidation,  $\beta$ -oxidation of fatty acids, metabolism of branched-chain amino acids such as leucine, valine that can produce acetyl-CoA under the effect of deacetylases. In some cells such as neurons, ketone body formation during starvation can generate acetyl-CoA (Pietrocola et al., 2015). In the cytoplasm and nucleus, acetyl-CoA can be produced by two enzymes; ATP-citrate lyase (ACL), which converts citrate (exported to the cytoplasm from mitochondria) to acetyl-CoA and acetyl-CoA synthase (ACSS2), which generates acetyl-CoA from acetate. The metabolic status of the cell mainly controls the rate of production of acetyl-CoA by these two enzymes (Choudhary et al., 2014, Pietrocola et al., 2015, Wellen and Thompson, 2012).

#### ***1.1.4 Enzymatic control of lysine acetylation***

As mentioned earlier that lysine acetylation is mediated by families of KATs and reversed by KDACs; the reciprocal action of these enzymes enables acetylation to be reversible and, therefore, a regulatory process (Drazic et al., 2016, Choudhary et al., 2014). The modulation of cellular signalling pathways by lysine acetylation is facilitated by three classes of proteins called: writers, erasers, and readers; those names are not frequently used, but it provides a

clear idea about the functions of those proteins lysine acetylation (Verdin and Ott, 2015, Choudhary et al., 2014). The first class is the KATs (writers) which use an acetyl group donated by acetyl-coenzyme A to acetylate lysine residues on proteins. The name changed from Histone acetyltransferase (HAT) to KATs to reflect that acetylation is not exclusive to histones. There are 22 different KATs known in mouse and human genomes; KATs are grouped into three families: GCN5, MYST and CBP/p300.

Next, we have the erasers (KDAC) enzymes, so called that as they remove acetyl groups from proteins with the help of NAD<sup>+</sup> or Zn<sup>2+</sup> molecules. There are four classes of KDACs based on their structure, with around 18 enzymes in human and mouse genomes (Choudhary et al., 2014, Glozak et al., 2005). Class I, II and IV KDACs are Zn<sup>2+</sup>-dependent histone deacetylases (HDACs 1-11), Class I and II are localised to the nucleus and cytoplasm, while class IV localise only to the nucleus. Class III is NAD<sup>+</sup>-dependent and includes Sirtuins (SIRT1-7), localised in the nucleus, mitochondria, and cytoplasm. It is worth mentioning that, to date, many of these enzymes have shown either weak or no deacetylase function, and some are targeting other acylation modifications, for example, SIRT4 (Anderson et al., 2017) SIRT5 (Du et al., 2011), and SIRT6 (Jiang et al., 2013). Figure 1.2 demonstrates the cellular localisation of KDACs enzymes.

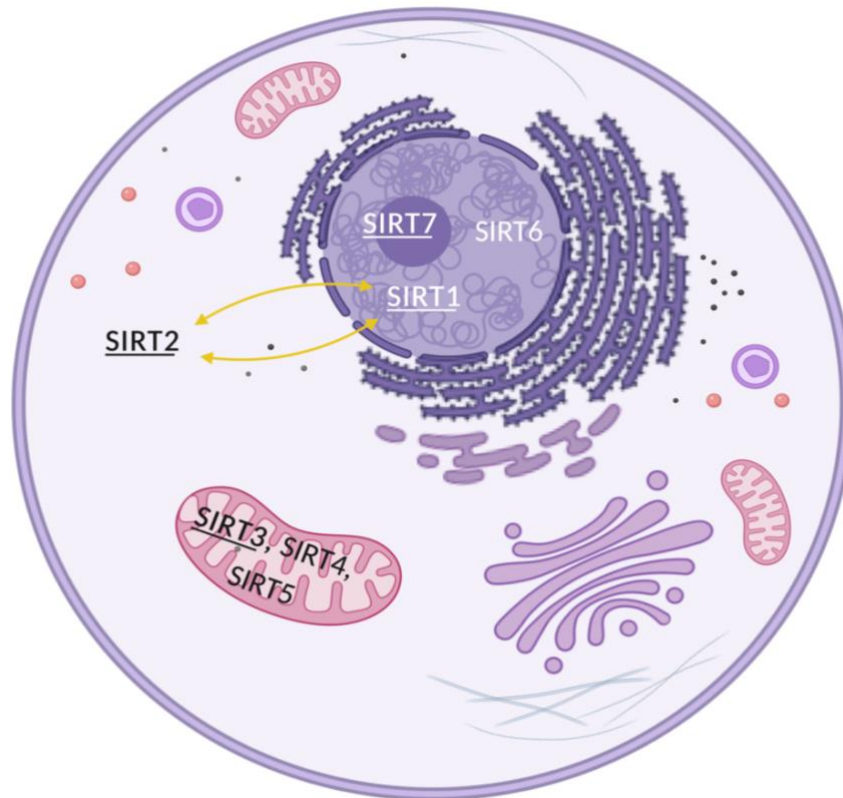


**Figure 1.2 – Sub-cellular localisation of Sirtuins.** Underlined SIRTs represent the deacetylase function of SIRT1, SIRT2, SIRT3 and SIRT7. SIRT1 and SIRT7 are mainly expressed in the nucleus, SIRT2 is expressed in the cytoplasm, but it can shuttle between cytoplasm and nucleus, and SIRT3 is localised in mitochondria.

The last protein group is the readers, which do not act as an enzyme; instead, they bind to and recognise the acetylated (K) residue on proteins. Nearly 60 acetyl-lysine readers are known in the human genome, including a bromodomain, a protein domain with less than 120 amino acids that mediate acetylation-dependent protein-protein interactions (Choudhary et al., 2014). Bromodomains are found in many KATs such as P300, CREBBP, GCN5 (KAT2A) and PCAF (KAT2B) (Svinkina et al., 2015, Choudhary et al., 2014, Drazic et al., 2016, Pietrocola et al., 2015). Most of those proteins target histone acetylation, but recent studies showed an interaction with non-histone acetylation and other acylation types (Marmorstein and Zhou,

2014, Fujisawa and Filippakopoulos, 2017). Overall, the acetyl reader group and their functions are poorly studied and widely unappreciated.

#### ***1.1.5 non-enzymatic acetylation***

In addition, to KATs, acetylation has been suggested to occur non-enzymatically under conditions where acetyl-CoA is abundant and a high pH by a direct reaction between acetyl-CoA and proteins; this was first discovered to occur on Histones. Interestingly, these conditions are commonly found in mitochondria. As mentioned earlier, most KATs enzymes are localised in the nucleus and cytoplasm, suggesting that many mitochondrial proteins are non-enzymatically acetylated (Drazic et al., 2016, Ali et al., 2018, Verdin and Ott, 2015). In organisms such as bacteria, acetylation can occur directly (chemically) through acetyl-phosphate (ACP) (Drazic et al., 2016, Wang et al., 2017c, Weinert et al., 2013), but further investigation is needed to prove the existence of non-enzymatic acetylation in mammalian cells.

### ***1.1.6 Detection of lysine acetylation.***

As mentioned earlier, acetylation was first classified as a nuclear modification, specifically histone proteins modification. Two papers were published by Allis (Brownell et al., 1996) and by Schreiber (Taunton et al., 1996) in the mid of 1990s, they uncover a direct relationship between histone acetylation and gene activation via acetyltransferase (Brownell et al., 1996). As well as the role for histone deacetylase as a major regulator of eukaryotic transcription (Taunton et al., 1996). Those significant observations were followed by many investigations of protein acetylation and the enzymes that regulate it (Verdin and Ott, 2015, Ali et al., 2018, Glozak et al., 2005).

Over time it has become apparent that acetylation occurs on other proteins (Svinkina et al., 2015, Verdin and Ott, 2015). After that evidence, more attention has focused on the acetylation of non-histone protein, and researchers are interested in uncovering its biological, regulatory, and therapeutic roles.

In 2006, Kim and his colleagues (Kim et al., 2006b) published the first acetylome profile, using immunoaffinity enrichment of acetylated peptides with pan-anti-acetyl-lysine antibodies and analysis using high-resolution mass spectrometry-based proteomics. This approach successfully identified 388 ac(K) sites from HeLa cells and mouse liver mitochondria. In subsequent studies by Choudhary et al. (Choudhary et al., 2009b), with more refined methodologies, more significant numbers were reported with 3,600 lysine acetylation sites identified on 1,750 proteins from human leukaemia cells (MV4-11, A549 and Jurkat) treated with deacetylase inhibitors.

The analysis of acetylated proteins and peptides can be performed using many types of MS instruments and methods such as top-down MS (analysis of intact proteins), e.g., for

investigation of histones, or bottom-up/shotgun (analysis of peptides after protein digestion) MS. Shotgun LC-MS/MS is widely used for acetylome analysis. This involves an enrichment of acetylated peptides using pan-anti-acetyl-lysine antibodies from digests of protein samples, e.g., whole-cell lysates (Choudhary et al., 2014, Svinkina et al., 2015). This approach was adopted later and followed by many other studies in different species (Zhang et al., 2009, Weinert et al., 2011). Most large scale acetylome profiles were generated using bottom-up (shotgun) proteomics (Lundby et al., 2012b, Kim et al., 2006a, Weinert et al., 2011), which involve protein digestion by enzymes (trypsin), anti-acetyl-lysine peptides enrichment, followed by LC-MS/MS analysis and bioinformatics analysis. Some studies add a fractionation step of acetylated peptides by chromatography to provide a less complex sample and a deep acetylome coverage (Choudhary et al., 2014, Verdin and Ott, 2015, Ludwig et al., 2018).

Owing to developments in mass spectrometry-based proteomics, a large number of acetylated proteins and individual acetylation sites in different cell types and tissues have been identified (Kim and Yang, 2011, Lundby et al., 2012b, Choudhary et al., 2009b). Figure 1.3 illustrates a brief timeline of the progress in identifying ac(K) from biological samples derived from mouse or human samples. A comprehensive proteomic analysis generated an acetylome dataset from 16 rat tissues/organs with 15,474 acetylation sites identified on 4,541 acetylated proteins. Of these, 4,782 acetylation sites were identified from 1,653 proteins in the brain (Lundby et al., 2012b), including many receptors and ion channels in the plasma membrane pointing to a potential function for lysine acetylation in neurophysiological pathways (Lundby et al., 2012b). This work has revealed that acetylation is widely distributed in mammalian tissues but with enrichment in brain tissues compared to other tissue types (Lundby et al., 2012b).

These studies have provided novel regulatory functions and properties of lysine acetylation. This valid and robust evidence revealed that acetylation is one of the most common protein modifications. Acetylation is not specific to a protein group, a cellular compartment, and occurs at a wide range from bacteria to humans, showing that acetylation is a very conserved and widespread modification (Kim et al., 2006a, Choudhary et al., 2009b, Narita et al., 2018, Choudhary et al., 2014).

Despite these advances in mass spectrometry-based proteomics detecting non-histone acetylation using other methods is challenging. Stoichiometry is a critical factor for acetylation investigation studies until now is not very well studied nor understood (Bogi Karbech et al., 2019, Verdin and Ott, 2015).

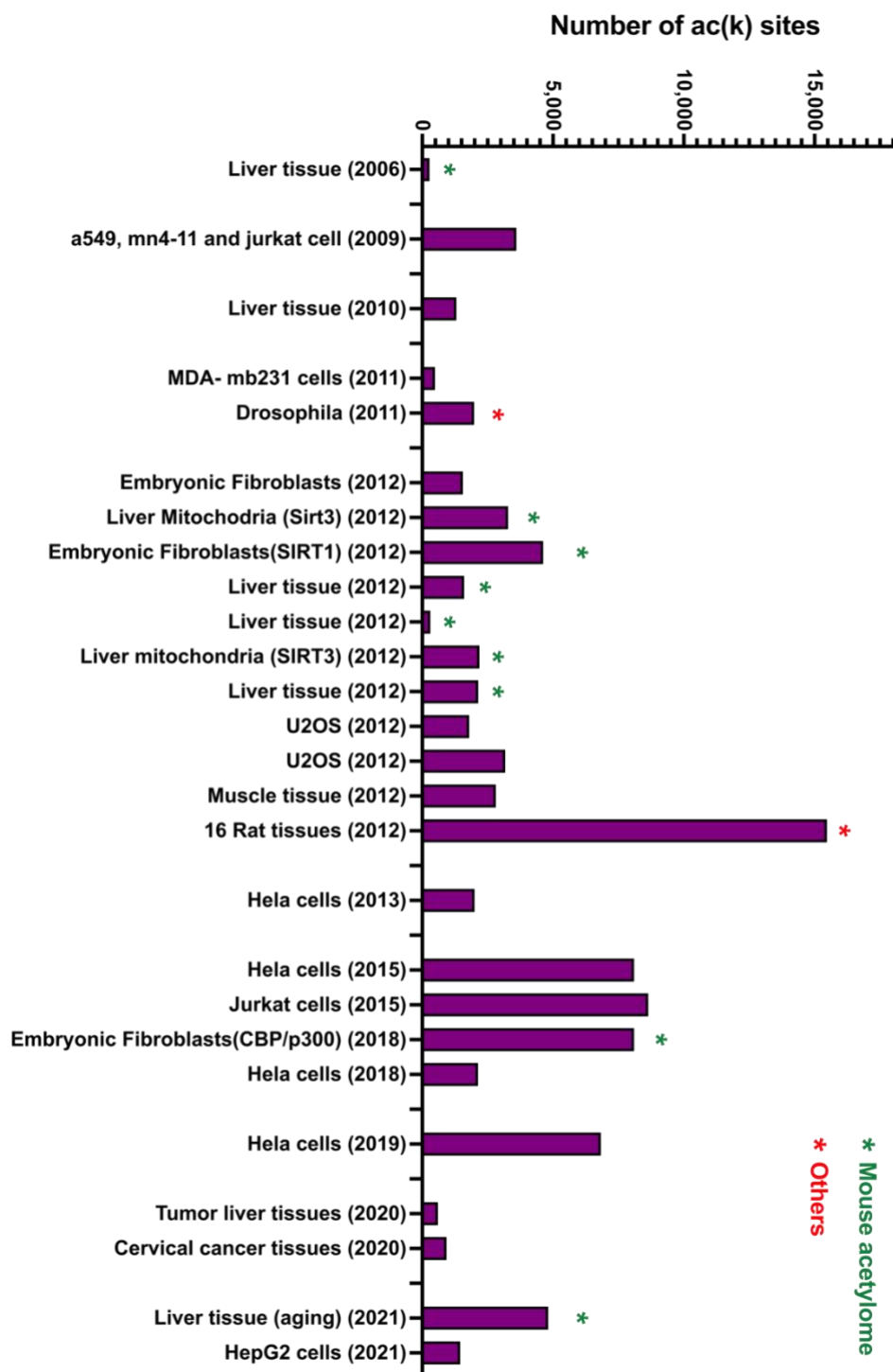


**Figure 1.3 – Timeline of acetylome datasets reported in the past decade.** The literature search was mainly focused on mouse and human samples and a few other acetylome datasets from other species. Column without stars represent acetylomes from the human samples, green stars represent acetylome from mouse tissues, red stars represent other species such as rat and drosophila.

### 1.1.7 Functions of lysine acetylation

Acetylation, in general, is well known for its role in the regulation of gene expression and epigenetic coding, which was first recognised for its occurrence in histones (Zhou et al., 2016b). Later, after many large scale acetylome studies, the role of lysine acetylation has expanded to many cellular functions, including the cell cycle, DNA damage repair, protein folding and aggregation, cellular signalling, and autophagy. Moreover, lysine acetylation has been found to regulate plasma membrane receptors, enzymes, and a wide range of proteins from all cell compartments. In addition to its impact on enzymes function regulation, protein-protein interaction, and protein degradation (Drazic et al., 2016, Narita et al., 2018, Choudhary et al., 2014). Figure 1.4 provide an example of roles and functions regulated by acetylation.

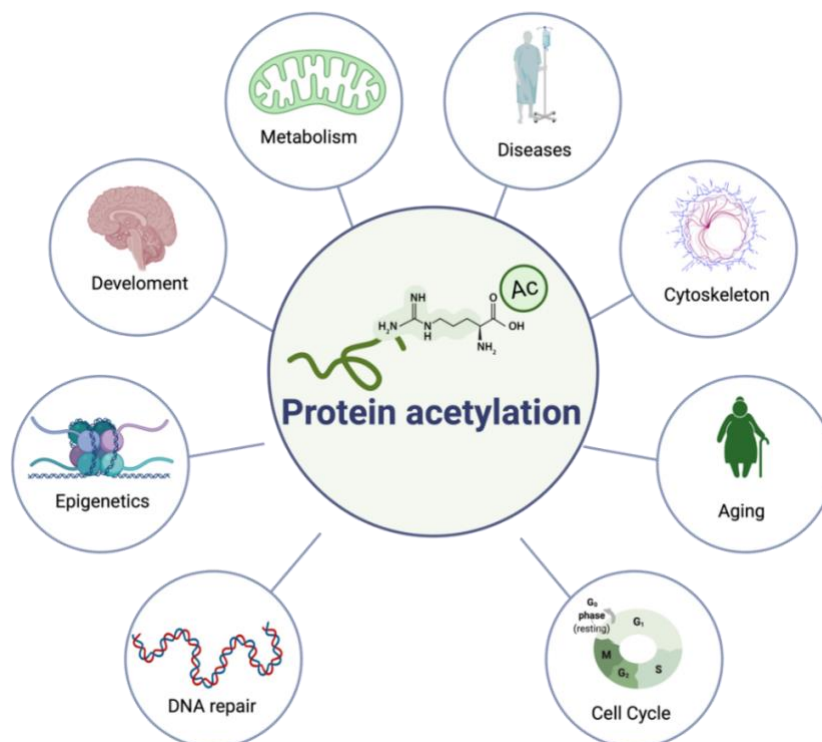


**Figure 1.4 – Acetylation regulates many cellular processes and is implicated in ageing and disease.**

A few years ago, an interesting review highlighted the recent progress on the functions and mechanisms of lysine acetylation modification, which revealed a summary of more than 380 functionally proteins associated with acetylation (Narita et al., 2018). Figures 1.5 and 1.6 provide an overview of lysine acetylation functions of KATs and KDACs regulated non-histone proteins (Narita et al., 2018).

These networks reveal the disproportionately large number of functionally studied acetylations are related to a few well-characterized KATs and KDACs. For example, SIRT1, P300, and CBP have been extensively investigated in comparison to others that might seem to be more functional than others. Another point is that proteins implicated in transcription control are significantly over-represented in these networks, accounting for more than 40% of functionally defined substrates. This corresponds to the nuclear localisation of the vast majority of canonical KATs, in addition to SIRT1.

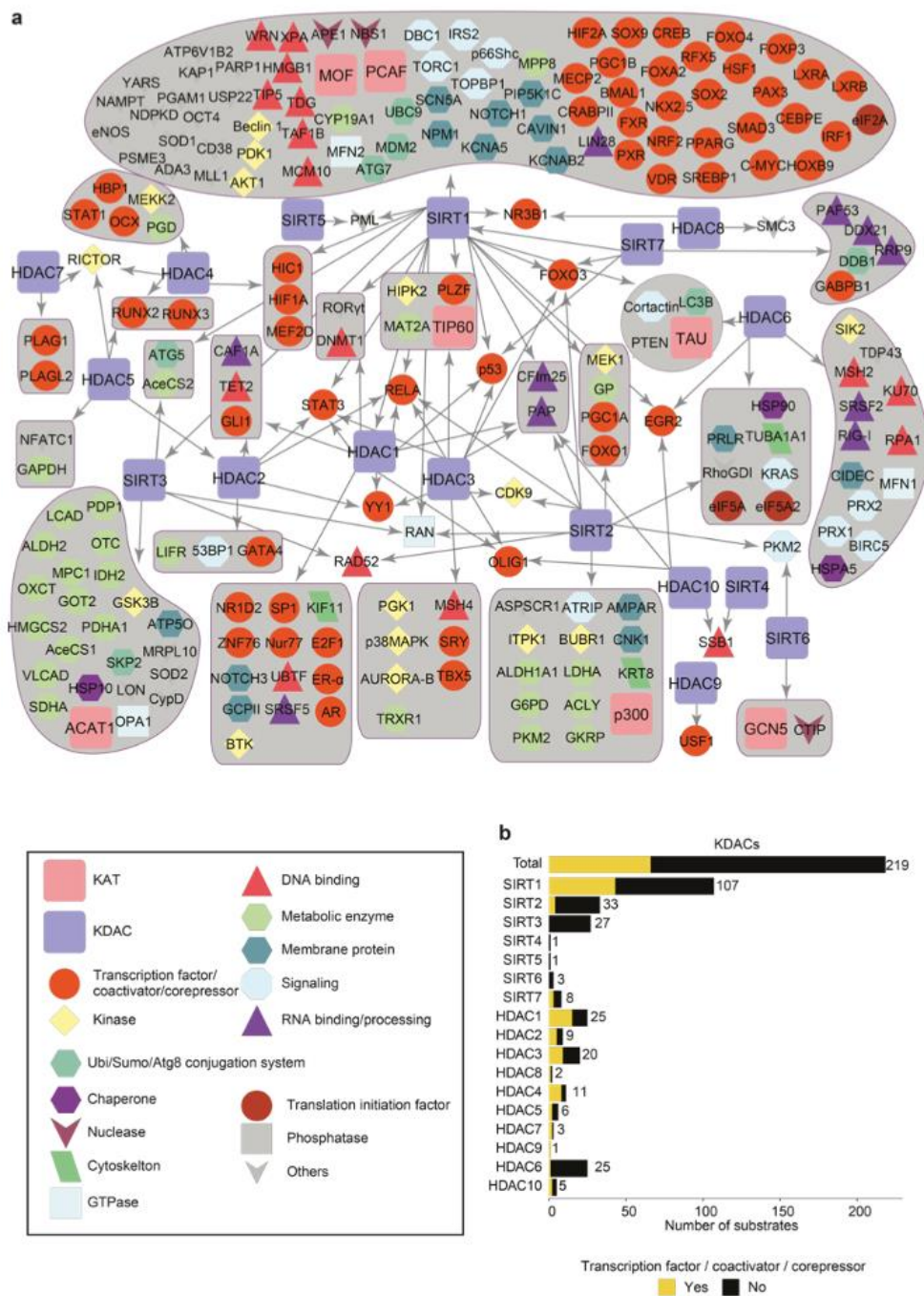


**Figure 1.5 – Functional networks of KDACs -regulated non-histone proteins. A)** schematic network of functionally characterised, acetylated non-histone proteins and their KDACs; each substrate is colour coded depending on their function. **B)** The Bar chart shows the number of proteins targeted by each KDACs and the fraction of the proteins linked to gene transcription. Network adapted from (Narita et al., 2018).

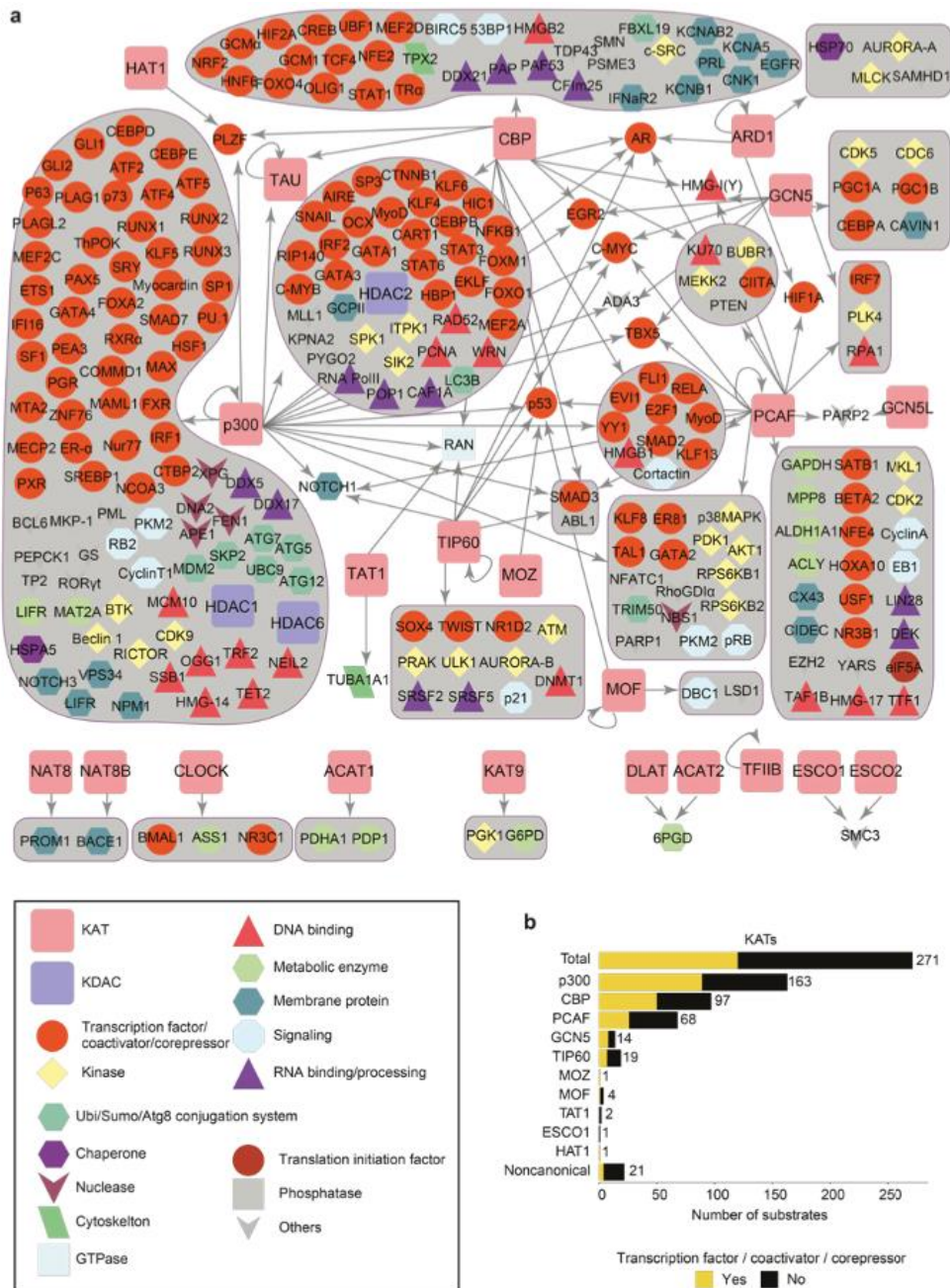


**Figure 1.6 – Functional networks of KATs-regulated non-histone proteins. A)** schematic network of functionally characterised, acetylated non-histone proteins and their KATs; each substrate is colour coded depending on their function. **B)** the Bar chart shows the number of proteins targeted by each KATs and the fraction of the proteins linked to gene transcription. Network adapted from (Narita et al., 2018).

Acetylation of one protein may occur in many different sites inside the cell and on many different sites with its protein sequence; several acetylated proteins are now understood to

be vital to complete many cellular and biological processes (Yang and Seto, 2008, Svinkina et al., 2015, Kim et al., 2006a, Ali et al., 2018). It has become apparent that different cellular functions require different patterns of acetylation; therefore, it is essential to identify where the protein acetylated in each tissue and organism, in addition to acetylation sites distribution of a particular protein.

Acetylation of K residues neutralises its positive charge, which is required for the interaction and activities of proteins—as a result, removing the positive charge can impact the stability, localisation, and enzymatic activity of proteins (Choudhary et al., 2014, Drazic et al., 2016, Narita et al., 2018). Studies have shown that acetylation regulates the activity of around 40 enzymes by inhibiting or enhancing their catalytic activity (Narita et al., 2018). For example, acetylation of both ACSS1 and 2 inhibit their catalytic activities (Schwer et al., 2006). Acetylation inhibits the formation of G6PD active form, which cause a loss in the enzymatic function (Wang et al., 2014). Both examples require deacetylation to restore their activity (Narita et al., 2018). On the other hand, the KAT enzyme p300 autoacetylates itself, enhancing its enzymatic activity to acetylate other proteins; here, deacetylase enzymes have a reverse function as deacetylation of p300 by Sirt2 reduces p300 enzymatic activity (Black et al., 2008, Narita et al., 2018). Other KAT enzymes activate their function by autoacetylation, such as KAT2B and KAT8 (McCullough and Marmorstein, 2016, Santos-Rosa et al., 2003). Studies show that acetylation can inhibit or promote protein-protein interactions. For example, acetylation of p53 prevents its interaction with other vital proteins primarily dependent on the positively charged K residues (Wang et al., 2016, Wątroba and Szukiewicz, 2016).

Lysine acetylation is known to prevent protein ubiquitylation that also occurs on lysine residues; thus, it promotes protein stability and prevents degradation (Yang and Seto, 2008). For instance, acetylation of the AMPA-selective glutamate receptor 2 (GluR1) on K831, 837,

840 and 885 prevents their ubiquitination. This decreases receptor internalisation and therefore increases cell surface expression of the receptor (Wang et al., 2017a). Similarly, acetylation of Tau, Arc (Arg3.1), ACLY, GLUL, and RUNX3 are shown to prevent their ubiquitination and degradation (Lalonde et al., 2017, Min et al., 2010, Guo et al., 2019, Narita et al., 2018, Jin et al., 2004). Interestingly, acetylation enhances ubiquitination and promotes the degradation of some proteins such as PCK1 (Jiang et al., 2011).

Another role of acetylation is to regulate protein localisation, which is more specific to non-histone acetylation. The interplay between KATs and KDACs enzymes can temporarily change protein localisation (Choudhary et al., 2014). For example, SKP2 and SOX2 are localised to the cytoplasm by acetylation or to the nucleus by deacetylation (Baltus et al., 2009, Wang et al., 2012). In contrast, acetylation of CtBP2 and HNF4 promotes their nuclear retention and prevent them from being exported to the cytoplasm (Soutoglou et al., 2000, Zhao et al., 2006). As mentioned earlier, the regulation of gene transcription through histone acetylation was the first function of acetylation to be discovered (Choudhary et al., 2014). However, acetylation of the transcription factor p53 is important for changing protein stability, interactions, and DNA binding; p53 is not the only transcription factor modified by acetylation; studies show that more than 100 acetylated proteins are involved in the gene transcription (Wang et al., 2016, Rothgiesser et al., 2010, Choudhary et al., 2014).

Acetylation is also involved in enhancing or inhibiting autophagy. Many KATs and KDACs enzymes are important enzymes that regulate autophagy. A study identified 421 sites on 296 proteins are significantly acetylated during autophagy (Zhou et al., 2019), in addition, studies showed that in many cell types, p300 regulates mTORC1 activity to regulate autophagy during starvation and refeeding (Son et al., 2020, Son et al., 2021). Sirt2 deficiency can cause

microtubule stability and the activation of autophagic-lysosomal pathway to degrade toxic A $\beta$  oligomers (Jeřko et al., 2016).

Acetylation alterations may have an impact on neurodegenerative illnesses, as many of the relevant proteins are autophagy substrates (Jeřko et al., 2016).

### ***1.1.8 The role of acetylation in disease***

The interplay between KATs and KDACs in regulating acetylation is important; thus, any dysregulation in this balance or any dysfunction of any acetylation enzymes could cause various diseases. Dysregulation of lysine acetylation is linked to and contributes to diabetes, lung, autoimmunity, cancer, cardiovascular diseases (Sarikhani et al., 2018a, Parodi-Rullán et al., 2018, Ali et al., 2018). Most diseases associated to acetylation are investigated in relation to one KAT or KDAC and their capacity to control and effect the pathogenesis of those diseases. For example, overexpression of Sirt1 in pancreatic  $\beta$  cells enhances glucose-stimulated insulin secretion in mice via regulating UCP2 which promotes the secretion of insulin (Bordone et al., 2006, Moynihan et al., 2005). Moreover, studies suggested that lysine acetylation is associated with many neurodevelopmental disorders and diseases (Donmez and Outeiro, 2013, Tapias and Wang, 2017).

### ***1.1.9 Lysine acetylation and neurodegenerative diseases***

Misfolded tau protein aggregates into fibrils during Alzheimer's disease (AD) due to the phosphorylation of tau. Tau is also acetylated by p300 and deacetylated by SIRT1; studies showed that the level of SIRT1 decreased in brains of AD patients during fibrils accumulation; thus, deacetylated tau increases the chances for its ubiquitination and degradation and, as a result, prevent its accumulation and aggregation and vice versa (Min et al., 2010, Min et al., 2018b, Julien et al., 2009, Sun et al., 2021).

Parkinson's disease (PD) is another common neurodegenerative disease that is characterised by the loss of dopamine levels and formation of Lewy bodies; studies have shown that changes in lysine acetylation and deacetylation of many proteins, including histones and non-histone proteins, may be closely linked to the pathogenesis of Parkinson's disease (Wang et al., 2020b, Bhattacharjee et al., 2019).

SNCA protein (Alpha synuclein), like many other proteins, are modified by both N-terminal acetylation (irreversible) and lysine acetylation (Spinelli et al., 2014, Wang et al., 2020b). Mutation in SNCA and SNCA acetylation contribute to PD pathogenesis mechanisms. First, the deacetylation of SNCA promotes its aggregation and neurotoxicity, which means that acetylated SNCA is crucial to inhibit toxicity and protect from PD (Rita Machado de et al., 2017, Wang et al., 2020b). Ep300 and Sirt2 are responsible for the acetylation of SNCA. Second, SNCA activates the deacetylase function of Sirt2 and promotes  $\alpha$ -tubulin deacetylation (Wang et al., 2020b). As a result, both deacetylated SNCA and  $\alpha$ -tubulin form the neural toxicity complex. Studies showed that deletion of the KDAC enzyme Sirt2 will block the deacetylation of SNCA and, as a result, prevent neural toxicity. Thus, inhibition by Sirt2 inhibitors (AGK2, and AK7) or genetic deletion of Sirt2 is a possible therapeutic avenue for PD (Chen et al., 2015, Spinelli et al., 2014, Outeiro et al., 2007).

In contrast, activating both SIRT1 and SIRT3 is considered a promising therapeutic route for PD. Studies showed that SIRT1 exhibited a low expression level or loss of activity in MPTP/MPP<sup>+</sup>- and 6-OHDA-induced PD model and PD patients (Wang et al., 2020b, Singh et al., 2017a). Which may be responsible for the defect of many cellular functions such as autophagy, oxidative stress and neuroinflammation (Wang et al., 2020b, Singh et al., 2017a, Guo et al., 2016). Like SIRT1, SIRT3 showed a loss in activity related to PD pathogenesis; as

SIRT3 is mainly responsible for maintaining mitochondrial acetylation balance, the failure of its activity causes many disturbances and leads to mitochondrial dysfunction (Wang et al., 2020b, Martens et al., 2018, Gleave et al., 2017).

Furthermore, studies have shown differences in acetylation of the ALS-disease gene SOD1 between ALS and non-ALS mouse models (Liu et al., 2013a). In addition, acetylation of the ALS gene TDP-43 controls its propensity to aggregate and acetylated TDP-43 lesions are detected in the spinal cord from ALS patients (Todd et al., 2015). Together, these examples illustrate the potential role of acetylation on the pathogenesis of several neurodegenerative diseases.

#### ***1.1.10 Lysine acetylation and synaptic proteins***

Synaptic proteins regulate most brain functions because of their involvement in synaptic plasticity, an activity-dependent change in the strength of synaptic connections that underlies learning and memory (Wang et al., 2017a, Zhang et al., 2021). Synapses are the junctions between the axon and the dendrite of two neurons. The changes that occur at synapses to allow communication between neurons is called synaptic plasticity. These changes can be a strengthening (long term potentiation (LTP)) or a weakening (long term depression (LTD)) of the synaptic connections. Studies show that many brain disorders and neurodegenerative diseases occur due to synaptic plasticity deficits (Bliss et al., 2014). Synaptic plasticity is regulated by protein modifications, protein synthesis and gene transcription (Zhang et al., 2021). Lysine acetylation through KATs and KDACs is linked to synaptic plasticity regulation via histone acetylation (Guan et al., 2009, Alarcón et al., 2004).

Studies showed that mouse synapse isolated from both post-synaptic density (PSD) and synaptosome (SYN) fractions contains around 4,142 proteins (Bayes et al., 2017). 1,145

proteins were significantly enriched in SYN while 687 proteins enriched in PSD with an overlap of 2,492 proteins (60%).

This mouse synaptic proteome dataset will be beneficial to address acetylated proteins and their function in synapses. In addition, studies provided a comprehensive proteomics analysis of mouse brain regions and found around 11,000 protein groups (Sharma et al., 2015). Moreover, a study showed an overlap of 70% between human and mouse PSD proteomes (Bayes et al., 2012). Thus, mice are considered a suitable model to represent human synaptic diseases and these proteomics data are valuable to use to understand lysine acetylation roles in relation to physiological, behavioural, and neurological studies (Bayes et al., 2017, Bayes et al., 2014, Itzhak et al., 2017, Sharma et al., 2015).

The mouse synaptic proteome dataset (Bayes et al., 2017) contains three KDACs, Hdac6, Hdac11 and Sirt2, however Sirt2 showed a higher abundance than the others as shown in Figure 1.7. Sirt2 is the only non-histone deacetylase present at synapses, and a comparison of protein levels between synaptosomes and post-synaptic densities indicate that Sirt2 is equally abundant in both fractions. These data are considered as valuable evidence to support that Sirt2-dependent lysine deacetylation may have a major role in regulating synaptic proteins and, as a result, regulate many molecular and cellular processes in the synapse and brain in general (Bayes et al., 2017).

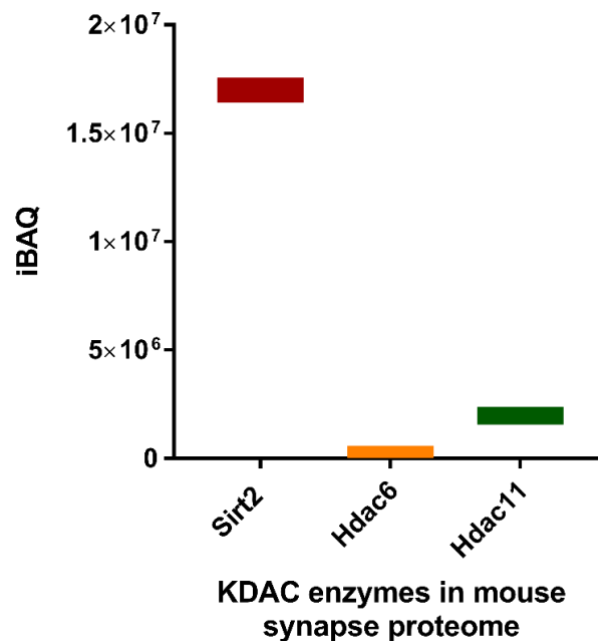


**Figure 1.7 – IBAQ intensity of KDAC enzymes found in mouse synaptic proteome.** Data showed an higher abundance of protein level of Sirt2 enzymes compared to Hdac6 and 11 (N=4) (Bayés et al., 2017).

There is little known about the role of non-histone lysine acetylation on synaptic proteins. Few studies have demonstrated the effect of lysine acetylation and cognate KATs or KDACs on synaptic proteins. AMPA receptors are important mediators of neurotransmission, synaptic plasticity, learning and memory (Wang et al., 2017a). These receptors are regulated by lysine acetylation, which occurs at their c-terminus and results in higher cell surface expression and prolongs the half-life of the receptor. AMPAR deacetylation by Sirt2 reveals a lysine residue that becomes ubiquitinated and targets the receptor for destruction by the proteasome (Wang et al., 2017a). Prevention of AMPAR deacetylation blocks ubiquitination at this site and therefore stabilises the receptor at the cell surface. AMPAR acetylation is

regulated by synaptic activity; it is reduced by upregulation of synaptic activity while increased in response to decreased synaptic activity (Wang et al., 2017a, O'Connor et al., 2020).

Moreover, studies showed that AMPA receptors are significantly reduced in AD models, which cause a lower amount of AMPA receptor localised in synapses (O'Connor et al., 2020). As a result, it showed a loss in synaptic activity and function and impaired memory. Thus acetylation of AMPA receptor (GluA1/ Gria1) contributes to its stability and rescue synaptic functions and memory loss (O'Connor et al., 2020).

Arc protein (also known as Arg3.1) is another important synaptic protein regulated by lysine acetylation. Arc is an immediate-early gene, and Arc protein is rapidly synthesised in response to synaptic activity. It is involved in regulating synaptic plasticity and has been shown to mediate homeostatic synaptic scaling of AMPA receptors by its ability to activate endocytosis of AMPA receptors (Shepherd et al., 2006). Arc has recently been established to form protein complexes with the synaptic scaffolding protein, PSD-95 (Fernandez et al., 2017). These complexes are enriched with genes associated with several neurological disorders, including schizophrenia, intellectual disability, autism, and epilepsy (Fernandez et al., 2017).

Calmodulin (CaM), a calcium ion sensor synaptic protein, had an essential role in the activation of CaMKII $\alpha$ , which is crucial for many brain functions (Storm and Xia, 2005). A study found that acetylation of CaM is critical for synaptic plasticity functions such as fear and memory. Acetylation of CaM activates the kinase CaMKII $\alpha$  which subsequently phosphorylates the AMPA receptor, which crucially contributes to brain function (Zhang et al., 2021).

These examples have stimulated a growing interest to understand and further study non-histone lysine acetylation and its role in cell signalling, synaptic plasticity learning and memory.

## **1.2 Sirt2**

Sirtuins are a conserved class III KDAC NAD<sup>+</sup> dependant enzymes (Rumpf et al., 2015). There are seven members of the Sirtuin family in mammals, all of which are related to the yeast homolog called Silent Information Regulator 2 (Sir2) protein (Gil et al., 2017). As mentioned previously, sirtuins are widely expressed (Wang et al., 2019b) and are present in several different cellular compartments. This variation in localisation provides an opportunity for Sirtuins to regulate many cellular processes. They regulate many cellular functions such as the cell cycle, metabolism, response to DNA damage, gene expression, and promotion of cell death and autophagy (Jayasena et al., 2016, Esteves et al., 2017). Consequently, Sirtuins are also associated with many diseases such as cancer, diabetes, obesity and neurodegenerative diseases (Gil et al., 2017).

### **1.2.1 Structure and expression**

Human Sirt2 has five isoforms; isoform 1 (43kDa) consists of a 389-amino acid, contains a conserved catalytic domain (residues 65-340), five NAD<sup>+</sup> binding sites (residues 85-89, 95-97, 167-170, 262-263 and 286-288) and a nuclear export region (residues 41-51) (de Oliveira et al., 2012, Pavletich et al., 2001, North et al., 2003). Figure 1.8 illustrates the domain organisation of Sirt2 domain. The catalytic domain is a conserved region among all sirtuins, and it is essential for deacetylation activity (North et al., 2003, Pavletich et al., 2001). Sirt2 is an NAD<sup>+</sup> dependant enzyme; thus, it has NAD<sup>+</sup> binding sites located within the deacetylase domain. The nuclear export signal region is essential for Sirt2 to maintain its localisation to the cytoplasm (Eldridge et al., 2020).



**Figure 1.8 – Sirt2 domain structure.** Linear representation of Sirt2 domains, catalytic region (65-340), conserved region for deacetylase function (green), Nuclear export signal (red), NAD<sup>+</sup> binding regions distributed along catalytic region (purple).

Sirt2 isoform 2 (39.5 kDa) and 3 (41 kDa) have a missing residue in disordered region 1-37 and 1-38, respectively (North et al., 2003, de Oliveira et al., 2012). Both isoforms exhibit no change in deacetylase activity so far; studies have shown that isoforms 1, 2 and 3 can deacetylate TUBA1A (Maxwell et al., 2011b, North et al., 2003). Isoform 4 (30 kDa) has different or missing residues (266-271 and 272-289), which contain most of the catalytic domain, while isoform 5 (35.6 kDa) has a missing residue (6-76) which involves the nuclear export region. As a result, both isoforms lack deacetylase activity, in addition to the predominant localisation of isoform 5 in the nucleus due to its inability to export into the cytoplasm (North et al., 2003, Piracha et al., 2020, Eldridge et al., 2020). Figure 1.9 illustrates a protein sequence alignment of all five isoforms, showing the deacetylase domain and NAD<sup>+</sup> binding sites. Overall, Isoform 1 is the most abundant form, and isoform 2 are more relevant to brain tissues; both forms are equally expressed in the heart, kidney, and liver (Eldridge et al., 2020, North et al., 2003).



Sirt2 has a 304-amino acid in catalytic domain and an N-terminal helical extension of 19, residues, the catalytic core of Sirt2 is elongated, with two domains: a larger domain (residues 53–89, 146–186, and 241–356) and a smaller domain (residues 90–145, and 187–240) connected by four polypeptide chains. The large domain can be found in a wide range of NAD(H)/NADP(H) binding enzymes, while the small domain has a structural zinc atom (Schiedel et al., 2016). Figure 1.10 illustrate the 3D structure of human Sirt2.

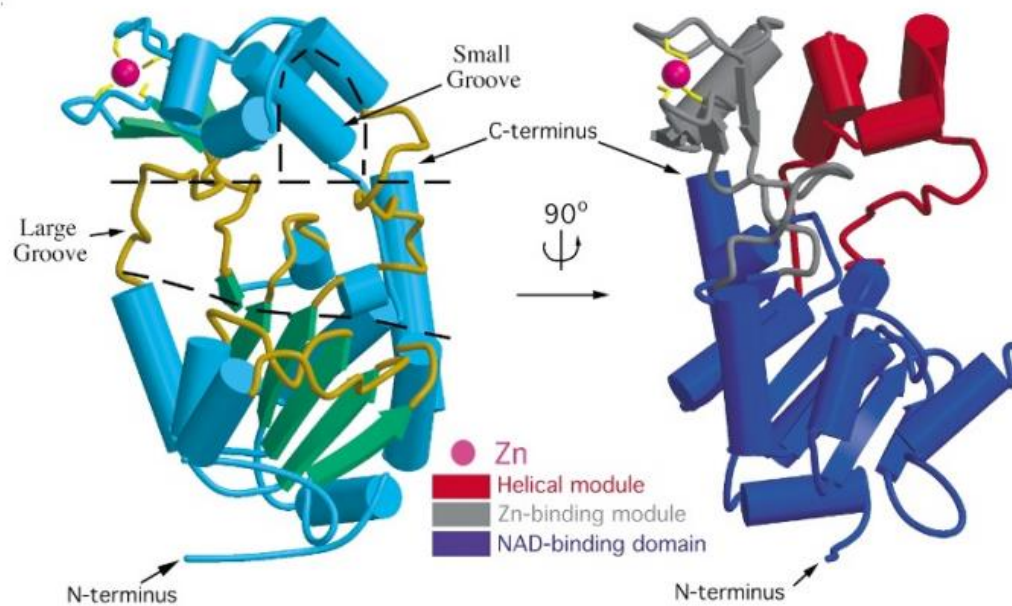


**Figure 1.10 – Human Sirt2 3D structure (Pavletich et al., 2001),** Sirt2 contains two domains that are connected by several conserved loops. Two views represent the structure of the Sirt2 catalytic core rotated by 90°. The large groove in Sirt2 (yellow) in the left panel, connect to the NAD-binding sites (blue) in the right panel. The smaller domain is made up of two modules. First model (grey) binds to a zinc atom (magenta), and the second hydrophobic pocket (red).

### 1.2.2 Sirt2 subcellular localisation

Sirt2 is predominantly localised in the cytoplasm, but evidence has shown its ability to shuttle into the nucleus and localise in nucleoli during G2/M transition and mitosis (Eldridge et al., 2020, North et al., 2003, North and Verdin, 2007). Figure 1.11 illustrates the localisation of Sirt2 to cytoplasm and nucleoli in U-251 cell line, which is derived from malignant glioblastoma tumour adapted from human protein atlas . Studies have shown that Sirt2 is co-localised with many substrates during its deacetylase activity. For example, Sirt2 co-localisation in microtubules with TUBA1A (Maxwell et al., 2011b).

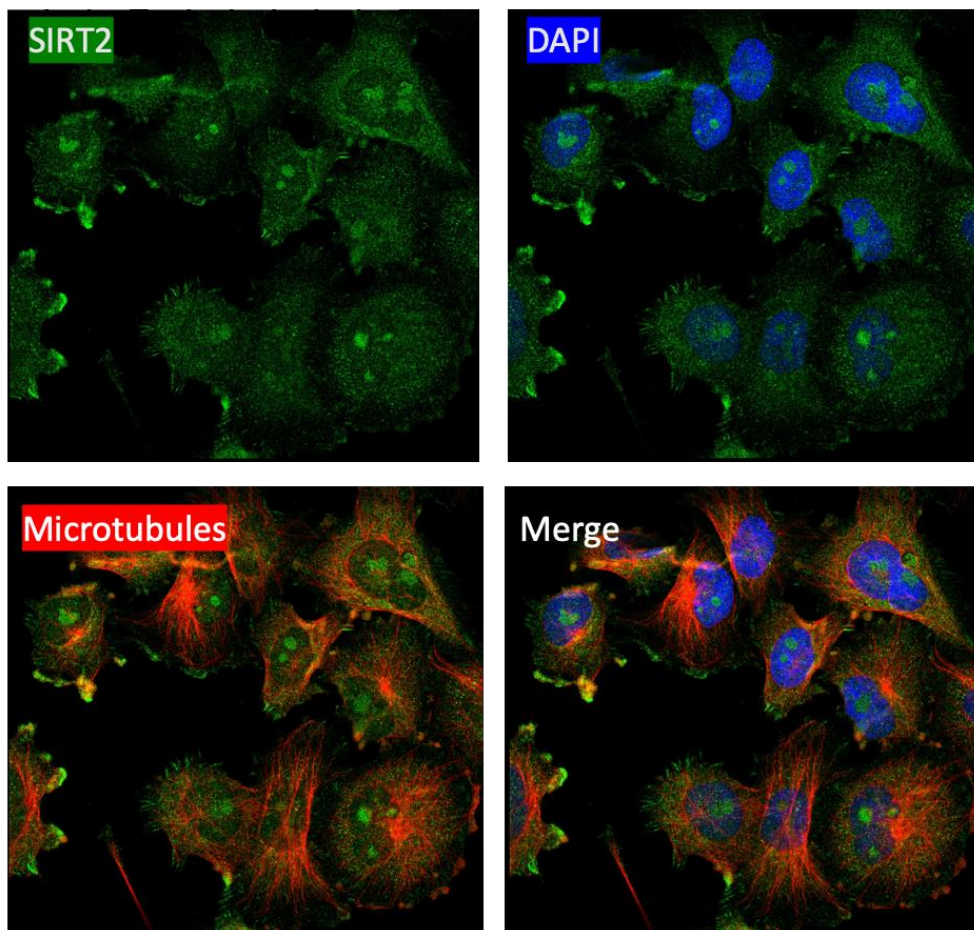


**Figure 1.11 – Sirt2 subcellular localisation in the U-251 cell line.** Sirt2 is localised in cytoplasm and nucleoli (green), DAPI labels the nucleus (blue), Sirt2 co-localised to microtubules (RED) and merge in yellow. Images adapted (Uhlén et al., 2015).

### ***1.2.3 Sirt2 protein expression***

Sirt2 is a ubiquitous protein that is expressed in the cardiovascular and digestive systems and is highly expressed in the nervous system. The ProteomicsDB (Schmidt et al., 2018) database for human proteins shows that Sirt2 is widely distributed in many tissues. Still, the highest expression is found in the spinal cord, brain and prefrontal cortex (Figure 1.12) (ProteomicsDB, 2017, Schmidt et al., 2018).

Interestingly, evidence has shown that Sirt2 expression level is low or undetectable in the mouse cortex during development, and it is considered a maturation marker for CNS (Maxwell et al., 2011a).

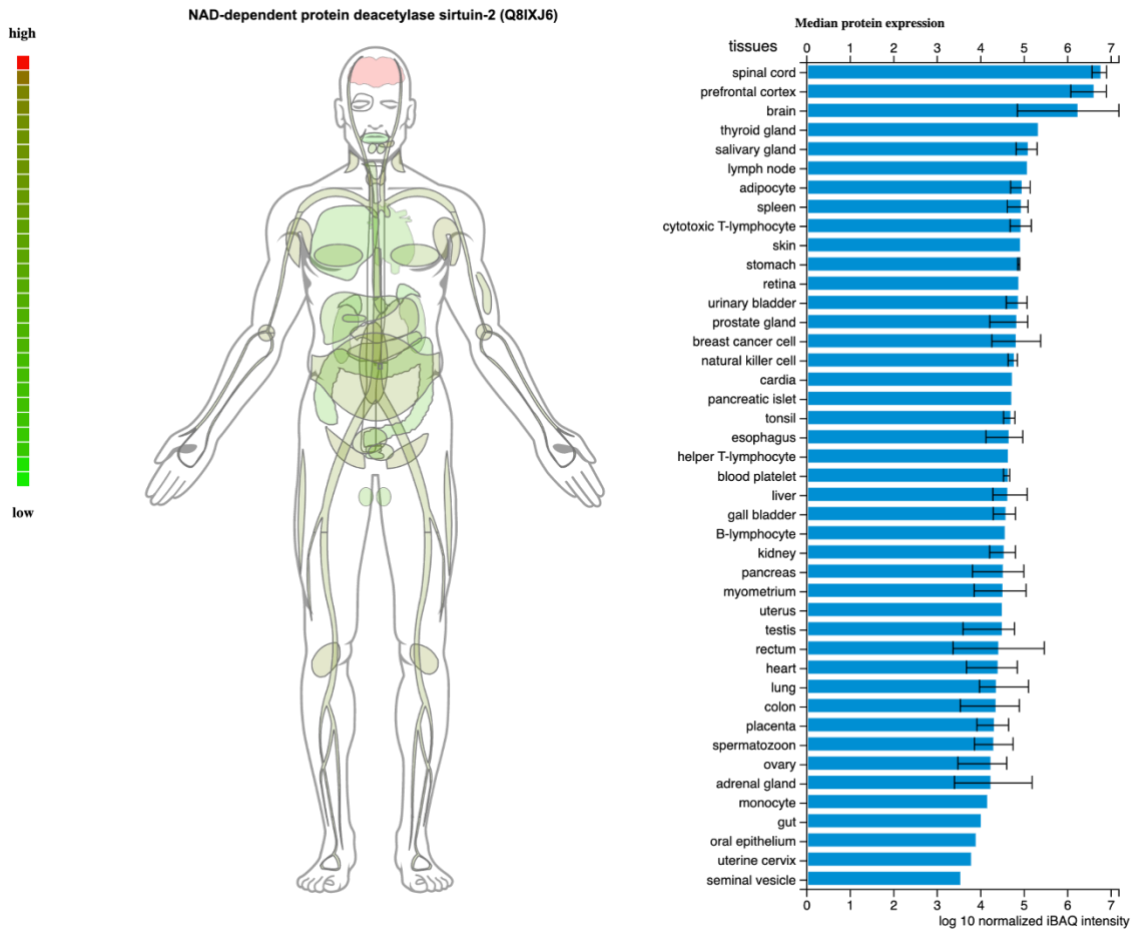


**Figure 1.12 – Distribution of Sirt2 expression across human tissues.** Sirt2 (Q8IXJ6) is widely expressed across many human tissues with a high expression level in the spinal cord, brain, and cortex. Data from (Schmidt et al., 2018).

#### 1.2.4 PTMs of Sirt2

Sirt2 is modified by phosphorylation, acetylation, and ubiquitination. Sirt2 acetylated by the KAT enzyme Ep300 at many sites and interacts with Sirt2. Acetylation of Sirt2 has been suggested to block its deacetylase activity towards TUBA1A (Han et al., 2008). There are few ac(K) site known for Sirt2 (Signling, 2017, Han et al., 2008). Sirt2 is highly phosphorylated, especially at the C-terminus; some studies show that phosphorylation regulates Sirt2 deacetylase activity. First, mutation of phosphorylated sites S368 and S372 resulted in a decrease in Sirt2 deacetylase activity, despite those sites being outside the catalytic domain

(Nahhas et al., 2007). Figure 1.13 illustrate Sirt2 PTM sites (Signling, 2017). Next, CDK5 and GSK3 $\beta$  phosphorylate Sirt2 at S331 and S327, S335 respectively, phosphorylation at S331 by CDK5 could block deacetylase activity of Sirt2; in contrast, phosphorylation by GSK3 $\beta$  led to an increase in activity in PD models (Liu et al., 2019b, Pandithage et al., 2008).

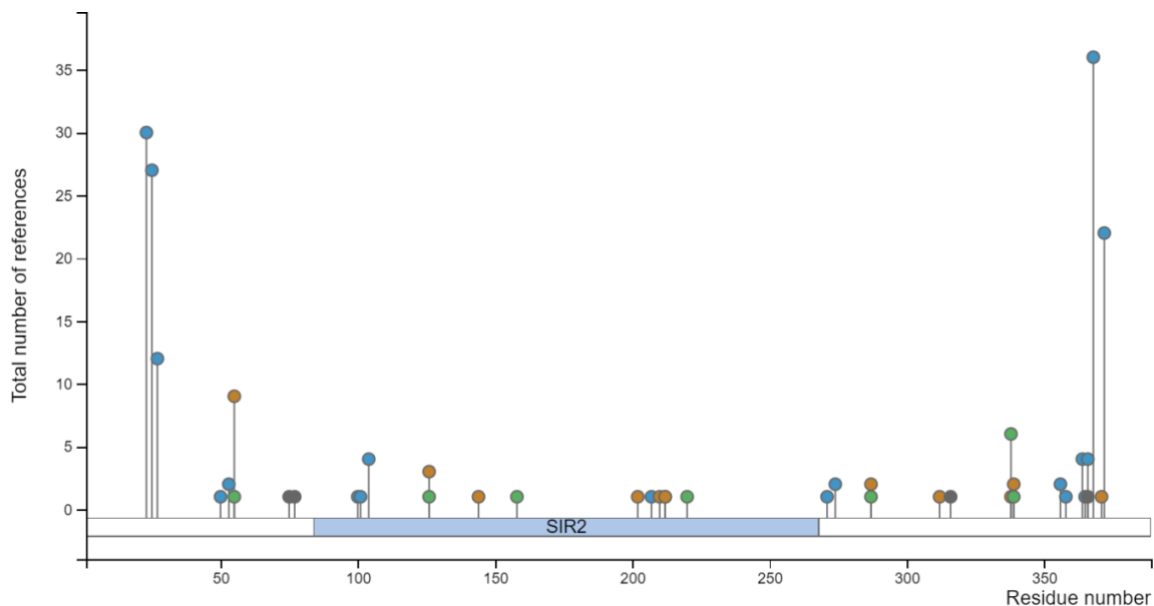


**Figure 1.13 – PTM sites of Sirt2; phosphorylation (blue), acetylation (green), ubiquitination (brown) and others (grey).** Image adopted from (Signling, 2017).

### 1.2.5 Known Sirt2 substrates and protein interactions

Recent evidence has shown that not all KDACs enzymes are functional in terms of deacetylase activity. Most of the deacetylation of histone or non-histone proteins are regulated by Sirtuins. Interestingly, 40% of known acetylation sites are controlled by SIRT1 as it can deacetylase many nuclear and some cytoplasmic proteins (Narita et al., 2018). The over-representation of SIRT1 in the literature is due to its ability to deacetylate essential transcription factors, which was one of the main focuses of acetylation studies, and the

availability of specific inhibitors compared to other KDACs (Yu et al., 2021, Min et al., 2018b, Michan and Sinclair, 2007, Narita et al., 2018). As shown in figure 1.5, Sirt2 is considered an active deacetylase enzyme that regulates more than 40 proteins in different mammalian tissue (Narita et al., 2018). Table 1.1 contains a list of the known Sirt2 substrates to date, along with associated ac(K) sites.

Sirt2 regulates the acetylation of the AMPA receptor GluA1 subunit, part of a crucial synaptic glutamate receptor complex. It was found that the GluA1 subunit can be modified at the same lysine site by both acetylation and ubiquitination, and this process is controlled by Sirt2 which has a key role in maintaining AMPAR stability and regulating synaptic plasticity and brain function (Wang et al., 2017a). Deacetylation by Sirt2 unmasks a lysine residue that can then be ubiquitinated, which causes AMPAR internalisation and protein degradation. Overexpression of Sirt2, deacetylates lysine residues of the GluA1 subunit, an effect that is abolished in a mutant GluA1 (lysine residues replaced by arginine residues) that cannot be acetylated (Wang et al., 2017a).

Another synaptic protein Arc (arg3.1) protein was recently shown to be regulated by Sirt2. Treatment of cells with Sirt2-specific inhibitors (AK-7) increased the level of lysine acetylation of Arc, a similar effect of KDACs inhibitors to AMPAR, which suggested that Sirt2 deacetylase Arc protein and maintain its turnover by balancing the competing between acetylation and ubiquitination (Lalonde et al., 2017).

As mentioned previously, Sirt2 is widely distributed in mammalian tissue and has an important role as a deacetylase enzyme in many diseases such as cancer and neurodegenerative diseases and could act as a promising therapeutic target (Chopra et al., 2012, Donmez and Outeiro, 2013, Chen et al., 2015). Unfortunately, there is little information about Sirt2 substrates in

particular tissues or organs. However, several studies have investigated the role of Sirt2 as the deacetylating enzyme for a specific protein or associated with a specific disease (Table 1.1).

<b>Substrate</b>	<b>Biological process/disease</b>	<b>Ac(K) Sites</b>	<b>Reference</b>
<b>ACLY</b>	Liver disease	K540, K546, K554	(Lin et al., 2013, Guo et al., 2019)
<b>ALDH1A1</b>	Breast cancer	K353	(Zhao et al., 2014)
<b>Alpha-tubulin</b>	Brain (microtubule)	K40	(Maxwell et al., 2011a)
<b>AMPA receptor</b>	Brain (synaptic plasticity)	K813/K819/K822/ K868	(Wang et al., 2017a)
<b>ASPSCR1</b>	Glucose homeostasis	K549	(Belman et al., 2015)
<b>ATRIP</b>	Cell cycle	K32	(Zhang et al., 2016)
<b>BubR1</b>	Cancer	K250, K668	(North et al., 2014, Qiu et al., 2018)
<b>c-Myc</b>	Neuroblastoma	K317, K323, K371	(Liu et al., 2013b)
<b>CDK9</b>	Ataxia	K48	(Sabò et al., 2008, Zhang et al., 2013)
<b>CNK1</b>	Cell proliferation and migration	K414	(Fischer et al., 2017)
<b>FOXO1</b>	Adipose tissue	K242/K245/K262	(Jing et al., 2007)
<b>FOXO3a</b>	Oxidative stress	K242/K245/K59	(Wang et al., 2007)
<b>G6PD</b>	NADPH homeostasis	K403	(Wang et al., 2014)
<b>GKRP</b>	Type 2 diabetes	K126	(Watanabe et al., 2018)
<b>GP</b>	Energy metabolic pathways	K470, K796	(Zhang et al., 2012)
<b>GSK3</b>	Cardiomyocytes	K150/K183	(Sarikhani et al., 2018c)
<b>HIF-1<math>\alpha</math></b>	Hypoxic tumour cells	K709	(Seo et al., 2015)

<b>HSP90</b>	Cell motility	NA	(Min et al., 2018a)
<b>JNKs</b>	Cell death	K153	(Sarikhani et al., 2018b)
<b>KRAS</b>	Tumorigenesis	K104, K147	(Yang et al., 2013, Song et al., 2016)
<b>KRT8</b>	Keratin solubility	K207	(Snider et al., 2013)
<b>LDH-A</b>	Pancreatic cancer	K5	(Zhao et al., 2013)
<b>LKB1</b>	Cardiac	K48	(Tang et al., 2017)
<b>MEK1</b>	MAPK pathways	K175, K362	(Yeung et al., 2015)
<b>MKP-1</b>	Inflammation	K57	(Jung et al., 2015)
<b>NF-<math>\kappa</math>B</b>	Brain Inflammation	K48	((Rothgiesser et al., 2010)
<b>NFAT</b>	Heart Failure	K612/K626	(Sarikhani et al., 2018a)
<b>NRF2</b>	Iron homeostasis	K506/ K508	(Yang et al., 2017)
<b>p300</b>	Acetylation	K418, K423, K1542, K1546, K1549, K1699, K1704, K1707	(Black et al., 2008)
<b>P53</b>	Apoptosis	K292/K382/K305/K315	(Donmez and Outeiro, 2013)
<b>P65</b>	Inflammation	K310	(Donmez and Outeiro, 2013)
<b>PEPCK1</b>	Gluconeogenesis	K70, K71	(Jiang et al., 2011)
<b>PGAM2</b>	Tumour / cell proliferation	K100	(Xu et al., 2014)
<b>PKM2</b>	Glucose metabolism	K305	(Park et al., 2016b)
<b>Slug</b>	Breast Cancer	K116	(Zhou et al., 2016c)
<b>SREBP-2</b>	Brain (HD)	K630/K363/K321	(Luthi-Carter et al., 2010a)
<b>STAT5</b>	Lung cancer	K697/K701	(Ma et al., 2010)

**TAU**

Brain (AD)

K280

(Diaz-  
Perdigon et  
al., 2020,  
Min et al.,  
2010)

---

***Table 1.1 Examples of known Sirt2 substrates***

Sirt2 is most known for its ability to interact and deacetylate TUBA1A, ACLY and Ep300 (North et al., 2003, Lin et al., 2013, Guo et al., 2019, Black et al., 2008). Moreover, Sirt2 interacts with other KDACs enzymes that share the deacetylase substrates, for example, HDAC6 interact with Sirt2 and both deacetylate TUBA1A (Yang et al., 2013, North et al., 2003, Nahhas et al., 2007, Tókési et al., 2010), Sirt2 also interacts with SIRT1, which deacetylates FOXO3 as well. (Wang et al., 2007, Wang et al., 2012). Another important interactor is Ep300; both enzymes regulate the acetylase/deacetylase activity of each other (Han et al., 2008, Narita et al., 2018, Black et al., 2008). Sirt2 interacts with more than 80 proteins localised in different cellular compartments, further showing that Sirt2 function is not limited to the cytoplasm; figure 1.14 illustrates the Sirt2 interaction network from the BioGRID database (Stark et al., 2006).

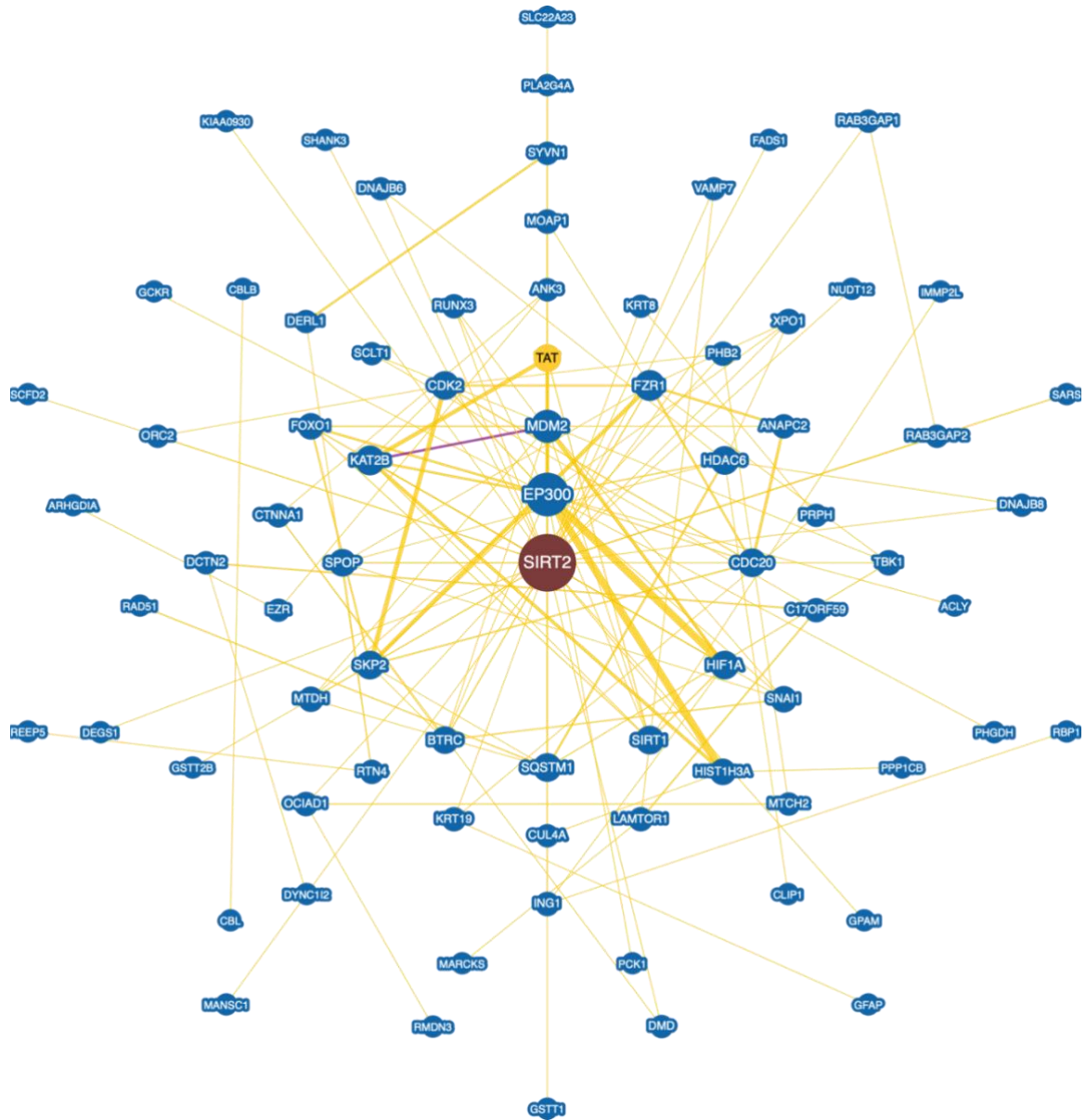


**Figure 1.14 – Sirt2 protein interactions.** Sirt2 interacts with ~ 80 other proteins. This network represents the interactions according to the BioGrid database with at least two evidences (Stark et al., 2006).

### 1.2.6 Sirt2 role in cells

Sirt2, as mentioned previously, is highly expressed in the brain and nervous system, and it is the most abundant of all Sirtuins in these tissues. However, its role in the brain and nervous system is not adequately explored. Studies have highlighted some cellular functions of Sirt2.

First, Sirt2 is vital for myelination, and studies showed that Sirt2 is expressed in oligodendrocytes (responsible for myelin production) and upregulated during oligodendrocyte cell differentiation (2021, Werner et al., 2007, Chamberlain et al., 2021). Sirt2 is considered an essential protein of the myelin proteome (Werner et al., 2007, Dugas et al., 2006). It was suggested that the expression of Sirt2 and MBP are gradually increased over time and stabilised during adulthood; this suggestion is still under study (Werner et al., 2007). Moreover, studies have shown that Sirt2 stimulates myelin formation by regulating the Par-3 protein acetylation in the peripheral nervous system, including Schwann cells (Beirowski et al., 2011, Wang et al., 2019b).

Sirt2 deacetylase activity contributes to dopaminergic neuronal differentiation; these neurons are essential for CNS functions, and any deficit in them can cause many neurological disorders such as PD (Szegő et al., 2017).

Sirt2 has been reported to be upregulated in response to oxidative stress, resulting in deacetylated FOXO3 and increases in the expression of genes targeted by FOXO3a, such as p27kip1, and MnSOD which reduce cellular reactive oxygen species (ROS) and influence cellular responses to oxidative stress (Wang et al., 2019b). The acetylation of autophagy protein 5 (ATG5), was considerably decreased in Sirt2<sup>-/-</sup> mice, suggesting that Sirt2 may directly interact with and deacetylate ATG5 (Gal et al., 2012).

FOXO1 is another protein that could be acetylated by dissociating from Sirt2 and attaching to autophagy protein 7 (ATG7) in response to oxidative stress, activating the autophagic process in malignancies (Mouchiroud et al., 2013). Studies showed after intracortical injection of lipopolysaccharide Sirt2<sup>-/-</sup> mice demonstrate morphological changes in microglia, an elevation in proinflammatory cytokines, and hyperacetylation of NF- $\kappa$ B, suggesting that Sirt2

may be a gatekeeper that inhibits excessive microglial activation by NF- $\kappa$ B deacetylation (Rothgiesser et al., 2010, Wang et al., 2019b).

### **1.2.7 The phenotype of *Sirt2* knockout mice**

*Sirt2*<sup>-/-</sup> adult mice exhibit impaired learning and memory and dysfunction in synaptic plasticity because of the role of Sirt2 in regulating AMPAR acetylation (Wang et al., 2017a, Wang et al., 2019b). In aged mice, *Sirt2* gene knockout causes locomotor dysfunction and disability due to the impact of Sirt2 on the axonal degeneration (Fourcade et al., 2017, Wang et al., 2019b). A decrease of dopaminergic neurons and a change in striatal fibre density in the substantia nigra were also observed in *Sirt2*<sup>-/-</sup> mice (Szegő et al., 2017, Wang et al., 2019b).

It has been shown that the loss of Sirt2 perturbs the acetylation status of a vital autophagy protein ATG5; thus, it might contribute to autophagy and mitophagy regulation (Fourcade et al., 2017, Liu et al., 2017c). Moreover, recent studies have observed a change in mitochondrial morphology in the cortex of *Sirt2*<sup>-/-</sup> mice. This was associated with reduced ATP production (energy failure). The striatum and the spinal cord of *Sirt2*<sup>-/-</sup> mice also showed a decrease in ATP levels (Fourcade et al., 2017, Liu et al., 2017c), although some of those phenotypes depend on ageing.

Moreover, in a gender-dependent manner, elevated susceptibility to cancers has been reported in *Sirt2* knockout mice. There is an increased prevalence of breast cancer in females and hepatic cell cancer in males (Kim et al., 2011, Serrano et al., 2013). Figure 1.15 shows major changes occur during *Sirt2* gene knockout in mice (Wang et al., 2019b).

Generally, brain *Sirt2* knockout is not lethal, but it is involved in first, neuron development such as myelin production and dopaminergic neurons (Fourcade et al., 2017, 2021, Wang et al., 2019b, Chamberlain et al., 2021). Second, behavioural, and cognitive impairment, and

synaptic damage that causes many neurological diseases (Wang et al., 2017a, Wang et al., 2019b).

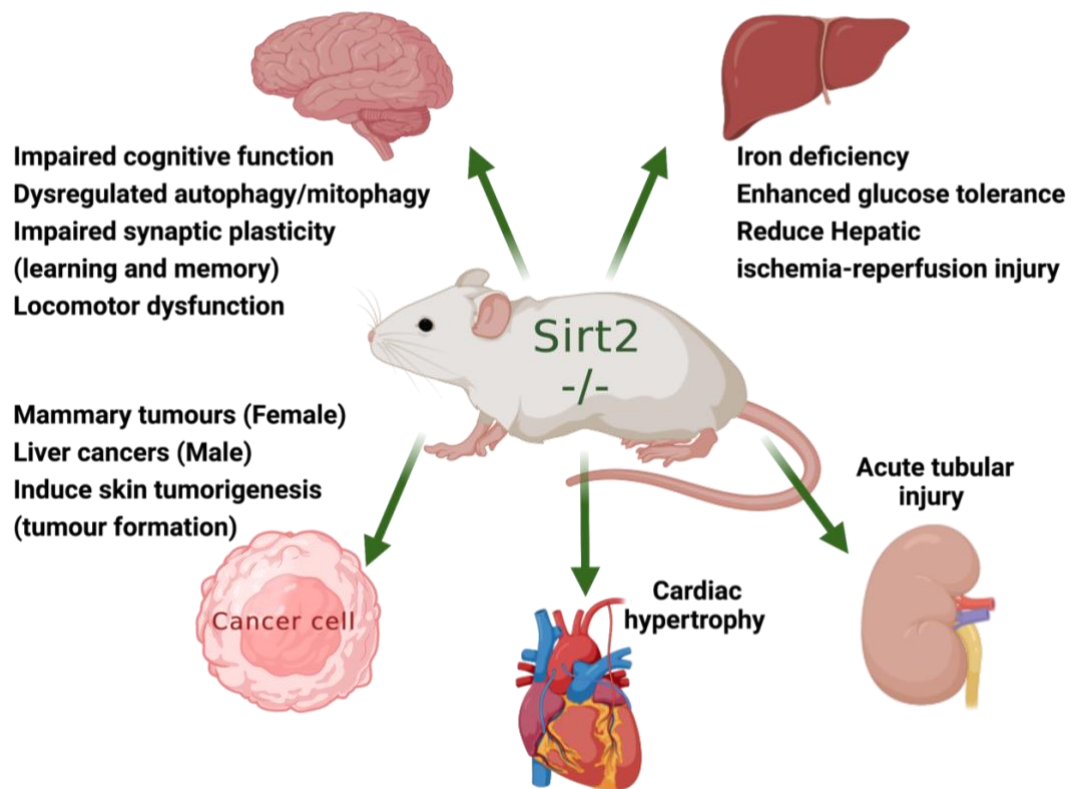
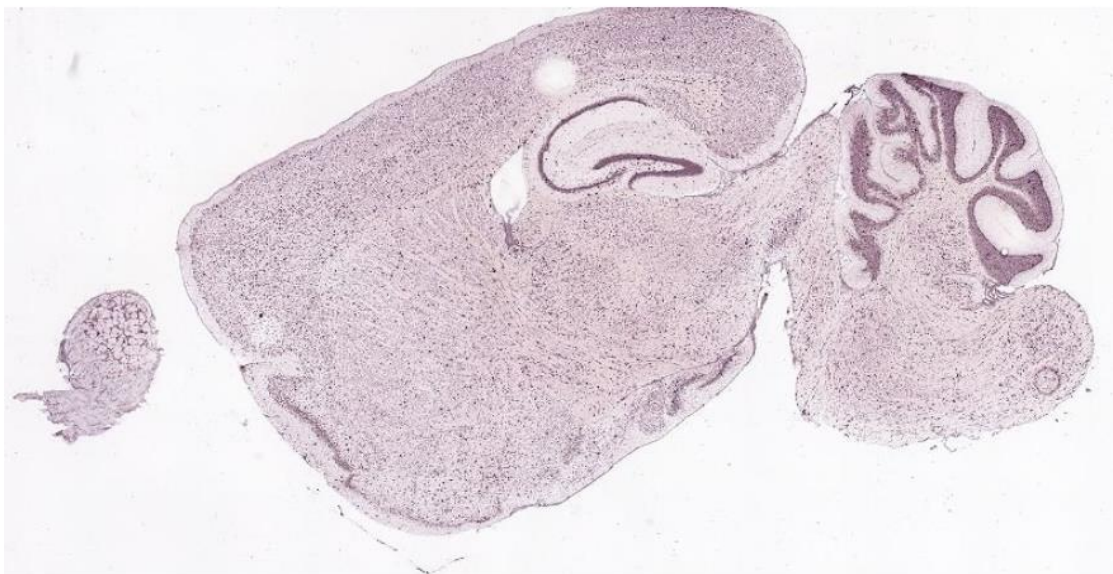


**Figure 1.15 – Phenotypes of *Sirt2*<sup>-/-</sup> mice.** Knockout of *Sirt2* results in a broad set of phenotypes but an enrichment of those affecting the nervous system (Wang et al., 2019b).

### **1.2.8 Sirt2 in diseases**

Sirt2 is widely distributed in human tissues and is highly associated with cancer, neurodegenerative and metabolic diseases. There is some evidence that Sirt2 is associated with neurological disorders such as Alzheimer's disease (AD), Parkinson disease (PD), Huntington's disease (HD) and amyotrophic lateral sclerosis (ALS). Sirt2 is highly expressed in the brain, as mentioned previously; it is present in schwann cells, oligodendrocytes, and neuronal synapses (Wang et al., 2017a, Herskovits and Guarente, 2013, Michan and Sinclair, 2007). Immunohistochemistry staining of Sirt2 in adult mouse brain tissue shows that it is widely expressed all over the brain but with high expression in the hippocampus and cerebellum (Figure 1.16).



---

**Figure 1.16 – Immunohistochemistry staining for Sirt2 in the adult mouse brain. Sirt2 is highly expressed in both hippocampus and cerebellum data from ([www.alleninstitute.org](http://www.alleninstitute.org)).**

### **1.2.9 Sirt2 and neurodegenerative disease.**

Previously, the role of lysine acetylation, especially Sirt2, in neurotoxicity was described. PD is caused by an accumulation of Lewy bodies (SNCA aggregation) and loss of dopaminergic neurons (Donmez and Outeiro, 2013, Wang et al., 2019b). Studies in post-mortem PD brain tissue showed an increase in the Sirt2 deacetylase activity (Wang et al., 2019b, Singh et al., 2017b). Other studies suggested that inhibition of Sirt2 activity could play an important role as a therapeutic target for PD. But there are several different PD disease models because of the different mechanisms that contribute to disease development. First, inhibition of Sirt2 activity increases the acetylation of SNCA and as a result prevent Lewy bodies formation and stop its toxicity (Bhattacharjee et al., 2019, Chen et al., 2015). Second, Sirt2 inhibition increases TUA1a acetylation, which can improve microtubules dynamics and, as a result, restore normal autophagy and neuronal functions (Rita Machado de et al., 2017, Wang et al., 2019b, Park et al., 2016a). Finally, although most studies provided valid evidence that Sirt2 inhibition leads to protection from developing PD, increased Sirt2 levels were observed to protect against cell death as a part of its role in the oxidative stress response (Singh et al., 2017b, Wang et al., 2019b).

In AD, the activity of Sirt2 has been reported to associate with the biomarkers Amyloid- $\beta$  peptides ( $A\beta$ ) and amyloid precursor protein (APP) metabolism (Gal et al., 2012). Studies showed that overexpression of Sirt2 in neuronal cell lines causes  $A\beta$  cytotoxicity. In some AD mouse models, inhibition of Sirt2 by AGK2 or AK-7 has demonstrated a decrease in  $A\beta$  production, reduction in the amyloidogenic pathway, and improved cognitive functions, including learning and memory (Biella et al., 2016, Herskovits and Guarente, 2013).

Hyperphosphorylation of Tau (MAPT) protein is widely considered a promising target for AD patients. Studies showed that inhibiting Sirtuin enzymes by Nicotinamide (NAM) restores cognitive functions and improves microtubule dynamics functions by increasing TUAB1a acetylation and decreasing tau phosphorylation. This mechanism results in the protection process from AD pathology by Sirt2 (Silva et al., 2017, Biella et al., 2016, Panza et al., 2019). Although studies were performed on different AD mouse models and showed that inhibition of Sirt2 deacetylase activity is associated with tau and A $\beta$ , further mechanistic understanding of the therapeutic role for Sirt2 inhibitors is required (Cacabelos et al., 2019, Wang et al., 2019b).

Sirt2 has also been linked to another important neurodegenerative disorder, Huntington disease (HD) (Chopra et al., 2012). HD is caused by a mutation in the HTT gene, which cause its misfolding and aggregation. Inhibition of Sirt2 by AK-7 and AGK2 has a significant effect on mutant HTT levels in the primary neuronal model of HD. Inhibition of Sirt2 plays a neuroprotective role by contributing to the sterol biosynthesis pathway (Luthi-Carter et al., 2010a, Donmez and Outeiro, 2013). Sirt2 inhibition decreases the level of SPEBP-2 and, as a result, decreases the sterol biosynthesis which results in decrease in Htt inclusion accumulation in HD models (Luthi-Carter et al., 2010a). Studies reported that the accumulation of cellular cholesterol contribute in mutant Htt binding to caveolae (Bobrowska et al., 2012, Luthi-Carter et al., 2010b). However, the involvement of Sirt2 in HD is still controversial as some studies have shown that depletion or deletion of Sirt2 had no neuroprotective role and did not show a difference in sterol biosynthesis pathways (Bobrowska et al., 2012, Chopra et al., 2012, Donmez and Outeiro, 2013, Luthi-Carter et al., 2010a). The provided evidence further implies the potential role of Sirt2 and its inhibitors as a therapeutic approach for neurological diseases (9, 13).

### **1.2.10 Sirt2 in ageing**

It is known that sirtuins are essential factors in ageing and lifespan (Yu et al., 2021, Wątroba and Szukiewicz, 2016). The effects of sirtuins in ageing are mediated by different mechanisms such as: delaying or suppressing cellular senescence, controlling telomere attrition, regulating genomic integrity (Imai and Guarente, 2014, Michan and Sinclair, 2007). For example, overexpressing SIRT1 and SIRT6 showed a decrease in cellular senescence, at the same time, inhibition of both enzymes enhanced premature senescence cells in endothelial cells (Zu et al., 2010, Lee et al., 2019). Overall, expression levels of both enzymes were significantly decreased in senescent cells derived from mouse embryonic fibroblasts (Lee et al., 2019).

Many studies have linked sirtuins to age, and many have considered sirtuins as anti-ageing targets. SIRT3 knockout results in mitochondrial dysfunction and increased oxidative stress, which contributes highly to the whole process of ageing. Many researchers are currently investigating how to overexpress and activate sirtuins using an NAD<sup>+</sup> booster, to extend lifespan and improve life quality (Lee et al., 2019, Wątroba and Szukiewicz, 2016).

Sirt2 has a controversial link to ageing; some evidence suggests that the mRNA expression level and protein expression level of Sirt2 is upregulated in a specific region of the rat brain called the occipital lobe with no significant increase observed in the other regions (Sidorova-Darmos et al., 2014). In addition, Sirt2 upregulation was found to be associated with stress-induced premature senescence, but not with quiescence or cell death. Increased Sirt2 is not a cause of senescence; rather, it is a consequence of senescence-related changes (Anwar et al., 2016).

Moreover, an accumulation of Sirt2 isoform 3 was found in aged mice CNS compared to isoform 1 and 2 (Braidy et al., 2015, Sidorova-Darmos et al., 2014, Maxwell et al., 2011a).

The role of Sirt2 is mainly related to lifespan and longevity; BubR1 is a cell cycle checkpoint kinase that decreases in levels with age due to a decline in Sirt2 and NAD<sup>+</sup> levels (Maxwell et al., 2011a, Wang et al., 2019b). BubR1 deacetylation by Sirt2 improves its stability, as Sirt2 activity reduces the ubiquitination of BubR1 and vice versa (Qiu et al., 2018, Rumpf et al., 2015, North et al., 2014). Moreover, Sirt2 overexpression improved the lifespan of many small organisms such as yeast, worms, and flies, yet further studies are needed for the mammalian sirtuins including Sirt2 (de Oliveira et al., 2012, Frankel et al., 2011, Rogina and Helfand, 2004).

### **1.2.11 KDAC Inhibitors**

A significant number of studies have linked lysine acetylation and its regulation by deacetylase enzymes with different diseases (Donmez and Outeiro, 2013). As a result, inhibitors are available for many deacetylase enzymes, and many of them have been tested on a cellular level and animal models. However, very few have been FDA approved to use in the clinic (Tan et al., 2010, Ali et al., 2018). A recent study used a proteomics approach to evaluate the specificity of KDAC inhibitors and identify substrate acetylation sites for several deacetylase enzymes (Christian et al., 2015). The action of these inhibitors are mainly to induce DNA damage, cell cycle interruption, activate apoptosis and proliferation, which was explained by hyper-acetylation induced by most KDAC inhibitors (Ali et al., 2018).

As the sirtuin family are similar in structure, this has raised issues concerning the specificity of Sirt2 inhibitors as a number of these inhibitors can also inhibit other sirtuins e.g. Nicotinamide and Sirtinol. On the other hand, these inhibitors distinguish between KDAC classes; Nicotinamide inhibits Class III, while Trichostatin A (TSA) inhibits Class I and II KDACs. The specificity of KDACi's is influenced by the level of the targeted enzyme (Ali et al., 2018, Christian et al., 2015). Sirt2 as a drug target is still under development as is inhibited by many inhibitors that does not specifically inhibit Sirt2 alone (Rumpf et al., 2015). Previous work has shown a weak correlation between deacetylation by Sirt2 and the inhibitors AGK2 and Sirtinol when used in mouse embryonic fibroblasts (Christian et al., 2015). However, other studies indicated that AGK2 is a selective Sirt2 inhibitor and it has been used as a benchmark to evaluate new Sirt2 inhibitors (He et al., 2012, Rumpf et al., 2015), e.g. SirReal2 (Rumpf et al., 2015), 33i (Erburu et al., 2017), aminothiazole (Schiedel et al., 2016).

SirReal2 is suggested as one of the most known selective Sirt2 inhibitors (Rumpf et al., 2015). SirReal2 can inhibit Sirt2 with very minimal effect on other Sirtuins members (SIRT1) . SirReal2 induces a rearrangement of Sirt2 active sites; one of these sites is the acetyl-lysine binding site. Instead of preventing Sirt2 from binding to acetyl-lysine peptide substrate, this inhibitor is only blocking the deacetylation process (Rumpf et al., 2015).

### **1.3 Hypothesis**

The main aim of this project is to investigate the role of lysine acetylation and its regulation by Sirt2 and during ageing in the brain. The hypothesis is that Sirt2 is the major synaptic acetyl-lysine deacetylase and that age-related changes in brain acetylation are related to Sirt2 activity.

### **1.4 Objectives**

1. Characterisation of acetylated proteins in mouse brain that are regulated (deacetylated) by Sirt2
2. Measurement of acetylation level changes in adult versus aged mouse brain tissue
3. Validation of putative substrates of Sirt2.

## **CHAPTER 2**

### ***Methods and Material***

## **2.1 Cell lines and tissue culture**

### **2.1.1 Culture of immortalised cell lines**

HeLa cells- Human cervical cancer cell line

HEK 293 cells- Human embryonic kidney cell line

Mouse motor neuron-like cells

Cells were cultured with at  $3-4 \times 10^5$  seeding density in 100mm plates containing Dulbecco's Modified Eagle Medium (DMEM- Gibco-11995-065) and supplemented with 10% FBS (Sigma-Aldrich-F7524) and 1% Penicillin-Streptomycin which then incubated in 37°C CO<sub>2</sub> incubator between 3 to 4 days or until ~ 70% confluency. Both HeLa cells and HEK293 cells were harvested and prepared for splitting by trypsinisation. Cells were washed with Phosphate-buffered solution (PBS-Alfa Aesar-J60801.K7) and cells were incubated with 3-5 ml of pre-warmed Trypsin-EDTA (Gibco-Trypsin-EDTA 0.05%-11590626) in 37°C CO<sub>2</sub> for 5 minutes. 1 ml of media was added to the cells and collected into a 15 ml tube which then centrifuged at 850 rpm for 5 minutes, the supernatant was removed, and cells were suspended in 1 ml of DMEM Media which then divided into new plates containing fresh media at the desired cell density and incubated in a 37°C CO<sub>2</sub> incubator. This process was repeated twice a week for HeLa cells and three times a week for HEK293 cells. On the other hand, NSC34 cells were cultured similarly except cells were harvested and prepared for splitting by aspirating 1 ml of media a few times until most cells were dissociated and collected.

### **2.1.2 Mouse Brain Tissue**

Sirt2 Knockout brain tissue was obtained from the Jackson Laboratory (J-012772). This knockout mouse line is a targeted homozygous mutant knockout of the Sirt2 gene at chromosome 7. Exon 5-6 and part exon 7 on Chromosome 7 were replaced with a floxed PGK-

neomycin to generate a targeted mutation (Knockout). Wild type brain tissue (The Jackson Laboratory- C57BL/6J-000664) was used as a control. Both strains were received as frozen tissues, all tissues were from a female mouse between 7-14 weeks of age with a total of 4 brain tissue samples for each strain.

Wild type brain tissues from mice at 24 months (old mice) or 7-14 weeks (young mice) of age were used as well in different experiments. Those tissues were collected by our lab.

## ***2.2 Acetylome analysis of mice brain tissue***

### ***2.2.1 Filter-Aided Sample Preparation (FASP)***

Digestion of forebrain tissues weighing ~ 0.30g were prepared according to FASP (filter-aided sample preparation) which been described previously (Ludwig et al., 2018, Wisniewski et al., 2009). Proteins were extracted with 4ml of lysis buffer containing 4% SDS (fisher scientific– s/5200/53), 100 mM Tris pH 8 (Sigma-Aldrich – T6066), 10 mM TCEP (Sigma-Aldrich – 646547) and Protease inhibitors 1:200 vol: vol ratio (Sigma-Aldrich – P8340). The mixture was homogenised for 20-25 times with dounce homogeniser, lysate was transferred into 4 tubes and homogenised using an electrical homogeniser (DLAB – D160) 3 times, for 10 seconds each, samples were then incubated for 15 minutes at 70°C with shaking at 800rpm in a thermomixer to denature protein and reduce disulfide bonds. DNA was sheared by passing the extract in a fine gauge needle 5-10 times and the lysate was clarified by centrifugation at 16,000xg for 10 minutes. Urea was added to a final concentration of 8 M and Iodoacetamide (IAA-Sigma-Aldrich –16125) was added to a final concentration of 20 mM to alkylate reduced cysteine residues (incubated in the dark for 30 minutes at room temperature). The total extracted protein was between 20 to 25 mg per forebrain.

Amicon centrifugal concentrator (ultra-15 30K MWCO) spin columns (Millipore – R6H A61952) were used to buffer exchange SDS with urea prior to tryptic digestion. Amicons were washed with 2ml of 8 M urea/100 mM Tris pH 8 and centrifuged at 4,000 x g for 20 minutes or until the retentate volume reached 250 µl. Samples were washed 3 times with 8 M urea/100 mM Tris pH 7.2 and twice with 8 M Urea (Sigma-Aldrich-U0631) and 0.1 M Ammonium bicarbonate (Ambic— Sigma-Aldrich— 09830). The upper chamber was transferred into a new falcon tube and 100 mM Ammonium bicarbonate was added to dilute a final concentration of urea to 1M. Sequencing grade modified trypsin (Promega – V51111) was added in a 1:20 (trypsin: total protein) ratio and left to digest at 37°C overnight with shaking at 300rpm.

### ***2.2.2 Acetone precipitation of proteins***

0.3g of forebrain tissue was lysed with 4 ml lysis buffer containing 50 mM Tris pH 8, 150 mM NaCl, 1 mM EDTA, 1% NP-40 (Thermo – 28324), 0.1% Sodium deoxycholate (Sigma-Aldrich-D6750) and protease inhibitors 1:200 (Sigma-Aldrich-P8340) and homogenised for 25 times with dounce homogeniser, the lysate was transferred into 4 different tubes and further homogenised by electrical homogeniser for 10 seconds, 3 times with 10 seconds in between pulses. Samples were denatured for 15 minutes at 70°C with shaking at 800 rpm then DNA was sheared by electrical homogeniser for few pulses before samples were centrifuged at 16,000xg for 15 minutes. The supernatant (extracted proteins) were collected into an acetone compatible tube and 20 µl of the sample was set aside for protein quantification using a BCA assay. Chilled (-20°C) acetone (Acros-Organics-268310025) was added to the samples in a 4:1 ratio (acetone: sample), the sample was vortex briefly before overnight incubation at -20°C. The mixture was centrifuged at 14,000 x g for 10 minutes at 4°C and the supernatant discarded with care not to disturb the pellet. 2 cycles of washes with 1 part of HPLC water (VWR-23595.328) and 4 parts of acetone were performed, then pellet was dried in an uncapped

tube for between 30-60 minutes at room temperature to allow full evaporation of acetone. The sample was then resuspended in 1 ml of 8 M of Urea/0.1M Ambic and 1 mM of Tecp and incubated for 30 minutes at room temperature with shaking at 750 rpm. Samples were then alkylated by adding IAA to a final concentration of 5.5 mM and incubated in dark for 30 minutes at room temperature. Ammonium bicarbonate was then added to reach a final concentration of 100 mM of Urea. Extracted proteins were digested with Sequencing grade modified trypsin at 1:20 ratio (trypsin: total protein) overnight at 37°C with shaking at 300rpm.

### ***2.2.3 S-TRAP sample preparation for brain tissue***

0.3g forebrain tissue from mice at 24 months (old mice) or 7-14 weeks (young mice) of age were lysed with 2 ml of chilled lysis buffer containing 1% Sodium deoxycholate, 50 mM Tris pH 8, 1 mM EDTA, and protease inhibitors 1:200 and homogenised for 25 times with dounce homogeniser. Samples were incubated for 1 hour end-over-end at 4°C, due to the high viscosity of the lysed both samples were supplemented with 1 ml of the same lysis buffer containing 60 mM Tris pH 8.5 and incubated for 30 minutes end-over-end at 4°C. Next samples were centrifuged at 16,000xg for 40 minutes and the supernatant was collected into 2 ml Eppendorf tubes, protein concentration levels were quantified using microBCA assay kit and extracted proteins. 1mM TCEP were added to the samples and incubated for 15 minutes at 70 °C which then alkylated with 0.5 M of IAA to a final concentration of 5 mM and incubated in the dark for 30 minutes at 37°C. Extracted proteins digested using S-trap midi column  $\geq$  300  $\mu$ g digestion column and analysed by LC-MS/MS.

11 mg of brain lysate were solubilised in 2% SDS, then 1 M of Triethylammonium bicarbonate (TEAB- Sigma-Aldrich – T7408) at a pH of 8.5 were added to a final concentration of 50 mM. Next 12% phosphoric acid (Sigma-Aldrich -79617) added at a ratio of 1:10 vol: vol (buffer:

sample) to acidify the sample and a ratio of 6.6: 1 vol: vol (buffer: sample) S-trap binding buffer containing 100 mM of TEAB pH 7.1, 90% methanol. The sample was then gradually added into the spin column, centrifuged at 3750 x g for 15 – 30 minutes or until the total sample volume passed through. S-trap column was washed 5 times with 3.5ml of S-trap binding buffer. Proteins were digested in 20 µl of 1 µg/µl grade trypsin was dissolved in 480µl of fresh 50 mM TEAB pH of 8.5 and incubated in a new tube overnight at 37°C. Tryptic peptides were eluted twice with 500µl of 50mM TEAB pH 8.5, followed by 500µl 0.2% of formic acid and 500 µl of 50% ACN, 0.2% of formic acid centrifuged at 3750 x after each elution step. Eluted peptides were then dried down for further analysis.

S-trap column (PROTIFI- S – Trap- column) was used to digest brain tissue protein extraction, extracted synaptosome and immunoprecipitation elution of tagged or endogenous proteins. Depending on protein concentration different columns were used and prepared for proteomics analysis according to the manufacture protocol (Zougman et al., 2014).

#### ***2.2.4 Peptide desalting***

Tryptically digested samples were acidified by the addition of Trifluoroacetic acid (TFA -Sigma-Aldrich - T6508) to bring the pH to less than 3 and centrifuged at 14,000 x g for 10 minutes at room temperature and the supernatant was retained. Peptide desalting was performed using SepPak C18 desalting cartridges (C-18 360mg-Water-WAT023501) column in a desalting bridge (Supelco – PRE–PY - 57160-U). Each cartridge was washed once with 10ml of 100% Acetonitril (ACN-Sigma-Aldrich- 271004) and twice with 5 ml of 50% of ACN/0.1% of TFA before it was equilibrated with 10 ml of 0.1% TFA. Next samples were loaded 3 times into the C-18 cartridge, washed with 5 ml of 0.1% TFA, and peptides eluted by adding 4 ml 50%

ACN/0.1% TFA. The elution was repeated twice, and eluted peptides were collected and dried down in a vacuum concentrator (Eppendorf DNA concentrator) at 45°C.

Acetylated peptides eluted with S- trap column were desalted by C-18 tips (Thermo Scientific Pierce - 87784). First columns were washed twice 50% ACN to activate the resins which equilibrated by washing resins twice with buffer containing 0.5 % TFA and 5% ACN. Next 3.8 µl of 10% of TFA was added to reach a finale concentration of 0.5% TFA that compatible with C-18 tips. Samples were loaded 3 times to the columns and incubated for 5-10 minutes at room temperature, columns were washed twice with buffer containing 0.5% TFA and 5% ACN. For elute 20µl of 50% ACN was added and incubated for 3 minutes at room temperature, Eluted peptides were collected using a mini microfuge (SciSpin- SS-6050). This step was repeated twice and dried down in a vacuum concentrator (Eppendorf DNA concentrator) at 45°C.

### ***2.2.5 Offline high pH reversed-phase peptide fractionation***

300 µg of dried desalted peptides was resuspended in 20 µl of HPLC H<sub>2</sub>O and transferred into HPLC vials. Prior to running the samples fractionation, 10 µg of BSA peptide mixture was run to check the performance of the separation.

The HPLC (Dionex) was operated using Chromeleon software and was equipped with a temperature-controlled auto-sampler at 6°C, fractionation was performed at a flow rate of 0.300ml/min with gradient starting from 100% of buffer A (10 mM ammonium hydroxide) to 40% buffer B (100% Methanol (Sigma-Aldrich- 34860) over 30 minutes using a 16µl of each sample was injected into the HPLC system and chromatograph was monitored using UV. 36 fractions were collected from each sample on 96 well plate containing 10% formic acid (Sigma-Aldrich-F0507) to neutralise the high pH fractions which were then dried down in a vacuum

concentrator for 3-4 hours. Fractions were resuspended in 50µl of 0.5% formic acid and concentrated into 10 final fractions to maximise orthogonality of the low pH chromatography during LC-MS/MS analysis. This was achieved by pooling initial fractions from the beginning, middle and end of the fractionation e.g., pooling fraction 1+13+25 and etc.

### ***2.2.6 Immuno-affinity purification of acetyl-lysine containing peptides (IAP)***

6 mg of dried peptides were subjected to acetyl-lysine (Ac-K) enrichment using a PTM-Scan Acetyl-Lysine motif kit (Cell-Signalling- 13416) which contained 10 x IAP buffer (Cell-Signaling-9977) Ac-K motif immuno-affinity beads. The samples were re-suspended in 1.4 ml of 1X IAP buffer and gently mixed. Top tips (Glygen –TT2EMT) were used to perform Ac-K immune-affinity purification, 40 µl of Ac-K beads were added to the top tip and washed 4 times with 1 ml of cold PBS applied slowly with 5 ml syringe. Later 100 µl of the sample was added to the washed beads to collect Ac-K beads in a new tube before the total volume of the sample was added and incubated in rotation for 2 hours at 4°C. Afterward, samples were washed twice with 1 ml of 1X IAP and 3 washes with 1 ml of HPLC water. Washing steps were performed using (W–zard Mini-columns - 70705) to avoid loss of beads. Acetylated peptides were eluted two times by adding 55 µl of 0.15% TFA and incubated at room temperature for 10 minutes with shaking at 750 rpm. A total volume of 110 µl of the eluted peptide was collected and kept at -20°C.

### ***2.2.7 Desalting peptides with stage tips***

Eluted acetylated peptides were desalted using stage tips which were washed with 100 µl of 0.1% TFA, 50%ACN, and centrifuged briefly for 30 second, Followed by another wash with 100 µl of 0.1% TFA. Solutions were loaded into the tips using 5 ml syringe, later the sample was added slowly into the stage tip, the sample was repeatedly loaded for 3 times before tips were

washed with 100  $\mu$ l of 0.1% TFA. Desalted peptides were eluted in a new collection tube by adding 100  $\mu$ l 0.1% TFA, 50% ACN, and dried down in a vacuum concentrator for 45 minutes.

### **2.2.8 Mass spectrometry**

Dried peptides were all suspended in 0.5% formic acid and mixed for 10 minutes before transferred to HPLC vials. Samples were analysed on an Orbitrap Elite hybrid mass spectrometry (Thermo-Fisher) with a nano-electrospray source connected to an Ultimate RSLCnano LC System (Dionex). Xcalibur 2.1 (Thermo-Fisher) and DCMSlimk 2.08 (Dionex) software were used to control this system.

18  $\mu$ l of peptides was loaded on to a capillary trap column (75  $\mu$ m I.D.X 20mm, Thermo Fisher) and separated using 125 minutes gradient from buffer A (0.1% formic acid to 40% buffer B (0.1% formic acid in 80% acetonitrile) on an Easy-Spray column (50 cm x 75  $\mu$ m ID, PepMap RSLC C18, 2 $\mu$ m, Thermo-Fisher). The Orbitrap Elite was operated with a cycle of one MS (in the Orbitrap) acquired at a resolution of 60,000 at m/z 400, with the top 20 most abundant multiply charged (2+ and higher) ions in a given chromatographic window subjected to MS/MS fragmentation in the linear ion trap. An FTMS target value of 1e6 and an ion trap MSn target value of 1e4 were used with the lock mass (445.120025) enabled. Maximum FTMS scan accumulation time of 500 ms and maximum ion trap MSn scan accumulation time of 100 ms were used. Dynamic exclusion was enabled with a repeat duration of 45 s with an exclusion list of 500 and an exclusion duration of 30s.

### **2.2.9 Mass spectrometry data analysis**

Orbitrap raw files were analysed by MaxQuant version 1.6.0.16 (Cox and Mann, 2008). Mouse sequence databases downloaded from UniProt at June 2015 were used to perform our peptides identifications. The following search parameters were used: digestion set to

Trypsin/P, methionine oxidation and N-terminal protein acetylation as variable modifications, cysteine carbamidomethylation as a fixed modification, match between runs enabled with a match time window of 0.7 min and a 20-min alignment time window, label-free quantification enabled with a minimum ratio count of 2, minimum number of neighbours of 3 and an average number of neighbours of 6. PSM and protein match thresholds were set at 0.1 ppm. A protein FDR of 0.01 and a peptide FDR of 0.01 were used for identification level cut-offs. For identification of acetylated or ubiquitinated peptides, acetylation of lysine residues or lysine glycine – glycine (Lys-Gly-Gly) for ubiquitination were set as variable modifications, respectively.

Raw data generated from MaxQuant was then analysed by Perseus 1.5.6 software (Tyanova et al., 2016) to perform a statistical analysis. LFQ intensities texts for each sample were loaded as a main column and protein groups for all runs were loaded at the text column. Analysis were then started by filtering and removing the potential contaminants, reverse sequence hits and only peptides identified by sites. PTMs were localised to specific sites in residues using a combination of a localisation probability of  $>0.75$  and a score diff of  $>5$ , these “Class 1” sites have an estimated false localisation probability of 1%. The filtered results were then log<sub>2</sub> transformed and grouped into 2 experiments groups (e.g., Sirt2 Knockout and Sirt2 wildtype groups). Rows were filtered based on valid values with minimum 3 values in one group and all missing values were imputed based on a downshift from the normal distribution. Two tailed student’s t-tests were performed with  $S_0$  set to 0.1 and a permutation-based FDR set at 0.05, Significant differences between the two groups were generated and data were plotted in volcano plots and exported.

### 2.2.10 Proteomics data analysis

Our proteomics results of Acetylome dataset and Sirtuin-2 interactors were mapped and compared to many different datasets in order to provide a better understanding to the data.

Dataset, study and purpose of analysis are provided in table2.1

<b>Dataset name</b>	<b>Purpose</b>	<b>References</b>
<b>Acetylation site</b>	To compare identified acetylated sites with known sites	(Signling, 2017)
<b>Ubiquitination site</b>	To compare identified acetylated sites with known Ubiquitinated sites	(Signling, 2017)
<b>Mouse synaptic proteome</b>	To identify acetylated synaptic proteins	(Bayés et al., 2017)
<b>Acetylome of rat brain tissue</b>	To identify known acetylated protein /sites in both species	(Lundby et al., 2012b)
<b>Sirtuin 2 interactors</b>	To compare identified Sirt2 substrates or interactors from our studies with known interactors	(Stark et al., 2006)

**Table 2.1 - Datasets used for bioinformatics analysis.**

## **2.3 Protein expression analysis**

### **2.3.1 Protein extraction and quantification**

Cells were washed with 3 ml PBS before being harvested by trypsinisation, cells were then centrifuged for 4 minutes at 500 x g and then resuspended in 1 ml of PBS and centrifuged again and the supernatant was removed and pellet stored at -20°C. 200 µl of protein extraction buffer containing 4% SDS (Thermo-Fisher-s/5200/53), 50 mM Tris pH 8 (Sigma-Aldrich-T6006), 5 mM TCEP (Sigma-Aldrich-646547), and protease inhibitors 1:200 (Sigma-Aldrich-P8340) were added to each sample which was then homogenised and denatured for 10 minutes at 70°C with shaking at 1200 rpm. Samples were then homogenised with an electrical homogeniser for 10 seconds for 3 cycles which then centrifuged at 12,000 x g for 5 minutes the supernatant were then retained as proteins and kept at 20°C. Protein concentration levels were measured using a microBCA assay kit (Thermo-Fisher-Pierce BCA Protein assay kit- 23225), a spectrophotometer (BioRad-SmartSec-Plus) was used to measure the absorbance at 562 nm.

### **2.4 Immunoblotting**

Extracted proteins were prepared for blotting by adding 2X Tris-Glycine SDS sample buffer (Novex-LC2676) to 25-35 µg of protein and denatured at 70°C with shaking at 850rpm for 10 minutes. Protein samples and Pre-Stained Molecular Weight Ladder (Thermo-Fisher-22612) were then separated using 10% - 12% gel electrophoresis at 140V for 60-90 minutes (SureCast-Thermo-Fisher-HC1001) in mini gel tank (Life Technologies-NW2000). Electrophoresed proteins were transferred to Polyvinylidene Difluoride membranes (PVDF-Thermo-Fisher-86520) in a 1x NuPAGE transfer buffer (Novex-NP0006-1) at 30V for 90 minutes according to the protocol provided (Life-Technologies-NW2000). The membrane was blocked for 60

minutes at room temperature with 5% skimmed milk (Sigma-Aldrich-70166) prepared in 0.1% tween-20 (Fisher-BP337) and PBS (PBST). Diluted primary antibodies at the desired concentration in 1% milk PBST were added to the membrane and incubated overnight at 4°C. Three washing cycles of PBST for 10 minutes were applied to the membrane before diluted secondary antibodies at the desired concentration with 1% milk PBST were added for 60 minutes at room temperature. The membrane was washed three times with PBST for 10 minutes and followed by 1 wash with PBS until the membrane is ready for imaging (table 2.2).

#### ***2.4.1 Imaging and Analysis***

Membrane was imaged either by image studio Lite (Version- 5.2) for non HRP antibodies or by adding ECL substrate solutions (Biorad-1705061) in 1:1 ratio to the membrane with anti-HRP antibodies for 5 minutes and washed with PBS for 2 minutes, the imaging was conducted using X-ray CL-Xposure film (Thermo-Fisher-34091) and the Optimax 2010 to visualise the desired protein bands. Developed X-ray was scanned and digitally imaged were created to perform analysis through ImageJ FIJI (version- ImageJwin64).

#### ***2.4.2 Immunofluorescence***

HeLa or HEK 293 cells were cultured on coverslips (VWR-631-0152) inside 12 well plates for 48 hours or until 70% confluency, cells were then washed 3 times with 500 µl of sterile PBS. Washed cells were fixed with 1ml of 4% Paraformaldehyde (PFA-Sigma-Aldrich-158127) and incubated for 20 minutes at room temperature which then were washed again with PBS for 3 times. Plates were then covered with para-film and kept at 4°C ready for the next steps. Permeabilising of fixed cells was performed by adding 1 ml of the permeabilised solution containing PBS and 0.3% of Triton-x-100 (Sigma-Aldrich- Triton-X-100) and incubated for 15 minutes at room temperature. Cells were then washed 3 times with 0.5 ml PBS and incubated

shaking for 5 minutes each. 1 ml of blocking solution containing PBS, 0.01% of Triton-x-100, and 0.2% of fish skin gelatine (Sigma-Aldrich-G7765) were added to the cells for 1 hour at room temperature. Meanwhile, primary and secondary antibodies were prepared in blocking solution at desired concentrations as showed in Table2.2. The primary antibody was added and kept at room temperature for 1 hour followed by 3 cycles of washing with PBS which were performed for 5 minutes. Later the secondary antibody was added to the cells and incubated overnight in dark at 4°C and then washed 3 times with PBS and two times with H<sub>2</sub>O.

Next coverslips containing fixed cells were removed from plates and left to air dry for few minutes before it was flipped onto microscopy slides (Apple-Woods-MS501) containing DAPI-Fluormount-G (Southern-Biotech-0100). Slides were then kept at 4°C ready for imaging (table 2.3).

#### ***2.4.3 Imaging and Analysis***

The NIKON A1 Confocal Microscope was used for imaging at the Wolfson Light Microscopy Facility. 405nm (blue), 488nm (green), and 561nm (red) were selected as the wavelengths. Images were acquired with a 40x objective lens and the Nikon instruments NIS software.

The software packages FIJI (imageJ) (Schindelin et al., 2012) were used to analyse all of the images. The colour channels were split to isolate the channel of interest in order to analyse protein signal in different compartment. The mean intensity and raw integrated density were measured using the free draw tool around a single cell. After that, the shape was moved within the cell and the same measurements were taken. The difference between the two means was then used to determine the level of protein signals.

## ***2.5 Immunoprecipitation (IP)***

### ***2.5.1 Pulldowns of tagged proteins from cell lines:***

Cells were harvested from two 100 mm plates or two T75 flasks at 70-80% confluency after 24-48 hrs of transfection of the desired tagged protein. Cells were lysed in 500  $\mu$ l of lysis buffer containing 50 mM Tris pH 7.2, 150 mM NaCl (Appllichem-A2942), 1 mM EDTA (Gibco-11590626), 1% Triton-X-100, and protease inhibitor 1:200 and incubated rotated end-over-end at 4°C for 1-2 hours. Samples were centrifuged at 12,000 x g for 10 minutes at 4°C, the supernatant was then retained as a cell lysate. 10-20% of the lysate was kept as input for immunoblotting analysis. 40  $\mu$ l of agarose resin (Anti-Flag M2-Sigma-Aldrich-A2220), (Anti-HA Sigma- Aldrich-A2095), or (GFP-nanotrap-Sepharose –prepared in house Smith’s lab) were washed 3 times by lysis buffer before 1.5-2mg of samples were added and incubated in rotation overnight at 4°C. Samples were then centrifuged at 3000 x g for 2 minutes and supernatant retained, resins were washed 3 times with lysis buffer. Proteins were eluted with 20  $\mu$ l of lysis buffer containing 0.05 M TECP twice by heating at 70°C with shaking at 800 rpm for 15 minutes, eluted proteins were kept at -20°C. Alternative elution was applied to elute flag fusion proteins from anti-Flag antibodies used for immunoblotting e.g. Sirt2 and CDK9 resins, samples were incubated for 30 minutes at room temperature in a ratio of 3:1 vol: vol (Single peptide: sample) with 2 mg/ml of single flag peptide (Sigma-Aldrich-F3290) dissolved in lysis buffer, which was then centrifuged at 800 x g for 5 minutes and the supernatant was retained as eluted proteins.

### **2.5.2 IP of endogenous proteins from mouse brain tissue**

Forebrain tissue was lysed in 5 ml of lysis buffer containing 1 mM EDTA, 50 mM of Tris pH 8, 150 mM of NaCl, and 1% of sodium deoxycholate and protease inhibitor 1:200 ratio and supplemented with 5 $\mu$ M of Trichostatin A (TSA -Cell Guidance Systems -SM36-1) and 20 $\mu$ M of AGK2 (Sigma-Aldrich-A8231) when indicated. Tissue lysate was homogenised for 20-30 times with dounce homogeniser before incubated for 30 minutes at 4°C and transferred into 2 ml Eppendorf tubes. The sample was centrifuged at 14,000 x g for 15 minutes at 4°C and supernatant were retained as extracted protein and quantified using a microBCA assay. Immune-complex was prepared as follows, a specific antibody of the chosen protein was added to 2mg of the sample in a ratio of 1:50 vol: vol (antibody: sample) and incubated rotated end-over-end for 60 minutes at 4°C. 60 $\mu$ l of protein A magnetic beads (Cell-Signaling-73778) were washed 3 times with 500 $\mu$ l of lysis buffer, mixed and separated for 10-20 seconds by the magnetic separation rack (Dynabeads – MPC– A13346). Protein A beads were precleared by adding 20 $\mu$ l of sample and incubated rotated end-over-end for 30mins at 4°C before beads were washed again 3 times before the immune-complex sample was added and incubated rotated overnight at 4°C. The supernatant was removed, and beads were washed 3 times by lysis buffer, later the sample was eluted by adding 60 $\mu$ l of 2 x Tris-Glycine SDS Sample Buffer (Thermo-Fisher-LC2676), mixed and centrifuged for 1 minute at 300 x g before the mixture was heated at 95°C for 5 minutes and supernatant retained as eluted proteins.

### ***2.5.3 IP of endogenous proteins from a cell line***

Two T-75 flask of desired cell lines were grown until it reached cell confluency of 70-80% before washed by cold PBS and incubated at 4°C for 5 minutes. 500µl of lysis buffer containing 50 mM Tris pH 7.2, 150 mM NaCl, 1 mM EDTA, 1% Triton-X-100, and protease inhibitor 1:200, supplemented with 2µM of TSA and 10µM of AGK2, was added to cells and scrapped into 2 ml tubes and kept in 4°C. cells were homogenised for 5 seconds 3 times with 5 seconds in between pulses which then centrifuged at 14,000 x g for 5 minutes at 4°C. The supernatant was retained as a cell lysate and 10-20 % of the lysate was kept as an input. Immune-complex was prepared by adding 200µl of the sample was added to 1:50 vol: vol (antibody: sample) ratio and incubated overnight rotated end-over-end at 4°C.

20µl of protein A magnetic (Cell signaling- 73778) beads were washed 3 times by adding 300µl of lysis buffer, vortex and separated for 10-20 seconds by the magnetic separation rack. Beads were initially precleared with 20µl of sample and incubated rotated end-over-end for 20 minutes at room temperature, 3 washing cycles with lysis buffer were applied before the immune-complex sample was added, and incubated rotated end-over-end for 20 minutes at 4°C. The supernatant was removed, and beads were washed 3 times by lysis buffer, proteins were eluted by heating the beads with 60µl of 2 x Tris-glycine SDS sample buffer at 95°C for 5 minutes before supernatant retained. Eluted samples of tagged proteins or endogenous proteins from immunoprecipitation were digest using S-trap ≤ 100µg digestion column and analysed by LC-MS/MS.

## 2.6 Antibodies

Name	Type	Conc.	Manufacturer
Acetyl lysine antibody	Primary	1/1000	ImmunoChem-ICP0380
Acetylated-lysine ( Ac-K-100) MultiMab	Primary	1/1000	Cell Signaling-9814S
Anti-Ubiquitin	Primary	1/1000	cell signaling-3933
Anti-GFP	Primary	1/1000	Peden lab, UoS
Anti-mouse IgG HRP-linked Antibody	Secondary	1/2500	Cell Signaling-7076
Anti-Sirt2 Antibody	Primary	1/1000	Atlas Antibodies-HP011165
Goat anti-Rabbit IgG (H+L) Poly-HRP	Secondary	1/2500	Thermo Fisher Scientific-32260
HA-antibody	Primary	1/500	BioLegend-901513
HA-tag antibody	Primary	1/1000	Bioss Antibodies bs-0966R
Monoclonal ANTI-FLAG M2	Primary	1/1000	Sigma-Aldrich - F1804
Normal Rabbit IgG	Control/Primary	1/1000	Cell Signaling-2729
VAMP2	Primary	1/1000	Cell Signaling-13508
VAMP3	Primary	1/200	Peden lab, UoS

**Table 2.2 Antibodies used for immunoblotting studies**

Name	Type	Conc.	Manufacturer
Donkey anti-Mouse IgG (H+L) Antibody Alexa Fluor 488	Secondary	1/2000	Thermo Fisher Scientific-A-21202
Donkey anti-Rabbit IgG (H+L) Antibody Alexa Fluor 594	Secondary	1/2000	Thermo Fisher Scientific A-21206
Monoclonal ANTI-FLAG M2	Primary	1/1000	Sigma-Aldrich -F1804
Anti-Sirt2 Antibody	Primary	1/500	Atlas Antibodies-HP011165

**Table 2.3 Antibodies used for Immunofluorescence studies.**

## **2.7 Plasmid preparation**

### **2.7.1 Agar plate preparation**

LB agar medium was prepared by adding 40 g of LB agar (Fisher-Scientific-LB Agar-Miller-Powder-BP1425) to 1L of distilled H<sub>2</sub>O in an appropriate glass bottle that was gently swirled to form the medium. The agar medium was autoclaved, later autoclaved agar medium was supplemented by 100ug/ml of Ampicillin (Sigma-Aldrich-A9393) or 50ug/ml Kanamycin (Thermo-Fisher-11815-024) before it was poured into 100mm plate and kept at 4°C.

### **2.7.2 Cell transformation and DNA isolation**

2 µl of DNA was amplified in the DH5-alpha competent E. coli (Thermo-Fisher-18265017) after been thawed for 10 minutes. The mixture was incubated for 30 minutes at 4 °C, DNA heat shock at 42 °C briefly for 40 seconds and incubated at 4 °C for 2 minutes. Pre-wormed 200µl of sterile Liquid broth (Fisher-scientific-LB-Broth-Miller-BP-1426) were added and incubated shaking at 300rpm at 37°C for 60 minutes. In sterile environment 100µl of cells was added into an agar plate containing compatible antibiotics. Agar plates were then incubated to allow

bacterial growth in 37°C for no longer than 17 hours, plates were kept at 4°C until further use. For stab culture or glycerol stock plasmids a sterile loop was inserted into the tube and the bacteria containing the DNA were streaked over the culture medium and incubated as described above.

1-2 bacterial colonies were picked from the transformed plates and added to 1L conical flask contains an autoclaved 250 ml of LB supplement with compatible antibiotics. Bacterial culture was incubated overnight with shaking in a 37°C incubator (Thermo – MAXQ 4000). Plasmid DNA isolated by GeneJET Plasmid Maxiprep Kit (Thermo-Fisher-K0492) according to the protocol provided.

### ***2.8 Transfection***

Cells were grown overnight in the desired plate depends on the experiment, constructs were transfected to the cells and incubated for 24-48 hours. 1µg/1µl stock of Polyethyleneimine (PEI-25kDa Linear-Alfa Aesar-34896) was used in a ratio of w: w (1:3) (plasmid DNA: PEI). 6 well plates were transfected with 2µg of plasmid DNA which were added to a tube containing 6µl of PEI and 60µl of Serum-free media (DMEM without FBS) and incubated for 20 minutes in room temperature. The transfection mixture was then added to the plates and incubated in 37°C CO<sub>2</sub> incubators. After 24-48 hours cells were harvested according to the desired experiment, transfection concentration of T-75flask, 100mm plates and 12 well plates were 10µg, 5µg and 1µg of DNA respectively.

Plasmids	Manufacturer
FLAG-Cdk9 T186A	AddGene-#28101
NC16 pCDNA3.1 FLAG NRF2	AddGene-#36971
Sirt2 Flag	AddGene-#13813
EGFP-alpha-synuclein-WT	AddGene- #40822
pTRE_GFP-GluR1	AddGene-#34857
6xHis-UB	A kind gift from Dr Guo, University of Sheffield
HA-UB	
GFP-VAMP2	A kind gift from Dr Peden, University of Sheffield
GFP-VAMP3 (mutant)	
HA-VAMP3	
HA-VAMP4	
RFP-VAMP2	

**Table 2.4 Plasmids used for transfection.**

## 2.9 siRNA

20uM stock of Sirt2 siRNA (DharmaFECT-SMARTpool-ON-TARGETplus-Sirt2 siRNA-L-004826-00-0005) was prepared by adding 250µl of resuspension buffer containing 150 mM NaCl and 10 mM HEPES pH 7.4. Resuspension was mixed gently by pipetting 3-5 times and incubated at room temperature for 30 minutes with shaking at 700 rpm. The siRNA was centrifuged for 1 minutes and stored at -20 °C ready to use.

HeLa cells were transfected with 25nM of Sirt2 siRNA and 25nM non-targeting control siRNA (DharmaFECT-ON-TARGETplus-Control-Pool-D-001810-10-05). 25nM of Sirt2 siRNA or negative siRNA were added to 100µl of serum-free DMEM media and mixed before incubated for 5 minutes, in another tube 4µl of DharmaFECT siRNA transfection reagent 4 (dharmacon, GE life sciences, T-2004-01) were incubated with 100µl f serum-free DMEM for 5 minutes. The Mixtures of both tubes were incubated together for 20 minutes at room temperature before it was added to the cells. Plates were incubated in a 37°C CO2 incubator for 48-72 hours before harvesting as described previously.

## 2.10 Drug treatments

AGK2, SIREAL2, and TSA were added to HeLa cells and HEK293 cells and different time points or concentrations were applied for acetylation and deacetylation studies. CHX and Mg132 were also applied to the same cell lines for protein stability studies and ubiquitination studies respectively, full information about the drugs is shown in the Table 2.5

<b>DRUG</b>	<b>Product</b>	<b>Manufacturer</b>	<b>Stock concentration</b>	<b>Working concentration</b>
<b>AGK2</b>	(A8231-5MG)	Sigma Aldrich	4.6mM	10uM
<b>Cycloheximide</b>	C4859-1ML	Sigma Aldrich	9.7mM	100uM
<b>Mg132</b>	M8699-1MG	Sigma Aldrich	10mM	10uM/100uM
<b>Nicotinamide</b>	72340-100g	Sigma Aldrich	1M	10mM /100uM
<b>SIREAL2</b>	SML1514-5MG	Sigma Aldrich	25mM	10,20,50uM
<b>TSA</b>	SM36-1 (0.5mg)	Cell Guidance Systems Ltd	25mM	1uM

**Table 2.5 different drugs used for treatments.**

## **CHAPTER 3**

# **Characterisation of the Sirt2-regulated mouse brain acetylome**

### **3.1 Introduction**

Lysine acetylation is a common PTM of many proteins in all mammalian tissues but with a particular enrichment in the brain (Lundby et al., 2012b). A global acetylation study of different rat tissues identified 4,264 acetylation sites in the brain (Lundby et al., 2012b). In addition, many studies have pointed out that acetylation is involved in neurophysiological functions. For example, Tau acetylation contributes directly to the accumulation of phosphorylated tau (p-tau) as neurofibrillary tangles by preventing ubiquitination, which is a hallmark of tauopathy. Moreover, the loss of tau acetylation may result in tau dysfunction by interfering with tau binding to microtubules. Tau acetylation affecting p-tau turnover and may modulate the activities of kinases involved in tau phosphorylation (Choudhary et al., 2009a, Lundby et al., 2012b, North and Verdin, 2007, Min et al., 2010).

We showed previously, one of the very few deacetylase enzymes that have been implicated in neurodegenerative disease beside SIRT1 is Sirt2. Moreover, Sirt2 is widely distributed in human tissues, but the highest expression is found in the spinal cord, brain, and prefrontal cortex. Sirt2 deacetylation of the AMPA receptor and Arc protein regulates their stability, turnover, and their function in synaptic plasticity (Wang et al., 2017a, Lalonde et al., 2017). The mechanism of this regulation lies in the fact that Sirt2 maintains the balance between acetylation and ubiquitination at individual lysine residues; deacetylation by Sirt2 reveals lysine residues that are then ubiquitinated, leading to degradation of the protein.

#### **3.1.1 Sirt2 substrates**

As mentioned before, Sirt2 is widely distributed in mammalian tissue and has a vital role as a deacetylase enzyme in many diseases such as cancer and neurodegenerations and could be a promising therapeutic target (Chopra et al., 2012, Donmez and Outeiro, 2013, Chen et al.,

2015). There is little information about Sirt2 substrates in particular tissues or organs. However, studies have investigated Sirt2 role as the deacetylase enzyme for a specific protein or a disease (Table 3.1), longer list was provided in chapter 1.

<b>Substrate</b>	<b>Diseases</b>	<b>Sites</b>	<b>REF</b>
<b>AMPA receptor</b>	Neurology	K813/K819/K822/ K868	(Wang et al., 2017a)
<b>Alpha-tubulin</b>	Neurology	K40	(North et al., 2003)
<b>BubR1</b>	Cancer	K250	(Qiu et al., 2018)
<b>Slug</b>	Cancer	K116	(Zhou et al., 2016c)
<b>JNKs</b>	Cell death	K153	(Sarikhani et al., 2018b)
<b>GSK3</b>	Cardiology	K150/K183	(Sarikhani et al., 2018c)
<b>NFAT</b>	Cardiology	K612/K626	(Sarikhani et al., 2018a)
<b>GKRP</b>	Hepatic	K126	(Watanabe et al., 2018)
<b>LKB1</b>	Cardiology	K48	(Tang et al., 2017)
<b>FOXO1</b>	Adipose tissue	K242/K245/K262	(Jing et al., 2007)
<b>FOXO3a</b>	Oxidative stress	K242/K245/K59	(Wang et al., 2007)
<b>P65</b>	Inflammation	K310	(Rothgiesser et al., 2010)
<b>NF-κB</b>	Neurology	K48	(Pais et al., 2013)
<b>CDK9</b>	Neurology	K48	(Zhang et al., 2013)
<b>NRF2</b>	Iron homeostasis	K506/ K508	(Yang et al., 2017)
<b>STAT5</b>	Cancer	K697/K701	(Ma et al., 2010)
<b>c-Myc</b>	Neurology	K317, K323, K371	(Liu et al., 2013b)
<b>MKP-1</b>	Inflammation	K57	(Jung et al., 2015)
<b>HIF-1α</b>	Cancer	K709	(Seo et al., 2015)
<b>SREBP-2</b>	Neurology	K630/K363/K321	(Luthi-Carter et al., 2010a)
<b>PGAM2</b>	Cancer	K100	(Xu et al., 2014)
<b>TAU</b>	Neurology	K280	(Ali et al., 2018, Min et al., 2010)

<b>P53</b>	Cancer	K292/K382/K305/K315	(Donmez and Outeiro, 2013)
------------	--------	---------------------	----------------------------

***Table 3.1 – Selection of characterised Sirt2 substrates.***

### **3.2 Aims**

The aim of this chapter was to perform an unbiased proteomic analysis to discover novel substrates of Sirt2 in the brain. First, acetylome analysis of Sirt2 knockout (KO) and wild-type (WT) mouse brain tissue was performed to identify changes in acetylation levels. In addition, I performed a whole proteome profiling of Sirt2 KO and WT mouse brain tissue to determine if the deletion of Sirt2 causes any changes in protein abundance.

### **3.3 Results**

#### **3.3.1 Lysine acetylation is a major PTM of synaptic proteins**

Recently, lysine acetylation has been found to regulate two essential synaptic proteins AMPA receptors and Arc protein (Wang et al., 2017a, Lalonde et al., 2017). To assess the extent of acetylation of synaptic proteins, we performed a bioinformatics analysis to annotate previously generated synaptic proteome datasets with publicly available data from large-scale acetylome studies (Signling, 2017). The synaptic proteome dataset is a dataset of proteins identified in mouse synaptosome (1,146) and post-synaptic density (PSD) (688) fractions and a total of 4,142 proteins using quantitative mass spectrometry (Bayés et al., 2017).

We found that 64% (2,652) of mouse synapse proteins are acetylated (Figure 3.1) at 16,691 sites compared to 32,000 sites of 9,561 mouse proteins, indicating an acetylation enrichment at the synapse. Given that lysine acetylation of the two synaptic proteins investigated so far regulates protein stability and degradation (Wang et al., 2017a, Lalonde et al., 2017) and is mediated by the opposing action of acetylation and ubiquitination at the same lysine residues, we investigated the occurrence of these PTM switches more widely. Annotation of the synaptic proteome dataset with publicly available ubiquitination and acetylation data from Phosphosite shows many ubiquitinated and acetylated modified proteins in the mouse synapse (Signling, 2017). Nearly 36% (6,032) of acetylated sites on synaptic proteins can also be modified by ubiquitination as well (Figure 3.2 A). Additionally, global acetylation and ubiquitination sites from the entire Phosphosite dataset indicate that 35% (11,596) of all acetylation sites can also be modified by ubiquitination (Figure 3.2 B).

The literature suggests that Sirt2 has a potential role in regulating the PTM crosstalk between acetylation and ubiquitination (Wang et al., 2017a, Guo et al., 2019). Therefore, we mined

our synapse proteome dataset for deacetylase and acetyl-transferase enzymes that could regulate synaptic acetylation. The result revealed that Sirt2 was one of a few lysine deacetylases present at synapses along with HDAC6 and HDAC11. A comparison of protein levels between synaptosomes and post-synaptic densities indicates that Sirt2 is present at both the pre-and post-synapse, but it is significantly enriched at the presynaptic side ( $p = 0.001$ , Permutation-based FDR 0.05). However, not all the KDAC enzymes have an active deacetylase function. Some of those enzymes target other types of acylation; for example, HDAC11 functions as a fatty acid deacetylase (Narita et al., 2018, Kutil et al., 2018). Mining of the synapse proteome dataset, on the other hand, failed to identify any lysine acetyltransferases that would mediate enzymatic acetylation. This raises the possibility of either non-enzymatic acetylation at the synapse, or that proteins are acetylated before being trafficked to the dendritic spine (Drazic et al., 2016, James et al., 2018).

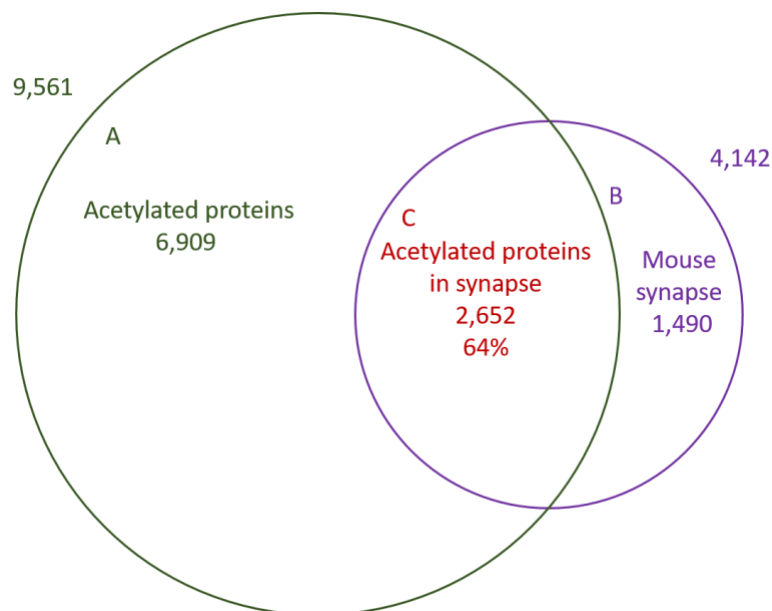


**Figure 3.1 – The majority of synaptic proteins are acetylated.** *The mouse synaptic proteome, which contains 4,142 unique proteins shown in (purple) (Bayes et al., 2017), was compared to the Phosphosite acetylated protein dataset that contained 9,561 proteins in (green) (Signling, 2017). Bioinformatics analysis of both datasets was compared by matching gene*

names from both data. Venn diagram revealed an overlap of 2,652 (64%) acetylated synaptic proteins.

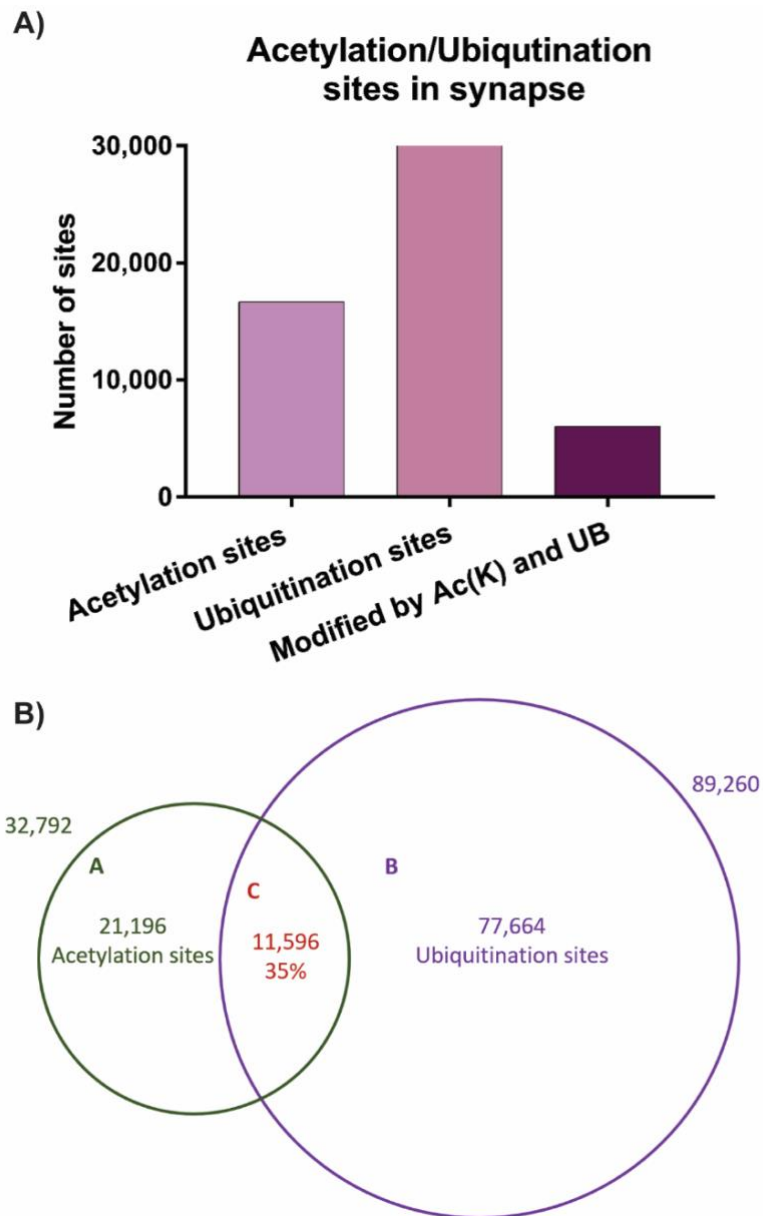


**Figure 3.2 – PTM Cross-talk of acetylation and ubiquitination; A)** Numbers of acetylation and ubiquitination sites in the synapse proteome. Bioinformatics analysis of mouse synaptic proteome containing 4,142 unique proteins was compared to Phosphosite ac(K) or Ub sites datasets (Signling, 2017). The peptides sequence window of each lysine site +/- 7 amino acids was compared to lysine sites +/- 7 amino acids from both datasets to identify ac(K) and Ub sites. The results were then matched to individual sites corresponding to those proteins (each protein may have more than one site). Bar chart representing synaptic proteins ac(K) sites in the first column, Ub sites in the second column, and both results were compared to define sites modified by acetylation and ubiquitination. **B)** Global cross-talk of acetylation and

*ubiquitination. Bioinformatics analysis of peptide sequence windows (lysine site +/- 7 amino acids) from both Phosphosite ac(K) and Ub sites datasets (Signling, 2017) were compared to identify the overlaps between ac(K) and Ub. The results were then matched to individual sites corresponding to those proteins (each protein may have more than one site).*

### **3.3.2 Acetylome analysis of Sirt2 knockout versus wild type mouse brain tissue**

#### **3.3.2.1 Optimisation of brain tissue acetylome analysis**

A workflow to enrich lysine-acetylated peptides and identify and quantify lysine acetylation sites using mass spectrometry is established in the Collins lab and has recently allowed the comparative analysis of >10,000 acetylation sites in HDAC1/2 knockout versus wild-type ES cells. The aim was to use this technology to identify novel Sirt2 substrates through a comparative analysis of acetylation in Sirt2 knockout versus wild-type brain tissue (Figure 3.3).

An initial optimisation was performed to test how well this workflow could be applied to brain tissue samples. Protein from a single adult wild type mouse forebrain was extracted and tryptically digested using FASP (Wisniewski et al., 2009). This sample preparation method has the advantage of maximising proteome coverage, particularly membrane proteins, and allows high peptide yield for downstream purification and analysis. Proteins were extracted using a lysis buffer containing 4% SDS to perform total solubilisation of the tissue a; all the detergents were then buffer exchanged with 8M Urea in a molecular weight cut-off centrifugal spin column. As SDS interferes with the following steps in the protocol, depletion of SDS using buffer exchange is essential to perform an effective analysis. All SDS can be removed from samples by repeated urea buffer exchanges in a filter concentrator 30K Device (Amicon ultrafiltration) (Wisniewski et al., 2009, Nagaraj et al., 2008). This approach was previously tested using lysates prepared from liver, brain, spleen and after desalting, produced purified

peptide samples ready for LC-MS/MS analysis (Nagaraj et al., 2008). Brain samples digested using FASP were desalted using a 360mg SEP Pak C-18 cartridge, eluted with 50% acetonitrile and 0.1% TFA and dried down in a speedvac. Acetylated peptides were then enriched by resuspension of the desalted peptides in immunoaffinity purification buffer, incubation with anti-Acetyl-lysine antibody resin (CST) overnight, several wash steps and elution with 0.15% TFA. The elution was desalted using C18 stage-tips and was performed to remove contaminating antibody chains (Wisniewski et al., 2009, Juri et al., 2007). Elutions from these acK IPs were analysed using 2-hour LC-MS/MS acquisitions on an Orbitrap Elite using a Top20 CID method. Data were processed and quantified using MaxQuant (Cox and Mann, 2008), and peptides and proteins were identified at an FDR of 1% using decoy database searching.

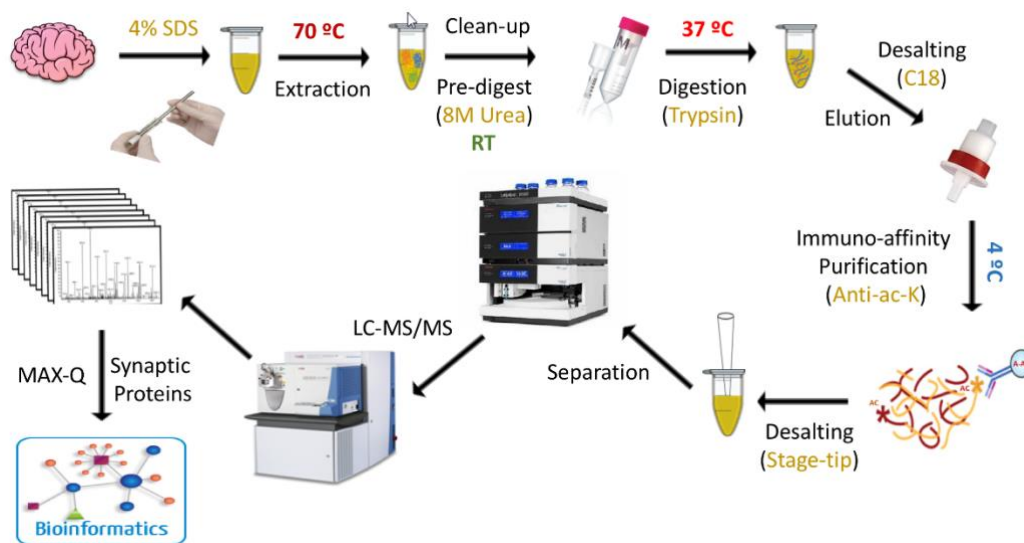


**Figure 3.3 Initial workflow for acetylome analysis of mouse brain tissue**

Three test experiments were performed using FASP to optimise the method with brain tissue before applying the optimised methods on our Sirt2KO/WT mouse brain samples. The first attempt was unsuccessful; I observed that the digested peptide sample had a visible cloudiness which may indicate that SDS was not removed properly that caused an ineffective

peptide digestion, enrichment and as a result caused a very low protein number with almost no detection of any synaptic proteins (Figure 3.4A). As a result, we were not able to identify many acetylated peptide/sites (Figure 3.4 B). In the second test experiment, a few changes were made to the protocol e.g., the digestion time was prolonged from 4-5 hours to overnight, and more care was taken to ensure the buffer exchange process was complete. An aliquot of the digest was analysed by LC-MS/MS analysis to check that the digest had been performed properly. Using a 30-minute LC-MS/MS analysis, >700 proteins were identified and features such as the charge state distribution and numbers of missed cleavages were checked and were found to be as expected. 84% of these proteins were known synaptic proteins which suggests that FASP method is improved compared to previous replicate (Figure 3.10 A). The remainder of this digested sample was desalted, subjected to acetyl-lysine immunoaffinity purification and MS analysis as described above. Although, this experiment worked to some degree: out of 758 proteins identified, 358 were acetylated proteins with 638 acetylation sites. 76% of the acetylated proteins identified in this experiment were synaptic proteins. (Figure 3.4 A, B).

In the third test experiment, to avoid SDS contamination during sample preparation, the lysis buffer was changed from 4% SDS to RIPA buffer with the same extraction methods. but we aimed to improve acetylated peptide enrichment by using new (new kit) anti-acetyl lysine resin. This experiment worked slightly better in terms of the number of identified proteins but the enrichments for acetylated peptides were unsuccessful (Figure 3.4 A, B).

The number of identified proteins and acetylated peptides from the three experiments using FASP was inconsistent and not as expected. Further optimisation was required to improve the protein yield to identify more synaptic proteins and acetylation sites.

Later, instead of FASP, we used acetone precipitation to improve detergent removal from the samples. A RIPA buffer extracted protein lysate was precipitated overnight at  $-20^{\circ}\text{C}$  by four volumes of ice-cold acetone (Weinert et al., 2011). This test experiment was performed in duplicate in parallel with one replicate of FASP digestion, as figure 3.4 A shows >1700 proteins were identified from acetone precipitation method, more than 70% were known as a synaptic protein compared to <1000 proteins identified from FASP. In terms of identifying acetylation sites acetone precipitation methods had a better result.

Furthermore, the number of identified acetylated peptides/sites is primarily determined by the total number of identified peptides. For example, in the first FASP experiment, we only identified 42 peptides (modified/unmodified), and only (9%) four of those peptides were acetylated. The optimised acetylome protocol led to the identification of 7,503 peptides, of which 2,776 (37%) were acetylated (Figure 3.4 B).

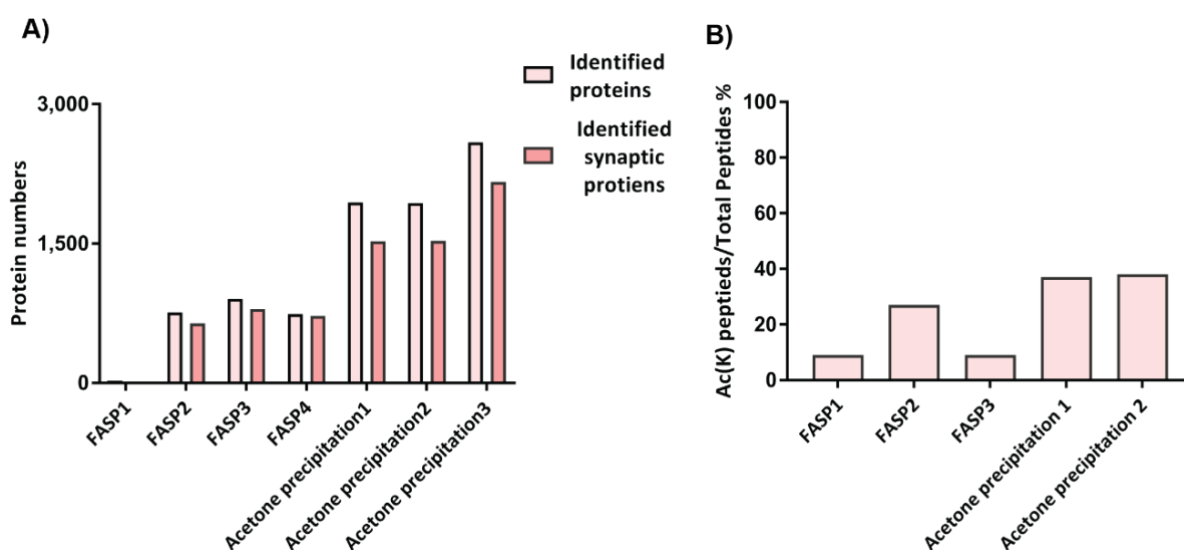


**Figure 3.4 – Optimisation of sample preparation for acetylome profiling.** Protein extraction from mouse brain tissue was optimised using different methods filter-aided sample preparation (FASP) and acetone precipitation. A) Bar chart represent the total proteins extracted from each repeat (pink) and identified synaptic proteins (red), proteins yield was a larger and more consistent using acetone precipitation. B) Bar chart represent the percentage of acetylated to total identified peptides.

### 3.3.2.2 Mouse brain acetylome profile

Based on the initial optimisation experiments, we chose acetone precipitation for detergent removal before acetyl-lysine immunopurification and applied this workflow to compare acetylation levels in wild-type and knockout brain tissue. Four Sirt2 knockout and wild-type brain tissue acetylome samples from adult mice (aged 7-14 weeks) were prepared (Figure 3.5). Proteins were extracted using a RIPA buffer to perform solubilisation of the protein. The protein lysate was precipitated with acetone overnight at  $-20^{\circ}\text{C}$  (Weinert et al., 2011). The protein pellets were resuspended in 8M urea/1 mM ammonium bicarbonate and digested

with trypsin overnight. Digested peptides were desalted using a 360 mg SEP Pak C-18 cartridge and eluted with 50% acetonitrile and dried down in a vacuum concentrator.

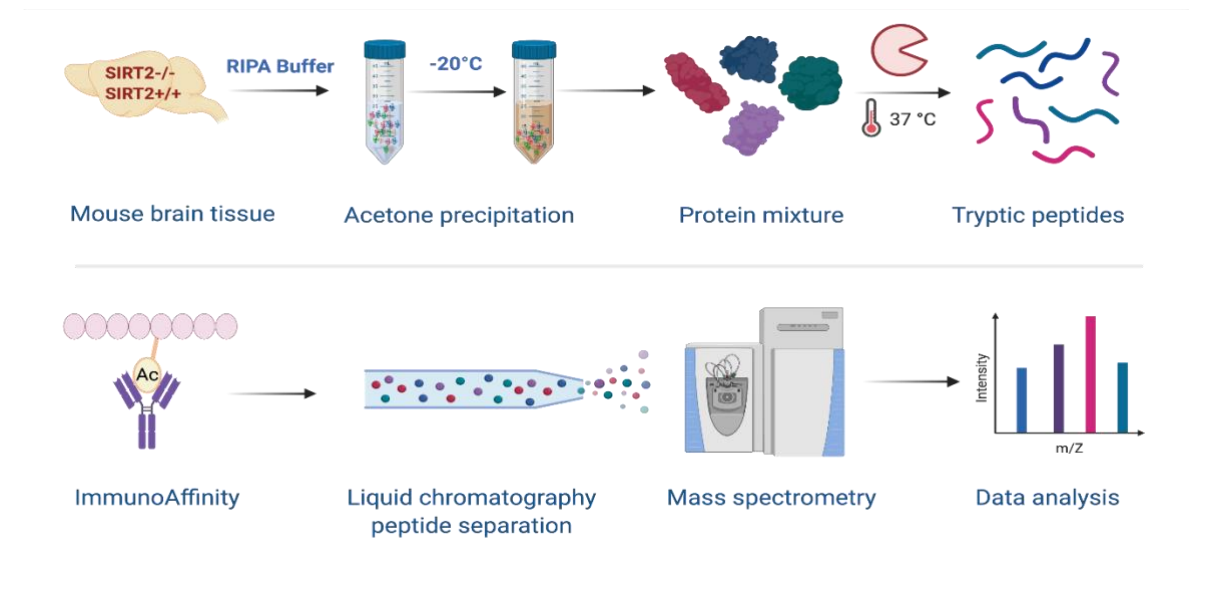
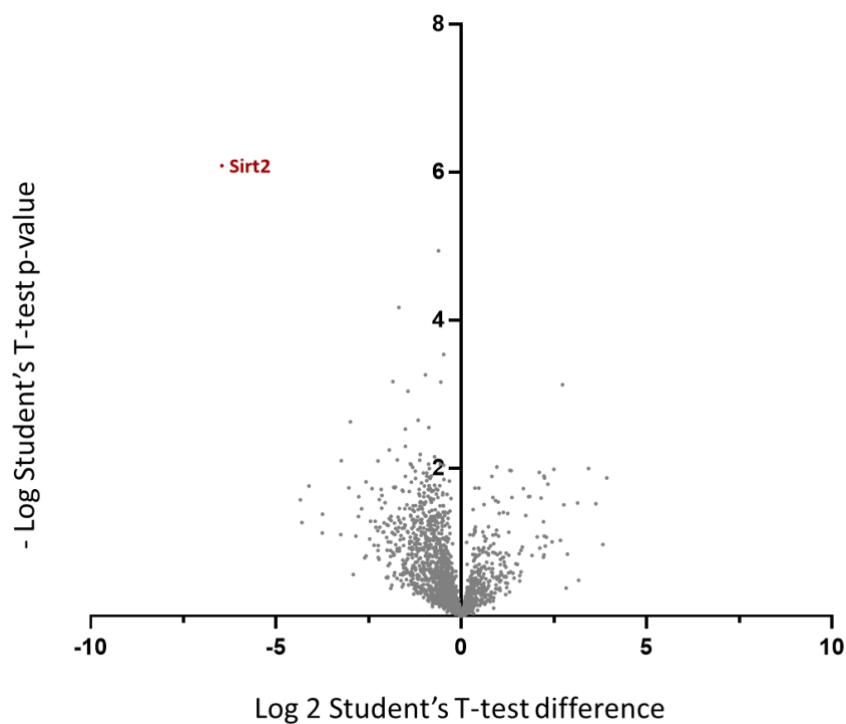


**Figure 3.5 – Workflow used for the acetylome analysis of wild-type and Sirt2 knockout brain tissue.** Protein from brain tissue was extracted using RIPA buffer and precipitated using cold acetone, followed by digestion with trypsin. Digested peptides were desalted and enriched for acetylation using immunoaffinity beads and analysed using LC-MS/MS. Raw data were processed using Maxquant, and statistical analysis of the quantitative data was performed using Perseus.

To test how well the protein extraction and digestion steps worked, an aliquot of each tryptic digest was analysed by a 2 hr LC-MS/MS analysis. Between 2,000 – 2,500 proteins were identified in each replicate shows that protein extraction and digestion performed well. Statistical analysis of the LFQ intensity data using Perseus (Stefka et al., 2016) confirmed that Sirt2 was significantly reduced in Sirt2 knockout brain tissue (Figure 3.6). Sirt2 was not detected in knockout samples but has a calculated t-test difference value and is represented in the volcano plot in Figure 3.12, because missing LFQ values in the knockout samples were imputed using a downshift from the normal distribution of the data from each sample.



---

**Figure 3.6 – Volcano plot showing Sirt2 significantly expressed in wild type tissue.** Student's T-test Difference between Sirt2 WT vs KO brain tissue. Extracted digested peptides were measured using Orbitrap MS. Sirt2 in far left (RED) was significantly reduced in Sirt2 knockout brain tissue. Statistical analysis of 4 replicates of Sirt2 KO and wild type was performed using t-testing (Permutation-based FDR of 0.05) using Perseus.

Next, those four samples were subjected to acetylated peptide enrichment using Acetyl-Lysine immunoaffinity beads, the elution from which was then desalted and concentrated using Stage-tips. Elutions were dried down in a vacuum concentrator, and peptides were resuspended in 0.5% formic acid and analysed using a 2-hour LC-MS/MS acquisition on an Orbitrap Elite using a Top20 CID method. Data were processed and quantified using MaxQuant (Cox and Mann, 2008). This approach identified 2,602 ac(K) sites on 983 proteins, at an FDR of 1 % at the peptide and protein level. Of which, 2,054 ac(K) sites (from 818 proteins) were quantified across a minimum of three replicates in either group (**\*\*Supplementary table 7.1**). Histogram plots of acetylation sites intensities were plotted to show that samples confirm that the data was normally distributed (Figure 3.7 A, B) To further check the quality of the data, correlation analysis of replicates of Sirt2 KO and WT acetylation sites, showed a good correlation across replicates within groups which confirms that our approach was robust and reproducible (Table 3.2).

\*\*(<https://figshare.com/s/13750b8c09063b5cb9eb>)

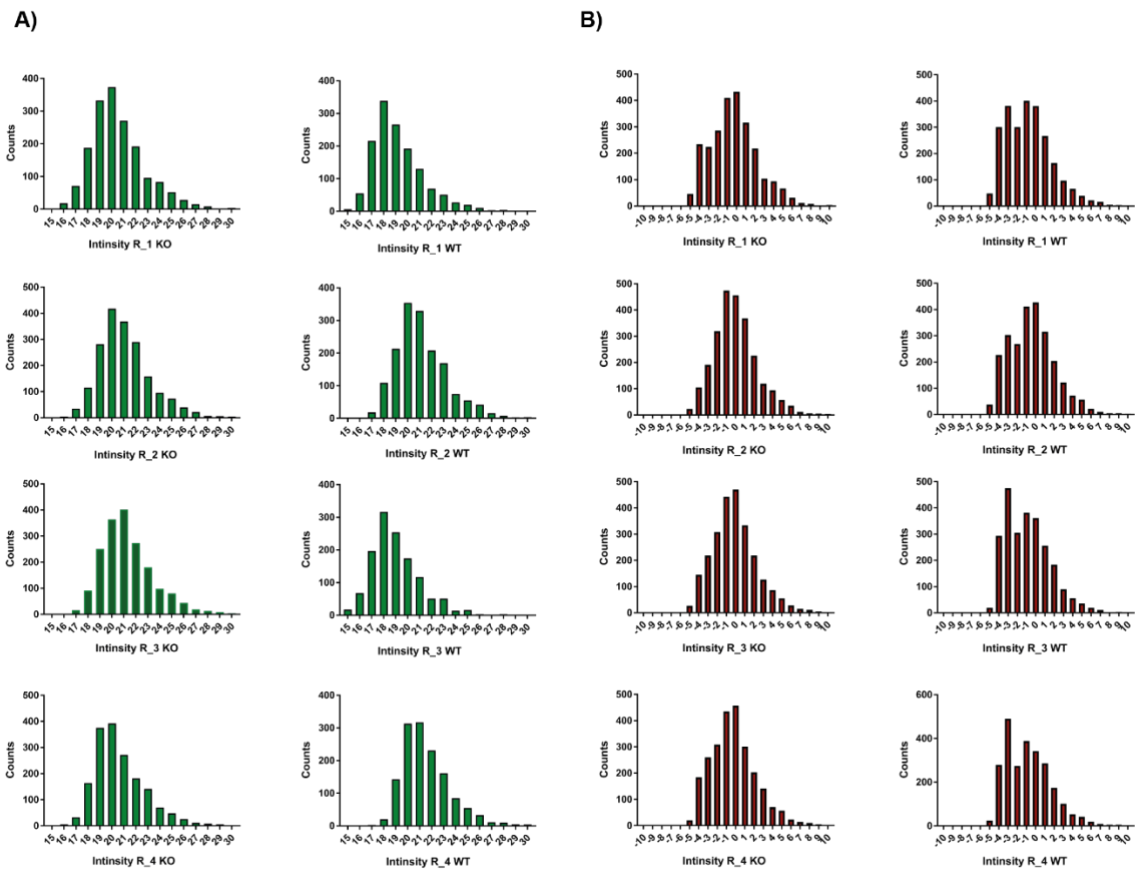


**Figure 3.7 – Histogram of LFQ intensity columns for replicates of *Sirt2* KO versus *Sirt2* WT. A) showing a normally distributed intensity. B) with normalised and imputed intensity values for statistical analysis.**

Intensity KO1	Intensity KO2	Intensity KO3	Intensity KO4	Intensity WT1	Intensity WT2	Intensity WT3	Intensity WT4	
NaN	0.931	0.895	0.811	0.806	0.834	0.826	0.805	Intensity KO1
0.931	NaN	0.946	0.876	0.833	0.848	0.842	0.848	Intensity KO2
0.895	0.946	NaN	0.916	0.825	0.835	0.808	0.868	Intensity KO3
0.811	0.876	0.916	NaN	0.844	0.771	0.739	0.852	Intensity KO4
0.806	0.833	0.825	0.844	NaN	0.821	0.819	0.892	Intensity WT1
0.834	0.848	0.835	0.771	0.821	NaN	0.902	0.839	Intensity WT2
0.826	0.842	0.808	0.739	0.819	0.902	NaN	0.792	Intensity WT3
0.805	0.848	0.868	0.852	0.892	0.839	0.792	NaN	Intensity WT4

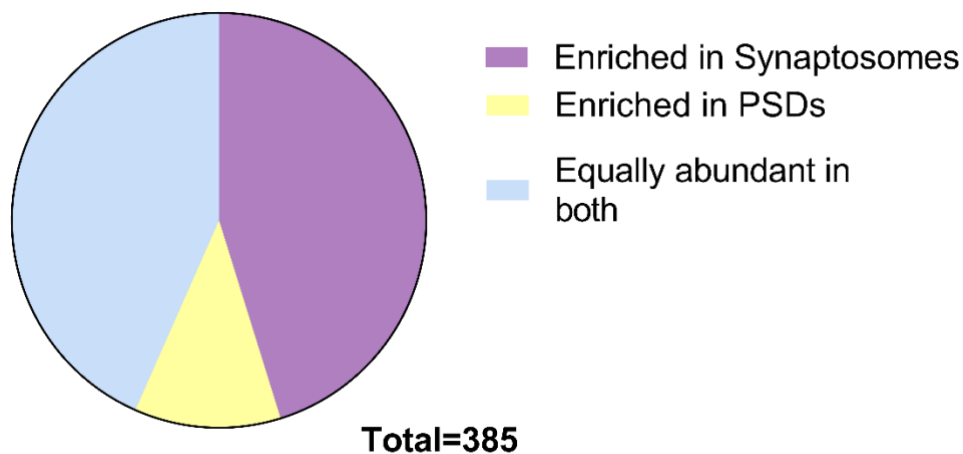
**Table 3.2 – Correlation values of Sirt2 WT and KO replicate datasets.** These show that biological replicates from 8 mouse brain tissue were mostly similar with very little difference between groups. Pearson correlation was 0.84 in same group, and 0.82 in different groups. Green and yellow boxes represent high and low correlation between samples respectively.

Table 3.3 details the number of identified proteins and acetylated peptides which was comparable with our optimisation data (figure 3.4). 3,418 Ac(K) peptides were identified, and the percentage of ac(K) peptides was 44% which show an improved performance than the data generated during method optimisation. This increase might be a result of Sirt2 knockout brain tissue which may contain acetylation sites not detectable in wild type tissue.

Identified Proteins	Identified Peptides	Ac(K) peptides	% Ac(K) peptides
1,631	7,654	3,418	44%

**Table 3.3 Summary of proteins and peptides identified in brain tissue from Sirt2 KO versus WT mice.**

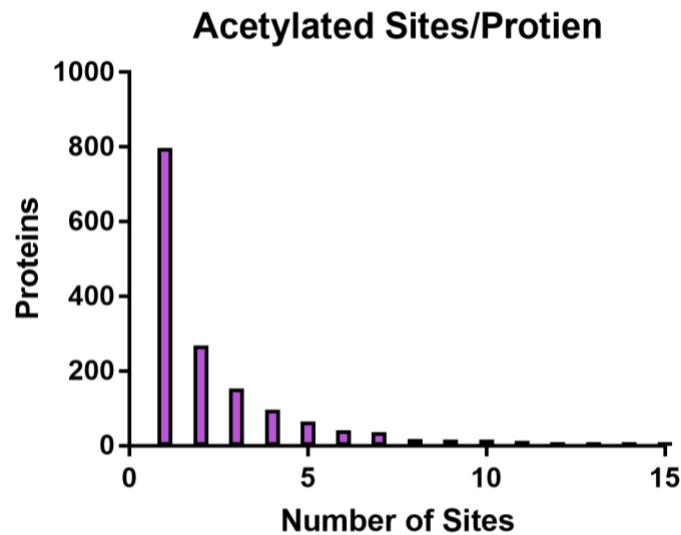
In the beginning of this chapter (figure 3.1) I pointed out that 64% of the mouse synaptic proteome is acetylated according to the Phosphosite database (Signling, 2017). Here we identified 1,676 ac(K) sites were acetylated on synaptic proteins which count for around 81% from the total identified sites. Identified sites were mapped on proteins identified from the mouse synapse proteome (Bayés et al., 2017). Next, we performed a comparison of the distribution of the proteins containing those identified sites between Synaptosome and PSD fractions and the results indicate that most of those proteins are equally abundant in both PSDs and synaptosomes as shown in figure 3.8.



---

**Figure 3.8 – Identified acetylated proteins are enriched in synaptosomes and PSDs** Bioinformatics analysis of identified ac(K) proteins mapped on mouse synapse proteome and its enriched level on both parts. synaptosomes (purple) and post-synaptic densities (yellow) and non-significant protein enrichments levels (Blue).

To further understand the distribution of identified ac(K) sites we performed a quantification of the number of acetylated sites per acetylated proteins as shown in figure 3.9 which revealed that the majority of identified acetylated protein (~800) contain one ac(K) site only.



---

**Figure 3.9 – Number of acetylated sites per acetylated proteins.** Bar chart represents the number of ac(K) site found in each protein. Around 800 proteins only contain one ac(K) site and very few proteins contain more than 10 ac(K) sites.

To assess the novelty of this dataset of lysine acetylation, a bioinformatics analysis was performed on the 2,054 ac(K) sites compared to the acetylation data in the Phosphosite database revealed that 873 sites were known and the majority (1,183) of those sites were novel (Figure 3.10A). This analysis was performed by matching peptide sequence windows containing the acetylated lysine residue +/- 7 Amino acids (Signling, 2017).

Given that acetylation can prevent ubiquitination and thus protein degradation, identifying acetylation sites that can also be ubiquitinated may help in prioritising potentially more important regulatory sites for further investigation. Studies have shown that acetylation and ubiquitination crosstalk on lysine sites are arising in many proteins, while other studies have

*focused on the importance of acetylation site modification as a preventable of site ubiquitination, which in many cases led to increased protein stability and improved many regulatory processes.(Choudhary et al., 2014, Wang et al., 2017a). Bioinformatics analysis of the ac(K) sites identified in our data and Phosphosite mouse ubiquitinated sites dataset revealed that 883 sites are modified by both acetylation and ubiquitination. Additionally, more than 442 of these ubiquitinated sites are also novel sites of acetylation from our data (Figure 3.10 B).*

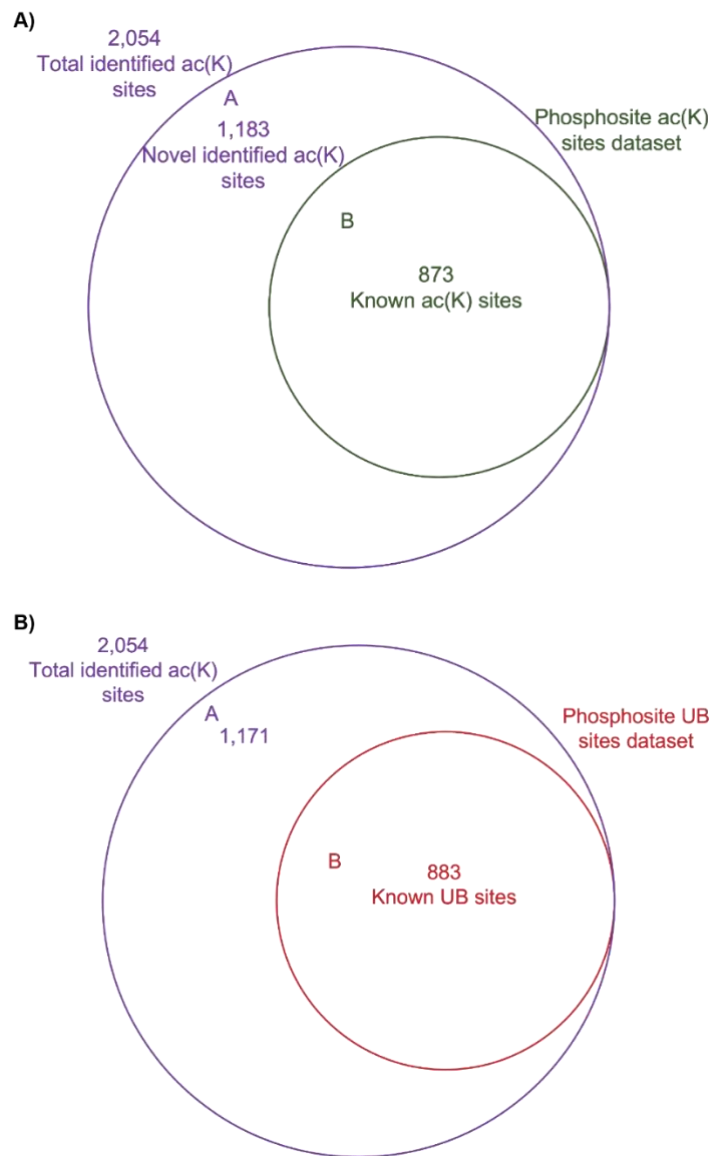


**Figure 3.10 – Venn diagram of known and novel acetylated sites;** 2,054 ac(K) sites identified (Purple) compared to Phosphosite (24). 873 known ac(K) sites (Green) and 1,183 were novel ac(K) sites. Bioinformatics analysis compared peptides sequence windows contains lysine site +/- 7 amino acids from acetylome profile and Phosphosite database (Signling, 2017). Venn diagram illustrating PTM Crosstalk between acetylation and ubiquitination sites. 883 sites (Red) out of 2,054 ac(K) sites (Purple) are known UB sites. Bioinformatics analysis compared peptides sequence windows contains lysine site +/- 7 amino acids from acetylome profile and Phosphosite UB dataset.

Next, to specifically compare identified ac(K) sites to brain ac(K) sites, we used a dataset of brain acetyome profile that was obtained from analysis of rat brain tissue (4,245 ac(K) sites) and compared it to our dataset by matching peptides sequence windows containing the acetylated lysine residue +/- 6 amino acids. Figure 3.11 shows an overlap of 647 ac(K) site (31%) between the two studies. Comparing dataset from different species by peptide sequence windows might be not optimal because those sites are not always conserved between species, thus any change of any amino acid of that sequence could eliminate the site from the results. We repeated this analysis, and we chose to compare gene names to compare the overlap of acetylated proteins instead of sites and 56% (459) out of 818 acetylated proteins were previously identified in the rat brain acetyome.

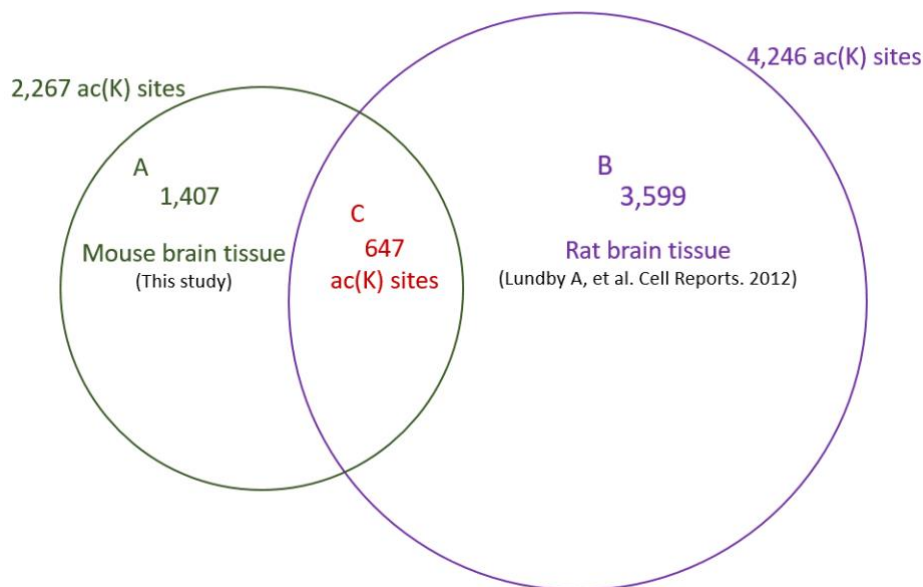


**Figure 3.11 – Ac(K) sites were previously identified in rat brain tissue.** Venn diagrams represent (A) 2,054 ac(K) sites from this study (green) compared to (B) 4,246 ac(K) sites from Rat brain tissue (Lundby et al., 2012b) (purple). Bioinformatics analysis compared peptides sequence windows contains lysine site +/- 6 amino acids from mouse and rat brain acetyome.

It is now well acknowledged that acetylation is not limited to nuclear proteins such as histones, studies shown that acetylation occurs in almost every cell compartment (Bogi Karbech et al., 2019, Lundby et al., 2012b). To investigate the distribution of identified acetylated proteins in our study, we annotated sub-cellular localisations determined by immunofluorescence-based protein localization from the human protein atlas . We found that the ac(K) proteins that we identified were distributed in almost all the subcellular compartments. The majority, with 31% found in the nucleus compared to 28% in the cytoplasm and 39%, were distributed in other compartments (Figure 3.12).

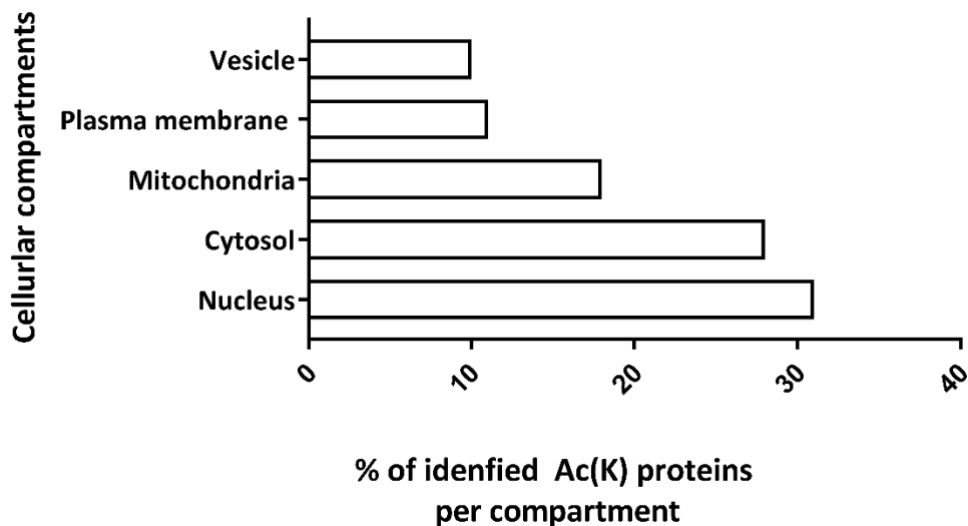


**Figure 3.12 –Cellular distribution of ac(K) proteins.** Proteins were assigned to subcellular compartments based on immunofluorescence data from the Human Protein Atlas and shows that lysine acetylation modification occurs in almost all cellular compartments.

Next, a Gene Ontology functional annotation analysis was performed to identify enriched gene ontology terms for cellular components, molecular function, and biological processes associated with the set of mouse brain acetylome. In figure 3.13, the analysis was performed using the mouse genome as a reference dataset and for a more specific the analysis, it was repeated using the brain proteome (Sharma et al., 2015) as a reference dataset (figure 3.13).

We found very interesting proteins associated with synapses and synapse parts such as (VAMP2-3, CamK2a, Mapt, Snap25, Snca and PCLO). Additionally, molecular functions were associated with many enzymes function, transmembrane protein, protein binding and activity, Figure 3.14 displays some of those annotation results (Michael et al., 2000, 2019).

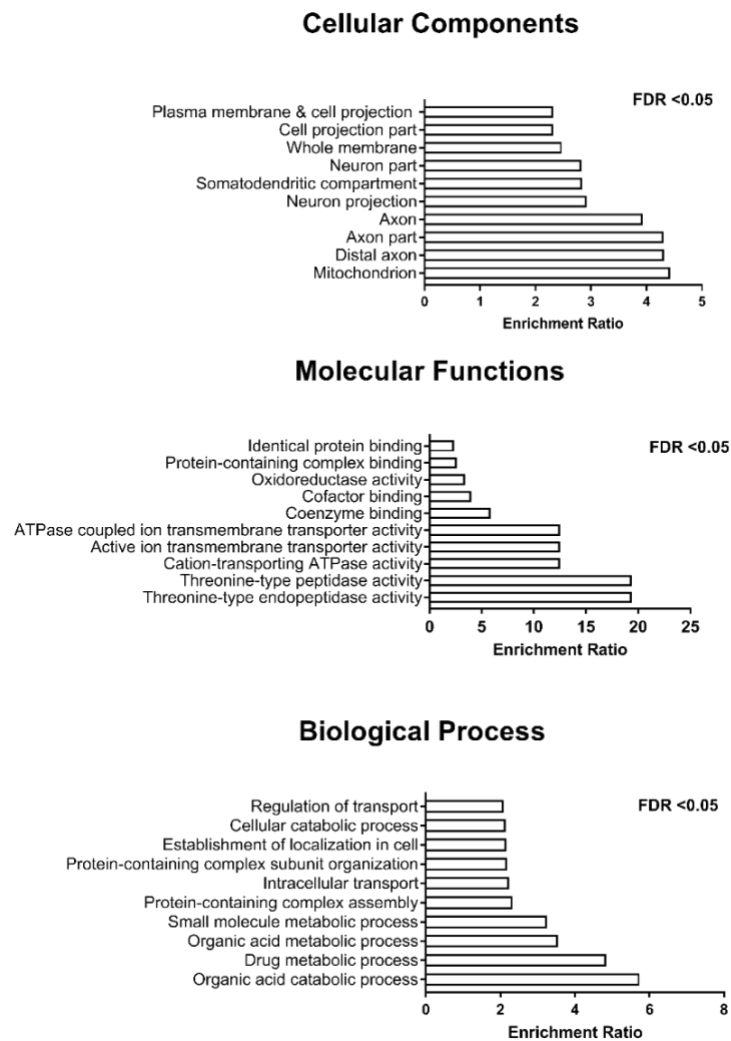
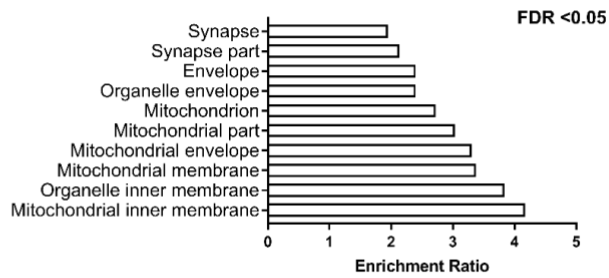
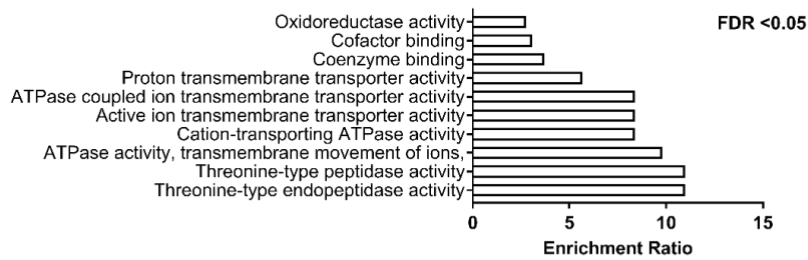


**Figure 3.13 – Significantly enriched proteins grouped into cellular component molecular pathways and biological processes** Gene ontology enrichment analysis of the total dataset of identified acetylated proteins at FDR <0.05 was generated using WebGestalt gene toolkit(Wang et al., 2017b) mouse genome used as a background.

### Cellular Components



### Molecular Functions



### Biological Process

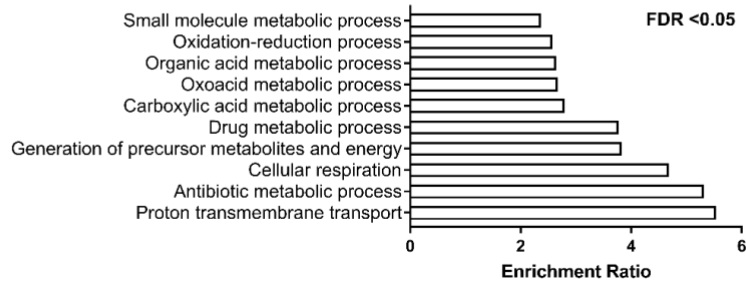


**Figure 3.14 – Significantly enriched proteins grouped into cellular component molecular pathways and biological processes.** Gene ontology enrichment analysis of the total set of identified acetylated proteins at FDR < 0.05 was generated using WebGestalt gene toolkit (Wang et al., 2017b) and brain proteome used as a background (Sharma et al., 2015).

In order to identify which pathways acetylated proteins are involved in, a pathway enrichment analysis was performed using the PANTHER pathways library. Table 3.4 lists some relevant pathways identified; acetylation is involved in Parkinson’s and Huntington’s disease, TCA cycle, glycolysis, synaptic vesicle trafficking and p53 pathways some of those results are consistent with results that reported previously (Lundby et al., 2012b, Bogi Karbech et al.,

2019). In addition, the same analysis was repeated to identify which protein classes are potentially regulated by acetylation in the brain. Table 3.5 lists the relevant protein classes that might require acetylation for its functions.

<b>PANTHER PATHWAYS</b>	<b>NUMBER OF PROTEINS</b>
Parkinson disease (P00049)	29 (Uchl1,Ywhab,Snca)
Huntington disease (P00029)	18
Wnt signaling pathway (P00057)	18 (Ep300)
Glycolysis (P00024)	12 (Pgk1, Pkm, Gapdh)
Synaptic vesicle trafficking (P05734)	9 (Snap25,Stx1a,B)
p53 pathway (P00059)	8 (Cdk5, Ep300)
TCA cycle (P00051)	5 (Mdh1, Pdha1)
Alpha adrenergic receptor signaling pathway (P00002)	3 (Snap25, Vamp3)

**Table 3.4 – Acetylated proteins grouped into Panther pathways.** Enrichment analysis of the identified acetylated proteins from mouse brain acetylome using panther analysis tools (Thomas et al., 2003).

<b>PROTEIN CLASSES</b>	<b>NUMBER of proteins</b>
Metabolite interconversion enzyme (PC00262)	216
Transporter (PC00227)	53
Protein modifying enzyme (PC00260)	46
Cytoskeletal protein (PC00085)	39
Nucleic acid metabolism protein (PC00171)	38
Membrane traffic protein (PC00150)	34
Protein-binding activity modulator (PC00095)	27
Gene-specific transcriptional regulator (PC00264)	23
Chromatin/chromatin-binding (PC00077)	18
Translational protein (PC00263)	16
Chaperone (PC00072)	16
Scaffold/adaptor protein (PC00226)	15
Transfer/carrier protein (PC00219)	11
Transmembrane signal receptor (PC00197)	7
Structural protein (PC00211)	6
Calcium-binding protein (PC00060)	5
Cell adhesion molecule (PC00069)	4
Intercellular signal molecule (PC00207)	4
Defense/immunity protein (PC00090)	4
Extracellular matrix protein (PC00102)	2
Cell junction protein (PC00070)	1

**Table 3.5 – Acetylated proteins grouped into protein classes.** Enrichment analysis of the identified from mouse brain acetylome by using panther analysis tools(Thomas et al., 2003).

To investigate whether acetylation of lysine residue occur more frequently with specific neighbouring amino acids, sequence motifs of the acetylome dataset were generated with a pLogo using the mouse genome as the background (Figure 3.15) (Joseph et al., 2013).

This figure reveals that the -1 position frequently contained the acidic residues glutamic acid (E) and aspartic acid (D). Whereas leucine (L), tyrosine (Y) and glutamic acid (E) are frequently found at +1 position. As mentioned earlier most of our acetylome data were enriched in synapses, and previous analysis failed to identify KATs enzymes in mice synaptic proteome (Bayés et al., 2017). These results suggesting that acetylation may have happened with chemical acetylation rather than enzymatic.

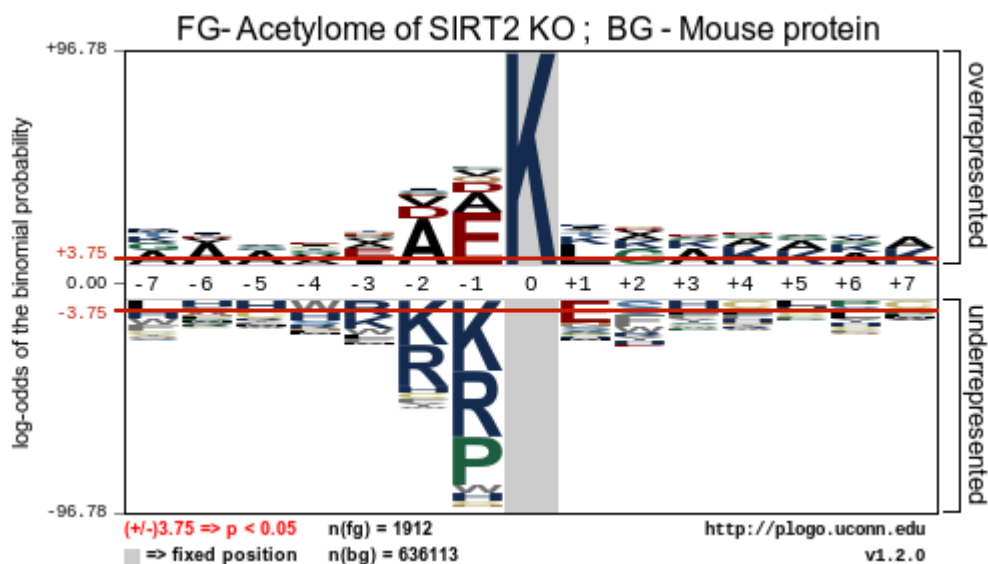


**Figure 3.15 – Sequence logo plots represent normalised amino acid frequencies for -/+7 amino acids from the lysine-acetylated site. A) represent sequence properties of overall identified ac(K) sites of Sirt2 KO vs. WT brain tissues at  $p < 0.05$  against mouse protein background. Logos generated with ([plogo.uconn.edu](http://plogo.uconn.edu))(Joseph et al., 2013).**

Acetylation may occur enzymatically by KATs on lysine residues on a protein or directly acetylated by acetyl-CoA, dependent on the acetyl-CoA concentrations and the accessible lysine residue in the tissue (Drazic et al., 2016, Bogi Karbech et al., 2019).

Interestingly, Ep300 an acetyl transferase enzyme was identified in our acetylome profile, to investigate the involvement of this enzyme on acetylation status of brain proteins. Previous study have generated a acetylome profile from CBP/EP300 knockout mouse embryonic fibroblasts and identified 2,783 ac(K) sites (Weinert et al., 2018). This dataset was compared to ac(K) sites from our study, and we found an overlap of 9% (193) ac(K) sites from our brain acetylome as a possible target for CBP/EP300 (Figure 3.16).

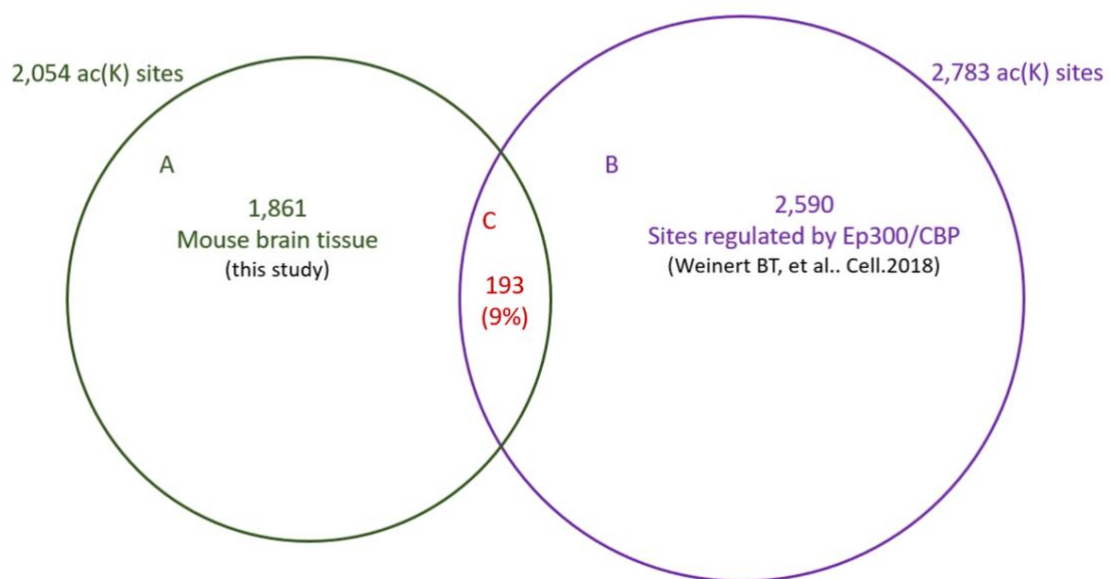


**Figure 3.16 – CBP/Ep300 acetyltransferase enzymes may regulate acetylation in brain tissue.** (A) Venn diagrams represent 2,783 ac(k) sites CBP/EP300 knockout Acetylome from mouse embryonic fibroblasts(Weinert et al., 2018) (purple), as compared to our brain Acetylome dataset that contain 2,054 Ac(K) sites(Green). 193 ac(K) sites of our brain Acetylome overlap with CBP/EP300 (red).

On the other hand, to investigate other potential KATs responsible for regulating the brain acetylome, we performed substrate predictions for each acetylation site in our dataset using GPS-PAIL. The results indicate that ac(K) sites might be acetylated by all KAT groups, but KAT2A and KAT2B are potentially critical KATs for those sites identified in brain acetylome (Figure 3.17) (Wankun et al., 2016). KAT2A and KAT2B are part of and localised to the nucleus, and the RNA expression of both shows high expression levels in the cerebral cortex, prefrontal cortex, and brain .

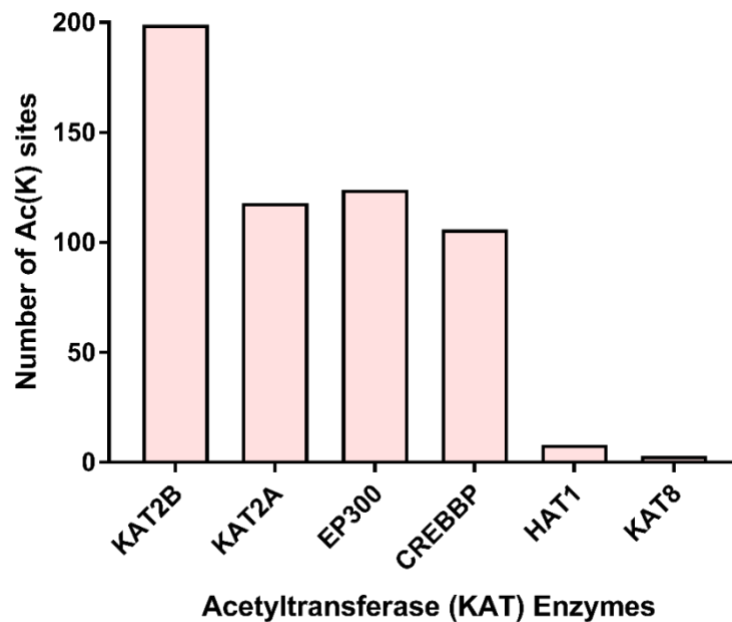


**Figure 3.17 – KAT2B and KATA2 are predicted to be the significant KATs regulating the brain acetylome** Bar charts Represent GPS predictions for acetyltransferase groups that regulate Identified sites from our study, peptide sequence windows of identified Ac(K) sites were analysed using GPS PAIL software (Wankun et al., 2016). a total of 554 ac(K) sites was recognised by different KAT enzymes.

### ***3.3.2.3 Characterisation and bioinformatics analysis of Sirt2 putative substrates***

Quantitative comparison of acetylation levels between wild type and Sirt2 KO mice was performed using Perseus (Tyanova et al., 2016). Data were filtered to proteins that only identified by sites in at least three replicates of each group, contaminate and reverse was removed. Data were also normalised by subtracting the median of the distribution, Statistical t-test performed with FDR 5% (Tyanova et al., 2016).

This approach enables the identification of 226 lysine sites that exhibit a significant increase in acetylation levels in Sirt2 KO brain tissue and are therefore potential as Sirt2 substrates. Volcano plot shows acetylated peptide distribution between two groups, peptides in the right side represent acetylated peptides that regulated by Sirt2 (Figure 3.17). Interestingly, 197 of those ac(K) sites were acetylated on synaptic proteins, and around 106 sites are also modified by ubiquitination.

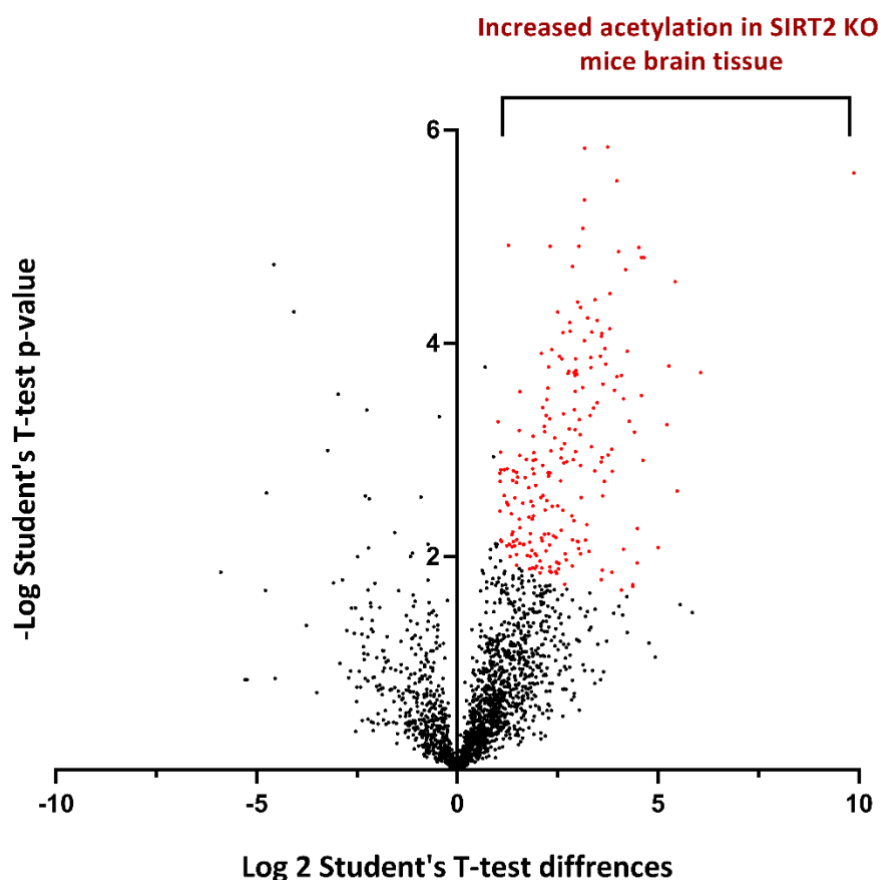


**Figure 3.18 – Volcano plot showing acetylation sites regulated by Sirt2;** acetylome data were flittered to proteins that only identified by sites in at least three replicates of each group, contaminate and reverse was removed. Data were then normalised by subtracting the median of the distribution, Statistical t-test performed with FDR 5% and s0 of 0.1. Red dots represent significantly acetylated peptides that regulated by Sirt2. Analysis was applied on 2,054 sites that identified in at least three replicates of each group. Statistical analysis of 4 replicates of Sirt2 KO and 4 replicate of wild type by the statistical package, Perseus.

As mentioned earlier we were able to identify more than 1000 ac(K) that were novel sites according to Phosphosite acetylation dataset (Signling, 2017). Table 3.6 demonstrate the percentage of acetylome ac(K) sites that previously identified, around 42% of the total ac(K) sites and 24% of Ac(K) sites regulated by Sirt2 were matched to acetylation dataset from Phosphosite (Signling, 2017). This result suggested that majority of novel ac(K) sites identified

might be a result of Sirt2 gene knockout and the loss of some deacetylase function in brain and in synapse as well.

	Identified ac(K) sites	Known ac(K) sites	%
<b>Total identified Ac sites</b>	2054	873	42
<b>Regulated Ac(K) sites by Sirt2 (increased in Sirt2 KO)</b>	226	56	24
<b>Other identified ac(K) sites</b>	1,828	817	44

***Table 3.6 known ac(K) sites found in Sirt2 knockout brain tissues.***

Given that Sirt2 was present in both synaptosomes and PSDs but enriched in the synaptosome fraction of our synapse proteome dataset, we performed a comparison of the distribution of these identified putative Sirt2 substrates between synaptosomes and PSDs fractions. The results indicate that the majority of Sirt2 substrates are equally abundant in both PSDs and synaptosomes, but more were significantly enriched in synaptosomes indicating a potentially larger role for Sirt2 in the regulation of pre-synaptic deacetylation (Figure 3.18).

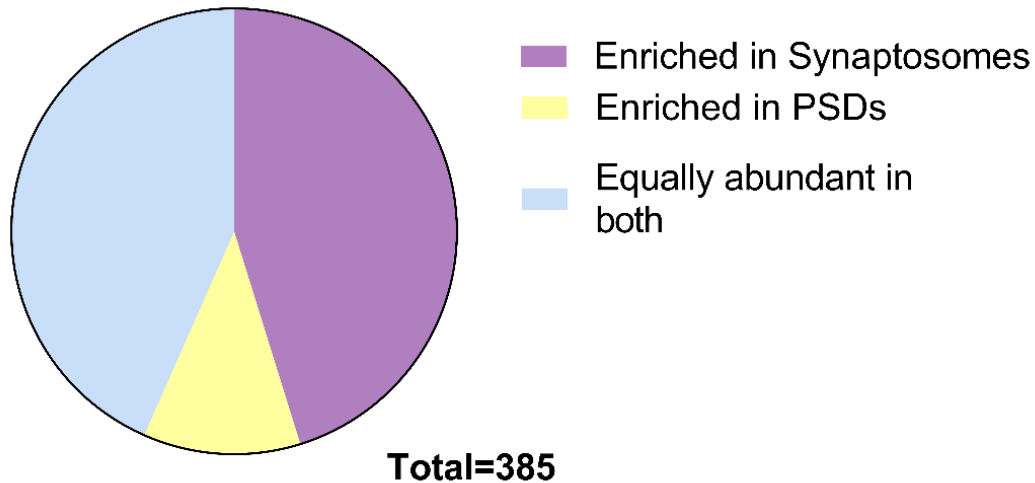


**Figure 3.19 – Identified putative Sirt2 are enriched in synaptosomes and PSDs.** Bioinformatics analysis of identified Sirt2 substrates showed protein that significantly enriched level on synaptosomes (purple) and post-synaptic densities (yellow) and non-significant protein enrichments levels (Blue).

To investigate whether identified putative Sirt2 substrates from our acetylome are interacting with Sirt2, we compared our data set to Sirt2 interactors dataset. Out of 179 acetylated proteins that might regulated by Sirt2 only four proteins were interactors all of those proteins were identified through high throughput proteomics studies (Stark et al., 2006).

Identified acetylated proteins from Sirt2 KO brain acetylome dataset require further validation to, first, investigate the acetylation as a modification for those proteins. Second to investigate a regulatory role of acetylation for these proteins. To prioritise potential Sirt2 substrates for further investigation, some criteria were established that well-suited with our hypothesis:

- Sites/proteins that significantly more acetylated in Sirt2 KO versus WT mice.
- Acetylation/Ubiquitination crosstalk on the identified site.
- Acetylated protein is known as a synaptic protein.

- Newly identified acetylated sites.
- The chosen substrate includes a site that is related to a specific function
- Proteins that are readily available for testing and compatible with our studies include tagged construct for transfection, reagents for immunoprecipitation, and antibodies for testing both immunofluorescence and immunoblotting.

Criteria were applied to the acetylome profile and resulted in 29 acetylated peptides that comply mostly with our aims of this project. Out of this list we choose the top 20 candidate Sirt2 substrate sites from synaptic proteins represented heat map in (Figure 3.19) that might be regulated by Sirt2 according to the KO/WT ratio difference.

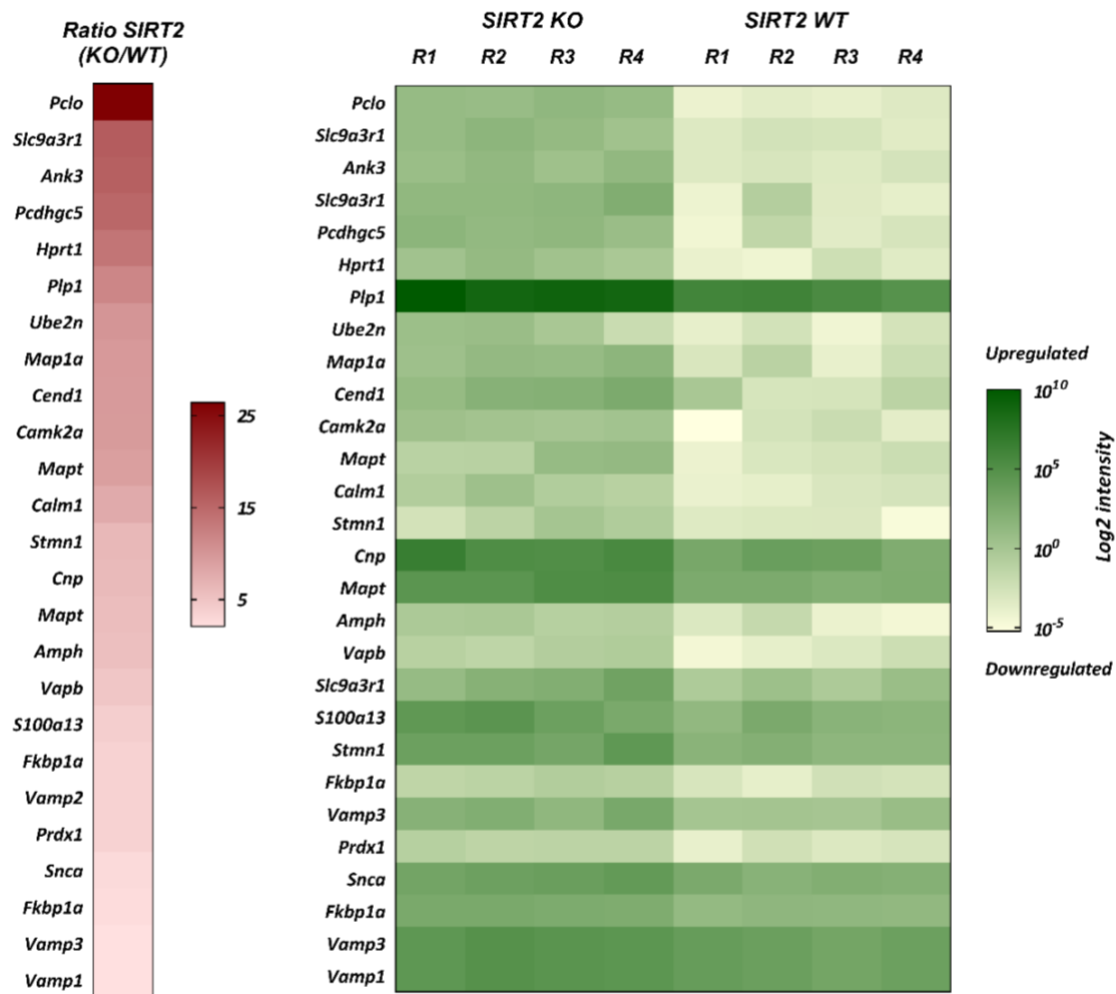


**Figure 3.20 – Heat map of highly acetylated peptides within the putative Sirt2 regulated dataset.** The first column represents highly acetylated peptides by fold change highest fold change (dark red). The second heat map was arranged according to fold change but demonstrated the (Log<sub>2</sub> intensity) of the acetylated peptides between four replicates of both groups Sirt2 KO (left), Sirt2 WT (right), highest intensity (dark green)

Sirt2 protein is localised in the cytoplasm and as far as we know it is the only cytoplasmic KDAC enzymes. To understand the impact of Sirt2 localisation on its deacetylase function we annotated the putative Sirt2 substrate to sub-cellular localisations determined by the human protein atlas using the gene names (Figure 3.19). As expected, we found that 41% were cytoplasmic proteins showing an over-representation compared to the complete set of acetylated proteins mentioned earlier in figure.3.12. 19%, 15% and 14% of identified putative Sirt2 substrates found in plasma membrane, mitochondria, and vesicle respectively. Interestingly, 32% of those substrates are localised to the nucleus.

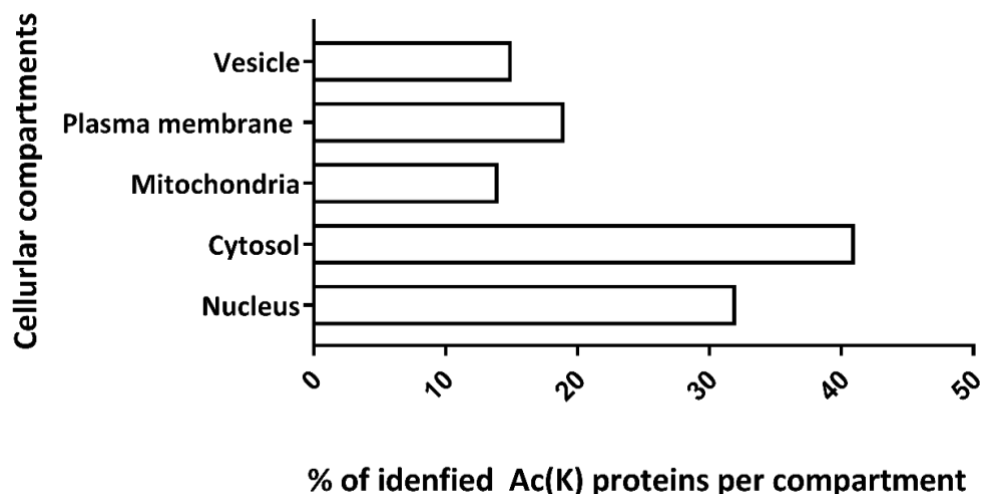
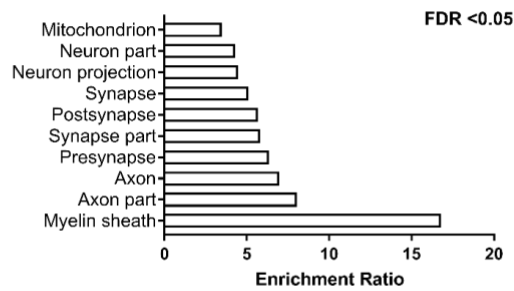


**Figure 3.21 –Cellular distribution of putative Sirt2 substrates.** Protein localisation annotation was mined from the Human Protein Atlas and shows that putative Sirt2 substrates are localised to many compartments, with the most localised to the cytosol.

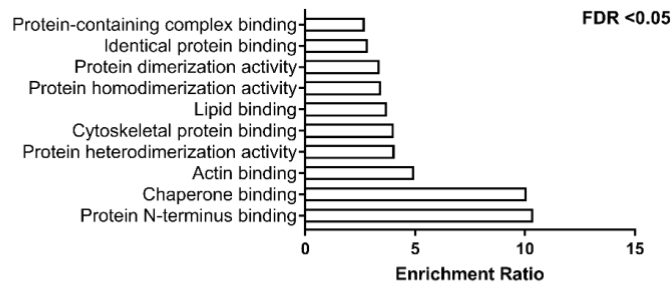
Next, a Gene Ontology (56) functional annotation analysis was performed to identify enriched gene ontology terms at  $p < 0.05$  for cellular components, molecular function, and biological processes associated with the set of putative Sirt2 substrates (Figure 3.20). Interestingly, in agreement with our previous results, Sirt2 and its potential substrates enriched significantly

in synapses, (pre-synapse) e.g. (VAMP1,2,3, SNCA and PCLO) were enriched. On the other hand, many identified substrates were related to myelin sheath (Slc25a5, Slc25a4 and Plp1), axon development and neuron development. Figure 3.20 displays some of those annotation results obtained using the mouse genome as a reference dataset and figure 3.21 using the brain proteome as a reference dataset to show results that are enriched within brain tissue (Michael et al., 2000, 2019, Carbon et al., 2021).

### Cellular Components



### Molecular Functions



### Biological Process

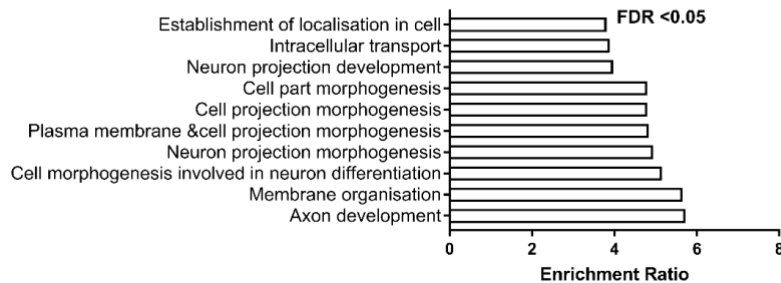
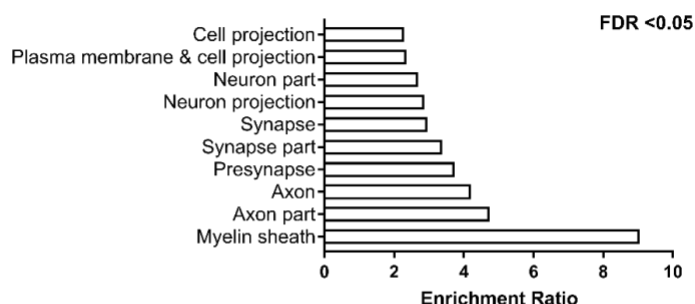
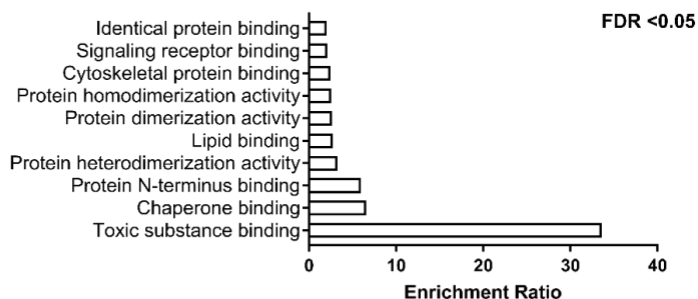


**Figure 3.22 – Gene ontology enrichment analysis of putative Sirt2 substrates compared to the mouse genome.** Significantly enriched proteins grouped into cellular component molecular pathways and biological processes. Gene ontology enrichment analysis was performed with an FDR < 0.05 using the WebGestalt gene toolkit (Wang et al., 2017b) with the mouse genome set as a reference for enrichment analysis.

### Cellular Components



### Molecular Functions



### Biological Process

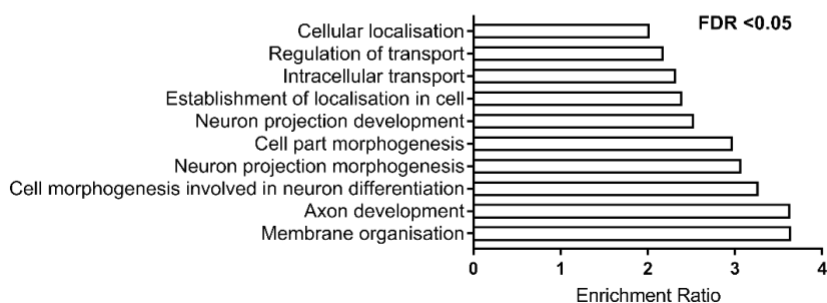


**Figure 3.23 – Gene ontology enrichment analysis of putative Sirt2 substrates compared to the brain proteome.** Significantly enriched proteins grouped into cellular component molecular pathways and biological processes. Gene ontology enrichment analysis was performed with an FDR <0.05 using the WebGestalt gene toolkit (Wang et al., 2017b) with the brain proteome set as a reference for enrichment analysis.

To understand the potential functions of Sirt2 through the identified putative substrates, we performed pathway enrichment analysis using PANTHER. Table 3.7 lists the most relevant pathways. The results show that Sirt2 substrates are involved with Parkinson's disease pathway, glycolysis and metabotropic/ionotropic glutamate receptor pathways. Interestingly, synaptic vesicle trafficking was enriched and included Vamp1 and Vamp2. Acetylation of these SNARE proteins has not been reported previously however, yet the identified lysine sites are known to be ubiquitinated (Yamazaki et al., 2013).

<b>Panther pathway</b>	<b>Numbers of proteins involved</b>
Metabotropic glutamate receptor group III pathway (P00039)	5
Parkinson disease (P00049)	5
Ionotropic glutamate receptor pathway (P00037)	5
Glycolysis (P00024)	4
Synaptic vesicle trafficking (P05734)	2
Cadherin signalling pathway (P00012)	2
p53 pathway (P00059)	1

**Table 3.7 Panther pathway enrichment analysis of the putative Sirt2 substrates.**

To investigate whether acetylation of lysine residues is correlated with neighbouring amino acids, sequence motifs of Sirt2 substrates were generated with pLogo with the mouse genome as the background, sequence windows +/- 7 amino acids were used in this analysis (Figure 3.22) (Joseph et al., 2013). This revealed that the -1 position frequently contained glutamic acid (E), alanine (A), glutamine (Q), whereas leucine (L) and arginine (R) frequently occur at +1 position. Consistent with previous acetylome studies, this result indicates that



The results indicate that ac(K) sites regulated by Sirt2 might be acetylated by all KAT groups, but KAT2B is potentially a critical KAT for those sites deacetylated by Sirt2 (Figure 3.23) (Wankun et al., 2016). Interestingly, KAT2B is a known Sirt2 interactor (Stark et al., 2006). In addition, KAT2A and KAT2B acetylate ACLY, a known Sirt2 substrate, which is identified in our study (Lin et al., 2013, Guo et al., 2019).

Another Sirt2 interactor EP300 was found in our brain acetylome data as mentioned earlier, EP300 acetylates Sirt2 resulting in a reduction of its activity (Han et al., 2008, Weinert et al., 2018). We compared our data to a CBP/EP300 knockout acetylome from mouse embryonic fibroblasts to identify which protein could be regulated by both enzymes (Weinert et al., 2018). 10% (23 sites out of 226) are possibly regulated by both Sirt2 and CBP/EP300. Given that the set of CBP/EP300 substrates was generated in a non-neuronal cell line, the overlap of substrates with Sirt2 would likely be higher in a neuronal system.

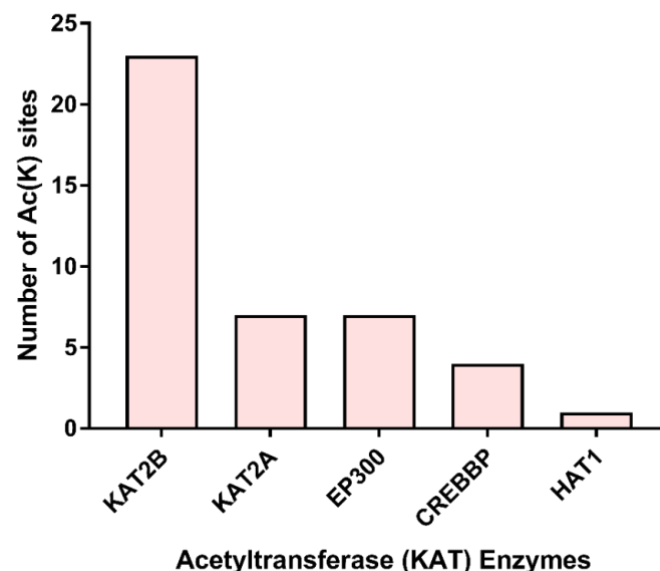


**Figure 3.25 – KAT2B and KATA2 are predicted to be the major KATs responsible for acetylation of putative Sirt2 substrates in the brain.** Bar charts represent GPS predictions for acetyltransferase groups that regulate identified sites from our study, peptide sequence windows of identified Ac(K) sites were analysed using GPS PAIL 2.0 software (Wankun et al., 2016).

### **3.3.3 Proteome profiling of Sirt2 knockout versus wild type mouse brain tissue**

In order to determine the effect of Sirt2 deletion of protein abundance, four Sirt2 KO and four Sirt2 WT brain tissue samples, (300µg of digested peptide) were collected for fractionation to perform protein expression profiling. Each sample was fractionated using high pH reversed phase chromatography into 36 fractions which were pooled into 12 final fractions for MS analysis. Each fraction was analysed using a 2-hour LC-MS/MS acquisition on an Orbitrap Elite using a Top20 CID method. Data were processed and quantified using MaxQuant (Cox and Mann, 2008). This approach was able to identify 5,797 proteins at an FDR of 1% at the peptide and protein 3,381 protein across a minimum of three replicates (**\*\*Supplementary Table 7.2**). Histogram plots of LFQ intensities were used to confirm that the data was normally distributed (Figure 3.24 A, B), shows a histogram plot for data before and after imputation. A multi-scatter was performed to check the data quality; replicates of Sirt2 KO and WT LFQ intensities showed a good correlation across replicates (Table 3.8).

\*\*(<https://figshare.com/s/13750b8c09063b5cb9eb>)

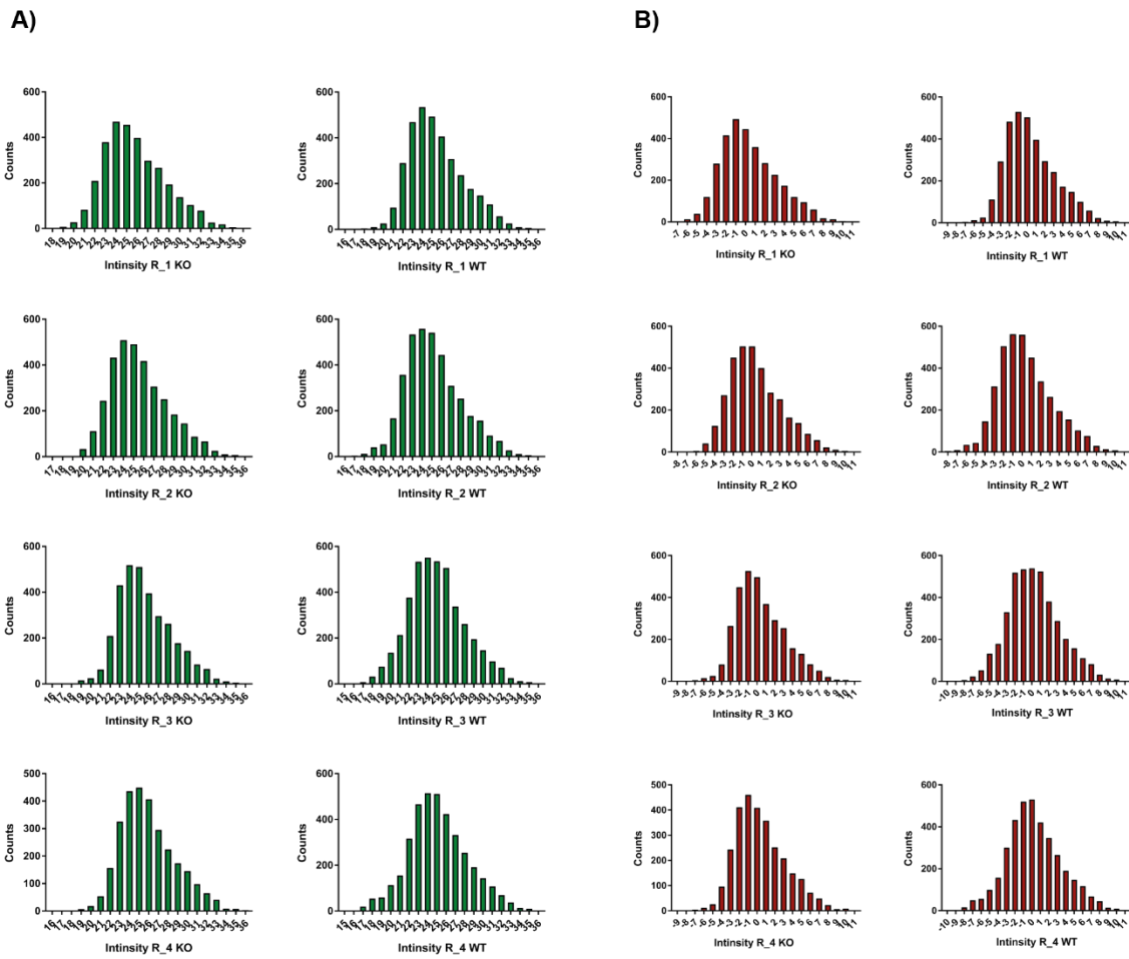


**Figure 3.26– Histogram of imputed LFQ intensity values for Sirt2 KO versus Sirt2 WT samples.**  
 A) Histogram of LFQ intensity values for replicates of Sirt2 KO versus Sirt2 WT proteome profiling samples. B) Histogram of imputed LFQ intensity values for replicates of Sirt2 KO versus Sirt2 WT proteome profiling samples.

LFQ intensity KO01	LFQ intensity KO02	LFQ intensity KO03	LFQ intensity KO04	LFQ intensity WT01	LFQ intensity WT02	LFQ intensity WT03	LFQ intensity WT04	
NaN	0.967	0.950	0.921	0.941	0.933	0.936	0.936	LFQ intensity KO01
0.967	NaN	0.976	0.945	0.966	0.957	0.945	0.947	LFQ intensity KO02
0.950	0.976	NaN	0.957	0.975	0.966	0.942	0.934	LFQ intensity KO03
0.921	0.945	0.957	NaN	0.954	0.932	0.901	0.928	LFQ intensity KO04
0.941	0.966	0.975	0.954	NaN	0.97261	0.942	0.934	LFQ intensity WT01
0.933	0.957	0.966	0.932	0.973	NaN	0.958	0.925	LFQ intensity WT02
0.936	0.945	0.942	0.901	0.942	0.958	NaN	0.931	LFQ intensity WT03
0.936	0.947	0.934	0.928	0.934	0.925	0.931	NaN	LFQ intensity WT04

**Table 3.8 – Multi-scatter plots of Sirt2 WT and KO proteome profiling samples.**

These Pearson correlation values show that biological replicates from 8 mice brain tissue were similar with very little difference between groups. Green boxes represent a high correlation between samples.

We performed a bioinformatics analysis of Sirt2 KO versus WT protein profile to proteins identified from brain proteome (Kirti et al., 2015) and found that 97% of those proteins were previously identified. On the other hand, we mapped identified proteins to mouse synapse proteome (Bayes et al., 2017); 2,492 proteins (73%) out of 3,381 proteins are known synaptic proteins.

A statistical analysis of the protein abundance levels between Sirt2 WT and Sirt2 KO mouse tissue was performed using Perseus (Tyanova et al., 2016). Data were filtered to keep proteins quantified in at least three replicates of each group. Data were normalised by subtracting the median values of each sample and missing data were imputed with a width of 0.3 and downshift of 1.8 from the standard deviation of the distribution. Statistical analysis (t-test) was performed to identify proteins with differential abundance with a permutation-based FDR of 5% (Tyanova et al., 2016). 16 proteins exhibited a significant expression level change, nine in Sirt2 KO (most prominent of which was Sirt2 itself which was absent in the KO samples) and seven in Sirt2 WT. A volcano plot shows protein expression profile changes between two

groups; the right side represents proteins that significantly increase because of Sirt2 gene knockdown, while the left side represents proteins that significantly decreased (Figure 3.25). The protein abundance profile was compared to the putative Sirt2 substrates identified from the acetylome profile shown earlier in figure 3.17. We found that proteins regulated by Sirt2 did not exhibit any changes in expression levels, which showed that changes in acetylation have not shown an effect on proteins stability for the proteins analysed.

On the other hand, 36 proteins are known as Sirt2 interactors according to BioGRID dataset (Stark et al., 2006), but none of those interactors expressed any significant changes in protein level. In addition, we were able to detect three KDAC enzymes SIRT5, Sirt2, and its interactor HDAC6, with no sign of any KAT enzymes. However, p300 was identified in our acetylome Sirt2 KO dataset. The KAT enzymes mentioned earlier are previously identified and expressed in brain tissue (64); thus, they might have a regulatory role.

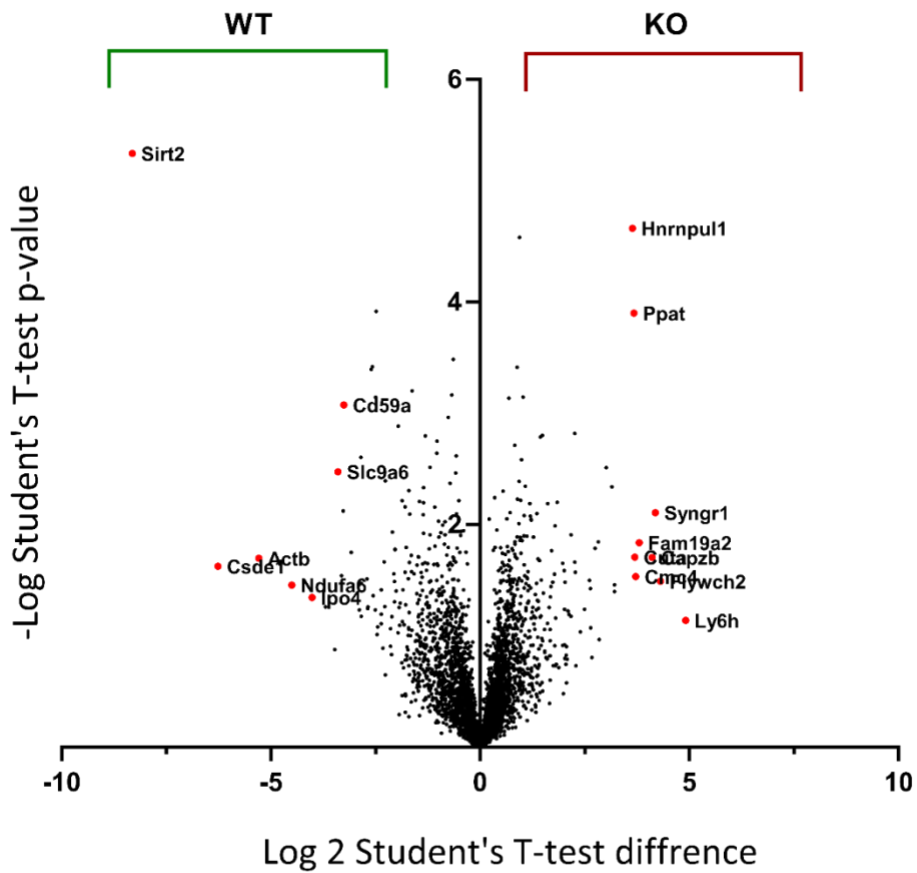


**Figure 3.27 – Volcano plot of differential protein abundance in Sirt2 KO versus WT brain tissue.** Statistical analysis was performed with a permutation-based FDR of 5%. Red dots represent peptides with significantly changed proteins level. Analysis was applied on 3,381 proteins identified in at least three replicates of one group.

### **3.4 Discussion**

#### **3.4.1 Mouse brain acetylome**

Overall, I successfully identified 2,602 ac(K) sites on 983 proteins from mouse brain tissue with a purity of 44% acetylated peptides; a previous study had identified 4,782 ac(K) sites on 1,653 proteins from rat brain tissue (Lundby et al., 2012b). Comparable methods were used; in the rat brain tissue study, both lys-C and trypsin enzymes were used for digestion. However, peptides were deep fractionated by strong cation-exchange (SCX) and immunopurification was performed on each fraction. Whilst our dataset is not as deep, it was generated using a cheaper/efficient method (Lundby et al., 2012b). Comparing those two datasets, we found 56% overlap in acetylated proteins; this suggested that Sirt2 KO brain tissue revealed new acetylation sites not previously detectable. 2,054 ac(K) sites quantified across a minimum of three replicates in either group, 1,676 (>80%) sites derived from synaptic proteins (Bayés et al., 2017), which count as supportive evidence to what we suggested earlier in this chapter that the majority of synaptic proteins identified are subject to acetylation.

According to the phosphosite acetylation database, the majority were novel ac(K) sites, with 58% of the identified mouse brain (Signling, 2017). Since identifying other KDACs enzymes in the protein expression profile of Sirt2KO/WT brain tissue is limited to SIRT5 and HDAC6, we suggest that the deletion of Sirt2 could have a more significant impact on the loss of deacetylase function in the brain. More evidence about the localisation of those sites, mainly nucleus as expected (Kim et al., 2006a, Yang and Seto, 2008, Choudhary et al., 2009b), cytoplasm, mitochondria, and cell membrane, this distribution agrees with literature. Lysine acetylation is not limited to the nucleus. Cytoplasmic and mitochondrial acetylation is related

to significant pathways and functions(Pereira et al., 2012, Liu et al., 2017a, Esteves et al., 2018, Choudhary et al., 2009a, Ali et al., 2018).

In terms of acetylation occurring in the brain, the protein expression profile of Sirt2 KO/WT has failed to identify KAT enzymes, yet EP300 was found in Sirt2 KO/WT acetylome profile. In addition, we could not identify any KATs in the mouse synapse proteome. But earlier, we found that some identified ac(K) peptides might be regulated by KAT2a and KAT2b. These results raise the possibility that either protein is acetylated before trafficked to synapses or that synaptic protein is acetylated by a non-enzymatic mechanism.

### ***3.4.2 Characterisation of the Sirt2-regulated mouse brain acetylome***

Previous proteomic studies have established that Sirt2 is the major KAT present in the synapse proteome. Studies have highlighted the importance of acetylation and its regulation by Sirt2 for synaptic proteins such as AMPAR and Arc protein (Wang et al., 2017a, Lalonde et al., 2017). However, our knowledge about the full complement of synaptic substrates of Sirt2 is limited. To address this, I optimised and applied a powerful MS-based quantitative acetylomics strategy to identify 226 ac(K) sites significantly increased in Sirt2 KO versus WT brain tissue. Although this is not a direct confirmation that Sirt2 is responsible for their deacetylation, this putative site dataset represents a useful dataset of acetylation sites likely regulated by Sirt2 in vivo. 197 of those ac(K) sites map to known synaptic proteins, some of which are enriched in pre-or postsynaptic fractions (Bayés et al., 2017). The fact that such a large fraction of putative substrates of Sirt2 are present at synapses reinforces our hypothesis that Sirt2 is the major synaptic KAT.

Given that only 24% of these putative Sirt2 sites were previously identified (Signling, 2017), it suggests that the deletion of the Sirt2 gene had a major impact on the deacetylate function

in the brain. Sites that would not normally remain acetylated under normal circumstances accumulate in the absence of Sirt2 and potentially contribute to the phenotypes of these mice. The Sirt2 gene deletion influences the nervous system's normal behavioural function. Adult Sirt2 KO mice demonstrated abnormal synaptic plasticity, as well as learning and memory deficits, as shown previously (O'Connor et al., 2020, Wang et al., 2017a). In another study, middle-aged Sirt2<sup>-/-</sup> mice showed locomotor dysfunction due to axonal degeneration, but this effect was not seen in young Sirt2 KO mice (Fourcade et al., 2017, Wang et al., 2017a). These are consistent with our findings; putative Sirt2 substrates were significantly enriched in pre-synapse and axon compartment, including protein that might be linked with phenotypes seen earlier, such as Map2, Map, Camk2a, Snap91, Amph and others (2019). However, existing literature suggests that the Sirt2 role may be age-dependent (Wang et al., 2019b).

As mentioned previously, we applied some criteria to the putative Sirt2 list that resulted in 29 acetylated peptides on synaptic proteins for prioritisation for functional analysis. First, protein piccolo (PCLO) is acetylated on three sites (K957, K373, and K616); Sirt2 regulates only one site (K957); those other sites are novel according to the Phosphosite database (Signling, 2017). PCLO is an essential synaptic protein involved in pre-synapse active zone functions such as vesicle clustering and exocytosis (Ivanova et al., 2015). There is no evidence in the literature about the functional effect of acetylation of this protein. Calcium/Calmodulin-dependent protein kinase type II subunit alpha (CAMK2a) is another crucial synaptic protein enriched in the postsynaptic density (Bayés et al., 2017) and involved in synaptic plasticity and long-term potentiation (Zhang et al., 2021, Incontro et al., 2018). We identified six acetylation sites in our data, and K68 site significantly increased Sirt2 KO brain tissue; this site is conserved among species and can also be ubiquitinated (Udeshi et al., 2013, Wagner et al., 2012).

Microtubule-associated protein Tau (MAPT) K613 and K661 sites were acetylated significantly in Sirt2 KO. MAPT acetylated on more than ten sites causes its accumulation, contributing to many neurodegenerative illnesses, specifically Alzheimer's disease (AD) and Tauopathies (Saha and Sen, 2019, Carlomagno et al., 2017, Cook et al., 2014). It has been reported that SIRT1 deacetylates MAPT but not Sirt2; however, our data suggest that this protein could be deacetylated by both enzymes (Min et al., 2018b, Carlomagno et al., 2017, Min et al., 2010). In addition, Vesicle-associated membrane protein2/3 (VAMP2/3) is acetylated on three sites, none of which were reported previously (Signling, 2017) and K59 and K83 was significantly increased in Sirt2 KO mice. Those sites are all conserved between VAMP2 and VAMP3 and among species and are known ubiquitination sites (Signling, 2017, Yamazaki et al., 2013). Previous studies have suggested that E3 ubiquitin ligases regulate the recycling endosome trafficking of VAMP3, which might be disturbed by acetylation (Yamazaki et al., 2013)

Alpha-synuclein (SNCA) is one of the most characterised acetylated proteins in the brain with significant involvement in neurodegenerative diseases. Our data found five ac(K) sites, of which K96 was significantly increased in acetylation in Sirt2 KO tissue. Studies suggest that deacetylation of SCNA by Sirt2 prevents neurotoxicity resulting from SNCA aggregation caused by acetylation (Bhattacharjee et al., 2019, Rita Machado de et al., 2017).

Sites related to the putative Sirt2 substrates showed an overrepresentation in the cytoplasm, which agrees with the Sirt2 localisation we showed in HeLa cells using immunofluorescence microscopy. As the literature suggested, it is the only KDAC present in the cytoplasm (ProteomicsDB, 2017, North et al., 2003).

Interestingly, our data revealed that more than 50% of those substrates are distributed in other compartments. The distribution of putative Sirt2 substrates is consistent with previous

studies showing Sirt2 activity in the mitochondria (2021, Liu et al., 2017c, Chamberlain et al., 2021) and nucleus (North and Verdin, 2007, de Oliveira et al., 2012) proteins, which provides further evidence to support that Sirt2 shuttle between cytoplasm and nucleus and deacetylate Histone 4 and 6 (North and Verdin, 2007, Herskovits and Guarente, 2013, Vaquero et al., 2006).

Amongst the set of putative Sirt2 substrates is an enrichment in proteins regulating the myelin sheath and axon development, a connection that has been previously discussed (Liu et al., 2017b, 2021, Chamberlain et al., 2021). Putative Sirt2 substrates such as Slc25a5, Slc25a4, Plp1, Mbp, and Mapt require the deacetylase function of Sirt2 to contribute to myelination and mitochondrial energy production especially in long axons and synapses (Liu et al., 2017b, 2021, Chamberlain et al., 2021). Furthermore, identified related pathways are primarily consistent with the Sirt2 function associated with Parkinson's disease, glycolysis, and metabotropic and ionotropic glutamate receptor pathways (Spinelli et al., 2014, Chen et al., 2015, Rita Machado de et al., 2017, Wang et al., 2017a).

### **3.4.3 Sirt2 KO versus WT proteome profile**

Finally, I successfully identified 3,381 proteins from Sirt2KO/WT brain tissue at FDR of 1%, 73% of those proteins were found previously in mouse synapse proteome (Bayés et al., 2017), and 97% in mouse brain proteome (Kirti et al., 2015). None of the putative Sirt2 substrates identified from the acetylome profile exhibited changes in expression levels, changes in acetylation do not affect protein stability. Still, as stated before, it contributes to many cellular and molecular functions.

Overall, these findings further support the hypothesis of the regulatory role of acetylation and the deacetylase enzymes Sirt2 on synaptic protein function. We believe these results will

advance the understanding of the involvement of Sirt2 in neurodegenerative diseases and help link those substrates with specific processes downstream of Sirt2.

#### ***3.4.4 Acetylome analysis technical points***

From a technical point of view, it was challenging to extract proteins from a complex sample such as a mouse brain. This experiment also requires an extracted protein and digested peptide compatible with acetyl-lysine enrichment and easy to measure with a sensitive method such as LC-MS/MS. Many studies have used the FASP sample preparation method with different tissue and cell lines, which was successful (Wisniewski et al., 2009). In addition, this method had been used in Collins's lab and was able to identify >10,000 Ac(K) sites in ES cells (data not published). Unfortunately, the FASP method was challenging for many reasons; the use of lysis buffer that contained SDS, which was challenging to remove, might cause poor protein digestion and acK peptide enrichments. Thus, sample preparation methods were changed to acetone precipitation, resulting in an improvement in the number of peptides/proteins identified in test digests and acetylated peptides from ac(K) enrichment from these samples.

## **CHAPTER 4**

### ***Acetylation profiling of young versus old mouse brain tissue***

#### **4.1 Introduction**

Lysine acetylation became a popular topic in the past decade; the fact that acetylation is not exclusive to histones or nuclear proteins has increased the curiosity to understand more about this modification which has been shown to occur in many other cellular compartments (Yang and Seto, 2008, Choudhary et al., 2009b, Lundby et al., 2012b, Zhou et al., 2016b, Revollo et al., 2004). Lysine acetylation has been linked strongly with neuronal function and dysfunction. Evidence shows it contributes to many neurodegeneration diseases such as AD, PD (5-7) and other age-related diseases such as cardiovascular diseases (Parodi-Rullán et al., 2018).

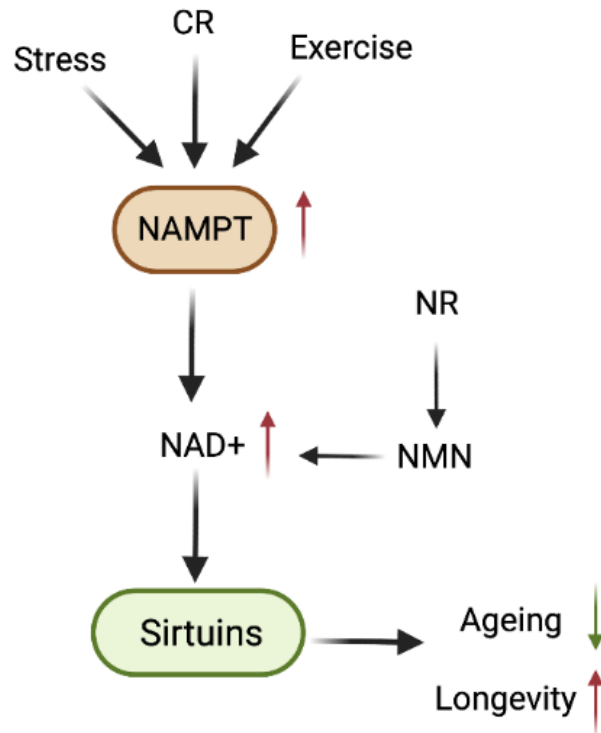
Global changes in gene expression were observed in ageing animals; when animals age, epigenetic marks such as histone acetylation change dramatically (López-Otín et al., 2013, Peleg et al., 2016). These age-dependent changes in histone acetylation are associated with changes in metabolic activity and, as a result, influence global gene expression (Pietrocola et al., 2015).

Studies showed that some ageing hallmarks are associated with acetylation, which may be altered because of mitochondrial dysfunction. It is known that acetylation depends on acetate/acetyl-CoA production in the mitochondria as a source of acetyl groups (Yu et al., 2021, Mouchiroud et al., 2013). In addition, mitochondrial contributes to many biological processes, such as the homeostasis of NAD<sup>+</sup>. NAD<sup>+</sup> biosynthesis is influenced by age as a result of CD38 protein upregulation which competes with sirtuins for NAD<sup>+</sup> as a substrate (Camacho-Pereira et al., 2016). Sirtuins de-acetylation activity is reduced by a lack of NAD<sup>+</sup>, resulting in hyper-acetylation of some key proteins, which may contribute to age-related mitochondrial dysfunction and oxidative damage (Imai and Guarente, 2014).

Although, acetylation is highly enriched in the brain (Lundby et al., 2012b), although it was suggested that acetylation levels changes with age, many studies were interested in investigating the role of KDAC enzymes and how acetylation levels changes during ageing (Braidy et al., 2015, Satoh et al., 2017, Wagner and Payne, 2011).

As previously mentioned, overexpression of Sir2 gene showed an improvement in longevity in flies, worms and yeasts (Rogina and Helfand, 2004, Frankel et al., 2011). Studies showed that at least three members of the sirtuin family, SIRT1, SIRT3, and SIRT6, have contributed to healthy ageing in mammals (López-Otín et al., 2013, Santos-Barriopedro et al., 2018, Camacho-Pereira et al., 2016). For example, overexpression of SIRT1 in transgenic mice enhances aspects of health during ageing, such as genomic stability and metabolic efficiency, but not longevity (Serrano et al., 2010, López-Otín et al., 2013). On the other hand, SIRT3 has been reported to mediate some of the longevity-promoting effects of caloric restriction (CR) via SIRT3 role in impact on mitochondrial protein de-acetylation.

It was proposed that in response to calorie restriction, exercise, and stress, NAD<sup>+</sup> levels increase and activate sirtuins. Upregulation of nicotinamide phosphoribosyl transferase (NAMPT) activates the NAD<sup>+</sup> biosynthesis pathway, which stimulates Sirtuins activity in the nucleus and mitochondria, leading to increased longevity and decreased ageing as show in (figure 4.1) (Revollo et al., 2004). However, until now, little is known about how acetylation levels in the brain change during ageing.

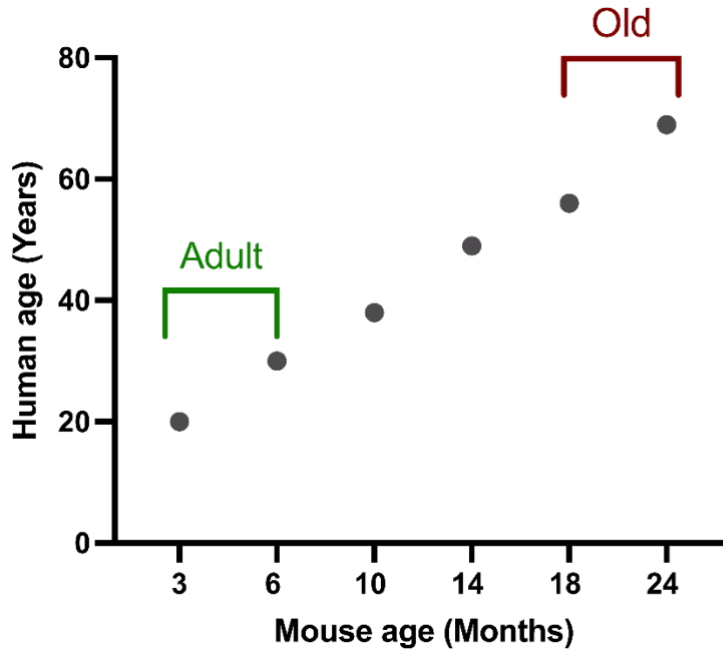



---

**Figure 4.1 – NAD<sup>+</sup> biosynthetic enzyme (NAMPT) and sirtuin responses to dietary and environmental changes control ageing and longevity.** caloric restriction (CR), Nicotinamide riboside (NR), nicotinamide mononucleotide (NMN) (Imai and Guarente, 2016).

Mice and human age are different, but it is comparable, and mouse and mouse tissue have been used in many ageing studies. For example, adult mouse 3 to 6 months equals 20-38 years in humans while 18-24 months is comparable to 56-69 years old in humans (Fox, 2006).

Life phase equivalences of mice and humans are shown in figure 4.2.



---

**Figure 4.2 – Life phase equivalences of mouse and human.** This graph illustrates mouse age in months and its correspondence to human age in years. Adult (young) mouse 3 to 6 months equals 20-38 years in human while 18-24 months considered as old in mouse compared to 56-69 years old in human. Adapted from (Fox, 2006).

## **4.2 Aims**

This chapter investigates the changes in acetylation levels in the brain with ageing. This aim will be achieved by performing a quantitative acetylome analysis of old (24 months old) versus young (2 months old) mice brain tissue using immunoaffinity enrichment of acetylated peptides and LC-MS/MS to quantify changes in acetylation levels.

## **4.3 Results**

### **4.3.1 Acetylome analysis of Old (24 months) versus Young (2 months) mouse brain tissue**

#### **4.3.1.1 Optimisation of brain tissue acetylome using S-trap digestion column**

According to many studies and our work in the Collins lab, the S-trap digestion method provides very reliable results in a short sample processing time compared to acetone precipitation and FASP methods used in chapter 3 (Ludwig et al., 2018). Three test experiments were performed using S-trap midi columns ( $\geq 300 \mu\text{g}$ ) to optimise the method with brain tissue before applying the optimised methods to old and young mouse brain samples. Brain tissues used during the optimisation steps were aged (24months). In the first attempt, we used 5% SDS extraction buffer as advised, results were satisfactory with of 1,766 proteins identified from 35ug of a protein digest analysed using a 2 hour- Top20 LC-MS/MS method, 80% of those proteins identified were synaptic proteins (Bayés et al., 2017) as demonstrated in (Figure 4.3.A). Extracting 1,489 synaptic proteins shows the ability of SDS to extract cell membrane proteins. However, when these results were compared to our Sirt2 KO acetylome profile, we noticed a loss of around 30% of total identified proteins, which may affect the number of ac(K) sites that need to be identified later. In addition, in chapter 3, SDS detergent was avoided because our data showed that SDS is not compatible with acetyl-lysine peptide enrichment.

In the second test experiment, protein extraction was repeated with 5% SDS buffer parallel with 1% sodium deoxycholate (Doc) buffer, as shown in figure 4.3.B. We were able to identify >2,400 proteins and >80% synaptic proteins from 35ug of a protein digest analysed by a 2-hour Top20 LC-MS/MS analysis. It was challenging to perform an acetyl-lysine enrichment during the optimisations for sample preparation, instead acetylated proteins identified from Sirt2 KO (1,533) were mapped to the identified protein from both buffers. 5% SDS was able

to identify 656 proteins, and 1% Doc identified 671. Both iBAQ and LFQ intensity were similar (Figure 4.3), suggesting that in our experiments 1% Doc could replace 5% SDS.

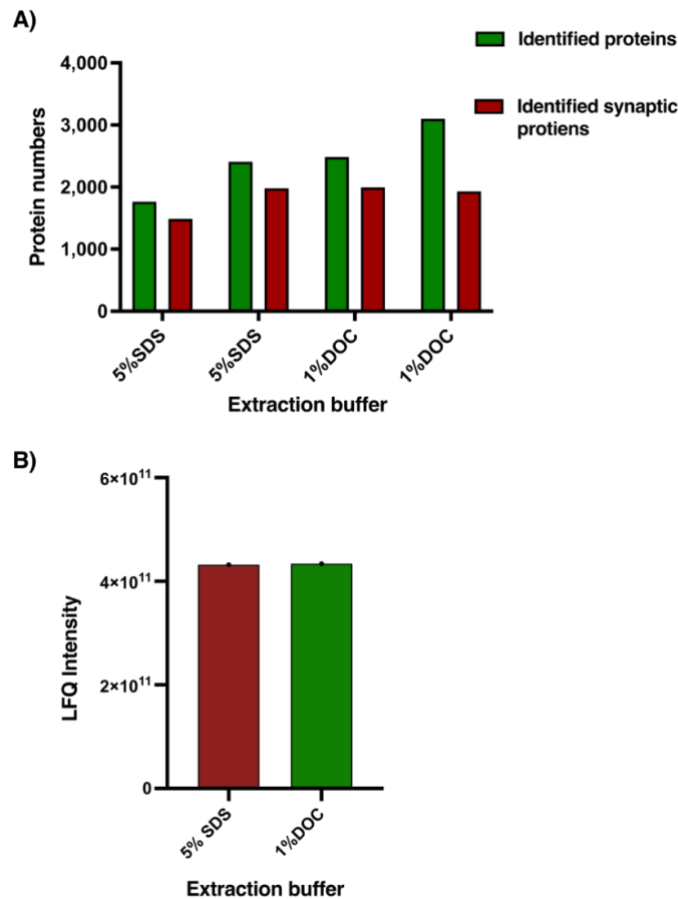


**Figure 4.3 – Optimisation of protein extraction from brain tissue samples for S-trap digestion.** **A)** Bar chart represents a comparison of total proteins number (green) and synaptic proteins number (red) (Bayés et al., 2017), of proteins extracted with buffers containing either 5% SDS or 1% Doc, from mouse brain tissues was optimised using S-trap digestion methods. Proteins extracted by 1% Doc buffer showed a better protein yield than the other with no observed change in synaptic proteins number. **B)** Bar chart represents a comparison of LFQ intensity of proteins extraction from mouse brain tissues was optimised using S-trap digestion methods. Proteins extracted with buffers containing either 5% SDS or 1% Doc, both were repeated twice. Both 5% SDS (red) 1% Doc (green) extracted similar protein numbers; results showed a similar sample intensity from both buffers.

#### 4.3.1.2 Quantitative acetylome analysis of old versus young mouse brain tissue

Next, four old (24 months) and four young (2 months) mouse brain tissues were used for acetylome analysis. Proteins were extracted with 1% Doc buffer and digested into peptides using an S-trap digestion column followed by acetylated peptide enrichment using acetyl-lysine immunoaffinity beads. Samples were desalted and concentrated using Stage-tips. Acetylated peptides were analysed using a 2-hour LC-MS/MS acquisition on an Orbitrap Elite using a Top20 CID method. Data were processed and quantified using MaxQuant (Cox and Mann, 2008). This approach enabled us to identify a total of 2,885 ac(K) sites on 3,563 ac(K) peptides from 1,223 proteins at an FDR of 1% (\*\***Supplementary Table 7.3**). The overall purity of these acetyl-lysine purifications was 37% which was lower than that achieved for Sirt2KO versus WT samples (44%), but the higher level of acetylation in the absence of Sirt2 may have led to an increase in ac(K) peptide purity in these samples (table 4.1).

Identified Proteins	Identified Peptides	Ac(K) peptides	% Ac(K) peptides
1,922	9,516	3,563	37%

**Table 4.1 – Summary of proteins and peptides identified in an acetylome analysis of brain tissue from old versus young mice.**

We performed a statistical analysis on four replicates of each group (old and young) using Perseus, 2,496 ac(K) sites from 1,091 proteins were quantified in at least 3 replicate samples in one group. 77% (1,932) of those sites were acetylated on synaptic proteins (Bayés et al., 2017).

\*\*(<https://figshare.com/s/13750b8c09063b5cb9eb>)

Histogram plots of Log2 transformed intensities of each replicate confirm that the data was normally distributed (Figure 4.4). The fourth replicate of the young brain tissue had low peptide intensities and was reanalysed again by mass spectrometry using the same volume of the same sample. The intensity distribution was slightly higher than other replicates from both groups. A multi-Scatter plot in (Table 4.2) illustrates the quality of the experiments we performed, a good correlation within the group, and a slightly low correlation between the two groups because of the fourth replicate of the young brain tissue group; overall, the results from this approach shown a reproducible result.

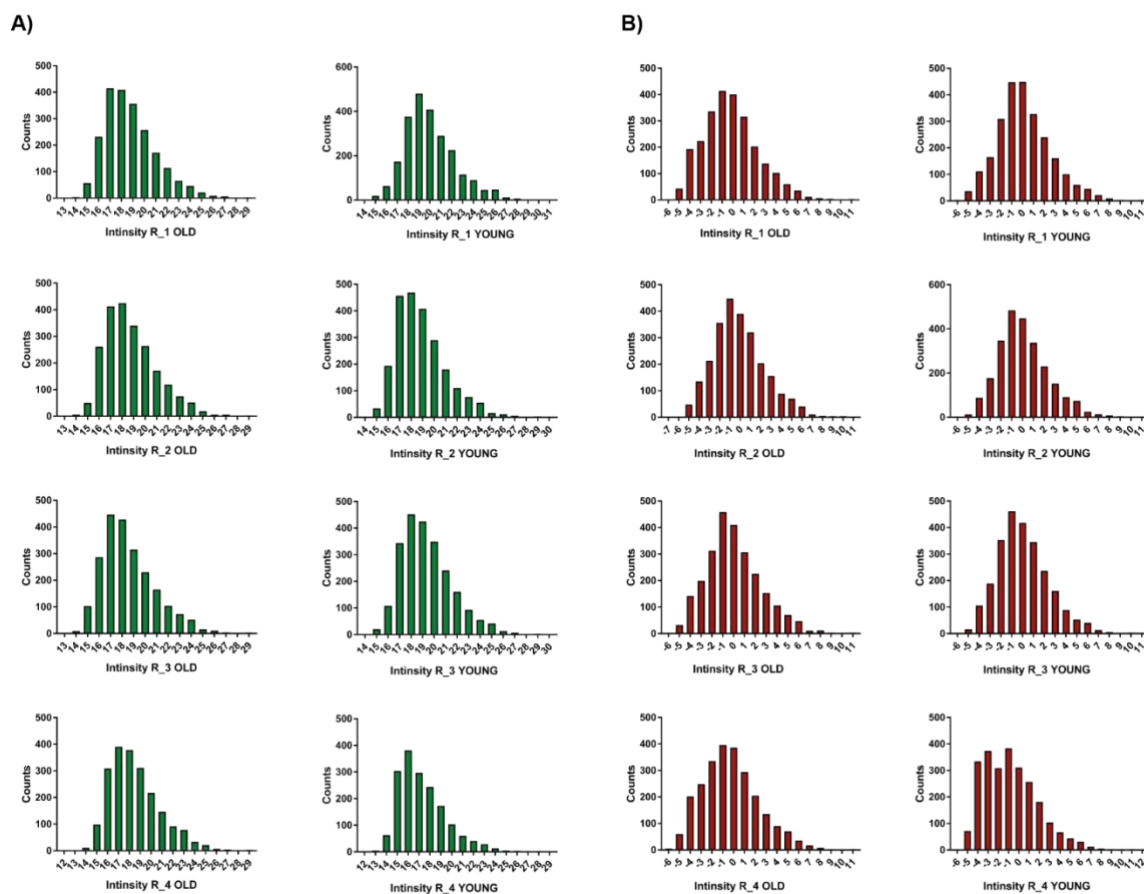


**Figure 4.4 – Histogram of ac(K) site intensity values for replicates of old versus young acetylomes. A) showing a normally distributed intensity. B) normalised with imputed intensity values for statistical analysis.**

Intensity Old-R1	Intensity Old-R2	Intensity Old-R3	Intensity Old-R4	Intensity Young-R1	Intensity Young-R2	Intensity Young-R3	Intensity Young-R4	
NaN	0.944	0.920	0.938	0.950	0.865	0.873	0.757	Intensity Old-R1
0.944	NaN	0.958	0.947	0.895	0.864	0.898	0.774	Intensity Old-R2
0.920	0.958	NaN	0.963	0.897	0.883	0.896	0.824	Intensity Old-R3
0.938	0.947	0.963	NaN	0.912	0.853	0.873	0.822	Intensity Old-R4
0.950	0.895	0.897	0.912	NaN	0.857	0.851	0.767	Intensity Young-R1
0.865	0.864	0.883	0.853	0.857	NaN	0.942	0.827	Intensity Young-R2
0.873	0.898	0.896	0.873	0.851	0.942	NaN	0.784	Intensity Young-R3
0.757	0.774	0.824	0.822	0.767	0.827	0.784	NaN	Intensity Young-R4

**Table 4.2- correlation values of old and young replicate datasets.**

The table represents the Pearson correlation of the biological replicates high (green), middle (yellow), low (red). Correlation in the same group was highest of 0.95; in between groups, the lowest was 0.76. These show that biological replicates inside the same groups were reproducible.

Next, we performed a bioinformatics analysis to determine which sites were novel or previously known. 2,496 ac(K) sites were compared to the mouse acetylation sites dataset in the Phosphosite database and revealed that 1,222 ac(K) sites were known, and (1,274) sites were novel (Figure 4.5.A) (Signling, 2017). In addition, to assess the crosstalk between lysine acetylation and ubiquitination in this dataset of 2,496 ac(K) sites, they were mapped to the mouse ubiquitination site dataset from Phosphosite. We found that 1,072 Ac(K) sites (42%) were previously shown to be ubiquitinated (Figure 4.5.B).

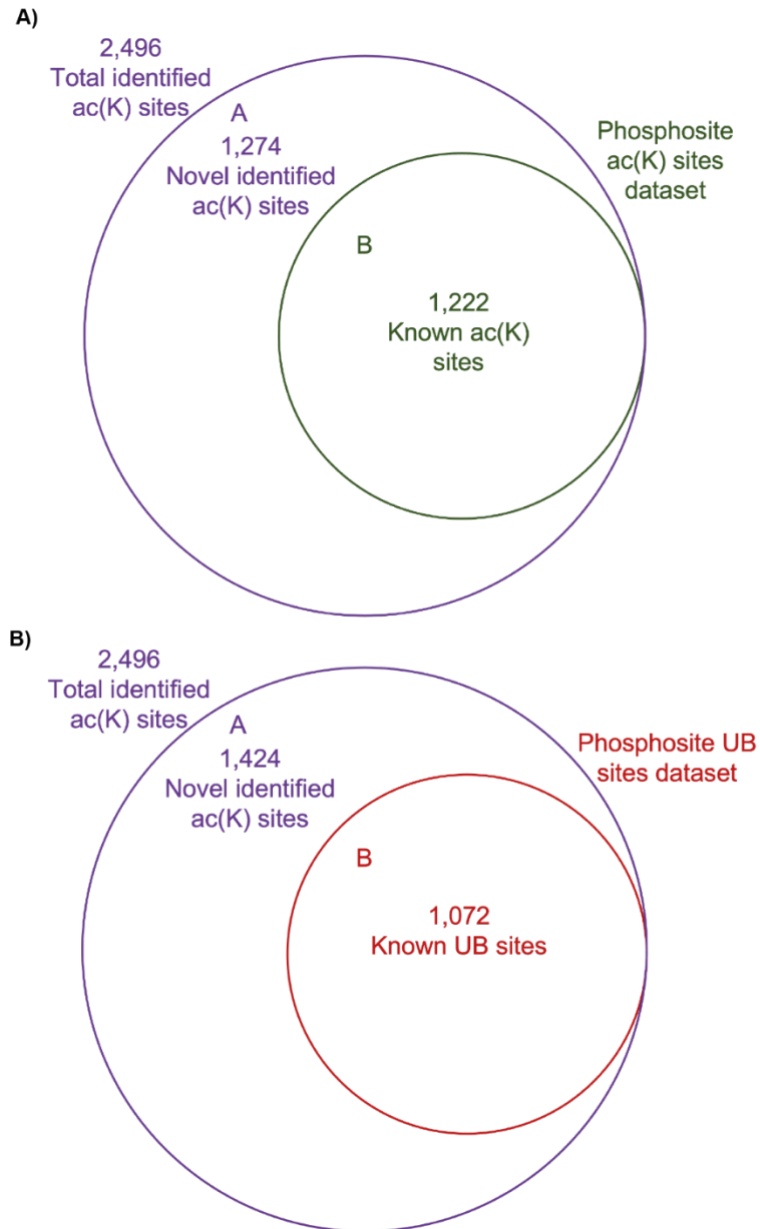
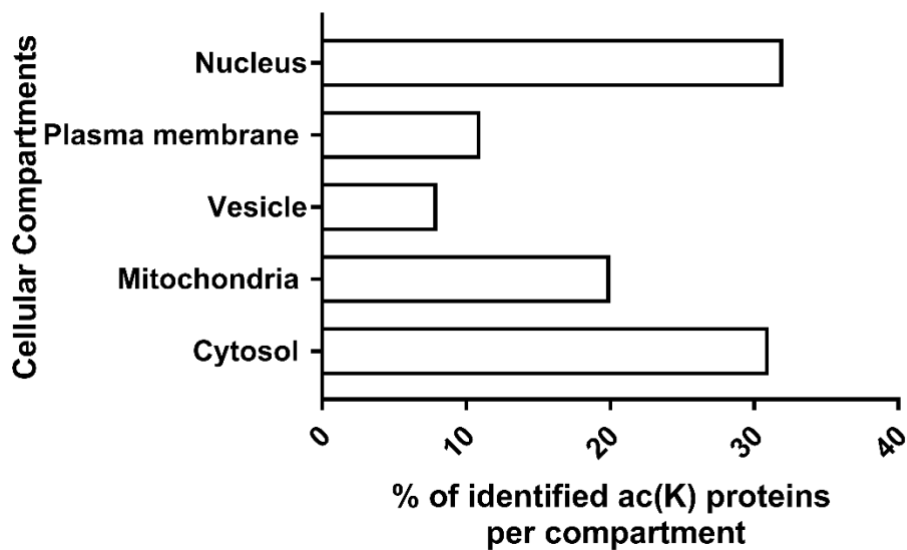


**Figure 4.5 – Known acetylated and ubiquitinated sites** **A)** Venn diagram of known and novel acetylated sites in the old versus young brain acetylome dataset. 2,496 ac(K) sites identified (purple) were compared to a mouse acetylation site mouse dataset (24). 1,222 are known(K) sites (green) and 1,274 are novel. Bioinformatics analysis compared peptide sequence windows containing lysine sites +/- 7 amino acids from both datasets. **B)** Venn diagram illustrating PTM crosstalk between acetylation and ubiquitination sites 1,072 sites (red) out of 2,496 ac(K) sites (purple) are known ubiquitination sites. Bioinformatics analysis compared peptides sequence windows containing lysine site +/- 7 amino acids from our acetylome dataset and the Phosphosite ubiquitination sites dataset.

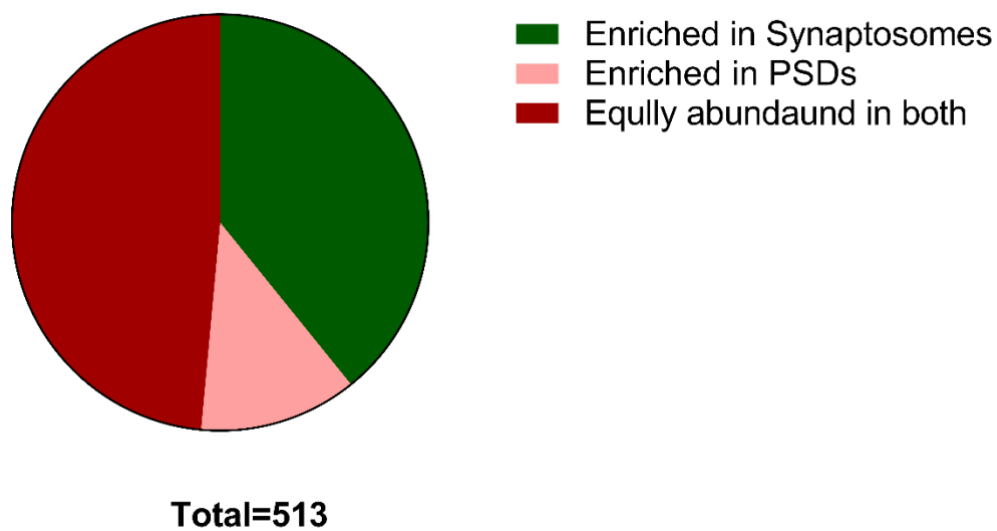
Since lysine acetylation modification occurs in almost all cellular compartments, the cellular distribution of old versus young brain acetylome profile was investigated by annotating to sub-cellular localisations determined by the human protein atlas . Identified ac(K) proteins were distributed in almost all the subcellular compartments, with 32% localised to the nucleus, 30% in the cytoplasm, and 20% in mitochondria (Figure 4.6). Unsurprisingly, many histones >300) ac(K) sites were identified in our dataset.



---

**Figure 4.6 –Cellular distribution of ac(K) proteins and sites identified from old versus young mouse brain tissue.** Protein localisation annotation was mined from the Human Protein Atlas (14), showing that *lysine acetylation modification occurs in almost all cellular compartments.*

As mentioned above, the majority of the identified ac(K) sites (1,932) from old versus young acetylome profiles occurred on synaptic proteins (Bayés et al., 2017). We performed a bioinformatics analysis of acetylated synaptic proteins and their enrichments in synaptosome and PSD fractions of our synapse proteome dataset. As shown in figure 4.7, most identified acetylated are equally abundant in both PSDs and synaptosomes. Still, more were significantly enriched in synaptosomes with 202 proteins out of 513, indicating a possible role of acetylation in pre-synaptic function.



---

**Figure 4.7 – Identified acetylated proteins are enriched in synaptosomes, and PSDs**  
Bioinformatics analysis of identified acetylome from old and young brain tissue showed protein that significantly enriched level on synaptosomes (green) and postsynaptic densities (light red) and non-significant protein enrichments levels (red).

Next, we used a rat brain acetylome dataset containing 3,895 ac(K) sites and compared it to our old versus young acetylome dataset (Lundby et al., 2012b). Both peptides sequence windows containing the acetylated lysine residue +/- 6 amino acids and gene names were used in this analysis. We found an overlap of 946 ac(K) site (37%) of old versus young are previously identified in rat brain tissue (Lundby et al., 2012b) (Figure 4.8). To provide more optimal results, a comparison of gene names was performed to avoid sequence windows changes between different species. An overlap of 57% (631) out of 1091 acetylated proteins was previously identified in the rat brain acetylome profile.

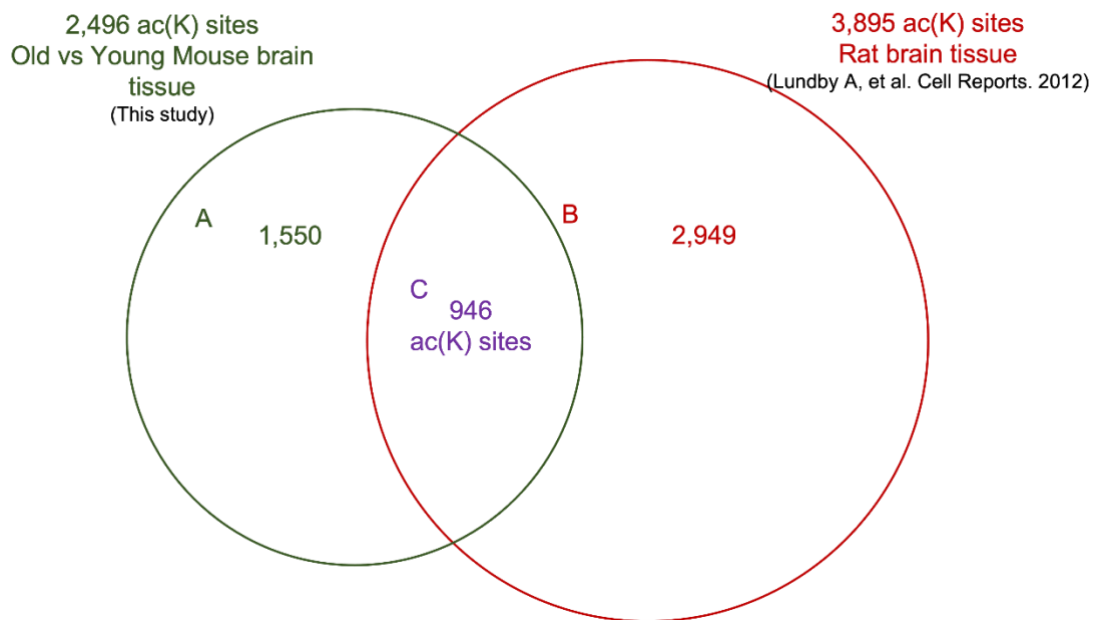


**Figure 4.8 – ac(K) sites previously identified in rat brain tissue.** Venn diagrams represent (A) 2,267 ac(K) sites from this study (green) compared to (B) 3,895 acetylated sites from rat brain tissue (Lundby et al., 2012b) (purple). Bioinformatics analysis compared peptides sequence windows containing lysine site +/- 6 amino acids from acetylome profile and RAT brain acetylome profile.

#### ***4.3.1.3 Characterisation of acetylation sites changes in the aged brain***

Next, to investigate whether ageing affects acetylation levels in mouse brain tissue, we performed a quantitative comparison of acetylation levels between old and young mouse brains was performed using Perseus (Tyanova et al., 2016). Data were filtered to proteins that were only identified by sites in at least three replicates of each group; contaminate and reverse were removed. Data were also normalised by subtracting the median of the distribution, missing values were imputed (using a downshift of 1.8, width 0.3) from the data distribution of each sample, and then a t-test was performed with a permutation-based FDR of 5% (Tyanova et al., 2016).

This analysis identified 60 ac(K) on 56 different proteins that are significantly different in old versus young brain tissue. The volcano plot in Figure 4.9 shows the distribution of acetylated peptides between two groups, acetylated peptides on the right side represent significantly increased acetylation. 36 ac(K) sites out of 60 are downregulated with age (increased acetylation in young brain tissue), and 24 ac(K) sites are upregulated (increased in old brain tissue). In addition, we found that 47 of those ac(K) sites were acetylated on synaptic proteins (Bayés et al., 2017), and 30 sites are also modified by both acetylation and ubiquitination (Signling, 2017).

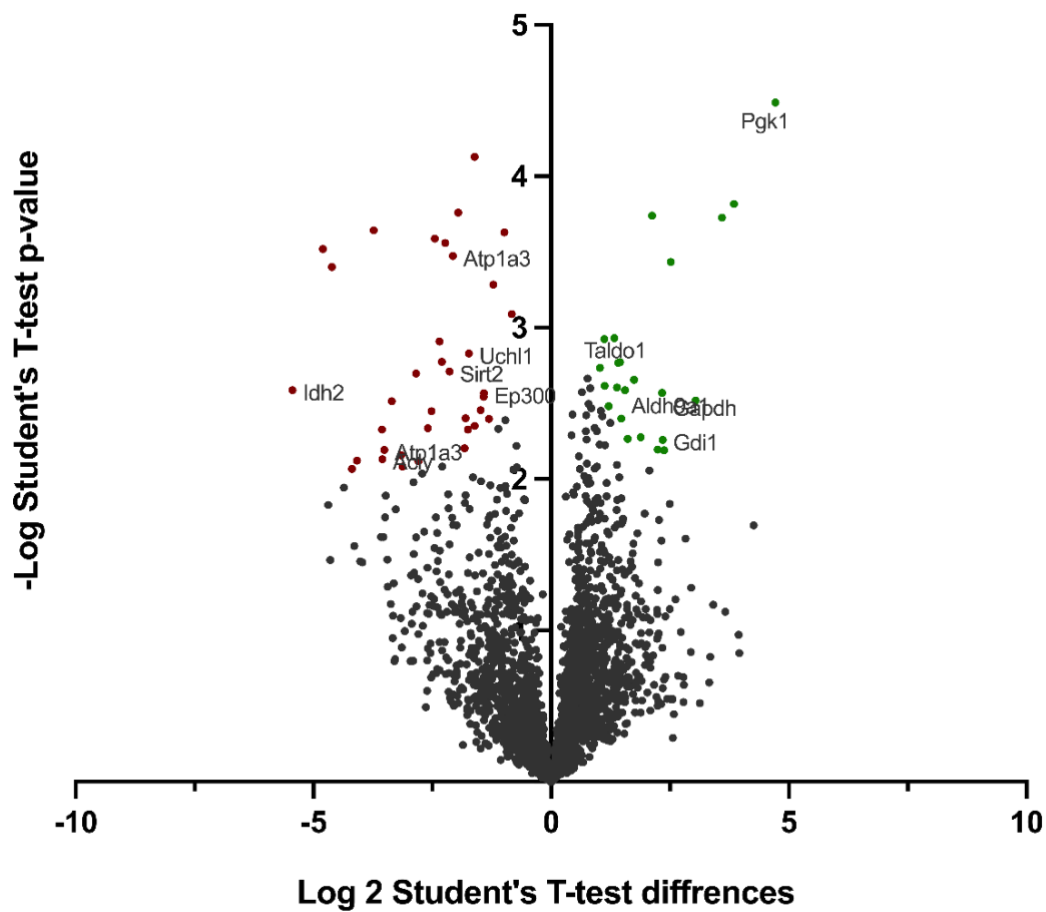


**Figure 4.9 – Volcano plot showing acetylation sites significantly regulated by ageing.** Data from the analysis of 4 replicates of *Sirt2* KO and 4 replicates of wild type acetylomes was filtered to retain acetylation sites quantified in at least three replicates of one group (2,496 sites). The data were normalised by subtracting the median intensity value of each sample, and statistical analysis was performed using *t*-testing with a permutation-based FDR 5% and *SO* of 0.1. Green dots represent acetylated sites significantly upregulated with ageing, and red dots represent acetylated sites significantly downregulated with ageing.

To further understand how the cellular distribution of acetylated proteins changed significantly with age, 60 ac(K) and their proteins were mapped to the human protein atlas . Interestingly, downregulated ac(K) sites were equally distributed between compartments while the upregulated was concentrated more in the cytoplasm, as shown in table 4.3.

	<i>Cytoplasm</i>	<i>Nucleus</i>	<i>Mitochondria</i>
<b>Upregulated (24 sites)</b>	10	4	2
<b>Downregulated (36 sites)</b>	10	11	11

**Table 4.3 – Cellular distribution of acetylated proteins regulated by ageing.**

The heat map in Figure 4.10 represents 60 ac(K) sites on 56 proteins identified as significantly regulated in old versus young brain tissue; the first heat map represents the fold change difference between the two groups. The second heat map represents the LFQ intensity of each ac(K) site in all the four replicates as shown; the first 25 ac(K) upregulated sites have a higher intensity in the old brain replicates. The rest of the ac(K) sites have a higher intensity in the young brain replicates (Figure 4.10). Pgc1 is an ATP/ADP binding protein highly involved in the glycolysis pathway. In our data, Pgc1 was highly acetylated on 11 ac(K) sites; most of these sites are previously known as Ub and ac(K) sites (Choudhary et al., 2009b, Lundby et al., 2012b). K156 was significantly increased in acetylation in old brain. Gapdh is another protein involved in glycolysis and is acetylated on nine ac(K) sites, K225 was significantly upregulated in old brain. Gapdh K sites are modified by UB and ac(K) (Lundby et al., 2012b, Signling, 2017). Interestingly, in our data, we found that the KDAC Sirt2, its interactor KAT Ep300 (Stark et al., 2006, Han et al., 2008), and the enzymes responsible for acetate production (Acaa2) (Cao et

al., 2008), were all decreased significantly in acetylation with ageing. Sirt2 was acetylated on two sites but significantly reduced in acetylation at K333. Nine ac(K) sites were identified on Ep300, with one significantly decreased site (K1674). Acaa2 had significantly decreased acetylation on K269, in addition to two other sites that were not statistically significant.

Most of those proteins have only one site except for (Taldo1) and (Uqcrc2), with two sites for each. Interestingly, according to the human protein atlas dataset, both proteins are classified as mitochondrial proteins.

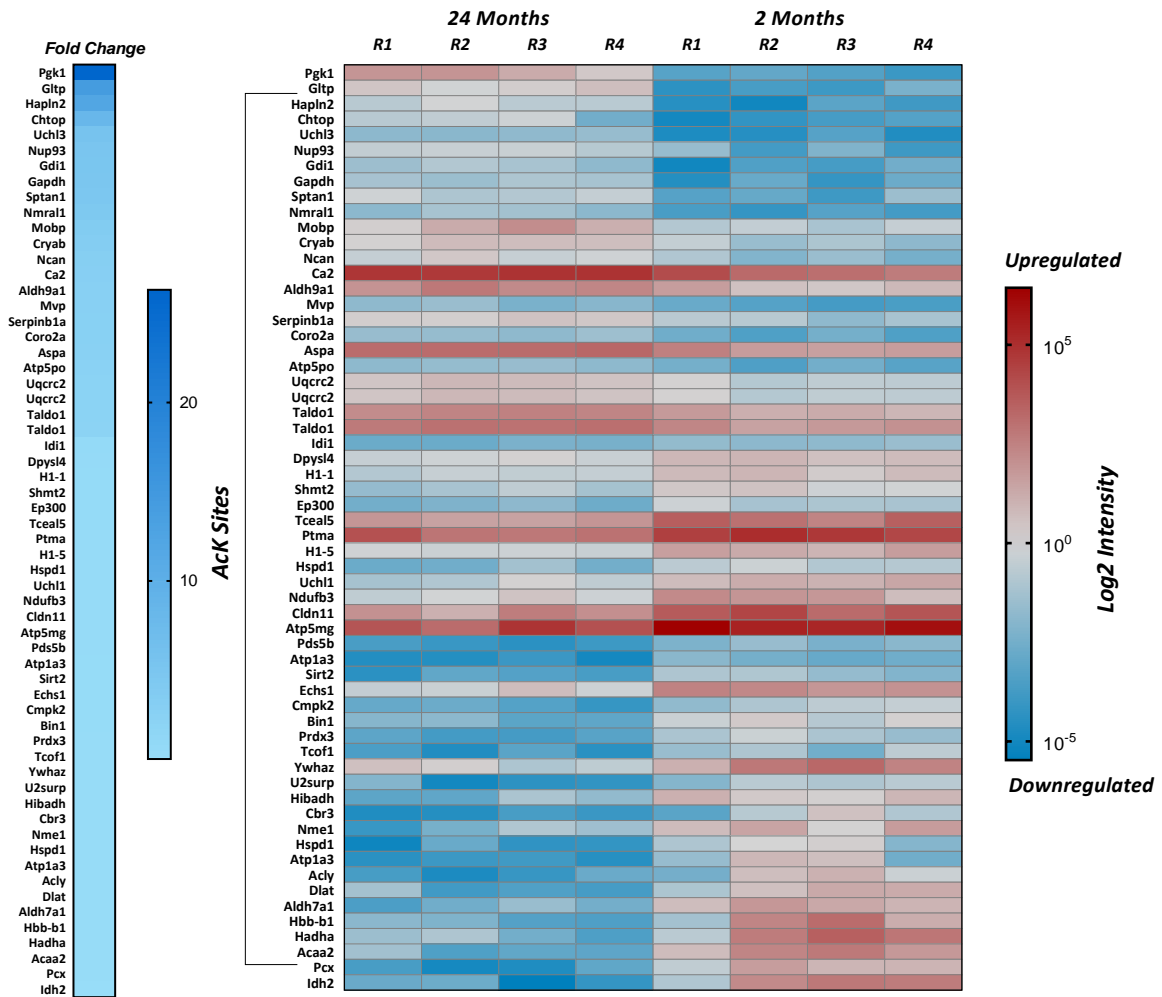


**Figure 4.10 – Heat map of identified acetylated peptides within the putative ageing regulated dataset.** The first column represents highly acetylated peptides by fold change highest fold change (dark blue). The second heat map was arranged according to fold change but demonstrate the (Log<sub>2</sub> intensity) of the significantly upregulated and downregulated in old/young brain acetylome acetylated sites across 4 replicates of each group, old brain (left), young brain) (right), highest intensity (dark red), lowest intensity (dark blue).

Functional annotation analysis of cellular components, molecular function, and biological processes associated with ac(K) sites upregulated and downregulated in old versus young mouse brain tissue (Michael et al., 2000). First, this analysis was performed to identify enriched terms compared to the whole mouse genome at FDR < 0.05. We found an enrichment in localisation in the cell membrane and mitochondria, but the highest enrichment was in the myeline sheet containing (Sirt2, Atp1a3, and Uchl1). Most of those genes contribute to enzymatic functions, cofactor, and NAD binding or metabolic processes; small molecule metabolic and oxidation-reduction metabolic processes, as shown in figure 4.11.

To identify acetylated proteins significantly enriched in brain functions, gene ontology annotation was repeated using the mouse brain proteome as a reference at FDR < 0.05 (Figure 4.12) (Sharma et al., 2015). This analysis avoids a general enrichment of terms associated with the brain. Any enrichment of terms will be above the frequency for proteins expressed in the brain. This analysis revealed 12 proteins significantly enriched and localised to the myelin sheath, both upregulated (Gdil, Uqcrc2, and Cryab) and downregulated (Sirt2, Uchl1, and Hspd1). Interestingly, 19 proteins were significantly enriched in mitochondria, suggesting a positive correlation between age and acetylation levels of mitochondrial proteins in the brain (Parodi-Rullán et al., 2018).

The only molecular function term significantly enriched in the analysis with the brain proteome as a reference was “NAD binding” with five proteins. Interestingly, four proteins were significantly downregulated with age, including Sirt2 and its substrates Idh1 and EP300 (Michael et al., 2000, 2019). This finding is consistent with studies showing the role of NAD<sup>+</sup> in ageing (Zhu et al., 2015, Mouchiroud et al., 2013). In addition, the oxidation-reduction

(redox) process was significantly enriched; the redox system is known to contribute to many age-related diseases (Jones, 2015, Mercurio et al., 2020), including neurodegenerative diseases (Anderson and Maes, 2013).

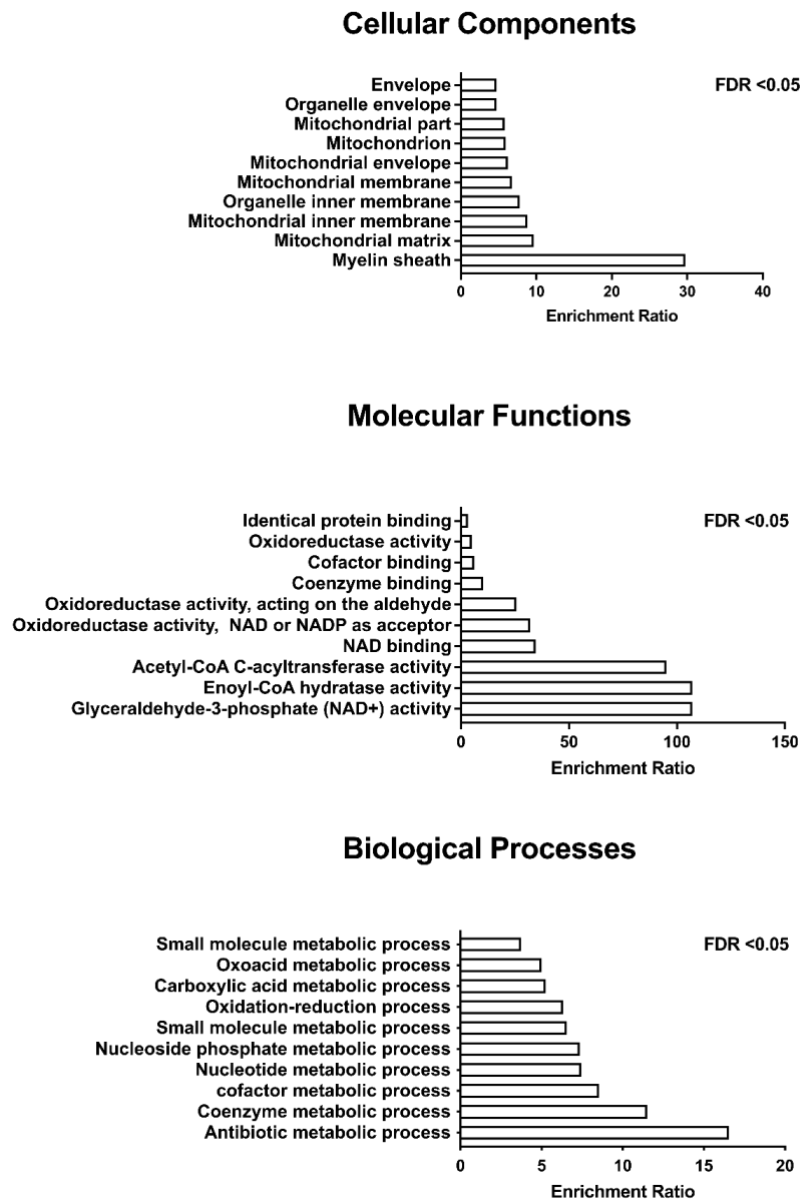


**Figure 4.11 – Gene ontology enrichment analysis of acetylated proteins regulated by ageing compared to the mouse genome.** Significantly enriched proteins are grouped into cellular component molecular pathways and biological processes. Gene ontology enrichment analysis was performed with an FDR < 0.05 using the WebGestalt gene toolkit (Wang et al., 2017b) with the brain proteome set as a reference for enrichment analysis.

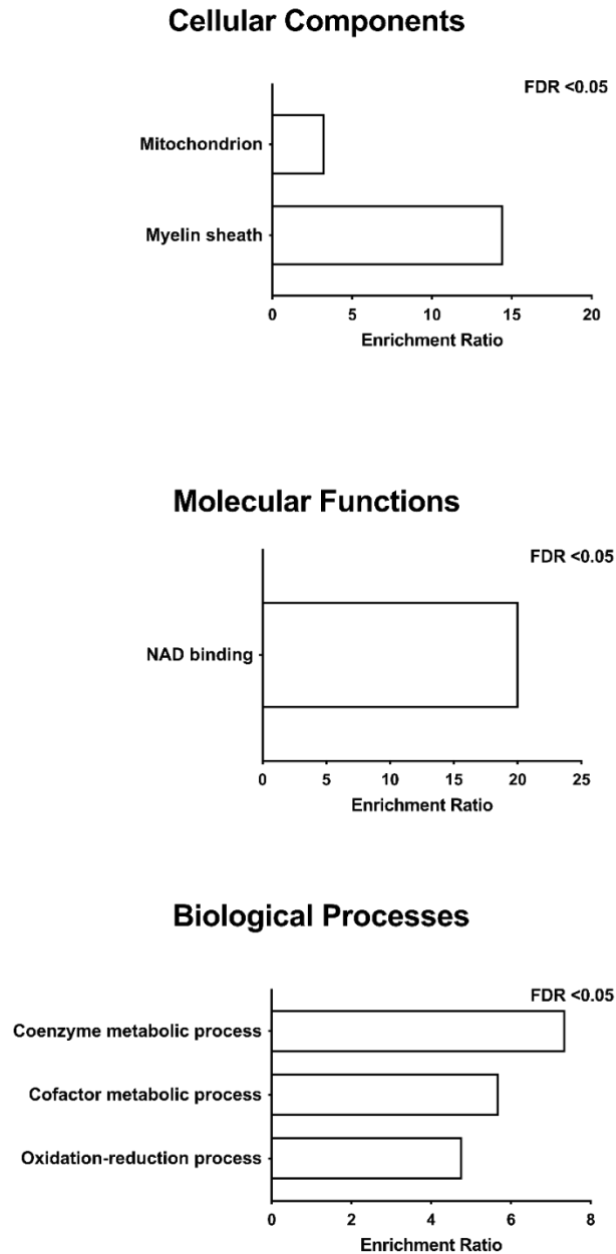


**Figure 4.12 – Gene ontology enrichment analysis of acetylated proteins regulated by ageing compared to the brain proteome.** Significantly enriched proteins are grouped into cellular component molecular pathways and biological processes. Gene ontology enrichment analysis was performed with an FDR < 0.05 using the WebGestalt gene toolkit (Wang et al., 2017b) with the brain proteome set as a reference for enrichment analysis (Carbon et al., 2021) .

We analysed pathways associated with these proteins and ac(K) sites upregulated and downregulated with age using PANTHER. Table 4.4 lists the most relevant pathways

annotated in our dataset. Consistent with the literature, this analysis revealed that ac(K) sites identified are involved in Parkinson’s and Huntington’s disease, and Sirt2 appears in the Parkinson’s disease pathway (Spinelli et al., 2014, Chen et al., 2015, Rita Machado de et al., 2017, Donmez and Outeiro, 2013). Glycolysis and pyruvate metabolism pathways were enriched in our dataset, which reflects their important role in both acetylation and ageing (Gray et al., 2013, Harris et al., 2014).

<b>Panther pathways</b>	<b>Proteins number</b>
Parkinson disease (P00049)	2
Huntington disease (P00029)	2
Pyruvate metabolism (P02772)	2
Glycolysis (P00024)	2
Axon guidance mediated by semaphorins (P00007)	1
Angiogenesis (P00005)	1
EGF receptor signalling pathway (P00018)	1
Pentose phosphate pathway (P02762)	1
Gonadotropin-releasing hormone receptor pathway (P06664)	1
PI3 kinase pathway (P00048)	1
Cholesterol biosynthesis (P00014)	1
Serine glycine biosynthesis (P02776)	1
p53 pathway (P00059)	1
Wnt signaling pathway (P00057)	1
VEGF signaling pathway (P00056)	1
Transcription regulation by bZIP transcription factor (P00055)	1
TGF-beta signaling pathway (P00052)	1
FGF signaling pathway (P00021)	1

**Table 4.4 – Panther pathway enrichment analysis of the acetylated proteins regulated by aging.**

To investigate which KATs regulate the old versus young brain acetylome, we performed acetyl-transferase substrate predictions for each ac(K) site using GPS-PAIL (Wankun et al., 2016). GPS PAIL is a software developed to help predict which KATs enzymes modify substrates, but it is currently restricted to predictions for seven KATs (CREBBP, EP300, HAT1, KAT2A, KAT2B, KAT5 and KAT8). This software performs predictions on imputed peptide sequence windows containing  $\pm 7$  amino acids surrounding ac(K) sites. It outputs two values, a score representing the potential of those K residues for acetylation. For our data, it is already known as we used our experimentally determined ac(K) sites. The second value is a cut-off value under the chosen threshold. We chose high threshold prediction for our analysis, which means the software output only identifies sites with high specificity for the corresponding KATs (Wankun et al., 2016). The results from this analysis indicate that ac(K) sites are regulated by many KATs enzymes, but KAT2B is potentially a crucial KATs for brain acetylation by potentially regulating >200 ac(K) sites (Figure 4.13) (Wankun et al., 2016). KAT2A, Ep300, and CREBBP showed a similar result regulating between 100 to 150 Ac(K) sites. As mentioned previously, KAT2B is localised to the nucleus and shows high RNA expression levels in the cerebral cortex, prefrontal cortex, and brain . In addition, KAT2B interacts with SIRT1, Sirt2, and SIRT7 deacetylase enzymes in the nucleus, cytoplasm (Stark et al., 2006). Studies showed that In HCT116 and HeLa cells, Sirt2 suppression causes an increase in KAT2B levels via stables acetylated KAT2B (Li et al., 2019, Fulco et al., 2003). in addition, SIRT1 interact with KAT2B via its conserved catalytic core domain and deacetylate KAT2B (Li et al., 2019, Fulco et al., 2003).

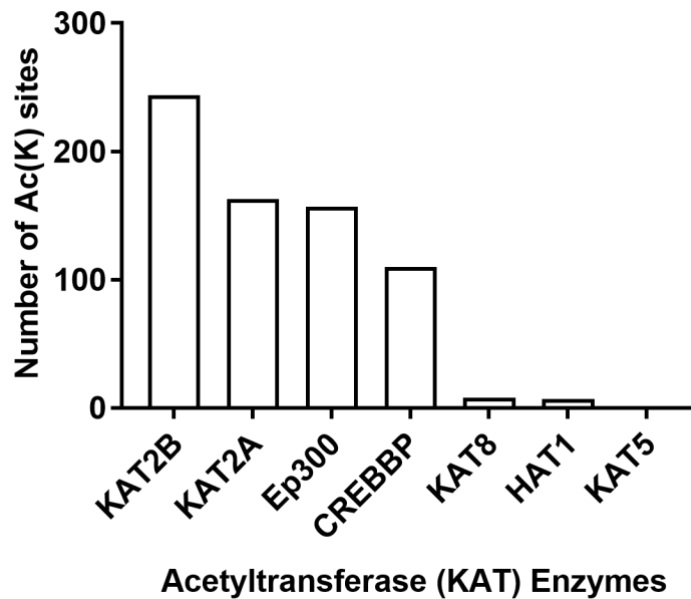


**Figure 4.13 – KAT2B is predicted to be the major KAT regulating the old versus young brain acetylomes.** Bar chart illustrating GPS predictions for acetyltransferases that regulate acetylated sites from our study, peptide sequence windows of identified Ac(K) sites were analysed using GPS PAIL 2.0 software at a high threshold (Wankun et al., 2016).

To investigate whether neighbouring amino acids influence acetylation of lysine residues, sequence motifs of peptides regulated by ageing were generated with pLogo with the mouse genome as the background, sequence windows +/- 7 amino acids were used in this analysis (Figure 4. 14) (Joseph et al., 2013). This result reveals that glutamine (E) and alanine (A) occur with high frequency at -1, and leucine (L) and arginine (R) frequently occur at +1 position. These results are consistent with what we identified in the Sirt2KO acetylome study and previous studies (Zhang et al., 2020, Weinert et al., 2011).

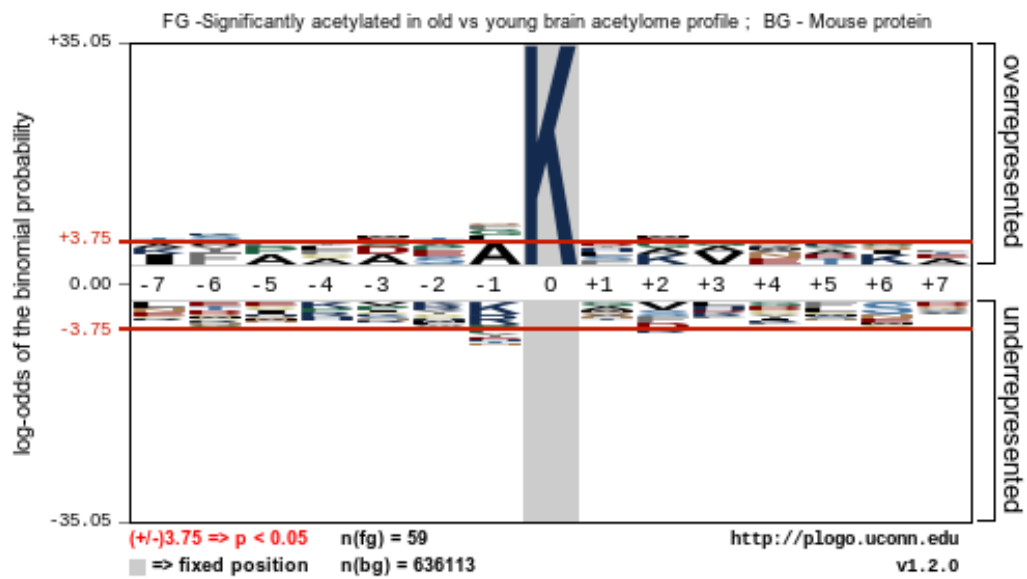


**Figure 4.14** – Sequence logo plots of normalised amino acid frequencies for  $-/+7$  amino acids of acetylated sites regulated during ageing from old versus young acetylome profile compared to the mouse genome. Logos generated with ([plogo.uconn.edu](http://plogo.uconn.edu)) (Joseph et al., 2013).

### **4.3.2 Proteome profile of old brain tissue versus young brain tissue**

To understand the effect of lysine acetylation modification and its role during ageing, we performed proteome profiling to identify differences in protein abundance between old and young brain tissue. We performed a 2-hour LC-MS/MS analysis of the digested peptides of each replicate before acetylated peptides were enriched. We identified a total of 3,103 proteins in mouse old and young brain tissue. 2,142 proteins were quantified identified across three replicates in at least one group; data were normalised, and missing values were imputed as described previously (\*\***Supplementary Table 7.4**). Proteins with differential protein abundance were identified using t-testing with a permutation-based FDR of 5% using Perseus. Histogram plots of each replicate show a normally distributed LFQ intensity (Figure 4.15). Correlation values of LFQ intensities across replicates and groups in Table 4.5 shows that the data was of high quality with excellent Pearson correlation values. Overall, these results show our sample preparation and MS analysis provided reliable and reproducible results.

\*\*(<https://figshare.com/s/13750b8c09063b5cb9eb>)

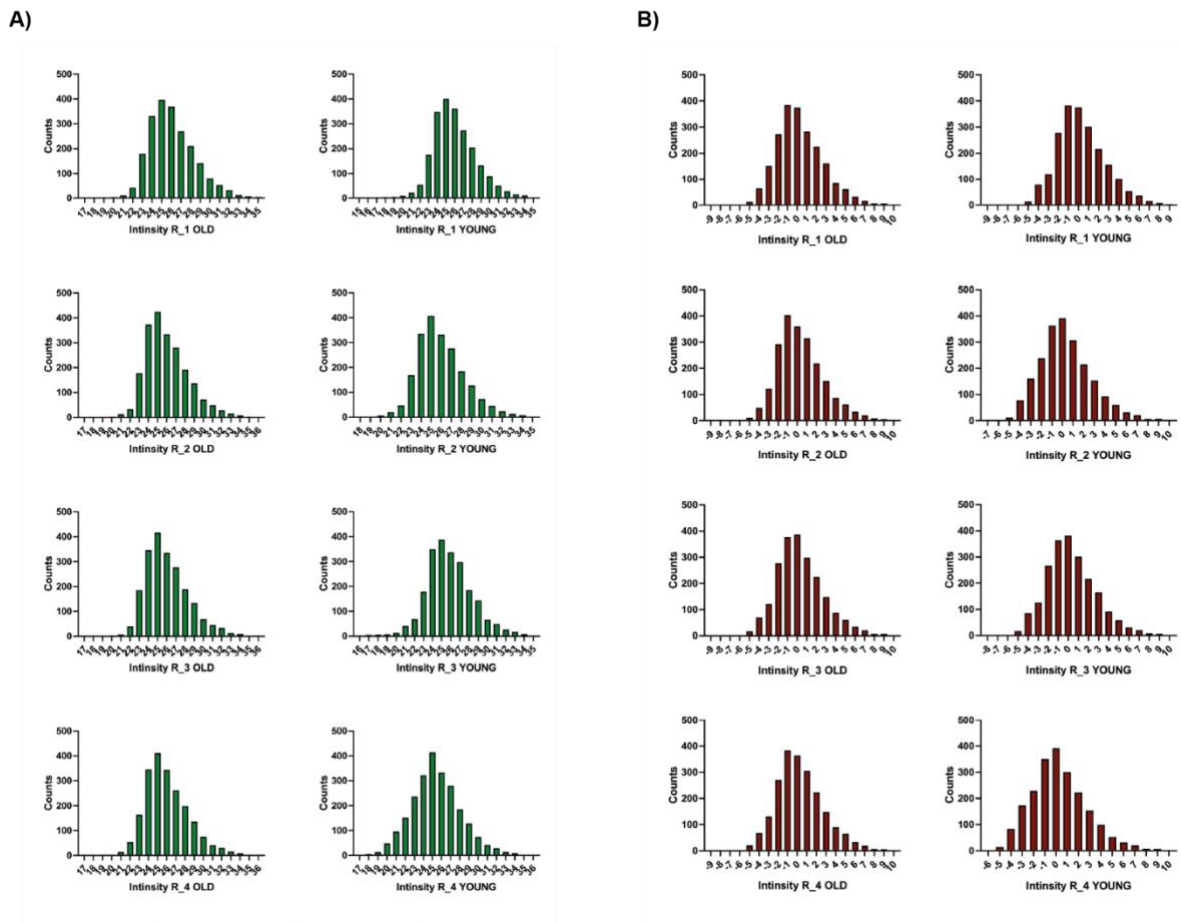
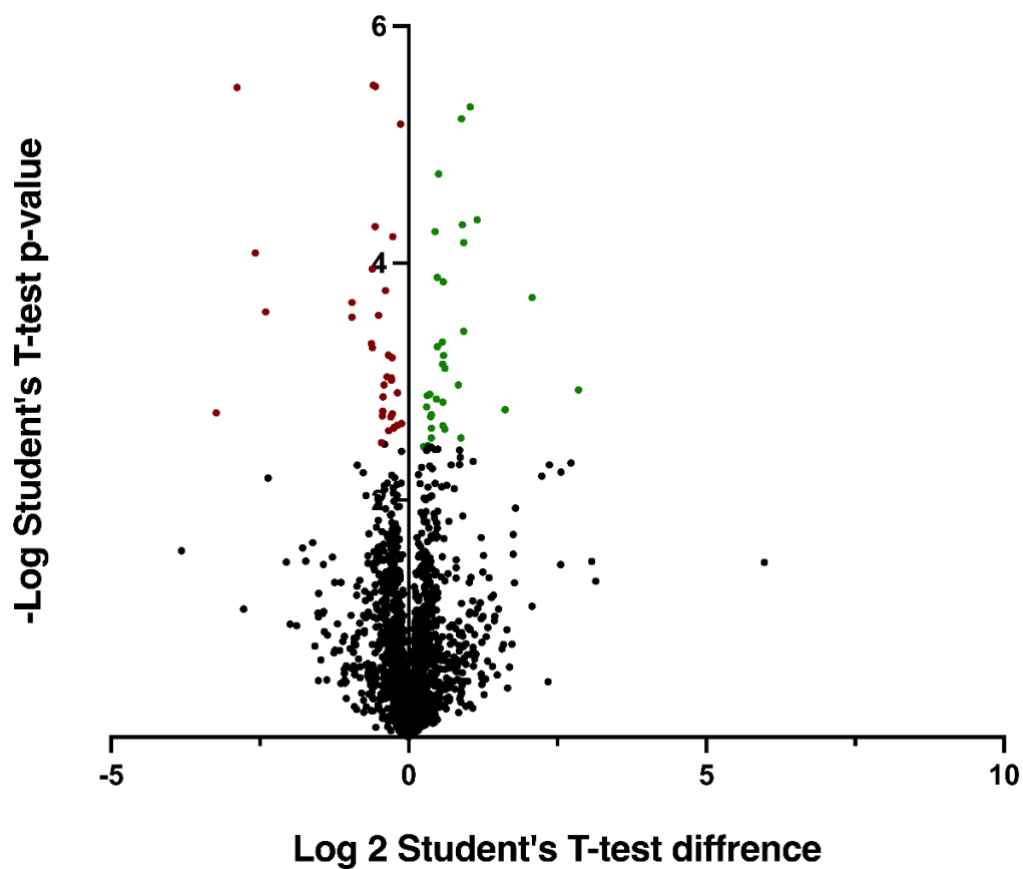


**Figure 4.15 – Histogram of LFQ intensity values for replicates of old versus young samples, A) showing a normally distributed intensity. B) normalised with imputed intensity values.**

Intensity Old-R1	Intensity Old-R2	Intensity Old-R3	Intensity Old-R4	Intensity Young-R1	Intensity Young-R2	Intensity Young-R3	Intensity Young-R4	
NaN	0.985	0.985	0.982	0.987	0.980	0.980	0.976	Intensity Old-R1
0.985	NaN	0.993	0.992	0.979	0.985	0.989	0.983	Intensity Old-R2
0.985	0.993	NaN	0.993	0.979	0.985	0.989	0.984	Intensity Old-R3
0.982	0.992	0.993	NaN	0.976	0.984	0.988	0.985	Intensity Old-R4
0.987	0.979	0.979	0.976	NaN	0.981	0.980	0.977	Intensity Young-R1
0.980	0.985	0.985	0.984	0.981	NaN	0.987	0.987	Intensity Young-R2
0.980	0.989	0.989	0.988	0.980	0.987	NaN	0.986	Intensity Young-R3
0.976	0.983	0.984	0.985	0.977	0.987	0.986	NaN	Intensity Young-R4

**Table 4.5 – Correlation values of old and young proteome profile replicate datasets.** These show that biological replicates from 8 mouse brain tissue were mostly similar within and between groups. Pearson correlation was above high (Green), middle (yellow), and low (red).

Analysis of protein abundance levels between old and young mouse brain tissue identified 67 proteins with a statistically significant difference at a 5% FDR. 32 proteins increased, and 35 proteins decreased during ageing. A volcano plot shows protein abundance changes between two groups; the right side represents proteins that significantly increased, left side represents proteins that significantly decreased in old brain mouse tissue (Figure 4.16).



---

**Figure 4.16 – Volcano plot showing the results of statistical analysis of old versus young brain proteomes. Data were filtered to retain proteins quantified in at least three replicates of one group. Data was Log<sub>2</sub> transformed, normalised by subtracting the median LFQ intensity of each sample. Statistical analysis using a t-test was performed with a permutation-based FDR of 5%. Green and Red dots represent proteins that showed significant increases or decreases in proteins abundance in ageing, respectively. Analysis was performed using the statistical package Perseus.**

This protein profiling data was compared to significantly acetylated sites from the young versus old acetylome analysis in figure 4.9; We found that 8 ac(K) sites on seven proteins exhibit a significant change in protein abundance as well as acetylation (Table 4.6). A change at the level of protein abundance and at the acetylome level could mean that the change was, in fact, not a change in acetylation but instead a change in the abundance of a protein. However, in 7/8 of these cases, the change in acetylation was substantially larger than the change in protein abundance, which strongly suggests both a change in abundance and acetylation. These results indicate that increased acetylation levels of those sites may regulate protein stability through inhibition of ubiquitination and degradation. K86 on Aldh7a1 exhibited a decrease in acetylation levels but an increase in protein abundance suggesting a more complex relationship between acetylation and protein stability in this case.

<b>Protein Name</b>	<b>Student's T-test Difference Old_Young (Protein levels)</b>	<b>Student's T-test Difference Old_Young (acetylation level)</b>	<b>Acetylation/Protein s ratio</b>	<b>Acetylome status</b>	<b>Ac(K) sites</b>
<b>Serpinb1a</b>	0.90	3.89	4.3	upregulated	K248
<b>Taldo1</b>	0.48	3.81	7.9	upregulated	K265
<b>Taldo1</b>	0.48	3.49	7.3	upregulated	K321
<b>Gltp</b>	0.58	6.91	11.8	upregulated	K133
<b>Hapln2</b>	2.85	6.62	2.3	upregulated	K168
<b>Ca2</b>	0.47	3.75	8.0	upregulated	K167
<b>Aldh7a1</b>	0.38	-6.48	-17.0	downregulated	K86
<b>H1-5</b>	-0.95	-4.34	4.6	upregulated	K17

**Table 4.6 – List of significantly changed proteins in acetylated and protein abundance levels in old versus young brain tissue.**

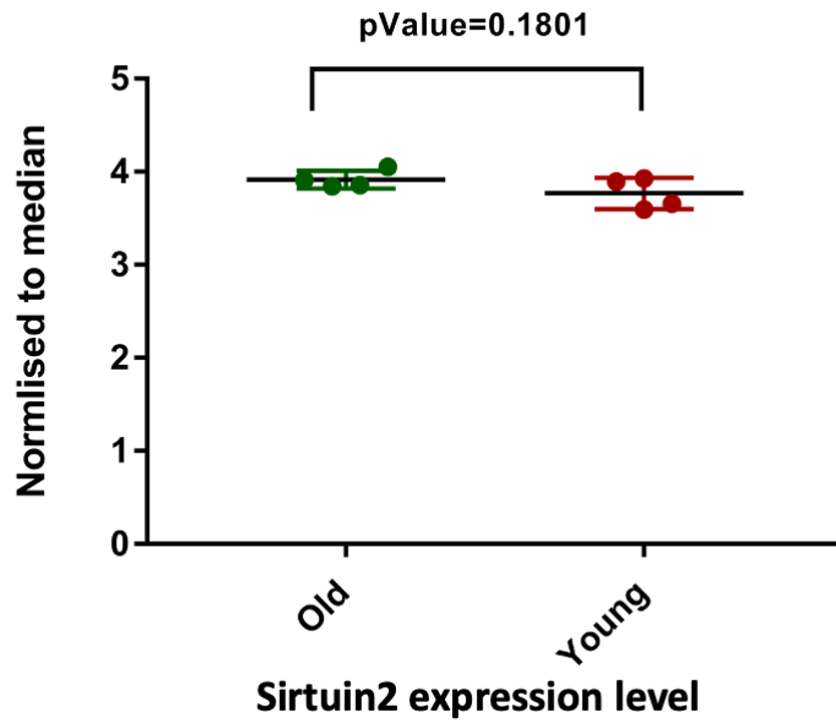
Functional annotation enrichment analysis of cellular component, molecular function, and biological processes associated with 67 proteins with significantly altered abundance during ageing was performed using the mouse brain proteome as a reference to provide results

specific to brain function at FDR of <0.05 (Sharma et al., 2015). This analysis revealed these proteins were significantly enriched with terms associated with the dendritic shaft, neurons, and neurons/cells projections. Most importantly, 10 proteins out of 67 were significantly enriched in the glutamatergic synapse, including Gabbr2 (Gamma-aminobutyric acid type B receptor subunit 2), which showed a significant decrease in mouse brain tissue with ageing, which validates data from a previous study of this receptor during ageing (McQuail et al., 2012). Calmodulin binding and cytoskeletal protein binding are two molecular functions highly enriched in our ageing-regulated protein abundance dataset, but no significant enrichment for any biological process was found. In addition, PANTHER analysis of those proteins revealed many interesting pathways such as metabotropic glutamate receptor group 1 and 2, synaptic vesicle trafficking, GABA-B receptor II signalling, and wnt signalling, as shown in table 4.7.

<i>Panther pathways</i>	<i>Proteins number</i>
Metabotropic glutamate receptor group III pathway (P00039)	3
Dopamine receptor-mediated signaling pathway (P05912)	3
Pyrimidine Metabolism (P02771)	3
Beta2 adrenergic receptor signaling pathway (P04378)	2
Axon guidance mediated by semaphorins (P00007)	2
Beta1 adrenergic receptor signaling pathway (P04377)	2
Ionotropic glutamate receptor pathway (P00037)	2
5HT1 type receptor-mediated signaling pathway (P04373)	2
Synaptic vesicle trafficking (P05734)	2
GABA-B receptor II signaling (P05731)	2
Heterotrimeric G-protein signaling pathway-Gi alpha and Gs alpha mediated pathway (P00026)	2
Wnt signaling pathway (P00057)	2
Nicotinic acetylcholine receptor signaling pathway (P00044)	2
Muscarinic acetylcholine receptor 2 and 4 signaling pathway (P00043)	2
Metabotropic glutamate receptor group II pathway (P00040)	2
Gonadotropin-releasing hormone receptor pathway (P06664)	2

**Table 4.7 – Example of some significantly enriched proteins grouped into panther pathways.** Panther analysis enrichment analysis of the significantly upregulated and downregulated in old/young brain proteome (Thomas et al., 2003).

Two KDAC enzymes (Hdac6 and Sirt2) and one KAT enzyme (Crebbp) were identified the protein expression profile of old versus young mouse brain tissue but it did not show major significant difference. The literature suggested that Sirt2.3 accumulated in CNS during ageing (Maxwell et al., 2011a), in our data we identified Sirt2.2 and the expression level of Sirt2 was not altered during ageing, as shown in figure 4.17.



---

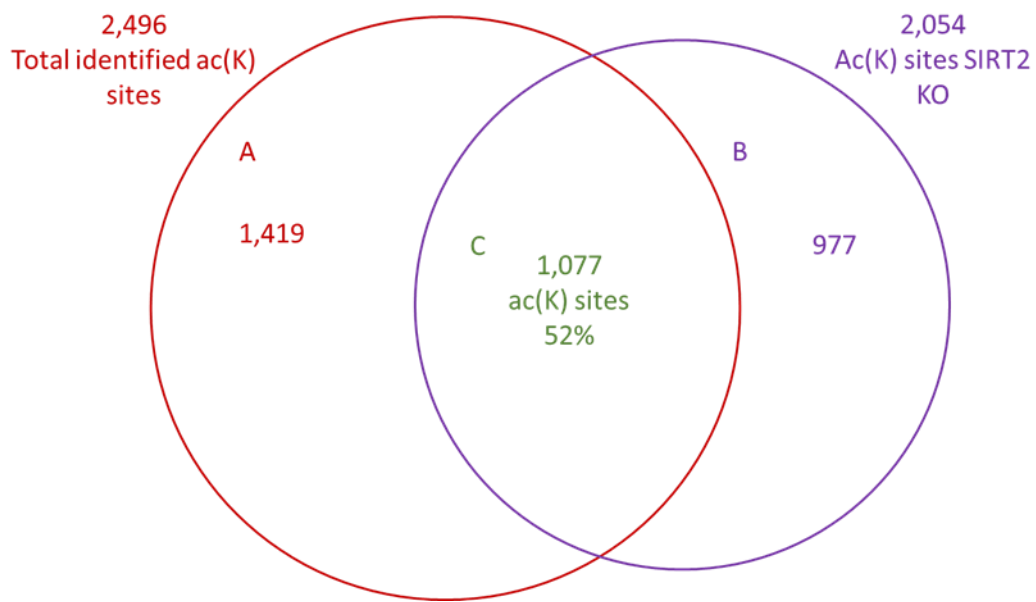
**Figure 4. 17 – Sirt2 protein expression difference between old and young mouse brain tissue.** LFQ intensity of Sirt2 of 4 biological replicates of each group. Chart shows no significant difference in Sirt2 levels with p value=0.1801. Analysis by the statistical package, Perseus.

### ***4.3.3 Understanding the relationship between Sirt2 substrates and changes in acetylation during ageing.***

#### ***4.3.3.1 Sirt2 KO versus old/young acetylome profiles.***

Studies have connected the sirtuins (NAD<sup>+</sup> dependent deacetylase enzymes) to age-related diseases. It is known that NAD<sup>+</sup> levels decline with age, and it is one of the hallmarks and signs of ageing. In addition, it is a long-standing discussion about increasing the activity of Sirtuins and NAD<sup>+</sup> levels contribute to and regulate ageing and longevity (Mouchiroud et al., 2013, Imai and Guarente, 2014).

To understand the role of Sirt2 in age-related diseases, I performed a bioinformatic analysis to compare the ac(K) sites of Sirt2 KO/WT mouse brain in chapter 3 to the ac(K) sites of old versus young mouse brain. In order to do this, peptide sequence windows surrounding (+/- 7 amino acids) Sirt2 KO versus WT ac(K) sites were compared to the total old versus young acetylome shown in Figure 4.19. We found an overlap of 1,077 sites identified in both datasets, suggesting we could identify more than 50% of the ac(K) identified in Sirt2 KO acetylome.




---

**Figure 4.18 – Venn diagram represents Ac(K) sites between *Sirt2*KO/WT and old/young mouse brain acetylome profile, 1,077 sites out of 2,496 ac(K) sites identified in old /young acetylome profile were identified in *Sirt2* KO/WT acetylome.**

Next, I compared the quantified ac(K) sites from Sirt2 KO/WT acetylome profile and old/young acetylome profile, an overlap of 52% (1,077) was found, and 28% of ac(K) sites regulated by Sirt2 were found in old/young acetylome as shown in table 4.8.

64 ac(K) sites significantly regulated by Sirt2 that also identified in old/young acetylome profile are presented in Table 4.9. Uchl1 K71 was the only ac(K) site regulated by Sirt2 and showed a significant decrease in acetylation level with age. Proteins with regulated acK sites in the Sirt2 KO and ageing datasets in some cases the regulated sites were not the same sites in both datasets. Two proteins (Gapdh and Sptan1) showed a significant increase in acetylation level with age. In contrast, three proteins (Hspd1, Uchl1, and Tcof1) were significantly decreased in acetylation with age.

	Identified ac(K) sites	Overlap with old/young acetylome	Percentage
<b>Regulated ac(K) sites by Sirt2</b>	226	64 known in old/young acetylome	28%
<b>Identified ac(K) site from Sirt2 KO Acetylome</b>	2,054	1,077 known in old/young acetylome	52%

**Table 4.8 - a comparison of Sirt2 KO acetylome dataset to old versus young acetylome (Signling, 2017).**

<i>Proteins</i>	<i>Ac(K) site</i>	<i>Proteins</i>	<i>Ac(K) site</i>
<b>Uchl1</b>	71	<b>Map7d2</b>	267
<b>Plp1</b>	105	<b>Slc32a1</b>	8
<b>Prdx6</b>	56	<b>Aldoc</b>	42
<b>Glrx</b>	9	<b>Npm1</b>	154
<b>Hrsp12</b>	13	<b>Sh3gl2</b>	7
<b>Hspd1</b>	202	<b>Ywhag</b>	69
<b>Fkbp1a</b>	53	<b>Mapt</b>	661
<b>Hbbt1</b>	145	<b>Ank3</b>	2574
<b>Acadl</b>	81	<b>Erh</b>	12
<b>Cnp</b>	174	<b>Arfgap1</b>	263
<b>Dync1h1</b>	4281	<b>Ctnnd2</b>	275
<b>Dbi</b>	51	<b>Hist1h2bb</b>	13
<b>Synrg</b>	508	<b>Psat1</b>	127
<b>Dbi</b>	14	<b>Ywhah</b>	69
<b>Pebp1</b>	148	<b>Cct6a</b>	5
<b>Amph</b>	101	<b>Dpysl2</b>	525
<b>Lasp1</b>	42	<b>haemaglobin</b>	17
<b>Purb</b>	77	<b>Hist1h2bb</b>	13
<b>Arl6ip1</b>	96	<b>Cend1</b>	61
<b>S100a13</b>	85	<b>Gap43</b>	37
<b>Ywhaq</b>	9	<b>Tpm3-rs7</b>	11
<b>Aldh1l1</b>	205	<b>Fasn</b>	673
<b>Aldoa</b>	42	<b>Dbi</b>	55
<b>Slc25a5</b>	105	<b>Ube2n</b>	92
<b>Slc1a2</b>	569	<b>Synrg</b>	735
<b>Dlgap4</b>	541	<b>Uqcrb</b>	96
<b>Hpca</b>	147	<b>Tcof1</b>	153
<b>Nefm</b>	296	<b>Mbp</b>	72
<b>Eef1a1</b>	439	<b>Got2</b>	90
<b>Bcas1</b>	163	<b>Capzb</b>	199
<b>Rgs10</b>	173	<b>Zyx</b>	24
<b>Sptan1</b>	2180	<b>Ndufs3</b>	55

**Table 4.9** *Overlap of regulated acetylated proteins from old and young acetylome and Sirt2 putative substrates. Old/Young acetylome datasets were matched to Sirt2 putative substrates dataset, and 64 ac(K) sites were identified as potential regulated. Those sites are not significantly acetylated by Sirt2. Bioinformatics analysis compared peptides sequence windows containing lysine site +/- 7 amino acids from Old/Young acetylome and Sirt2 KO acetylome.*

## **4.4 Discussion**

### **4.4.1 aged mouse brain acetylome**

Overall, we successfully identified 2,885 ac(K) sites on 1,223 proteins from mouse brain tissue, with an acetyl-lysine purity of 37% (acK peptides/total peptides ratio). This chapter used the S-trap digestion column instead of the acetone precipitation digestion method used in Sirt2 KO acetylome profile experiments. S-trap digestion is a fast and reliable method that provides similar results (Ludwig et al., 2018).

2,496 ac(K) sites at 1,091 proteins were statistically comparable across a minimum of three replicates in either group at an FDR of 1%. According to the Phosphosite database, 1,274 ac(K) sites were novel sites, and around 1,072 sites can be modified by both ac(K) and UB. These results further support the crosstalk between acetylation and ubiquitination (Caron et al., 2005, Kozuka-Hata et al., 2020, Seo and Lee, 2004, Zhou et al., 2016a)

1,932 ac(K), around 77% of total identified sites were found on synaptic proteins. Most sites found in proteins are equally distributed in synaptosomes and PSD, yet nearly half of them are significantly enriched in synaptosomes. Interestingly, similar results were found in the Sirt2 KO acetylome profile, which indicates that lysine acetylation may regulate many synaptic portions, specifically pre-synaptic proteins, and their functions.

### **4.4.2 acetylation sites level changes during ageing**

We found 60 ac(K) that significantly changed with ageing, 24 sites were increased in acetylation (upregulated), and 36 sites decreased in acetylation (downregulated) with age. 47 ac(K) sites (78%) were derived from synaptic proteins, and 50% of those sites can also be ubiquitinated. This result further confirms the suggested hypothesis about the role of

acetylation on synaptic proteins and the existence of the crosstalk between ac(K) and UB modifications. This result agrees with the findings in chapter 3.

We noticed putative ac(K) sites regulated by ageing were significantly enriched in mitochondria at an FDR of <0.05 (Wang et al., 2017b). In addition, most downregulated sites are localised to the nucleus and mitochondria, while almost all upregulated sites are found in the cytoplasm according to the human atlas proteome. This is in agreement with the literature, showing NAD<sup>+</sup> depletion is considered one of the hallmarks of ageing. In addition, the loss of NAD<sup>+</sup> would reduce the activity of sirtuins (Mouchiroud et al., 2013, Imai and Guarente, 2014). For example, Pgc1 showed a significant increase in acetylation with ageing; pgk1 acetylation promotes cancer cell proliferation and carcinogenesis by increasing Pgc1 activity (Hu et al., 2017). Studies reported that SIRT7 overexpression effectively reduced PGK1 acetylation levels in 293T cells (Hu et al., 2017). Moreover, studies showed an increase in GAPDH acetylation in WT versus Sirt2 KO T cells (Hamaidi et al., 2020). Thus, alterations in SIRT7 and Sirt2 activities may be influenced by NAD<sup>+</sup> deficiency during ageing. We observed that NAD<sup>+</sup> binding was significantly enriched at an FDR of <0.05, and as mentioned earlier, mostly specific to downregulated ac(K) sites.

Recent evidence suggests linking ageing and the sirtuin family (59, 60), utilising Sirt1 (9) and other sirtuins as anti-ageing agents controversial (61). A comparison of old/young acetylome and Sirt2 KO/WT shows whether Sirt2 plays an ageing role. We found an overlap of 1,071 ac(K) (42%) in the Sirt2 KO acetylome profile, and 1,027 ac(K) (41%) were found in the Sirt2 WT acetylome profile, yet the expression level of Sirt2 did not show any significant change between young and old brain tissue. We found 64 regulated ac(K) sites by Sirt2 in old versus young acetylome; among those, Uchl1 (Ubiquitin carboxyl-terminal hydrolase isozyme L1) K71

showed a decrease in acetylation during ageing. Uchl1 is an abundant neuronal protein, it is one of the ubiquitin-proteasome systems, and it contributes to autophagy pathways. It is controversial how Uchl1 contributes to Parkinson's diseases (Coulombe et al., 2014). As studies showed that Uchl1 is important for maintaining cellular architecture via regulating the MT network, and its suppression inhibits the development of SNCA aggregates and activates the autophagic pathway. (Pukaß and Richter-Landsberg, 2015, Choi et al., 2004). We reported that K71 is an ac(K) site and a site of ubiquitination (Signling, 2017). This result suggests that deacetylation of Uchl1 may have a role in neurodegenerative or age-related diseases.

#### ***4.4.3 Old versus young proteome profile***

The proteome profile of old versus young brain tissue revealed that the expression levels of 67 proteins were significantly changed with age. Those proteins contribute highly to synaptic protein and synapse functions (Bayes et al., 2017). This result agrees with previous studies suggesting the decline in synaptic function with age in different species (Morrison and Baxter, 2012, Leal and Yassa, 2015).

This chapter successfully generated an acetylome profile of old versus young mouse brain tissue. We showed that 60 ac(K) sites were significantly regulated during ageing. These results advance our understanding of the function of acetylation during ageing and help provide more information about the brain functions that might affect with age.

## **CHAPTER 5**

### ***Validation of putative Sirt2 substrates***

## 5.1 Introduction

Sirt2 is distributed widely in human tissue; it deacetylates and interacts with many substrates related to essential molecular functions and cellular compartments. In chapter 3, we highlighted the critical role of Sirt2 in synapses and the brain, and our data revealed that Sirt2 might regulate up to 190 synaptic proteins via deacetylase activity. Interestingly, most of the putative Sirt2 substrates were novel acetylated proteins which provided new information and uncovered many biological processes and molecular pathways potential regulated by Sirt2. Many exciting candidates were identified from the Sirt2 KO/WT acetylome dataset. However, for the general aims of this study, the focus was to validate acetylation sites identified on selected synaptic proteins.

To prioritise putative substrates of Sirt2 for further analysis, we short-listed candidates based on the following: (i) newly identified ac(K) sites (ii) acetylation sites were also known to be ubiquitinated, (iii) acetylated proteins that are localised to synapses. In addition, other aspects were considered, such as proteins that are readily available for testing and compatible with our studies. For example, tagged constructs for transfection, reagents for immunoprecipitation, and antibodies for immunoblotting. The complete list of putative Sirt2 substrates is listed in chapter 3.

The prioritised putative Sirt2 *substrates* (Figure 3.26) were involved in many interesting pathways and functions, For example, axon development (PLP1 and MAPT), synaptic vesicle trafficking (SNCA, VAMP2,3) and many others. This list contains proteins known to be deacetylated by Sirt2 and are, therefore, positive controls, such as; SNCA (Diaz-Perdigon et al., 2020, Rita Machado de et al., 2017) and MAPT (Biella et al., 2016). It includes other known acetylated proteins from previous acetylome studies, such as PCLO and VAMP3 (Lundby et al., 2012b).

## **5.2 Aims**

The primary aim of this chapter is to attempt to validate the acetylation status of Vamp2/3 and other putative Sirt2 substrates identified from the Sirt2 KO/WT mouse brain tissue acetylome profile. Second, to investigate and identify Sirt2 interactors in the HEK239 cell line to determine whether Sirt2 stably interacts with its substrates.

## **5.3 Results**

### **5.3.1 Challenges in the detection of non-histone acetylation**

To validate putative Sirt2 substrates, we attempted a series of in vitro lysine acetylation detection assays of chosen substrates, with known substrates as a control. Detection of non-histone acetylation is difficult, which is one of the main reasons why the roles and significance of this PTM have only recently been investigated (Drazic et al., 2016, Choudhary et al., 2014). In this chapter, we faced many challenges while examining the role of acetylation and Sirt2 on VAMP2/3. These issues also occurred with known Sirt2 substrates such as CDK9, GLUA1 and NRF2 (Wang et al., 2017a, Yang et al., 2017, Zhang et al., 2013). We aimed to follow the investigating assays previously used in similar studies (Wang et al., 2017a). However, acetylation could not be detected using many different approaches for any of the proteins listed above.

A combination of detecting methods, tagged/endogenous immunoprecipitation with immunoblotting using a pan acetyl-lysine antibody or LC-MS/MS analysis for detection. Different cell types and brain tissues were used to validate acetylation sites. We maximised the scale of pulldowns to increase the amount of target proteins in pulldown elutions by increasing cell numbers and transfection concentrations. To boost acetylation levels, we treated cells with KDACs inhibitors at concentrations that were optimised to prevent toxicity. Furthermore, lysine deacetylation was prevented during cell lysis and immunoprecipitation by inhibiting deacetylase activity using KDACs inhibitors added to IP lysis buffer. Although our pulldown assays worked very well with both tagged/endogenous proteins to enrich target proteins, we further optimised the IP lysis buffer composition and volume to prevent any alteration in acetylation status. Overall, we were able to identify proteins and ac(K) peptides,

but we were unable to detect acetylation sites of interest. Figure 5.1 summarises the steps taken to optimise detection of acetylation of Sirt2 substrates.

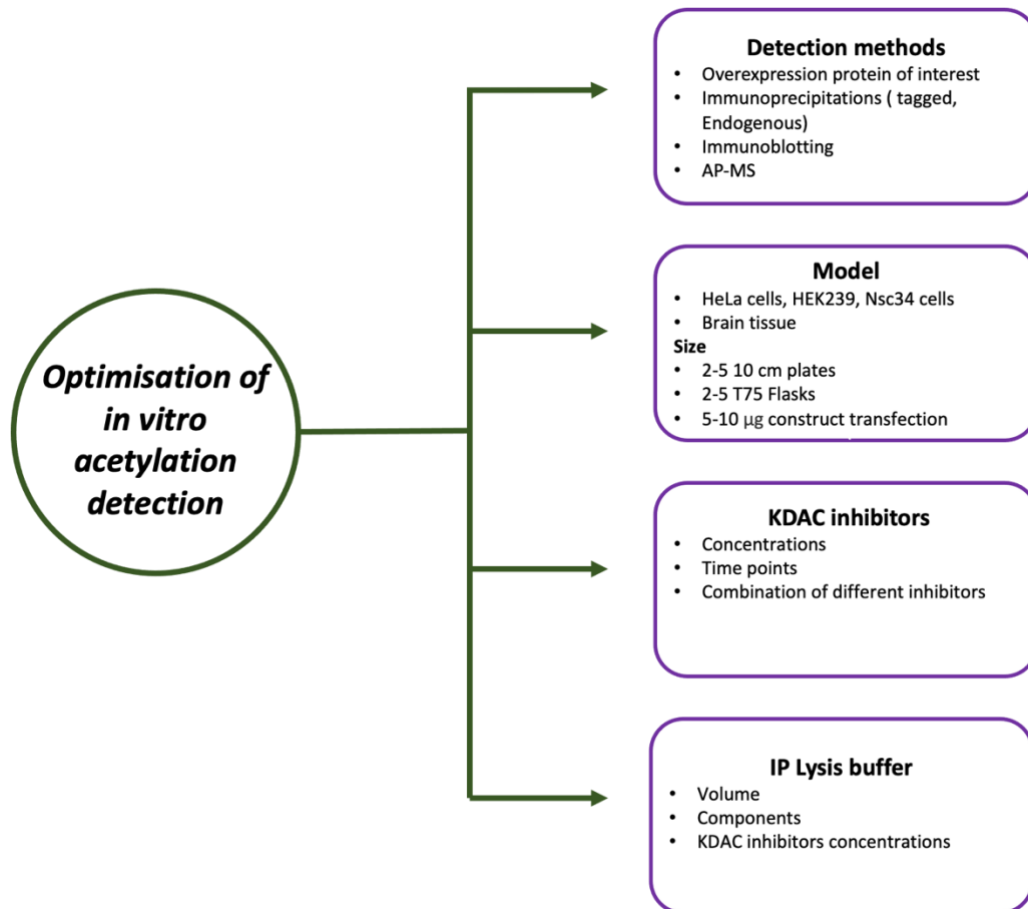


**Figure 5.1 – Flowchart summarised optimisation of detection acetylation to validate Sirt2 putative substrates.**

### **5.3.2 Manipulation of Sirt2 activity in cells and detection of acetylation**

To achieve the aims of this chapter, first, we needed to optimise our method of validation using different assays to measure the ability of Sirt2 to deacetylate substrates in cell culture. Most deacetylase studies are performed *in vitro* by manipulating KAT/KDAC levels by small-molecule inhibition, overexpression, or enzyme knockdown (Sabò et al., 2008, Zhang et al., 2013, Wang et al., 2017a, Yang et al., 2017, Guo et al., 2019). As mentioned previously, *in vivo*

knockout technique was used to identify Sirt2 substrates in mouse brain tissue. To validate putative Sirt2 substrates, we chose to measure acetylation changes in different cell lines using various manipulations such as Sirt2 overexpression, inhibition, and knockdown. Acetylation levels were measured via immunoblotting (IB), immunoprecipitation (IP), immunofluorescence and affinity purification mass spectrometry (AP-MS).

To prove that our techniques can manipulate Sirt2 expression or activity. First, inhibition of endogenous Sirt2, HeLa cells were treated with AGK2 (Sirt2 inhibitor) and another KDAC inhibitor TSA at different concentrations for 8 hours. Cells were collected, cell lysates prepared, and 35  $\mu$ g was used for immunoblotting using pan anti-acetyl-lysine antibodies to detect changes in acetylation level. Figure 5.2 shows the differences in acetylation between different inhibitor concentrations. The control sample had fewer acetylation bands than the others, except the sample treated with 10  $\mu$ M AGK2, which had an apparent reduction in acetylation levels and  $\beta$ -actin at the same time. This experiment was repeated many times before we got these results, and one of the main reasons was that the signal for histone acetylation is very strong. The higher intensity was detected after using the inhibitors, especially TSA, making it difficult to detect other bands and distinguish the changes. Thus, the PVDF membrane was cut around 20 kDa after the transfer step to separate histones band from the others every time TSA was used. Inhibition of endogenous Sirt2 by AGK2 was used

previously; this assay will be beneficial in the validation of Sirt2 substrates (Wang et al., 2017a).

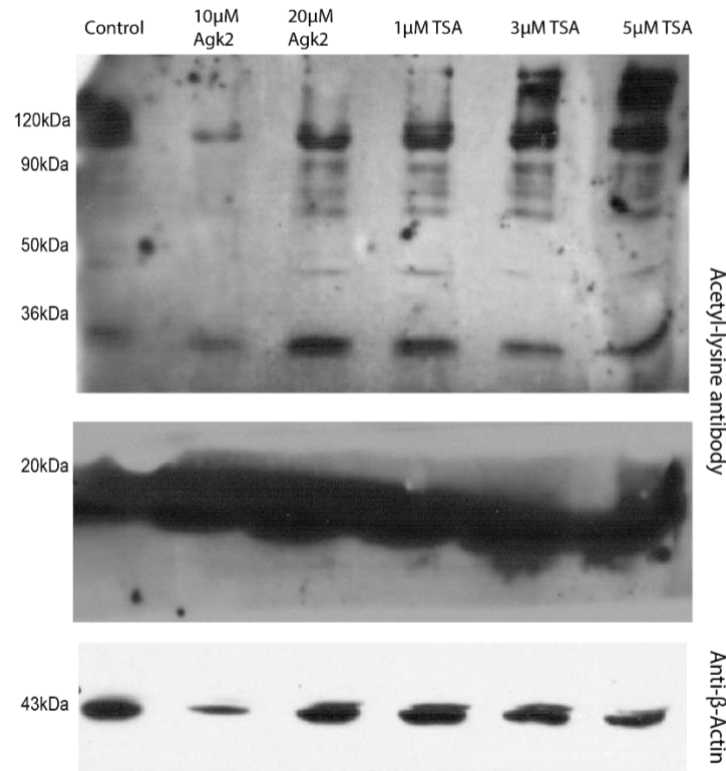


**Figure 5.2 – Optimisation of KDAC inhibitor concentrations.** Immunoblotting of acetylation levels between different KDAC inhibitors in HeLa cells. Cells were treated with 10 μM, 20 μM of AGK2 and 1 μM, 3 μM and 5 μM TSA 8 hrs, DMSO used as control. 35 μg of protein were immunoblotted using an anti-acetyl-lysine antibody. The membrane was cut above 20 kDa to separate the strong acetylation signals from histones from the rest of the membrane; β actin was used as a loading control.

Next, we repeated the experiment, but this time used anti-Lys40 acetyl-tubulin antibody to detect changes in ac-tubulin levels when endogenous Sirt2 was inhibited. HEK293T cells were treated AGK2 and NAM + 1M μTSA (8 hrs), TSA was added to inhibit HDAC6, another KDAC enzyme that deacetylase tubulin (Figure 5.3) The results were normalised to actin and control +1 μM TSA and showed an observed change in tubulin acetylation. Treatments with 20 μM

AGK2 showed an increase in acetylation levels that was unexpected compared to higher concentrations of the same inhibitor, but the AGK2 had larger error bars than the others.

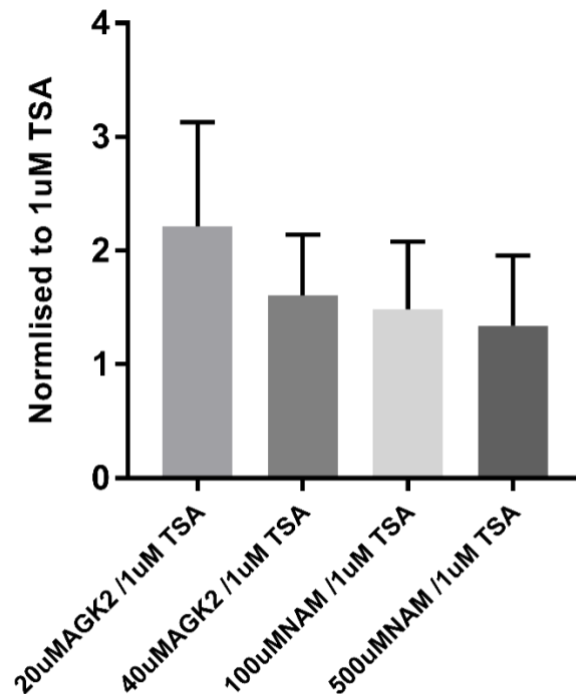


**Figure 5.3 – Sirt2 (KDAC) inhibitors increase ac tubulin levels.** A) Immunoblotting represent changes of tubulin acetylation levels in HEK293T cells were treated AGK2, and NAM + 1 μM TSA (8 hrs) and measured using an anti-acetyl-tubulin-Lys40 antibody, β-Actin used as control. Unpaired T-test was used to determine the significance of the difference between ac tubulin levels with different KDAC inhibitors, results normalised to control/1 μM TSA, n=3.

Next, to determine the extent to which Sirt2 regulates global acetylation levels, I first performed a test experiment where the influence of overexpression of Sirt2 on acetylation levels in HeLa/HEK cells was investigated. KDAC inhibitors (TSA and NAM) and Sirt2 inhibitors (AGK2 and SirReal2) were used to inhibit the deacetylase activity of Sirt2 and, as a result, induce hyper-acetylation, which was demonstrated previously. In parallel, hypo-acetylation was induced by HeLa or HEK cells transfection with a Flag-tagged construct of Sirt2. Figure 5.4 shows the overexpression of Sirt2 detected by an anti-flag antibody in HeLa cells (Rumpf et al., 2015, North et al., 2003).

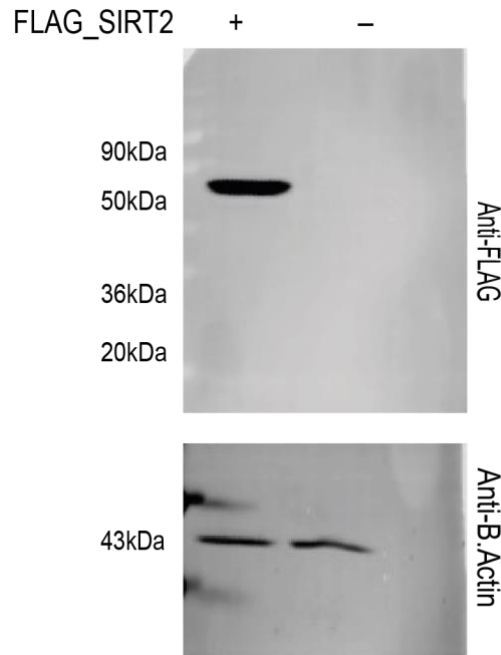


**Figure 5.4 – Overexpression of FLAG-tagged-Sirt2.** Sirt2-FLAG overexpressed in HeLa cells for 24 hrs. 25  $\mu$ g of the protein lysate was immunoblotted using an anti-FLAG Antibody.  $\beta$ -Actin used as a control n=1

Next, HeLa cells were transfected with C-terminally FLAG-tagged Sirt2 construct for 24 hours. In parallel, cells were treated with AGK2, SirReal2 (Sirt2 inhibitor) and TSA for 8 hours before harvesting. 25  $\mu$ g of extracted proteins were immunoblotted against anti-acetyl-lysine and  $\beta$ -actin antibodies. In Figure 5.5, multiple acetylation bands were detected in all conditions, but we observed a reduction in Sirt2-FLAG compared to control. Inhibiting overexpressed Sirt2 by AGK2 and SirReal2 showed slightly higher acetylation levels compared to control. An observed difference in both acetylation levels and ac-tubulin compared to Sirt2-Flag. However, results showed that AGK2 had a better effect on inhibiting overexpressed Sirt2. This approach will help provide further information about Sirt2 substrates acetylation levels changes +/- Sirt2 at a cellular level which was used successfully in many previous studies (2, 3).

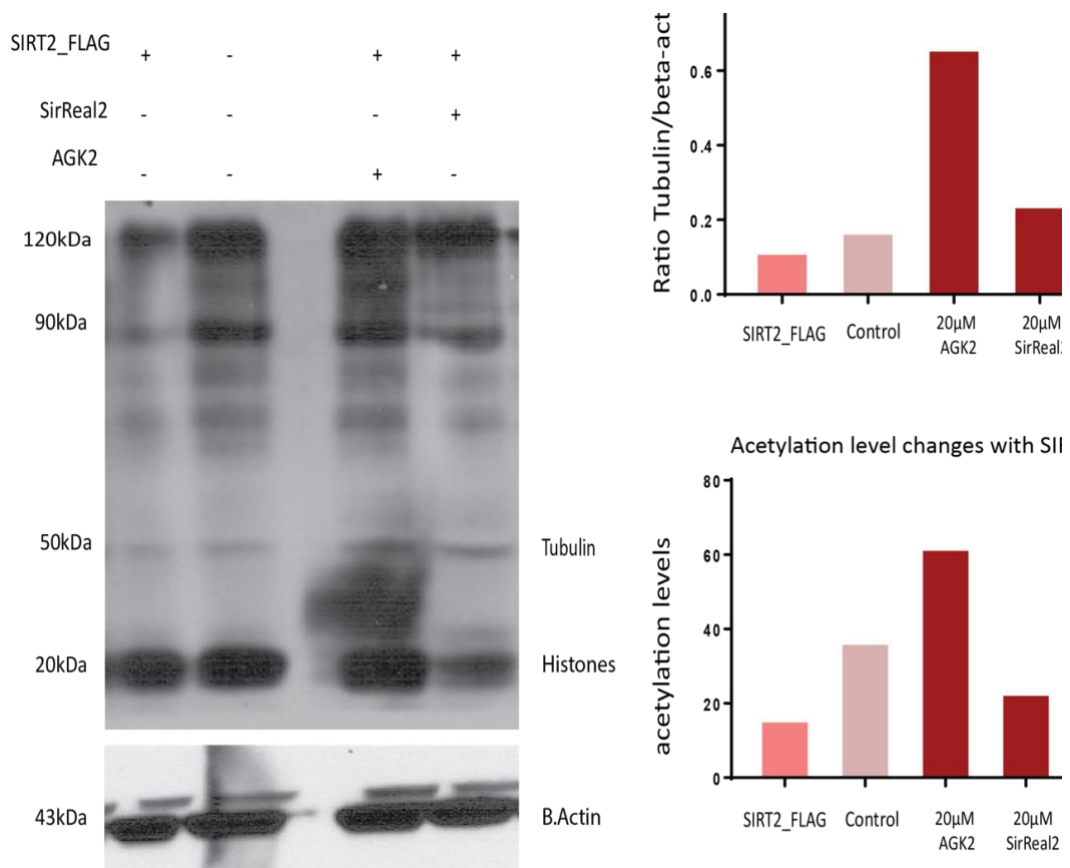


**Figure 5.5 – Optimisation of overexpression and inhibition of Sirt2.** Immunoblotting of changes of acetylation levels between overexpression and inhibition of Sirt2 in HeLa cells. Cells were transfected with Sirt2-FLAG for 24 hours then treated with inhibitors 20  $\mu$ M AGK2 and 20  $\mu$ M SirReal2 for 8 hours. 25  $\mu$ g of protein was separated on a gel, and immunoblotting was performed using an anti-acetyl-lysine antibody. The acetylation intensity was normalised to  $\beta$ -Actin n=1 PEI/DMSO (control)

Levels of acetylation were assessed by immunoblotting with a pan acetyl-lysine antibody. An observed change in acetylation levels in both conditions is evident in total cell lysates, Expression of Sirt2-FLAG resulted in a decrease in the acetylation of several bands as expected (Figure 5.6). An anti-acetylated-tubulin antibody was used to detect tubulin acetylation specifically. An observed change in intensity of the band at 50kDa due to overexpression of Sirt2-FLAG is consistent with previous research that showed that Sirt2 deacetylates tubulin.

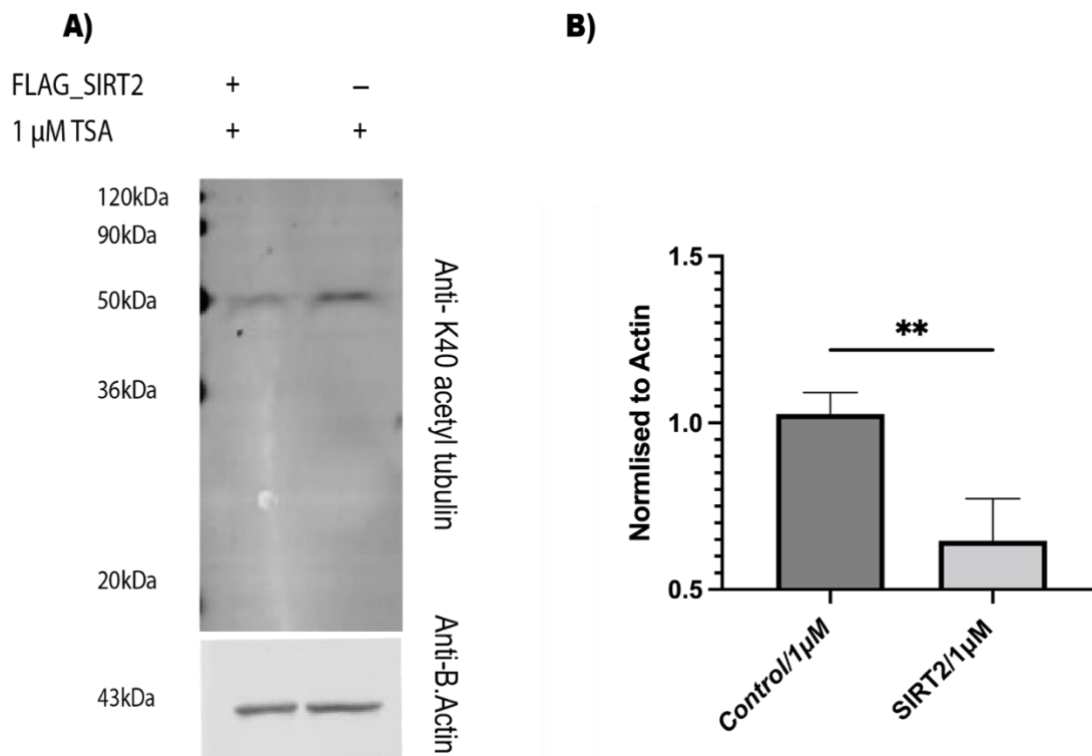


**Figure 5.6 – Overexpression of Sirt2 reduces acetylated-tubulin levels.** **A)** Representative Immunoblot showing reduced Tubulin acetylation levels in HEK293T cells after overexpression of Sirt2(24hrs) + 1 $\mu$ M TSA (8hrs) detected by anti-Lys40 acetyl-tubulin antibody,  $\beta$ -Actin used as a loading control. **B)** An unpaired T-test was used to determine the significance of the change in ac-tubulin levels with or without Sirt2 overexpression ( $p$ -value <0.0029). Results are normalised to the control condition— $n$  =3.

As mentioned previously, Sirt2 is the only cytoplasmic KDAC, but it is also localised to the nucleus and has nuclear substrates. HeLa cells were transfected with 1 $\mu$ g of Flag-Sirt2 for 24hrs, and we performed immunofluorescence microscopy with staining using anti-Flag and anti-acetyl-lysine antibodies. These results showed that Sirt2 is localised mainly to the cytoplasm (Figure 3.7) (Narita et al., 2018).

In addition, the deacetylase function of Sirt2 on different cellular compartments results showed a reduction in nuclear acetylation levels (mainly histone acetylation) in Sirt2 transfected compared to non-transfected cells. The detection of acetylation levels in other

compartments was difficult due to the high signal from histone acetylation. It can be seen that there is minimal overlap between acetylation and Sirt2-FLAG staining, which confirms that Sirt2 may reduce cytoplasmic and nuclear acetylation (North and Verdin, 2007).

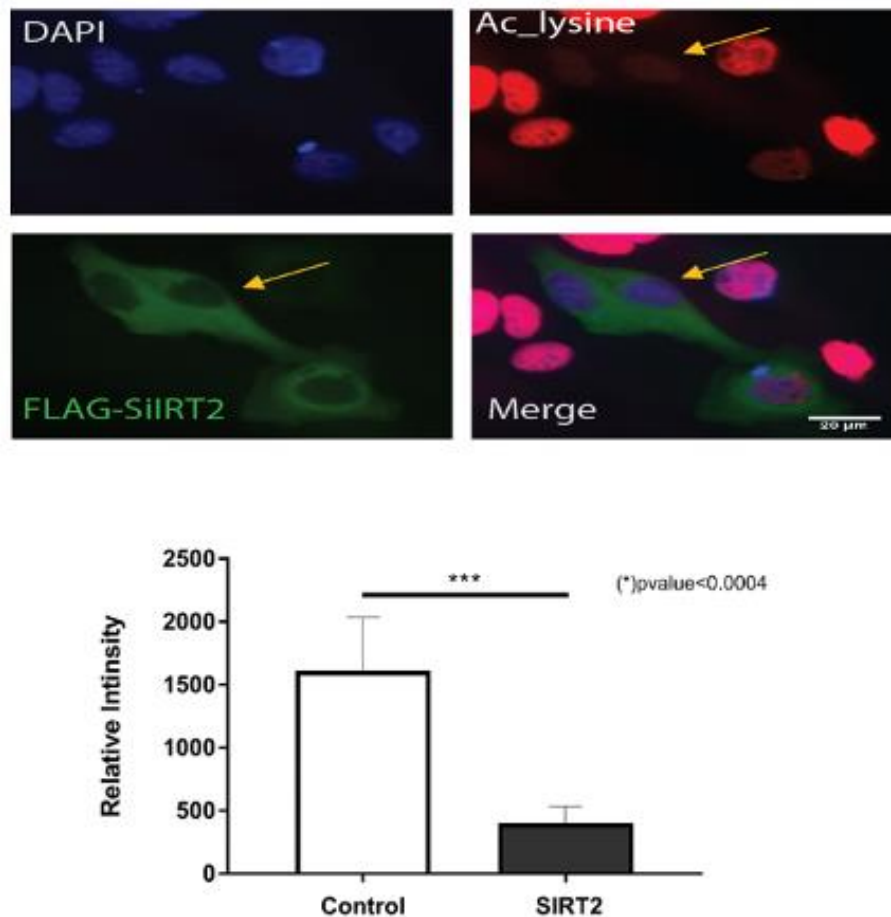


**Figure 5.7 – Overexpression of Sirt2 significantly reduces acetylation levels.** Representative images of Immunofluorescence staining after overexpression with Flag-tagged Sirt2. DAPI (Blue) 1:250 Anti-Flag (Green) and 1:250 Anti-Acetyl-lysine (RED). Quantification of acetylation level changes +/-Sirt2 was conducted using ImageJ software (mean + SEM unpaired t-test from two independent experiments with two technical replicates for each) n=4, \*\*\* p<0.0004. Scale bars represent 20μm.

Next, we used IP/pulldowns to enrich proteins of interest and measure the acetylation levels with or without Sirt2 activity. Moreover, IP will provide information about Sirt2 and substrates protein-protein interactions. The Sirt2-FLAG construct was transfected as stated before, cells

were harvested with IP lysis buffer, and Sirt2 were immunoprecipitated with anti-FLAG agarose resin, eluted and immunoblotted using anti-FLAG antibody. Figure 5.8A displays an immunoblot of input, elution, supernatant, wash 1 and 2 of Sirt2 and control pulldowns. FLAG bands were detected in the input and elution of Sirt2-FLAG but not the control sample, supernatant, wash 1 and wash 2. As the molecular weight of Sirt2 is between 42-44kDa, it showed an overlap with the anti-Flag antibody heavy chain at 50kDa as pointed with red and yellow arrows representing Sirt2 and heavy chain, indicating that the boiling elution released anti-FLAG antibody. The same experiment was repeated but with a competitive elution using FLAG peptide to minimise contamination with antibody chains. We detected a strong band corresponding to Sirt2 in input and peptide elution at 42-44 kDa of Sirt2-FLAG pulldown but not in control (Figure 5.8 B), demonstrating that the IP worked well.

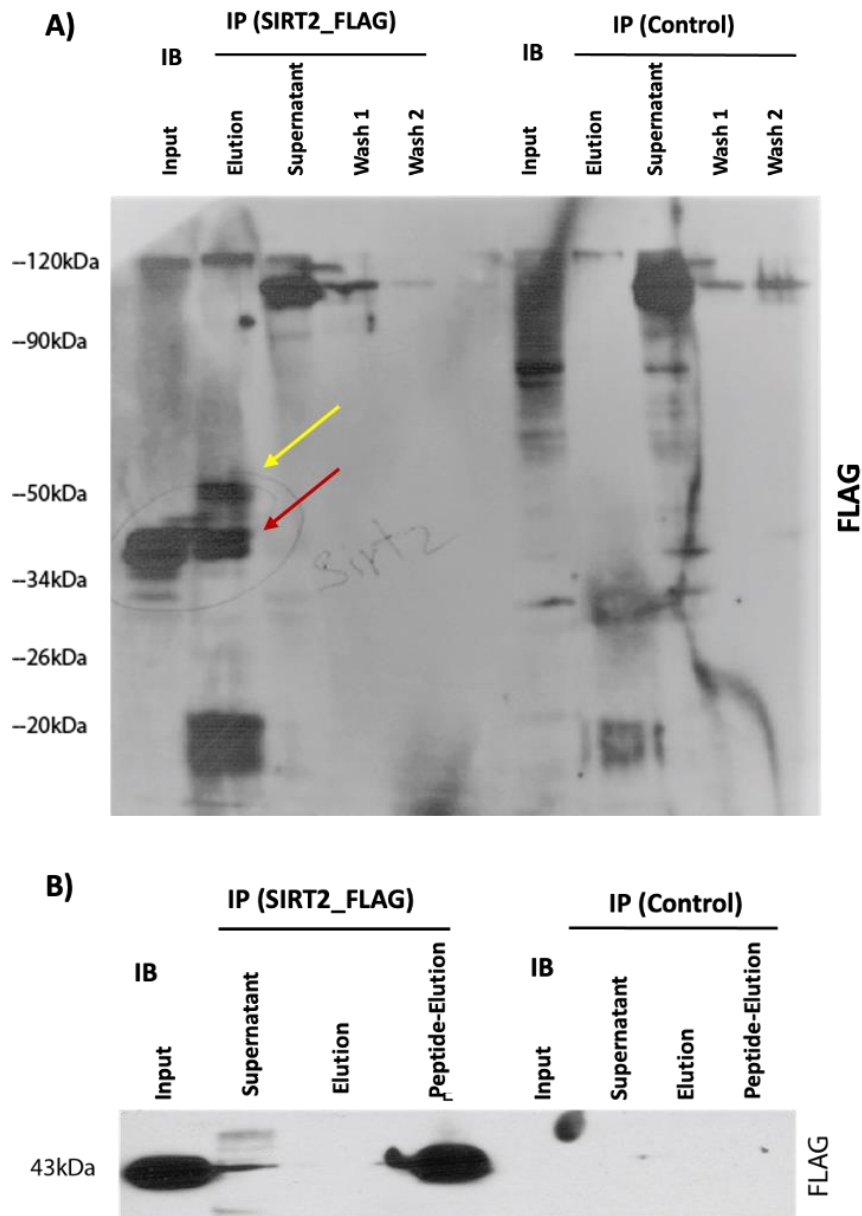
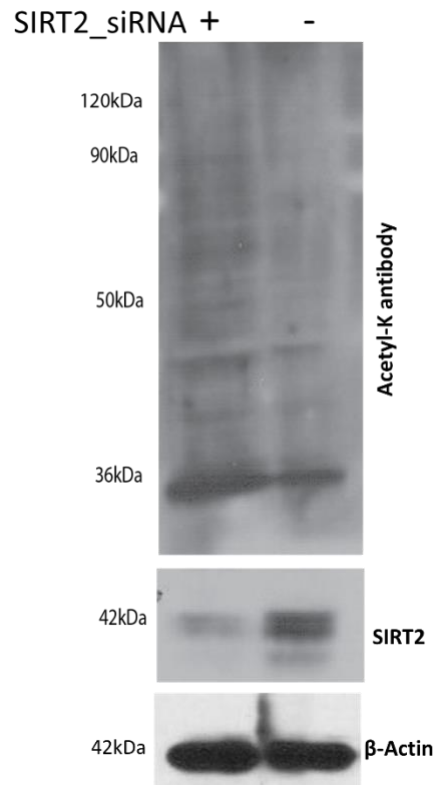


**Figure 5.8 – Immunoprecipitation of Sirt2-FLAG; A)** FLAG pull-downs from control and Sirt2-FLAG transfected HeLa cells (24 hours) with boiling elutions and immunoblotting with anti-FLAG antibody. The first lane for cell lysate (input) and the second lane for pull-down (elution) showed Sirt2 a band at 42-44 kDa, and those bands were absent in the control input and elution. No FLAG signals were detected in supernatant washes, although some extra bands appeared in both pull-downs. The yellow arrow represents the anti-FLAG antibody heavy chain at 50kDa, and the red arrows show the Sirt2 band. **B)** FLAG pull-downs from control and Sirt2-FLAG transfected HeLa cells (24 hours) with FLAG peptide elutions and immunoblotting with anti-FLAG antibody. The first lane for input and the fourth lane for peptide elution showed Sirt2, a band at 42-44 kDa; those bands were absent in control input and peptide elution. No Sirt2 band was detected in the subsequent boiling elution for both pull-downs indicating an efficient, competitive elution with FLAG peptide.

As mentioned previously, Sirt2 overexpression reduces acetylation levels, and the opposite occurs with Sirt2 inhibition with KDAC inhibitors (Zhang et al., 2013, North et al., 2003). Depleting Sirt2 using small interfering RNA (siRNA) is likely to be much more specific than using small molecule inhibitors, which can have off-target effects. Therefore, we used siRNA to reduce Sirt2 levels to increase acetylation of Sirt2 in cell culture and hopefully show a similar result to the in vivo study.

HeLa cells were treated with Sirt2 RNAi and control RNAi for 24 hours; cells were then harvested and immunoblotted against Sirt2 and pan acetyl-lysine antibodies to observe changes in total acetylation levels. Figure 5.9 shows that transfection with Sirt2 siRNA decreased Sirt2 levels but did not provide a complete depletion. Next, a very minimal change happened in acetylation levels as a slight increase with Sirt2 RNAi were observed.



---

**Figure 5.9 – Optimisation of Sirt2 knockdown in HeLa cells.** HeLa cells were transfected with 25 nM Control or Sirt2 RNAi for 24 hours, and cell lysate was immunoblotted with acetyl-lysine antibody, Sirt2 and  $\beta$ -Actin. Results show a slight change in acetylation levels and an observed change in Sirt2 levels.

Next, the same experiment was repeated with a longer treatment time and higher concentration. Figure 5.10 A Sirt2 levels were depleted with 25 nM and 50 nM Sirt2 siRNA but not with the control. We detected the two isoforms of Sirt2, Sirt2.1 at 43kDa and Sirt2.2 at 39.5 kDa, which was slightly apparent in previous results.

However, the acetyl-lysine immunoblot showed no changes between samples, which was unexpected. Although the antibody used was not protein specific, we expected more acetylation bands to appear more intense with Sirt2 knockdown. Immunoblotting of the same samples was repeated, and acetylated BSA (control sample) was added to show if acetyl-lysine antibody could detect, as shown in figure 5.10 B. We could detect BSA acetylation at 66 kDa, but there is no observed acetylation change between other samples. Here we noticed that there are some issues with this antibody's sensitivity, the histone bands aren't as intense as they used to be, and the sensitivity has decreased.

Overall, Sirt2 knockdown can provide more specific modulation of acetylation levels changes with an IP of a protein of interest. This approach is commonly used with KATs and KDACs substrate acetylation validation, and it has been used before with Sirt2 in many studies (North et al., 2003) (Wang et al., 2017a, Zhang et al., 2013).

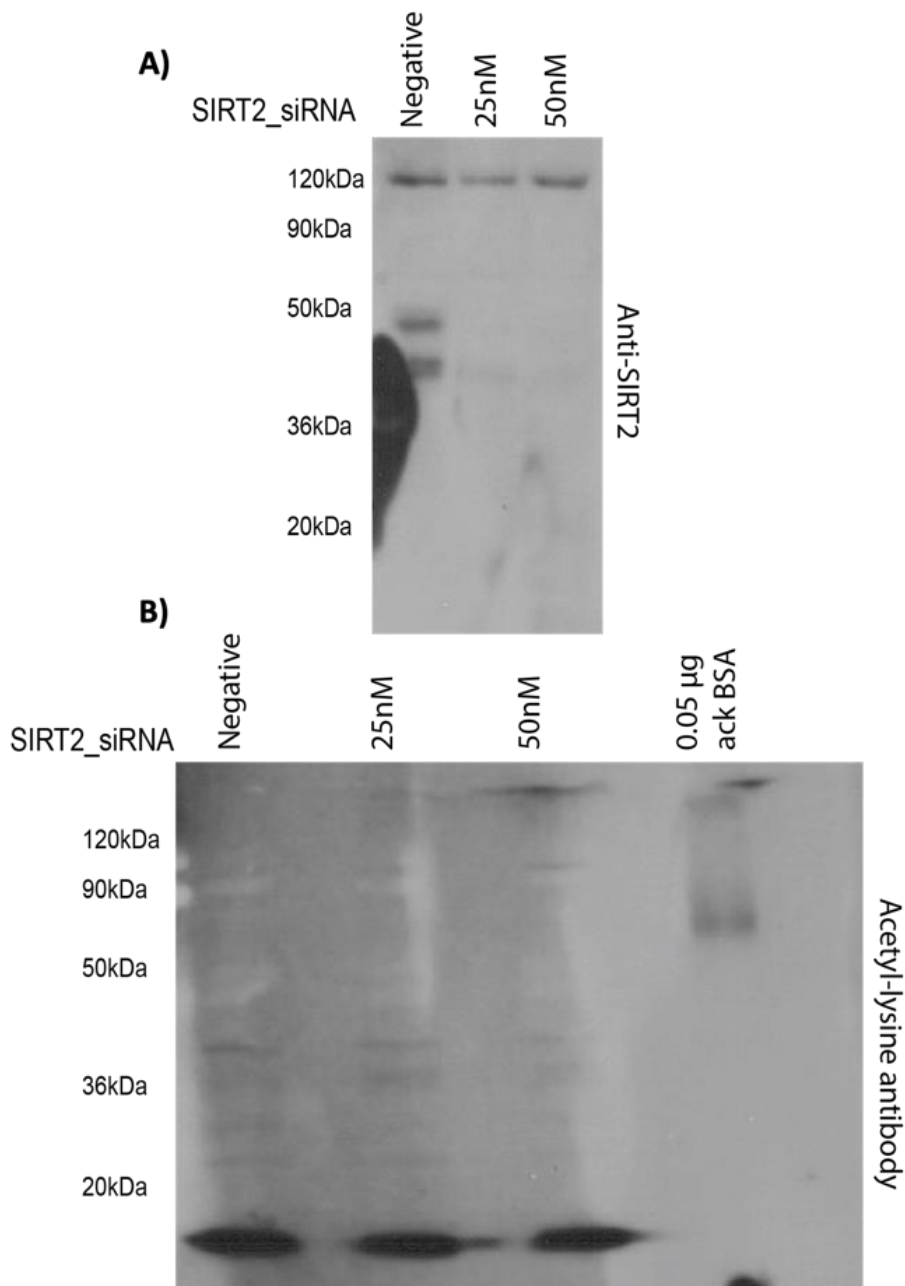


**Figure 5.10 – Optimisation of Sirt2 knockdown and measurement of acetylation levels in HeLa cells.** HeLa cells were transfected with control, 25 nM, 50 nM Sirt2 RNAi for 48 hours, and 35 µg of protein extracted from cell lysate was immunoblotted with acetyl-lysine antibody and anti-Sirt2, 0.05 µg of acetylated BSA were used as a positive control for the acetyl-lysine antibody. **A)** Results show a change in Sirt2 levels between control and treated samples. **B)** There was no observed change in acetylation levels; a signal of acetylated BSA was detected at 66 kDa. Sirt2 has a role in regulating the crosstalk between acetylation and ubiquitination. Studies showed that an increase in GluA1 (AMPA) receptors subunit ubiquitination is coupled with a decrease in acetylation levels due to Sirt2 overexpression and vice versa.

These experiments were conducted in cultured hippocampal neurons and HEK239 cells (Wang et al., 2017a). Our identified putative Sirt2 substrates in the Sirt2 KO acetylome found that ubiquitination and acetylation shared and regulated more than 49% (Signling, 2017). Thus, ubiquitination sites were one of the criteria applied to putative Sirt2 substrates for further investigation. Here Sirt2 was overexpressed in HeLa cells and immunoblotted against ubiquitin antibodies. As shown in Figure 5.11, there was a change in ubiquitination levels because of increased Sirt2 levels. Our plan was to change Sirt2 levels and activity and Mg132 to block protein degradation for a protein of interest and provide more specific results than global changes.

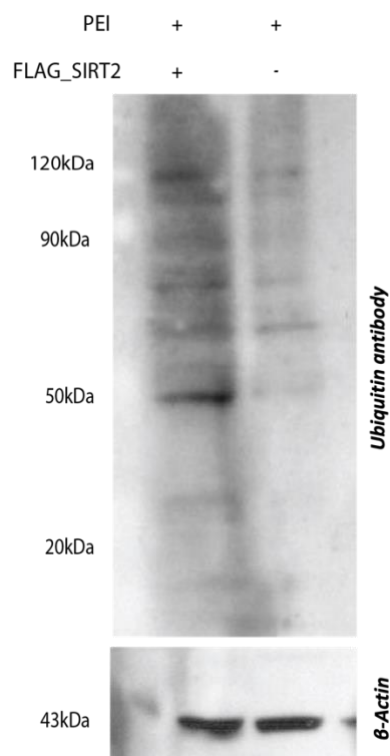


**Figure 5.11 – Detection of a change in ubiquitination levels in response to Sirt2 overexpression in HeLa cells.** HeLa cells were transfected with 2  $\mu$ g Sirt2-FLAG and PEI control expressed in HeLa cells for 24 hours and immunoblotting with an anti-ubiquitin antibody and  $\beta$ -Actin. Results show a potential increase in ubiquitination levels with Sirt2-FLAG overexpression.

### 5.3.3 Testing VAMP2/3 deacetylation by Sirt2

From the Sirt2 KO/WT acetylome data, VAMP2 and VAMP3 were identified as putative Sirt2 substrates. Vamp2/3 are acetylated on three ac(K) sites (K35, K42 and K66), two of which (K42 and K66) showed a significant increase in acetylation in Sirt2 KO mouse brain tissue. It indicated that Sirt2 might regulate the acetylation of those sites. K35, K42 and K66 sites were identified as Vamp3 sites from the acetylome profile. However, these sites map to a highly conserved sequence region shared between Vamp1/2/3. Figure 5.12 illustrates a multiple sequence alignment of the sequences of VAMP1, 2 and 3 from human and mouse; all these three proteins shared a highly conserved area shown inside the green box and labelled with a star symbol. Few changes in the sequence were found, mostly in VAMP1. As shown in this figure, the three identified sites were located inside the conserved area, this is not limited to humans and mice only, but it is also conserved in rats (Bateman et al., 2021, Signling, 2017).

```

SP|Q15836|VAMP3_HUMAN -----MSTGPTAATG|SNRRLQQTQ|NQVDEVVDIMRVNV|DKVLERDQ| 41
SP|P63024|VAMP3_MOUSE -----MSTGVPSGSSAATG|SNRRLQQTQ|NQVDEVVDIMRVNV|DKVLERDQ| 45
SP|P63027|VAMP2_HUMAN MSATA--ATAPPAAPAGEGGPPAPPNLT|SNRRLQQTQ|AQVDEVVDIMRVNV|DKVLERDQ| 58
SP|P63044|VAMP2_MOUSE MSATA--ATVPPAAPAGEGGPPAPPNLT|SNRRLQQTQ|AQVDEVVDIMRVNV|DKVLERDQ| 58
SP|P23763|VAMP1_HUMAN MSAPAQPPAEGTEGTAPGGGPPGPPPNMT|SNRRLQQTQ|AQVEEVVDIIRVNV|DKVLERDQ| 60
SP|Q62442|VAMP1_MOUSE MSAPAQPPAEGTEGAAPGGGPPGPPPNMT|SNRRLQQTQ|AQVEEVVDIMRVNV|DKVLERDQ| 60
                                     *****  **.*.....*****

SP|Q15836|VAMP3_HUMAN KLSELDDRADALQAGASQFETSA|AKLKRKYWWKN|CKMWAIGITVLVIFIIIIIVVWVSS| 100
SP|P63024|VAMP3_MOUSE KLSELDDRADALQAGASQFETSA|AKLKRKYWWKN|CKMWAIGISVLVIIVIIIVVWCVS-| 103
SP|P63027|VAMP2_HUMAN KLSELDDRADALQAGASQFETSA|AKLKRKYWWKN|LKMMIILGVICAILIIIIIVYFST-| 116
SP|P63044|VAMP2_MOUSE KLSELDDRADALQAGASQFETSA|AKLKRKYWWKN|LKMMIILGVICAILIIIIIVYFST-| 116
SP|P23763|VAMP1_HUMAN KLSELDDRADALQAGASQFESSA|AKLKRKYWWKN|CKMMIMLGAICAIVVVVVIYFFT-| 118
SP|Q62442|VAMP1_MOUSE KLSELDDRADALQAGASQFESSA|AKLKRKYWWKN|CKMMIMLGAICAIVVVVVIYFFT-| 118
                                     *****  **.*.....*****

```

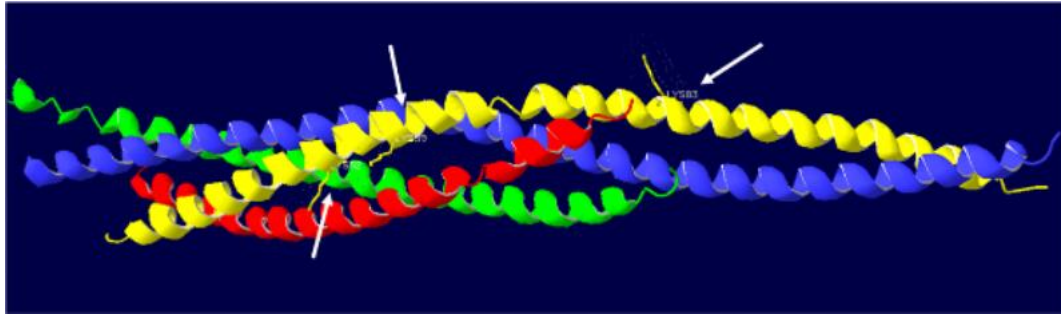
**Figure 5.12 – Multiple sequence alignment of VAMP 1,2,3 protein sequences.** Green box represents a ~100% identical region containing conserved acetylated sites of Vamp1,2 and 3 among human and mouse species. Identified ac(K) sites from sirt2 KO acetylome were highlighted (red). Proteins sequences were generated using UniProt alignment tools (Bateman et al., 2021).

Moreover, although those sites were not identified in the Phosphosite database search, K35 and K42 were identified in the acetylome profile of rat brain tissue (Lundby et al., 2012b,

Signling, 2017). Studies have shown that these lysines are also modified by ubiquitination (Yamazaki et al., 2013). Ubiquitination of VAMP3 prevents its interaction with other proteins and decrease its stability by protein degradation (Yamazaki et al., 2013). The three sites are located on coiled-coil (SNARE domain) on the Vamp2/3 structure.

VAMP3 is a member of the VAMP/synaptobrevin family containing other six proteins, of which VAMP1 and VAMP2 (Synaptobrevin-2). VAMP3 is involved in crucial molecular functions such as; SNARE complex assembly, vesicle fusion, proteins transportation and regulation of cell secretions VAMP3 is localised to cytoplasm and vesicles and is expressed widely across different human cells and tissues . Although acetylome data showed that VAMP3 is a primary protein for the three ac(K) sites, and given the higher level of expression of VAMP2 in the brain (Kirti et al., 2015), this is most likely the specific protein from which this acetylated peptide is derived.

VAMP2, also known as (Synaptobrevin-2) is localised in the cell membrane enriched in the nervous system within the presynaptic terminal. It is involved in many synaptic and developmental functions through its role in neurotransmitters release. It is an essential molecule in the SNARE complex, consisting of STX1A SNAP25 and VAMP2. The SNARE complex is involved in synaptic vesicle fusion from the presynaptic membrane and enables the vesicles to release their content into the synaptic cleft, activating postsynaptic receptors. Figure 5.13 illustrates the SNARE complex tertiary structure containing a four-helix bundle with VAMP2 shown in yellow, STX1A shown in blue and two copies of SNAP25 shown in red and green (Yamamoto et al., 2012, Yoon and Munson, 2018).



---

**Figure 5.13 – The tertiary structure of SNARE complex.** Vamp2 (yellow), Stx1A (blue), and Snap25 (red, green) showing Vamp2 ac(K) sites. White arrow showing LYS 35, 42 and 66 positions on VAMP2.

Studies have revealed that VAMP2 is a substrate of Botulinum neurotoxin, a protein produced by *Clostridium botulinum* bacteria, causing a severe neurological disorder called flaccid paralysis (Gray et al., 2018). Botulinum cleavage of VAMP2 at the site (58-59 or 76-77) might prevent SNARE complex formation, and therefore, this may have an impact on synaptic vesicle fusion and neurotransmitter release (Yamamoto et al., 2012, Michael and Raymond, 2000). Thus, deacetylase VAMP2 may regulate SNARE complex assembly by preventing cleavage of VAMP2 by Botulinum neurotoxin. Or by regulating the stability of VAMP2 by revealing lysine residues that can be ubiquitinated (Figure 5.14).

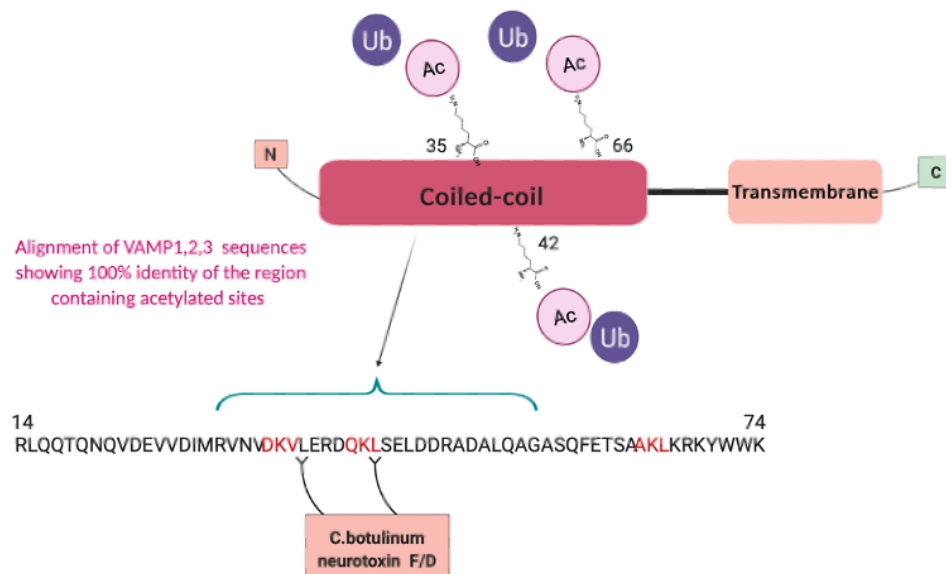


**Figure 5.14 – Domain structure and PTM sites of human VAMP3.** The acetylated/ubiquitinated sites identified by our Sirt2-regulated acetylome dataset and the cleavage site of Botulinum neurotoxin are indicated.

To validate if Sirt2 regulates VAMP2/3 acetylation, we needed to confirm that VAMP3 is acetylated. HeLa cells were transfected with a VAMP3-HA construct was transfected, as described previously for Sirt2 and CDK9. VAMP3 was then pulled down with anti-HA agarose resin and immunoblotted using anti-HA antibodies, as shown in Figure 5.15A. Bands at 12 kDa were detected in both the input and elution of the VAMP3-HA pulldown with no band detected in the control input. Results showed a light band in elution control corresponding to VAMP3 that might occur due to contamination. Afterwards, both pulldowns input and elution samples were immunoblotted using a pan anti-acetyl-lysine antibody. Multiple acetylation bands in the input samples of both pulldowns were observed. However, no bands were detected in control or VAMP3-HA elution samples (Figure 5.15B), indicating that we could not detect VAMP3 acetylation.

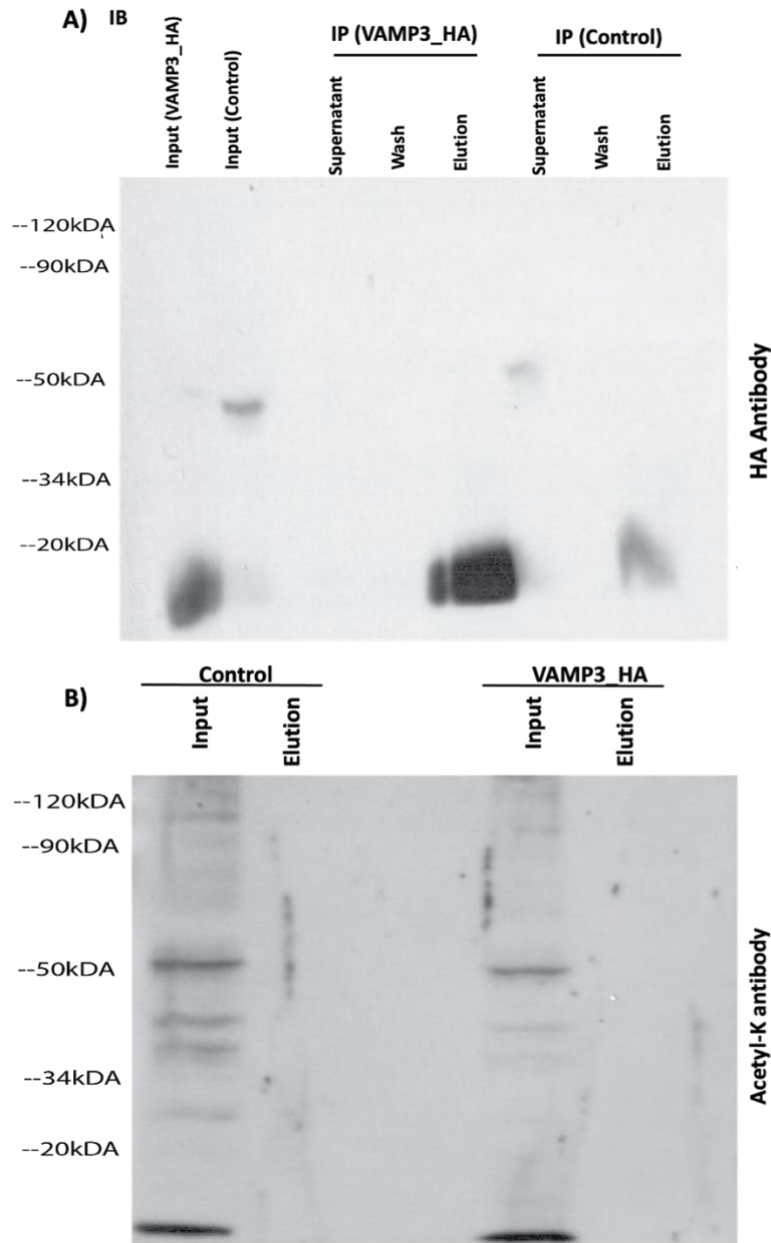


**Figure 5.15 – Immunoblotting of HA-tagged VAMP3 pulldowns. A)** Pulldown of HA for VAMP3 and control from cell lysates prepared from two 10 cm plates of transfected HeLa cells (24 hours) immunoblotted with anti-HA antibody. First, second lane inputs showed a band corresponding to VAMP3 at 12k Da but not in control. Pulldown elution for VAMP3-HA showed a strong band 12k Da; a similar but lighter band appeared at control elution. No HA signals were detected in the supernatant and wash for both pulldowns. **B)** inputs and elution samples of both pulldowns were immunoblotted using a pan acetyl-K antibody; multiple acetylation bands were detected in both inputs; no bands were detected in either elution.

To further optimise this experiment to detect VAMP3 acetylation, we changed the acetylation detection protocol. First, the VAMP3 pulldown was scaled up with each pulldown using a cell lysate prepared from four 10 cm plates of transfected HeLa cells, and transfection time was increased to 48 hours to allow more protein to be produced that might allow VAMP3 acetylation to be detected. Unfortunately, similar results were observed with no acetylation band detected in VAMP3 pulldown elution.

Next, we added an extra step; we used KDAC inhibitors to inhibit endogenous deacetylase activity, which should increase acetylation signals and make VAMP3 acetylation to be more easily detected. The same experiment was repeated, and cells were treated with 2  $\mu\text{M}$  of TSA and 20  $\mu\text{M}$  of AGK2 for 8 hours, then harvested using IP lysis buffer. The VAMP3-HA pulldown experiment was successfully performed. Unfortunately, there was no change observed from the previous experiment. However, the intensity of acetylation bands in the input samples was more apparent due to deacetylase activity inhibition. This experiment was repeated with CDK9, but no observed change was observed.

Then, we questioned the IP lysis as it is known that acetylation is reversible and dynamic modification. This might cause a loss in modification during sample preparation if there is a deacetylase activity in the sample. Thus, we repeated the same experiment and harvested cells using IP lysis buffer containing 2 $\mu\text{M}$  of TSA and 20 $\mu\text{M}$  of AGK2. Figure 5.16 A illustrates a successful VAMP3 IP that detected HA bands corresponding to VAMP3 in both input and elution samples of VAMP3-HA but not in the control samples. Input and elution of both pulldowns were immunoblotted using a pan anti-acetyl-lysine antibody, as shown in figure 5.16 B. We observed an increase in the intensity of multiple acetylation bands in the inputs compared to previous results. Still, there were no bands detected in elution samples which again indicate that acetylation of VAMP3 can't be detected.

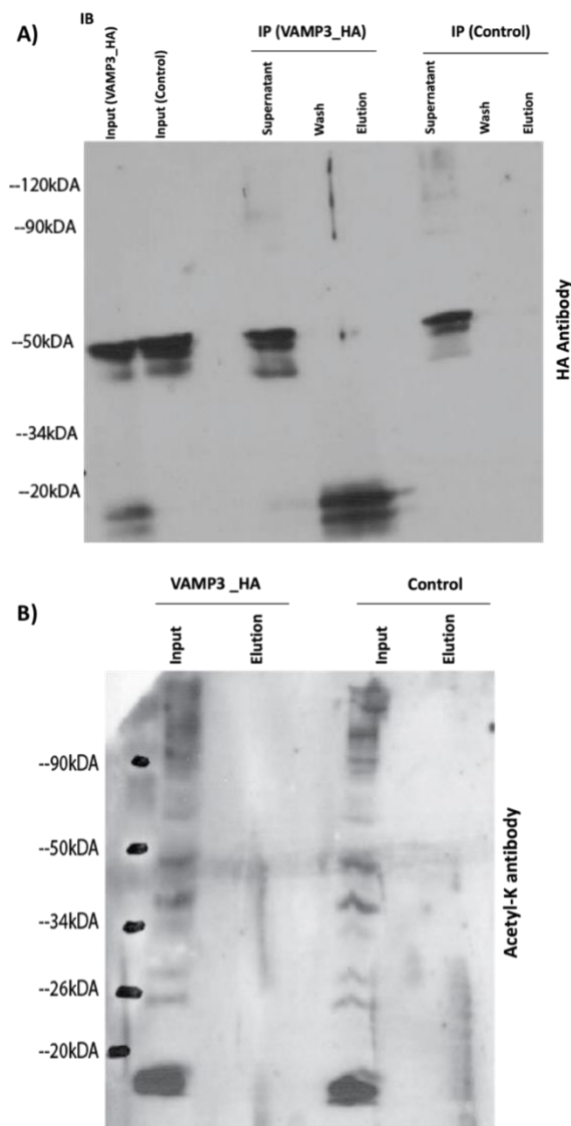


**Figure 5.16 – VAMP3-HA pulldown with inhibition of KDAC deacetylase activity. A)** Pulldown of HA for VAMP3 and control using lysates from four 10 cm plates of transfected HeLa cells (for 24 hours), treated with 2  $\mu$ M of TSA and 20  $\mu$ M of AGK2 for 8 hours, IP lysis buffer supplemented with 2  $\mu$ M of TSA and 20  $\mu$ M of AGK2, immunoblotting with an anti-HA antibody. First, second lane inputs, the first lane showed a band corresponding to VAMP3 at 12 kDa but not in control. Pulldown elution for VAMP3-HA showed a strong band 12 kDa, with no band detected in the control elution. No HA signals were detected in the supernatant and wash for both pulldowns. **B)** Inputs and elution samples were immunoblotted using a pan acetyl-K antibody. Multiple acetylation bands were detected in both inputs; no acetylation bands were detected in elutions.

Later, we noticed some unspecific bands repeatedly appearing in control elutions, which raises the question about the specificity of the band detected by the HA antibody. If VAMP3 pulldown was not performed well and bands detected were unspecific. Thus, immunoblot of input and elution samples against VAMP3 antibody was performed to detect the VAMP3 overexpressed protein, not the HA tag. Results found that a much more intense band corresponds to VAMP3 in the VAMP3 pulldowns than the control pulldowns (Figure 5.17). These results confirmed that the VAMP3 transfection and IP of VAMP3 worked very well. Although this approach was followed by many studies (Zhang et al., 2013, Wang et al., 2017a, Lalonde et al., 2017), detecting acetylation of VAMP3 and other known Sirt2 substrates is very challenging.

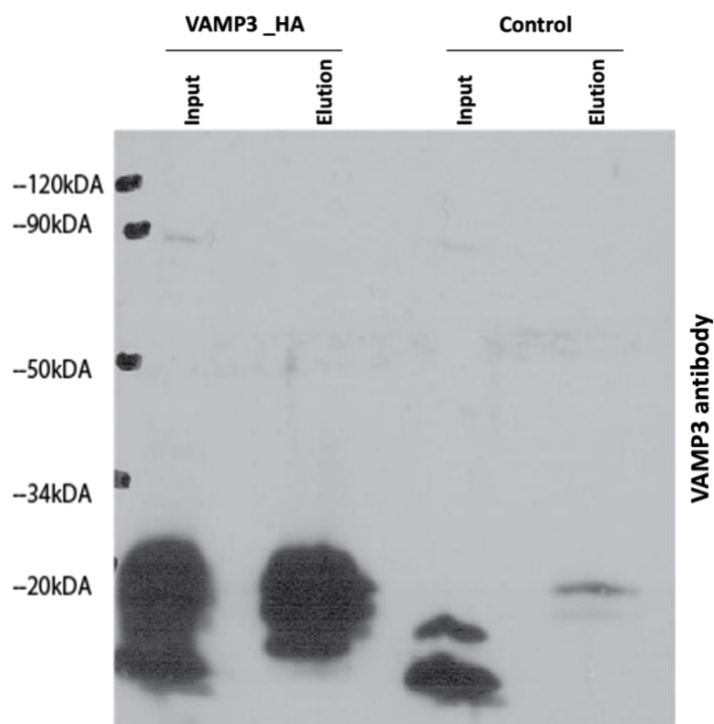


**Figure 5.17 – Detection of VAMP3 in VAMP3\_ HA pulldowns.** Inputs and elutions of both pulldowns were immunoblotted using an anti- VAMP3 antibody. Results showed a strong band of VAMP3 in VAMP3-HA pulldowns input and elution detecting the overexpressed VAMP3, and control input detects VAMP3 at a lower intensity representing endogenous VAMP3; this signal is absent in the control elution.

#### **5.3.4 Identification of VAMP2/3 acetylation sites with AP-MS**

After many attempts, we understand that acetylation detection by western blot is might be challenging. However, given that we detected putative Sirt2 substrates using LC-MS/MS in the first place, we decided to perform affinity purification-mass spectrometry (AP-MS) to attempt to validate VAMP2/3 acetylation in cell culture. VAMP3-HA was overexpressed in HEK239 cells. These were chosen because they can be transfected at high efficiency, and Sirt2 and VAMP3 are normally expressed in HEK239 cells (Thomas and Smart, 2005). Constructs transfected into two 10 cm plates HEK239 cells for 48 hours to allow protein production and treated with 20  $\mu$ M of TSA and 20  $\mu$ M of AGK2 for 8 hours, then harvested using IP lysis buffer with 2  $\mu$ M of TSA and 20  $\mu$ M of AGK2. Tagged proteins were pulled down with anti-FLAG agarose resin or anti-HA agarose resins. Elutions were cleaned up and digested with trypsin using the S-trap columns and analysed using LC-MS/MS. Data were processed and quantified, and acetylation sites were set as a variable modification in the MaxQuant analysis (43).

VAMP3 were identified as part of the most abundant proteins in their pulldowns as assessed by their iBAQ values, demonstrating that the pulldowns and sample preparation for LC-MS/MS was performed correctly. Furthermore, Sirt2 was not identified in VAMP3 pulldown. However, no acetylation sites were detected for any of the bait protein. Peptides covering the region of these proteins where acetylation sites of interest are located were identified with high intensity compared to other peptides. Table 5.1 lists the identified peptide sequences for VAMP3, the intensity of each peptide and its corresponding acetylation sites according to the Phosphosite dataset and the modification status for each peptide detected by MaxQuant (Signling, 2017, Jürgen and Matthias, 2008).

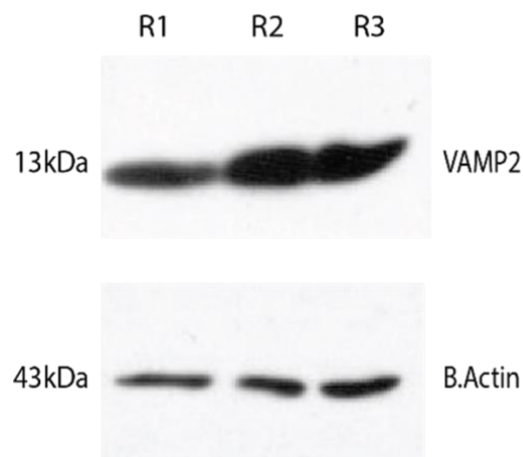
Peptides Sequence	Intensity	Acetyl (K)	Modifications
<b>VAMP3; VAMP2; VAMP1</b>			
LQQTQNQVDEVVDIMR	1.08E+08	–	Oxidation (M)
LQQTQNQVDEVVDIMR	2.43E+09	–	Unmodified
RLQQTQNQVDEVVDIMR	1.94E+08	–	Oxidation (M)
RLQQTQNQVDEVVDIMR	8.53E+08	–	Unmodified
STGPTAATGSNR	5.82E+05		Acetyl (Protein N-term)
LSELDDR	6.07E+05	–	Unmodified
VLERDQKLSELDDR	2.13E+06	K42	Unmodified
VNVDKVLER	3.95E+07	K35	Unmodified

**Table 5.1 – Bait peptides identified by LC-MS/MS of VAMP3-HA pulldown.**

Most Ac(K) peptides were identified with high intensity but detected in its unmodified status. Two 10 cm plates HEK239 cells, transfected with the different construct for 48 hours and treated with 2  $\mu$ M of TSA and 20  $\mu$ M of AGK2 for 8 hours. Cells were harvested with IP lysis buffer containing 2  $\mu$ M of TSA and 20  $\mu$ M of AGK2. Elution was digested with trypsin using the S-trap columns and analysed with LC-MS/MS. Data were processed and quantified using MaxQuant. No statistical tests were applied to the shown intensities because each construct has one replicate only.

### 5.3.5 Testing VAMP2 deacetylation by Sirt2

The tryptic peptide from VAMP2/3 bearing acetylation sites upregulated in the Sirt2 acetylome is identical in sequence in VAMP2 and VAMP3. Therefore, it is possible that those sites were detected on VAMP2, not VAMP3 in our acetylome dataset, given that VAMP2 is highly expressed in brain tissue with high sequence coverage (72%) in a mouse brain proteome dataset (Sharma et al., 2015). In order to assay VAMP2 acetylation in a neuronal line cell line, we chose to use NSC34 cell line (a hybrid motor neuron/neuroblastoma cell line) for endogenous VAMP2 pulldowns. Previous proteomic data conducted in Collins's lab showed that VAMP2 is expressed in NSC34 cells. We confirmed this by immunoblotting of NSC34 cell lysates with a VAMP2 antibody to detect endogenous VAMP2 (Figure 5. 18).



---

**Figure 5.18 – VAMP2 is expressed in NSC34 cells.** NSC34 cells (P12) were harvested and protein extracted. 35  $\mu$ g of proteins were used for immunoblotting with anti- VAMP2 and anti- $\beta$ -Actin used as control. Results showed that VAMP2 is expressed in NSC34 cells; three biological replicates were used for this experiment R1, 2 and 3.

To induce hyperacetylation of endogenous VAMP2, NSC34 cells were then treated with 2  $\mu$ M TSA and 40  $\mu$ M AGK2/ Endogenous VAMP2 was immunoprecipitated along with a non-specific IgG pulldown, which was used as a control. The endogenous pulldown of VAMP2 from NSC34 cells was successful with VAMP2 detected in both the input and elution (Figure 5.19A). VAMP2 and IgG pulldown samples were next immunoblotted using a pan anti-acetyl-lysine antibody (Figure 5.19B). The results showed non-specific bands in almost all samples with no bands corresponding to VAMP2; these results were not very promising as we were not able to detect regular acetylation bands pattern of acetyl-lysine antibody in the input samples, the lack of histone acetylation bands indicated a problem with detection of acetylation in this experiment.

A reciprocal immunoprecipitation also performed in an acetyl-lysine pulldown from the same cells and immunoblotted using an anti-acetyl-lysine antibody (Figure 5.19C) and anti- VAMP2 (Figure 5.19D). This experiment aimed to pulldown all acetylated proteins and then detect VAMP2. The result showed that we were able to detect VAMP2 in input and supernatant of both IgG and acetyl-lysine antibody but not in the elution samples. The lack of acetylated histone bands again indicated a problem with the detection of acetylation in this experiment, specifically the pan acetyl-lysine antibody.

Unfortunately, we had many problems with NSC34 since the cells were difficult to work with, especially when we needed to maximise pulldown and treat the cells with a lot of KDAC inhibitors. First, cells developed slowly in various batches obtained from multiple cell stocks. Then, we observed cell death when treated with a combination of KDAC inhibitors at different concentrations and time points needed for the following optimisation steps.

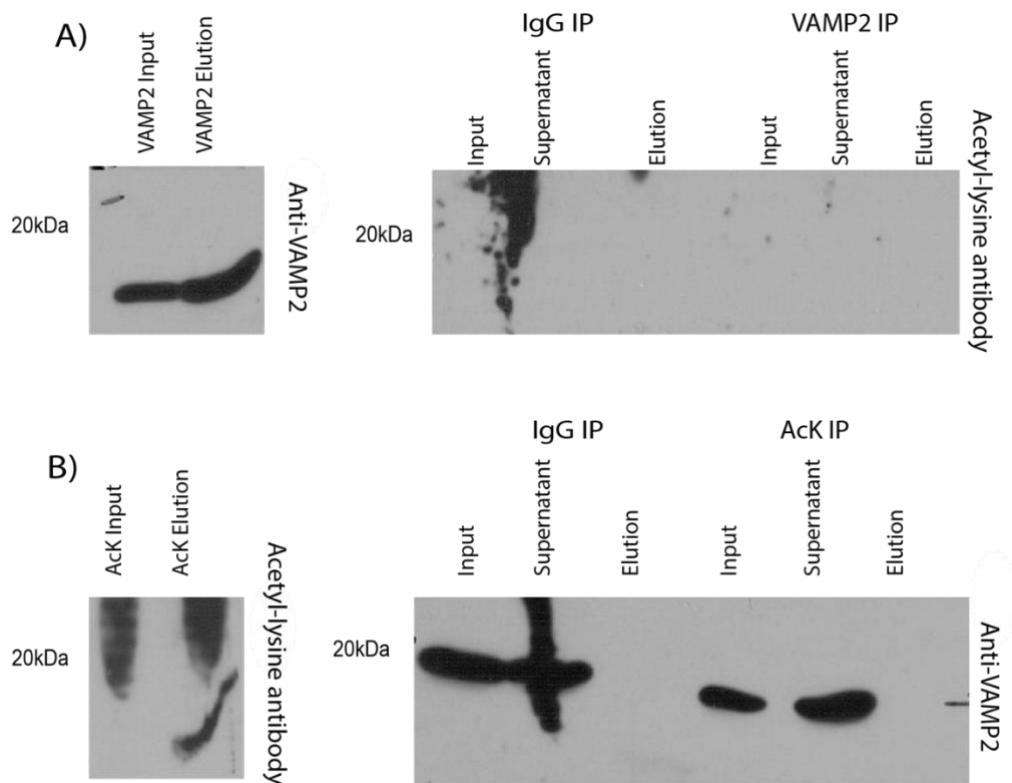


**Figure 5.19 – Endogenous IP of VAMP2 and IP of acetylated proteins in NSC34 cells.** Two T75 flasks of NSC34 cells were treated with 2  $\mu$ M of TSA and 40  $\mu$ M of AGK2 for 8 hours, IP lysis buffer supplemented with 2  $\mu$ M of TSA and 20  $\mu$ M of AGK2 were used to harvest cells and extract proteins, 2 mg of proteins were used for the endogenous IP of VAMP2, acetyl-lysine and IgG used as control. 1:50 vol/vol AB/S ratio were used. **A)** VAMP2 input and elution pull-down were immunoblotted against anti-VAMP2 antibody, showing VAMP2 signal at 12 kDa. IgG and VAMP2 pull-downs were immunoblotted using anti acetyl lysine antibody; results showed no signal corresponding to VAMP2 in all samples, both inputs and elution. **B)** An acetyl-lysine pull-down was immunoblotted against an anti-Acetyl-lysine antibody, showing multiple signals in both samples. IgG and Acetyl-lysine pull-downs were immunoblotted against anti-VAMP2 antibody, results showed an observed signal corresponding to VAMP2 in all the samples except for IgG and acetyl-lysine elution.

Thus, VAMP2 and acetyl-lysine endogenous pull-down experiments were repeated in HEK239 cells and the elution samples of VAMP2, acetyl-lysine and IgG were immunoblotted against anti- acetyl lysine antibody as shown in Figure 5.20. Non-specific bands were detected

between 90kDa to 50kDa in the three elution; however, more bands were expected to be detected in acetyl-lysine elution. VAMP2 acetylation was not detected in any elution samples.

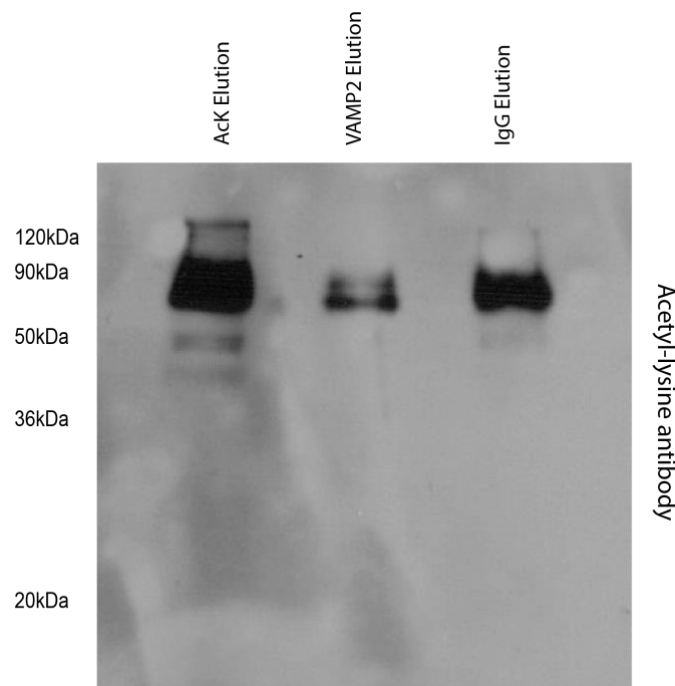


**Figure 5.20 – Endogenous IP of VAMP2 from HEK cells.** Two T75 flasks of HEK239 cells were treated with 2  $\mu$ M TSA and 40  $\mu$ M AGK2 for 8 hours, IP lysis buffer supplemented with 2  $\mu$ M of TSA and 20  $\mu$ M of AGK2 were used to harvest cells and extract proteins, 2 mg of proteins were used for Endogenous IP of VAMP2, acetyl-lysine and IgG used as control. 1:50 vol/vol AB/S ratio were used. **A)** acetyl-lysine, VAMP2 and IgG elution samples were immunoblotted using an anti-acetyl lysine antibody, results showed no signal corresponding to VAMP2 in all samples.

To assay VAMP2 acetylation by expressing a tagged version of the protein, we transfected VAMP2-GFP into two T75 flasks of HEK239 cells for 48 hours and treated with 2  $\mu$ M of TSA and 40  $\mu$ M of AGK2 for 8 hours, then harvested using IP lysis buffer containing 2  $\mu$ M of TSA and 40  $\mu$ M of AGK2. Tagged proteins were pulled down with GFP-trap resin. Pulldown elutions were digested with trypsin using S-trap digestion columns and analysed using LC-MS/MS.

Data were processed and quantified, searching for acetylated sites using MaxQuant (43). VAMP2 was identified as one of the most abundant proteins, showing transfections, pulldowns, and sample preparation for LC-MS/MS performed correctly, but we did not identify any acetylation sites. However, peptides covering the acetylated region of VAMP2 (residues 42-66) were identified at a high intensity compared to other peptides. In this experiment, we set MaxQuant to search for other PTMs such as phosphorylation as it is a common modification and ubiquitination as the identified VAMP2 ac(K) sites are also sites. Table 5.3 lists the identified peptides sequences for VAMP2, modification status, and peptide intensity (Signling, 2017, Jürgen and Matthias, 2008). Overall, we identified six VAMP2 peptides, including three ubiquitinated peptides, including K66, which was previously reported (Yamazaki et al., 2013, Signling, 2017). Three peptides identified known phosphorylation sites at residues S61, T79 and S80 (Signling, 2017). These results indicate that our method could detect VAMP2 at high intensity and detect PTMs sites other than acetylation, which might explain the difficulties in detecting acetylation sites with immunoblotting.

Peptide Sequences	Modification	Intensity
ADALQAGASQFETSAAK	Phospho (STY)	1.5E+07
ADALQAGASQFETSAAK	Unmodified	4.6E+09
ADALQAGASQFETSAAKLK	GlyGly (K)	1.5E+08
ADALQAGASQFETSAAKLK	Unmodified	2.5E+07
ADALQAGASQFETSAAKLKR	2 GlyGly (K)	2.5E+07
ADALQAGASQFETSAAKLKR	GlyGly (K)	1.2E+07
DQKSELDDRADALQAGASQFETSAAK	Phospho (STY)	2E+08
DQKSELDDRADALQAGASQFETSAAK	Unmodified	3.5E+07
LSELDDRADALQAGASQFETSAAK	Phospho (STY)	6.9E+07
LSELDDRADALQAGASQFETSAAK	Unmodified	6.5E+09
LSELDDRADALQAGASQFETSAAKLK	Unmodified	8963400

**Table 5.2 – VAMP2 peptides identified by LC-MS/MS of VAMP2\_GFP pulldowns.**

Two T75 flasks of HEK239 cells were transfected with VAMP2-GFP for 48 hours and treated with 2  $\mu$ M TSA and 40  $\mu$ M AGK2 for 8 hours. Cells were harvested with IP lysis buffer containing 2  $\mu$ M TSA and 40  $\mu$ M AGK2. VAMP2 was immunoprecipitated with GFP trap resin, and elutions were digested with trypsin using the S-trap digestion columns and analysed with LC-MS/MS. Data were processed and quantified using MaxQuant. No statistical tests were applied to the shown intensities because each construct has one replicate only. Ac (K42-66) peptides were identified with high intensity but detected in their unmodified state; other PTMs sites were also identified.

After many attempts to detect acetylation with different approaches, we faced a problem where detecting any acetylation bands was difficult even in cell lysates which we have previously shown many times. This issue needed to be solved before continuing optimisation.

(i) protein concentrations used in immunoblotting were increased to 50 µg instated of 25-35 µg. (ii) changed primary antibody concentration to 1:500 instated of the recommended concentration 1:1000 using a new antibody from the same company and another from different company. (iii) membrane exposure time during imaging were increased up to 15 from between 3 - 8 minutes. (iv) proteins were extracted just before immunoblotting to avoid freezing the samples. (v) results were compared to different antibodies than were used. (vi) Chemically acetylated BSA (AcK BSA) was used as a positive control for anti-acetyl lysine antibody as shown at different concentrations in Figure 5.21.

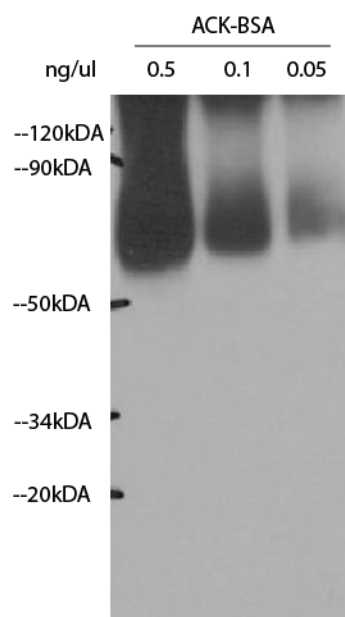
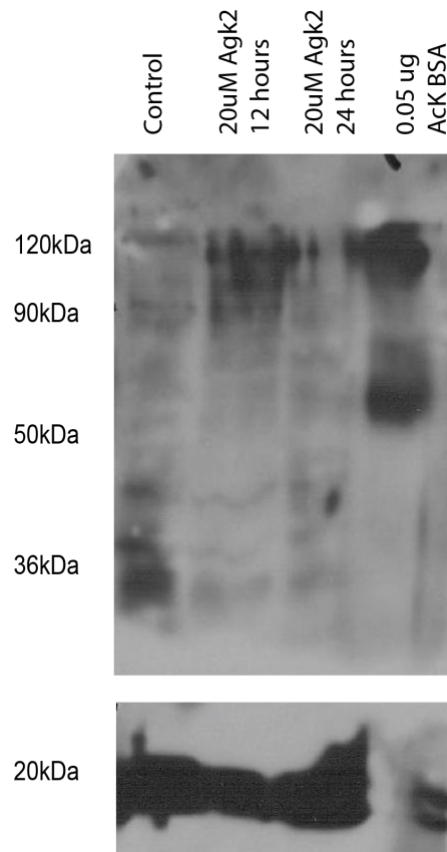


**Figure 5.21 – Testing the performance of a pan anti-acetyl-lysine antibody using chemically acetylated BSA.** Chemically 25ul acK-BSA was loaded at the following concentrations 0.5ng/ul, 0.1ng/ul and 0.05ng/ul in 2XSDS sample buffer and immunoblotted against 1;500 anti-acetyl-lysine antibody. Results show acK-BSA was detected in all samples at 66 kDa.

Each of those changes was tested separately and then were combined; AGK2 was used to inhibit deacetylase activity and detect more acetylation bands. Figure 5.22 shows acetylation levels between control and cells treated with AGK2, indicating that acetylation was successfully detected after those optimisation steps.



---

**Figure 5.22 – Detection of acetylation in AGK2 treated HEK293 cells.** Cells were treated with 20  $\mu$ M of AGK2 for 12 or 24 hours, DMSO was used as control and 0.05  $\mu$ g ack BSA as a positive control. 50  $\mu$ g of protein was immunoblotting against an anti-acetyl-lysine antibody. The membrane was cut above 20kDa to separate strong acetylation signals from histones.

After successfully detecting acetylation signals from different conditions, detection of VAMP2 acetylation was repeated with a few additional changes. First, cells were treated with nicotinamide (NAM) instead of AGK2 to inhibit all Sirtuins. NAM was also added to the IP lysis buffer for pulldown experiments. AcK BSA was used as a positive control to check that the acetyl-lysine antibody worked well. VAMP3, VAMP2 and IgG control pulldowns were performed as described previously. Figure 5.23 shows the acetyl-lysine blotting for VAMP3, VAMP2 and IgG pulldowns input and elutions. Results showed that AcK BSA was detected, demonstrating the ability of the antibody to detect acetyl-lysine proteins, and multiple acetylation bands appeared in all input samples.

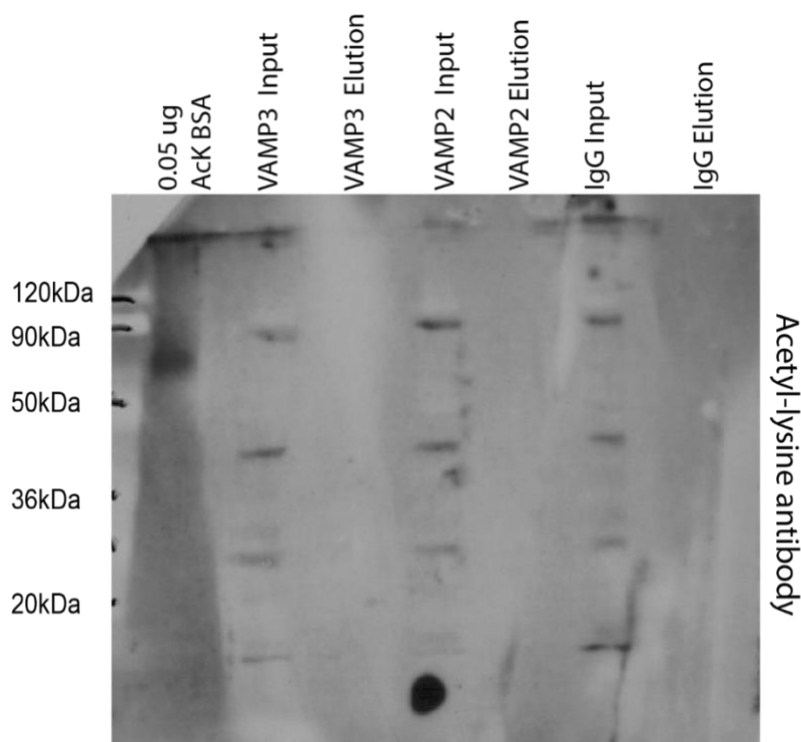


**Figure 5.23 – Endogenous IP of VAMP2** Two T75 flasks of HEK239 cells were treated with 2uM of TSA and 40uM of AGK2 for 8 hours, IP lysis buffer supplemented with 2uM of TSA and 20uM of AGK2 were used to harvest cells and extract proteins, 2mg of proteins were used for endogenous IP of VAMP3, VAMP2 and IgG used as control. 1:50 vol/vol AB/S ratio were used. VAMP3, VAMP2 and IgG elution samples were immunoblotted against anti acetyl lysine antibody; results showed no signal corresponding to VAMP2 in all samples. 0.05 µg ack BSA as a positive control.

Unfortunately, we have been unable to detect acetylation of VAMP2, 3 or any other Sirt2 known substrates so far. Thus, the concentrations were used for KDAC inhibitors were increased and combined, aiming for a global inhibition of deacetylase functions. Concentrations between 0.1-0.2mM of TSA and 1-5mM NAM were used previously (Guo et al., 2019, Wang et al., 2020a, Zhang et al., 2013). Unsurprisingly, using high concentrations led to cell death in most conditions, time points were changed, but similar results were found. Cells treated with lower concentrations survived for up to 6 hours.

Studies were able to detect acetylation of Sirt2 substrates using anti-acetyl antibodies designed for specific acetyl sites such as ACLY, CDK9 and IDH1 (Guo et al., 2019, Lin et al., 2013, Wang et al., 2020a, Zhang et al., 2013). In contrast, others successfully detected acetylation with pan acetyl lysine antibody (Wang et al., 2017a). In figure 5.24, anti-ac-tubulin antibodies were used to detect acetylation levels changes with different concentrations of KDAC inhibitors. Results showed an increase in acetylated tubulin levels with high concentrations of KDAC inhibitors. As shown in the last figure, ac-tubulin was clearly increased; we used the same KDAC inhibitors concentrations and repeated VAMP2 pull-downs for both endogenous and overexpressed versions to detect VAMP acetylation. Similar results were found as this approach could not detect acetylation of VAMP2.

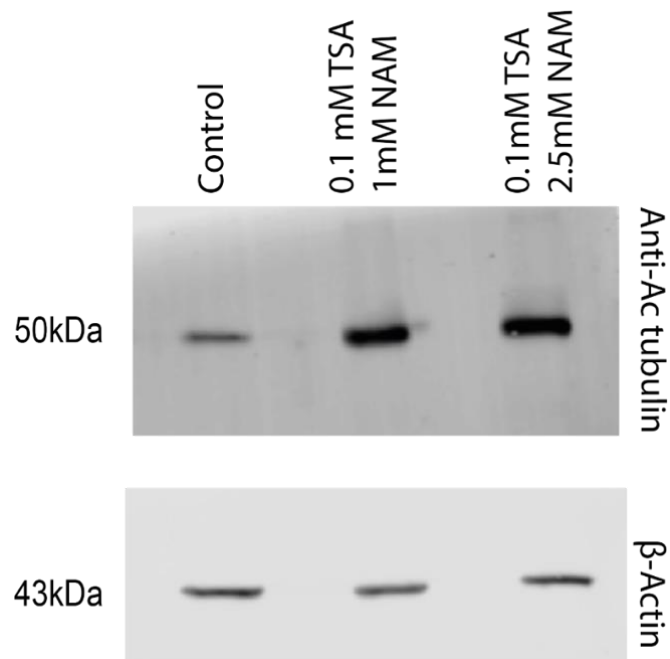


**Figure 5.23 – Inducing acetylation level by KDAC inhibitors.** 6 wells plate of HEK239 were treated with these conditions control, 0.2mM TSA 5mM NAM, 0.2mM TSA 2.5mM NAM, 0.2mM TSA 1mM NAM, 0.1mM TSA 2.5mM NAM and 0.1 mM TSA,1mM NAM for 6 hours. Cell deaths were observed in 0.2mM TSA 5mM NAM, 0.2mM TSA 2.5mM NAM and 0.2mM TSA 1mM NAM. Survived cells were harvested with trypsin, and 35  $\mu$ g were immunoblotted against anti-ac-tubulin antibody anti- and  $\beta$ -Actin as control. Results show an observed change in tubulin acetylation levels due to KDAC inhibition.

### 5.3.6 Testing known substrates of Sirt2

We could not detect acetylation of VAMP2/3, so we decided to test our acetylation detection assays on known Sirt2 substrates. CDK9 is a protein kinase involved in the regulation of transcription, mostly elongation factor B complex with cyclin T or K (Sabò et al., 2008). CDK9 is modified by acetylation at Lysine K48 and deacetylate by Sirt2, which is required for its activation (Kosciuczuk et al., 2018, Narita et al., 2018). Sirt2 deacetylates CDK9 and stimulates CDK9 kinase activity to promote recovery from replication arrest. Furthermore, by deacetylation of CDK9, Sirt2 can directly regulate DNA damage replication stress and promote innate immune responses (Zhang et al., 2013, Kosciuczuk et al., 2018).

This approach aimed to overexpress a specific protein, for example, CDK9 with  $-/+$  Sirt2, to observe the changes in the acetylation levels of those proteins. We performed a successful IP experiment of CDK9\_FLAG, which we transfected in HeLa cells for 24 hours (Figure 5.25 A, B). FLAG signals appeared at 42 kDa in CDK9-FLAG pulldown but were not in the control. CDK9 was eluted using FLAG peptide to avoid contamination of the elution with the antibody heavy chain. The anti-FLAG antibody detected CDK9 in the CDK9\_FLAG pulldown elution but not in the control. As shown in this figure, we achieved much better blotting that contains no additional bands.

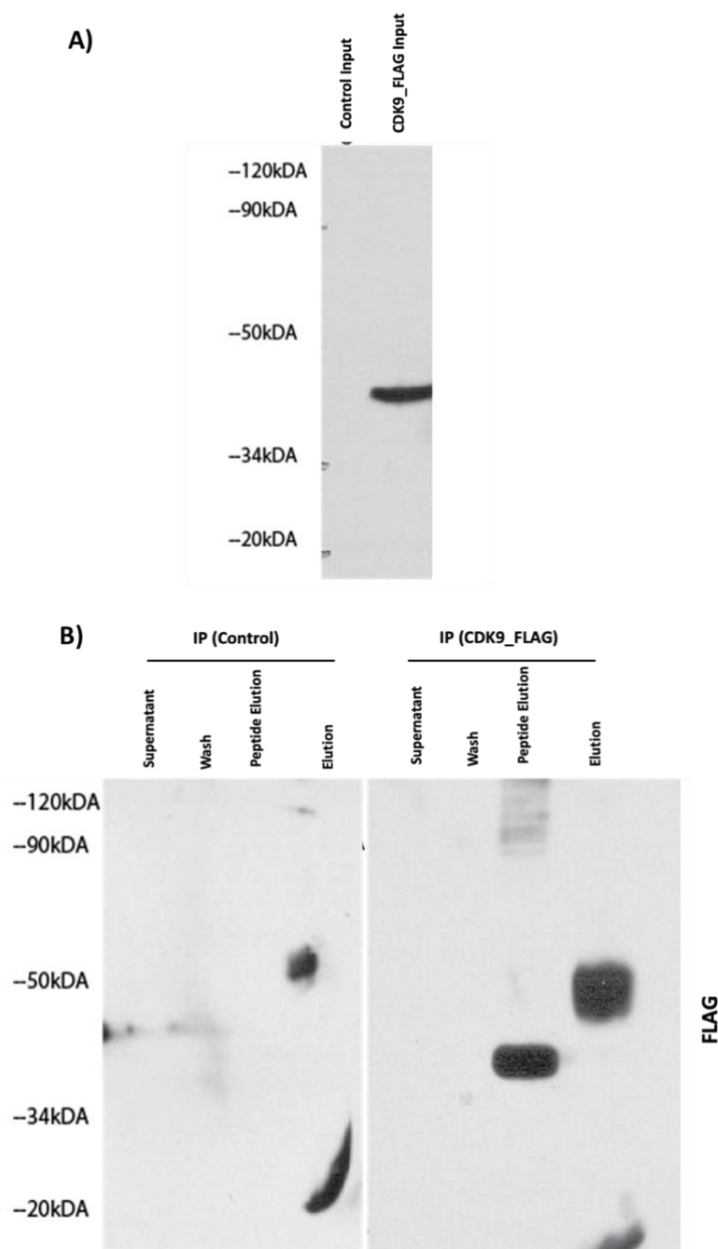


**Figure 5.24 – Immunoprecipitation of CDK9\_FLAG.** FLAG pulldown from control and CDK9\_FLAG transfected HeLa cells (24 hours) **A)** Inputs of both pulldowns immunoblotted against anti-FLAG showed a CDK9 band at 42 kDa but not in control. **B)** Pulldowns immunoblotted against anti-FLAG showed the CDK9 band at 42 kDa in the peptide elution for FLAG\_CDK9, which disappeared at control peptide elution. No FLAG signals were detected in supernatant, wash, and elution for both pulldowns. Note the appearance of anti-FLAG antibody heavy chain in the subsequent boiling elutions.

Next, we used the input and pulldown peptide elutions from this experiment to detect CDK9 acetylation by immunoblotting using a pan anti-acetyl-lysine antibody. Figure 5.26 A showed multiple acetylation bands in the input samples of both pulldowns, and no bands were detected in control peptide elution. However, there are some unclear bands in CDK9\_FLAG peptide elution, the membrane was imaged again with a shorter exposure time, and similar results were observed, as shown in Figure 5.26 B. This might happen due to high protein concentration or poor transfer steps. Moreover, some issues were faced with acK antibody as shown, inputs sample should represent histones bands that were not detect in this immunoblotting. Overall, we could not detect CDK9 acetylation, and the bands that appear in peptide elution do not correspond to the molecular weight of CDK9.

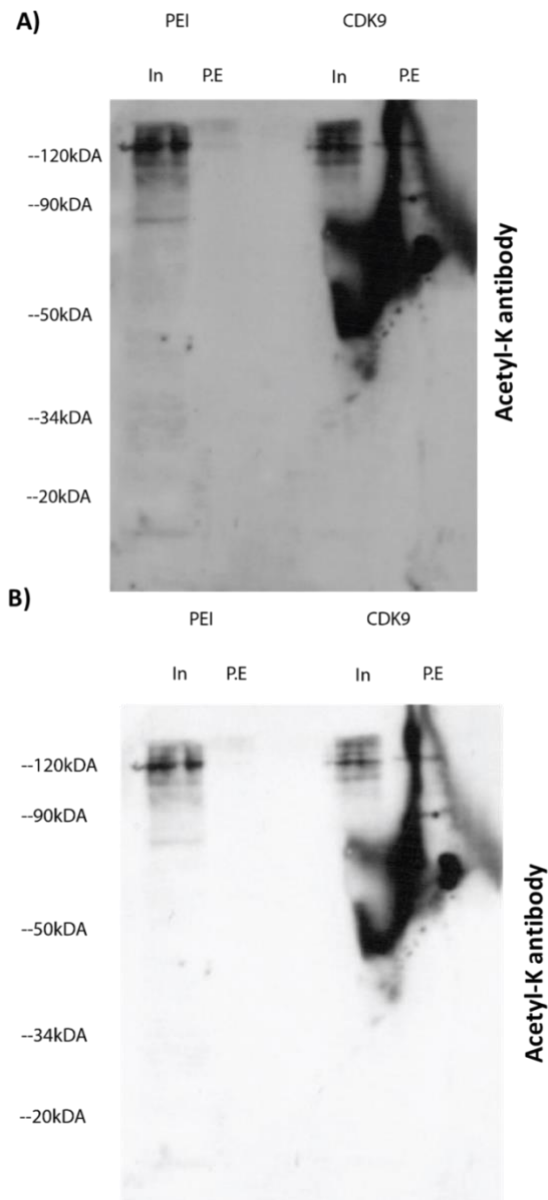
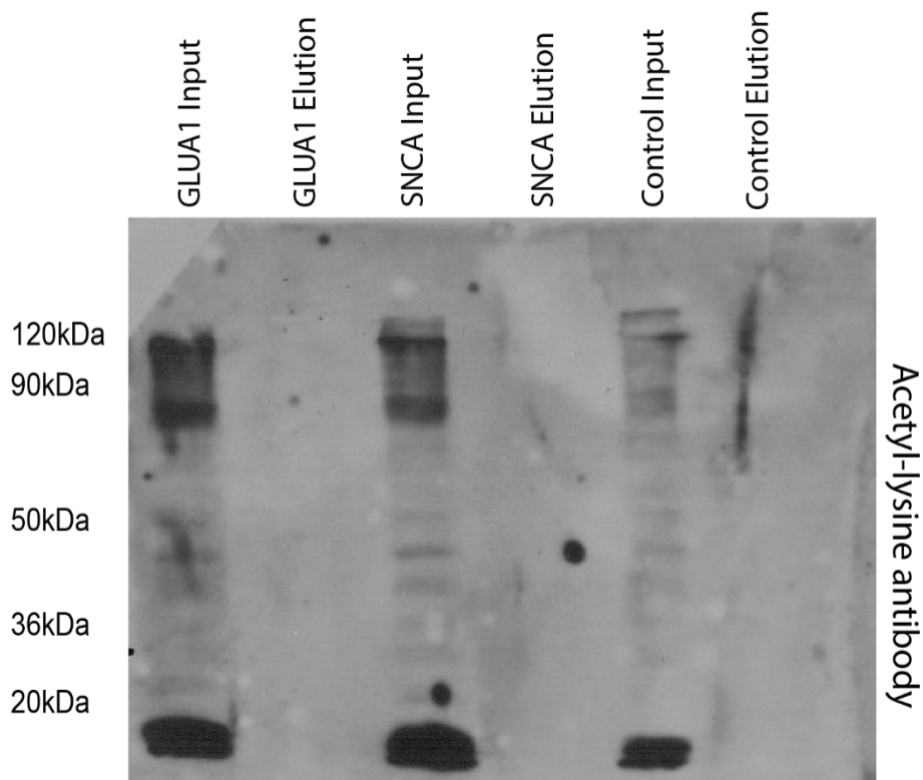


**Figure 5.25 – Anti-acetyl-lysine immunoblot of CDK9 pulldowns.** Inputs and peptide elution samples of both Flag\_CDK9 and control pulldowns were immunoblotted using an acetyl-lysine antibody. **A)** showed multiple acetylation bands in both inputs. No bands were detected in control peptide elution while some unclear signals in CDK9. **B)** showed the same results but with a short exposure time. Overall, all the bands do not correspond to CDK9 at 42kDa.

The same experiment was repeated with GLUA1-GFP and SNCA-GFP, and pulldowns were successful. Despite this, acetylation bands were not detected in any pulldown elutions. As previously stated, the intensity of the acetylation bands was much higher in the input samples, indicating that deacetylase activity was successfully inhibited (Figure 5.27).



---

**Figure 5.26 – Inhibition of KDAC deacetylase activity to detect GLUa1 and SNCA acetylation;** GLUA1-GFP, SNCA-GFP and control transfections (for 24 hours) of four 10 cm plates of HeLa cells for each pulldown were treated with 2  $\mu$ M of TSA and 20  $\mu$ M of AGK2 for 8 hours. IP lysis buffer supplemented with 2  $\mu$ M of TS and 20  $\mu$ M of AGK2. Inputs and elution samples of pulldowns were immunoblotted using a pan anti-acetyl-K antibody, multiple acetylation bands were detected in both inputs, no bands were detected in elutions.

After several attempts, we have concluded that detecting acetylation using a western blot may be difficult.

CDK9-FLAG and FLAG-NRF2, another known Sirt2 substrate, were overexpressed in HEK239 cells. Constructs were transfected into two 10 cm plates of HEK239 cells for 48 hours to allow protein production, then treated for 8 hours with 20 M TSA and 20 M AGK2, then harvested using IP lysis buffer with 2 M TSA and 20 M AGK2. Anti-FLAG or anti-HA agarose resins were used to pull down tagged proteins. Elutions were cleaned and digested with trypsin using S-trap columns, then LC-MS/MS was used to analyse these. The data was analysed and quantified, and in the MaxQuant analysis, acetylation sites were set as a variable modification (43).

CDK9 were identified as part of the most abundant proteins in their pulldowns as assessed by their iBAQ values, demonstrating that the pulldowns and sample preparation for LC-MS/MS was performed correctly. NRF2 was identified but showed a low intensity compared to other proteins in the same pulldown, which might be because of transfection time, or low-level expression of this particular plasmid. Furthermore, Sirt2 was identified in CDK9 pulldown but not NRF2. Studies show that Sirt2 deacetylates and interacts with CDK9 (Zhang et al., 2013). However, no acetylation sites were detected for any of the three bait proteins. Peptides covering the region of these proteins where acetylation sites of interest are located were identified with high intensity compared to other peptides. Table 5.3 shows the NRF2 and CDK9 peptide sequences found by LC-MS/MS, as well as the intensity of each peptide and its corresponding acetylation sites as determined by the Phosphosite dataset and the modification status of each peptide (Signaling, 2017, Jürgen and Matthias, 2008).

Peptides Sequence	Intensity	Acetyl (K)	Modifications
<b>NFE2L2</b>			
ALHIPFPVEK	5.34E+07	K472	Unmodified
DEDGKPYSPSEYSLQQTR	3.74E+07	_	Unmodified
EQFNEAQLALIR	9.86E+07	_	Unmodified
IINLPVVDFNEMMSK	1.45E+08	K487	Unmodified
KLENIVELEQDLHLKDEK	4.19E+06	K536	Unmodified
KLENIVELEQDLHLKDEKEK	6.07E+06	K538	Unmodified
LTEVDNYHFYSSIPSMEK	6.26E+07	_	Unmodified
LVETTMVPSPEAK	9.24E+06	_	Unmodified
<b>CDK9</b>			
QYDSVECPFCDEVSKYEK	1.62E+08	K21	Unmodified
AYVRDPYALDLIDK	1.69E+08	K294	Unmodified
DPYALDLIDK	2.26E+08	K294	Unmodified
DPYALDLIDKLLVLDPAQR	1.62E+07	K294	Unmodified
FTLSEIK	2.39E+08	K127	Unmodified
IDSDDALNHDFFWSDPMPSDLK	3.57E+08	-	Unmodified
IGQGTFGGEVFK	9.34E+08	-	Unmodified
KGSQITQQSTNQSRNPATTNQTEFER	3.72E+05	K354	Unmodified
QYDSVECPFCDEVSK	1.57E+08	-	Unmodified
SPIMQGNTREQHQLALISQLCGSITPEVW	2.50E+07	-	Unmodified
PNVDNYELYEK			
VLMENEKEGFPITALR	1.54E+08	K56	Unmodified

**Table 5.3 – Bait peptides identified by LC-MS/MS of FLAG\_NRF2 and CDK9\_FLAG pulldowns.**

Most Ac(K) peptides were identified with high intensity but detected in its unmodified status. Two 10 cm plates HEK239 cells, transfected with the different construct for 48 hours and

*treated with 2 μM of TSA and 20 μM of AGK2 for 8 hours. Cells were harvested with IP lysis buffer containing 2 μM of TSA and 20 μM of AGK2. Elutions were digested with trypsin using the S-trap columns and analysed with LC-MS/MS. Data were processed and quantified using MaxQuant. No statistical tests were applied to the shown intensities because each construct has one replicate only.*

To confirm our results, CDK9 and GLUA1 pulldowns were performed, CDK9 FLAG and GLUA1-GFP were overexpressed by transfection into two T75 flasks of HEK239 cells for 48 hours and treated with 0.1mM TSA 2.5mM NAM for 6 hours, then harvested using IP lysis buffer containing same KDAC's concentrations. Tagged proteins were pulled down with anti-FLAG or GFP-trap resins. Elution samples were digested using the S-trap digestion columns and trypsin and analysed using LC-MS/MS data were processed and quantified, searching for acetylated sites using MaxQuant (43). CDK9 and GLUA1 were among the most abundant proteins, unmodified peptides corresponding to the acetylation sites of CDK9 were identified at a good intensity, but no acetylation sites were identified. On the other hand, the data showed many GLUA1 peptides, but none contained known acetylated sites; thus, no acetylation sites were detected as well for GLUA1 (Table 5.4) (Signling, 2017, Zhang et al., 2013, Wang et al., 2017a).

Peptide Sequence	Intensity	Modification
<b>GLUA1 (AMPAR)</b>		
FALSQLTEPPK	2.35E+09	Unmodified
GVYAIFGFYER	2.59E+08	Unmodified
VLDTAAEK	1.31E+06	Unmodified
NWQVTAVNILTTTEEGYR	1.97E+09	Unmodified
MLFQDLEK	2.80E+09	Oxidation (M)
NGIGYHYILANLGFMDIDLNK	6.54E+07	Oxidation (M)
VMAEAFQSLR	3.49E+09	Unmodified
RGNAGDCLANPAVPWGQGIDIQR	2.70E+09	Unmodified
GNAGDCLANPAVPWGQGIDIQR	1.90E+09	Unmodified
FEGLTGNVQFNEK	2.88E+09	Unmodified
RTNYTLHVIEMK	9.21E+06	Unmodified
TNYTLHVIEMK	1.74E+08	Unmodified
KIGYWNEDDKFVPAATDAQAGGDNSSVQNR	3.72E+07	Unmodified
IGYWNEDDKFVPAATDAQAGGDNSSVQNR	1.87E+08	Unmodified
FVPAATDAQAGGDNSSVQNR	5.09E+07	Unmodified
TYIVTTILEDPYVMLK	9.96E+08	Oxidation (M)
TYIVTTILEDPYVMLKK	1.22E+07	Unmodified

KNANQFEGNDRYEGYCVLAAEIAK	2.83E+07	Unmodified
NANQFEGNDRYEGYCVLAAEIAK	2.64E+08	Unmodified
YEGYCVLAAEIAK	6.77E+07	Unmodified
HVGYSYR	5.07E+05	Unmodified
AWNGMVGELVYGR	1.30E+09	Oxidation (M)
ADVAVAPLTITLVR	2.19E+09	Unmodified
FSPYEWHSSEEFEEGR	4.16E+08	Unmodified
MVSPIESAEDLAK	3.67E+09	Unmodified
QTEIAYGTLEAGSTK	2.63E+09	Unmodified
TTEEGMIR	9.53E+05	Unmodified
NPVNLAVLK	6.19E+07	Unmodified
GFCLIPQQSINEAIR	2.45E+09	Unmodified
SMQSIPCMSHSSGMPLGATGL	6.55E+08	Oxidation (M)
GKYAYLLESTMNEYIEQR	1.76E+07	Unmodified
YAYLLESTMNEYIEQR	1.28E+09	Unmodified
VGGNLDSKGYGIATPK	3.10E+07	Unmodified
<b>CDK9</b>		
VMQMLLNGLYYIHR	2.13E+08	Unmodified
VVTLWYRPPPELLLGER	5.50E+08	Unmodified
DYGPPIDLWGAGCIMAEMWTR	2.80E+07	Unmodified

HENVVNLIEICR	5.69E+07	Unmodified
DPYALDLIDK	1.43E+08	Unmodified
IDSDDALNHDFFWSDPMPSDLK	9.26E+08	Oxidation (M)
AYVRDPYALDLIDK	3.75E+07	Unmodified
NPATTNQTEFER	5.73E+05	Unmodified
GMLSTHLTSMFEYLAPPR	1.84E+07	Unmodified
QYDSVECPFCDEVSKYEK	5.69E+08	Unmodified
VLMENEKEGFPITALR	2.21E+08	Unmodified

**Table 5.4 – Identified peptides by LC-MS/MS of GLUA1\_GFP and CDK9\_FLAG pulldowns.**

Two T75 flasks of HEK239 cells, transfected for 48 hours and treated with 0.1mM TSA 2.5mM of NAM for 6 hours. Cells were harvested with IP lysis buffer containing 0.1mM TSA 2.5mM of NAM. GLUA1 and CDK9 were pulled down with GFP trap and FLAG resins. Elutions were digested using the S-trap digestion column and analysed with LC-MS/MS. Data were processed and quantified using MaxQuant. No statistical tests were applied to the shown intensities because each construct has one replicate only.

### **5.3.7 Acetylation stoichiometry**

In recent years, non-histone lysine acetylation has become of interest to researchers as there have been several examples where specific acetylation sites have been shown to regulate protein function. The stoichiometry of non-histone acetylation is a critical aspect of this modification, and its difference compared to histone acetylation was reported during this PhD. A study published in 2019 (Bogi Karbech et al., 2019) measured acetylation stoichiometry through an acetylome analysis of HeLa cells which contained 6,829 acetylated sites on 2,535 proteins. The acetylome was measured using a combination of chemical acetylation (100% acetylated) and native acetylation, and SILAC labelling was used to pool these samples. Samples were digested, acetylated peptides were immunopurified, and LC-MS/MS analysis allowed the quantification of native versus full (chemical) acetylation, which was used to calculate stoichiometry. This study showed that the acetylation stoichiometry of the majority of ac(K) sites are very low, with a median of 0.02% and ~ 15% of the total identified ac(K) sites occur at median stoichiometry at >0.1%. Only 1% of the identified ac(K) sites have a high stoichiometry with a median of >1%; those are primarily sites on histone proteins (Bogi Karbech et al., 2019).

We searched for Sirt2 known substrates and putative Sirt2 substrates identified from Sirt2 KO acetylome in this dataset (Bogi Karbech et al., 2019). This study was able to identify VAMP2/3 sites (K35 and K66) at three peptides, but those sites were not found in all replicates. Median stoichiometry levels were calculated, and we found that the three ac(K) peptides of VAMP2/3 were acetylated at 0.009-0.03%.

Table 5.5 highlights the stoichiometry of known Sirt2 substrates; CDK9, ACLY and TUBA1 0.025%, 0.53% and 0.085% respectively (Guo et al., 2019, Lin et al., 2013, Bogi Karbech et al., 2019, North et al., 2003). Furthermore, Table 5.2 lists other putative Sirt2 substrate

stoichiometry, such as SNCA (0.12%) and MAPT (0.022%). HIST1H2BB was the only histone protein found significantly increased in acetylation in Sirt2 KO acetylome, and here it showed a stoichiometry level of 0.662%, which is considered relatively high compared to others (Rita Machado de et al., 2017, Bogi Karbech et al., 2019).

Gene names	Modified sequence	Stoichiometry
VAMP3; VAMP2	_LSEDDRADALQAGASQFETSAK (ac)LK_	0.029%
VAMP3; VAMP2	_ADALQAGASQFETSAK (ac)LK_	0.031%
VAMP3; VAMP2; VAMP1	_VNVDK (ac)VLER_	0.009%
ACLY	_ICRGIK (ac)EGR_	0.533%
ACLY	_YPFTGDHK(ac)QKFYWGHKEILI_	0.117%
ACLY	_DEVAPAK(ac)KAKPAMPQDS_	0.107%
CDK9	_IGQGTGGEVFK (ac)AR_	0.025%
SNCA	_TVEGAGSIAAATGFVK (ac)K_	0.068%
SNCA	_KGLSKA(ac)KEGVVAAAEEKTKQGVAAEAGK_	0.124%
TUBA1C;	_VKCDPRHGK(ac)YMACCLLYRGDV_	0.085%
TUBA1B;TUBA4A		
TUBA1C;TUBA1B;TUBA4A	_LDHKFDLM(ox)YAK(ac)R_	0.020%
TUBA4A	_DVNAAIAAIK(ac)TK_	0.019%
MAPT	_SEK(ac)LDFK_	0.022%
MAPT	_VQIINK(ac)K_	0.017%
CAMK2D;CAMK2A;	_KKLSARDHQK(ac)LEREARICRLLKH_	0.036%
CNP	_RPPGVLHCTTK(ac)FCDYGKAPGAE_	0.080%

<b>FASN</b>	_TPEAVQK(ac)LLEQGLRHSQDLAFL	0.107%
<b>FKBP1C;FKBP12</b>	_FDSSRDRNKPFK(ac)FMLGKQEVIR_	0.020%
<b>HIST1H2BB</b>	_KKGSKKAITK(ac)AQKKDGKKRKR_	0.662%
<b>VAPB</b>	EAVWKEAKPEDLMDSK(ac)LRCVFELPAENDKPH	0.214%
<b>VAPB</b>	AKVEQVLSLEPQHELK(ac)FRGPFTDVVTTNLKL	0.041%

**Table 5.5 Acetylation stoichiometry levels of some putative Sirt2 substrates.**

It is known that the detection of ac(K) peptides is mainly dependent on protein abundance, which was one of the reasons most studies prefer to overexpress proteins of interest and IP assays in acetylome studies (Wang et al., 2017a, Zhang et al., 2013). However, increasing the protein copy number will increase both modified and unmodified versions of the peptides. It might increase the difficulties in detecting acetylation without an enrichment step for ac(K) peptides. The stoichiometry study showed that only 0.17% of total identified peptides were detected as ac(K) peptides without antibody enrichment (Bogi Karbech et al., 2019). Similar findings were found in both of our Sirt2 KO/WT and old vs young proteome profiles, with 0.98 % and 0.46 % identified peptides being acetylated without enrichment.

These results further confirm that detecting ac(K) peptides without enrichment is very challenging, even with a deep proteome analysis (Bogi Karbech et al., 2019).

### **5.3.8 Sirt2 interactome**

Sirt2 has been shown to interact with several of its substrates, for example, CDK9, AMPA receptor, ACLY, SCNA and Ep300 (31). As another means to attempt to validate putative Sirt2 substrates identified in the Sirt2 KO/WT acetylome study, we sought to test whether Sirt2 interacts with them. Here, we investigated the protein interactions of Sirt2 using an unbiased AP-MS strategy using epitope-tagged Sirt2 expressed in HEK239 cells. First, we performed a pilot pulldown experiment of two different tagged versions of Sirt2, C-terminally FLAG-tagged or HA-tagged Sirt2. Both constructs were overexpressed in HEK239 cell lines (Thomas and Smart, 2005). Sirt2 was transfected into the cells for 24 hours, and cell pellets were harvested using immunoprecipitation lysis buffer, and pulldowns were performed using either anti-FLAG or anti-HA agarose resins. Elutions were then digested with trypsin using the S-trap columns and analysed using LC-MS/MS. Data were processed and quantified using MaxQuant (43). 803 proteins were identified from Sirt2 FLAG pulldown, and 863 proteins were found from Sirt2 HA, at an FDR of 1 % (Figure 5.28) Overall, both pulldowns showed similar results, and there was an overlap of 67% between both tagged versions. Sirt2-Flag pulldown, on the other hand, detected more interactors and putative Sirt2 deacetylase substrates than Sirt2-HA; this pilot experiment served as a guide for the replicate controlled Sirt2-Flag AP-MS experiment.

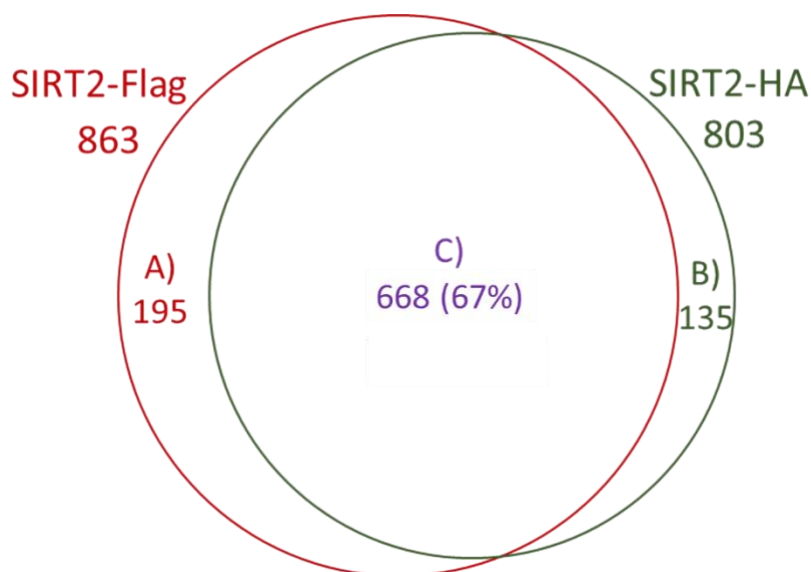


**Figure 5.27 – Venn diagram of the total number of proteins found in AP-MS from each tagged version, Flag or HA, including proteins shared between them. This experiment was used as pilot runs to choose the tag for the subsequent experiment.**

Affinity purification-mass spectrometry (AP-MS) of Sirt2–FLAG-tagged was performed with four replicates of control (mock-transfected) and four replicates transfected with Sirt2-Flag as described previously. This approach enabled the identification of 1162 proteins at an FDR of 1 % at the protein level (\*\***Supplementary Table 7.5**). Of which 486 proteins were quantified across a minimum of three replicates in either group. Histogram plots of proteins intensities were plotted to show that the data was normally distributed (Figure 5.29).

\*\*(<https://figshare.com/s/13750b8c09063b5cb9eb>)

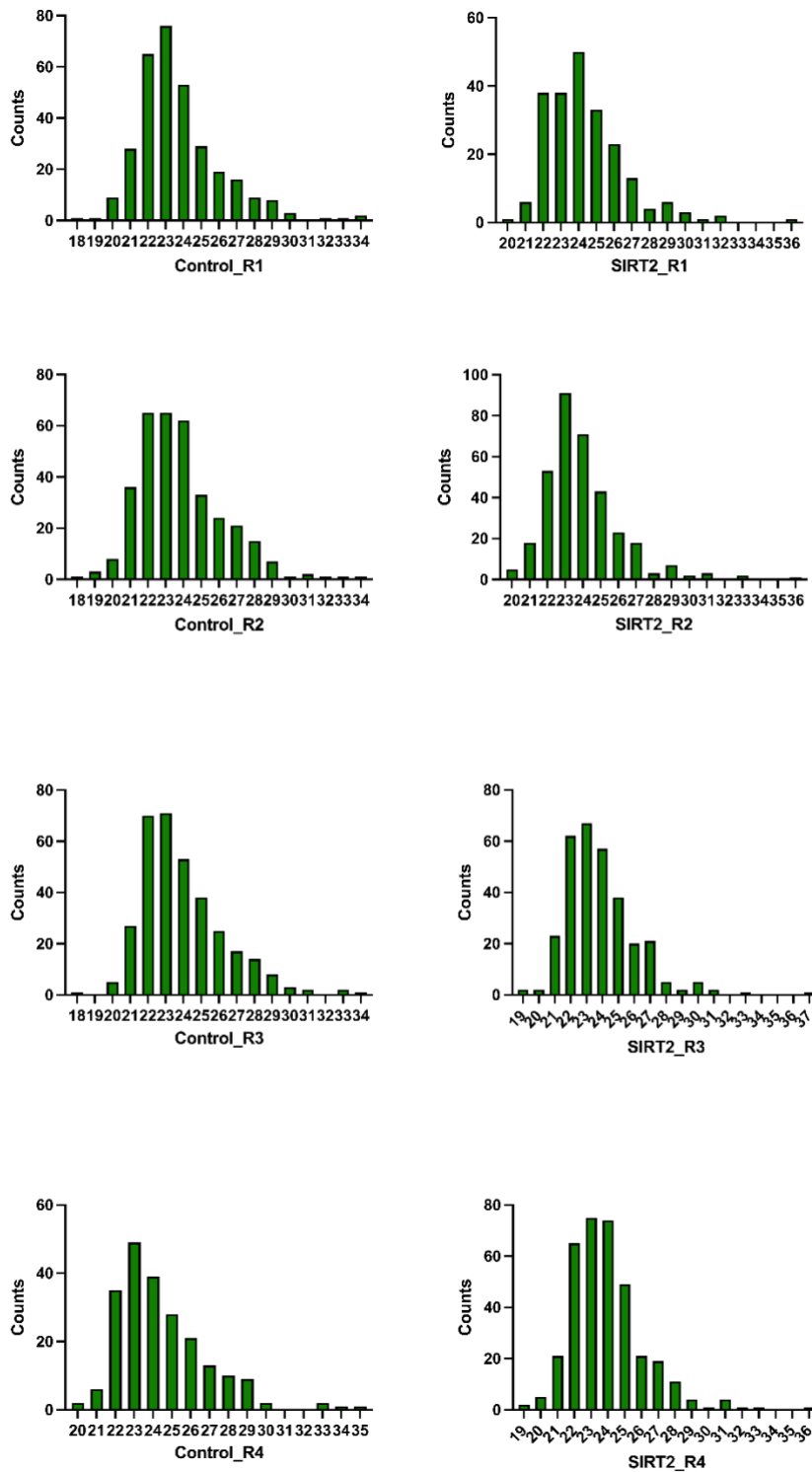


**Figure 5.28 Histogram of LFQ intensity values for replicates of Sirt2-FLAG versus control pulldowns.**

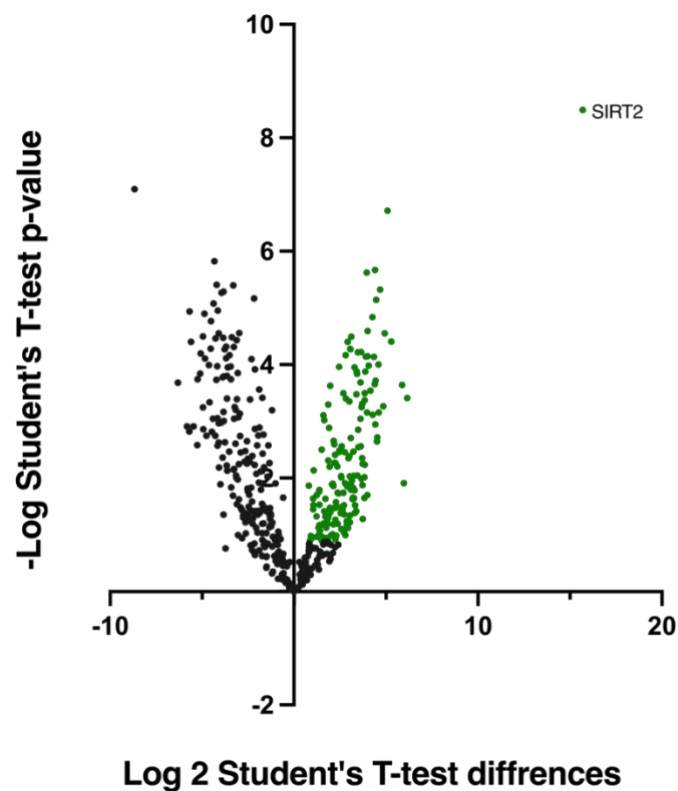
To further check the quality of the data, correlation analysis of replicates of Sirt2 and control proteins, the Sirt2 repeats were all highly correlated with very little difference between repeats. However, a comparison of Sirt2 compared to the control pulldowns shows a lower correlation, as there are several proteins highly enriched in Sirt2 pulldowns. Those proteins are significantly different proteins specific to the Sirt2 pulldowns. This confirms that our method was robust and reproducible (Table 5.6).

LFQ intensity Cont_R1	LFQ intensity Cont_R2	LFQ intensity Cont_R3	LFQ intensity Cont_R4	LFQ intensity SIRT2-R1	LFQ intensity SIRT2-R2	LFQ intensity SIRT2-R3	LFQ intensity SIRT2-R4	
NaN	0.932	0.953	0.929	0.477	0.540	0.537	0.474	LFQ intensity Cont_R1
0.932	NaN	0.952	0.922	0.323	0.375	0.373	0.318	LFQ intensity Cont_R2
0.953	0.952	NaN	0.923	0.309	0.372	0.350	0.308	LFQ intensity Cont_R3
0.929	0.922	0.923	NaN	0.308	0.387	0.352	0.357	LFQ intensity Cont_R4
0.477	0.323	0.309	0.308	NaN	0.940	0.943	0.922	LFQ intensity SIRT2-R1
0.540	0.375	0.372	0.387	0.941	NaN	0.924	0.951	LFQ intensity SIRT2-R2
0.537	0.373	0.350	0.352	0.943	0.924	NaN	0.926	LFQ intensity SIRT2-R3
0.474	0.318	0.308	0.357	0.922	0.951	0.9257	NaN	LFQ intensity SIRT2-R4

**Table 5.6 – Correlation values of Sirt2 and control replicate datasets.**

The table represents the Pearson correlation of the biological replicates high (green), middle (yellow), low (red). Correlation in the same group was increased at an average of 0.94; in between groups, the correlation was very low at an average of 0.385. those differences were expected as Sirt2 pulldown contain more specific proteins for Sirt2 that should not appear in control pulldowns. These show that biological replicates inside the same groups were reproducible

171 proteins were quantitatively enriched in Sirt2 versus control pulldowns with a permutation-based FDR of 0.05. Sirt2 was the most abundant protein in this dataset. This suggests that the transfection, a pulldown, and analysis were efficient. Figure 5.30 shows a volcano plot of the protein distribution between control and Sirt2. The right side shows protein highly abundant in Sirt2 pulldowns; green dots represent significantly enriched proteins with Sirt2.



---

**Figure 5.29 – Volcano plot of AP-MS data for FLAG-Sirt2 versus control pulldowns.** Data were filtered to retain proteins quantified in at least three replicates of either group (486 proteins), contaminants and reverse hits were removed. Data were then normalised by subtracting the median intensity of the distribution. Statistical analysis of four replicates of each group was performed using t-testing with a permutation-based FDR 5% and  $s_0$  of 2. Green dots represent significantly enriched proteins. Statistical analysis was performed using Perseus.

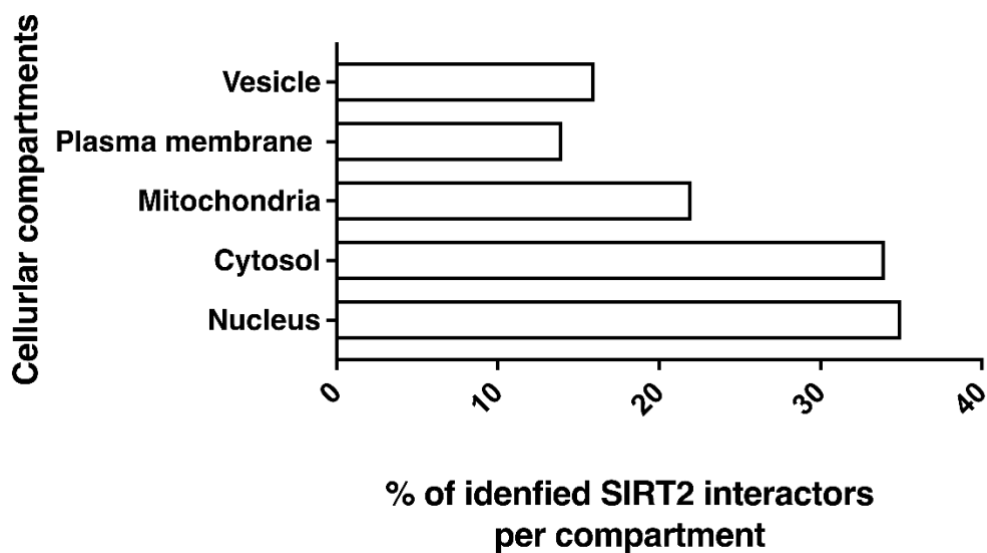
Putative Sirt2 interactors identified in this experiment were compared to different Sirt2 interactors datasets. First, the Biogrid database was used, and the result found that only three proteins are shared between our list and Biogrid interactors; those proteins are VAMP7, XPO1 and RAB3GAP2. Unfortunately, we could not detect CDK9, AMPAR, ACLY, or IDH1, which have previously been identified as Sirt2 deacetylase substrates and interactors but some of these proteins are not expressed/expressed at low levels in HEK cells (Zhang et al., 2013, Wang et al., 2017a). In addition, putative Sirt2 substrates identified in the Sirt2 KO acetylome study were mapped to this dataset, with the results indicating that 5 Sirt2 substrates interact with Sirt2 (FASN, HSPD1, SLC25a5, ALDH1I1 and DYC1h1).

We then compared our set of Sirt2 interactors to a recent study that explored the Sirt2 interactions in HeLa cells, which identified 450 proteins. Those proteins were mapped to the total identified proteins from Sirt2 pulldowns. We found an overlap of 114 proteins (figure 5.31A). Those proteins were mapped to the significantly upregulated proteins in Sirt2 pulldowns, and an overlap of 55 proteins was found, as shown in figure 5.31B (Eldridge et al., 2020).



**Figure 5.30 – Overlap between Sirt2 interactors in HEK239 and HeLa cells;** Venn diagrams represent; **(A)** 488 proteins identified from this study (red) compared to 450 proteins identified previously (green) (Eldridge et al., 2020), an overlap of 114 proteins (purple). **(B)** 171 proteins that significantly enriched in Sirt2 pulldowns (red) compared to overlap results from (A) (green) showed an overlap of 55 proteins (purple). Bioinformatics analysis compared gene names of proteins identified from Sirt2 interactors in HEK293 and HeLa cells.

Our Sirt2 KO/WT acetylome profile found that putative Sirt2 substrates are localised in almost every cell compartment (Bogi Karbech et al., 2019, Lundby et al., 2012b). To investigate the distribution of Sirt2 interactors from Sirt2 pulldowns, we annotated sub-cellular localisations determined by immunofluorescence-based protein localisation from the human protein atlas . We found 35% localised in the nucleus, 34% in the cytoplasm and 22%in mitochondria (Figure 5.32). This result further proves that Sirt2 has a broad impact on many cellular and biological processes.

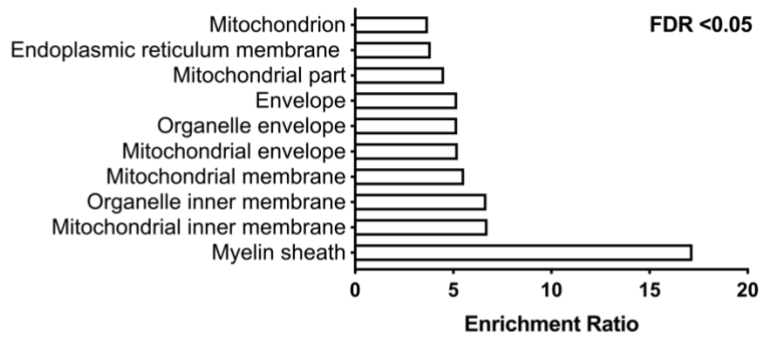


---

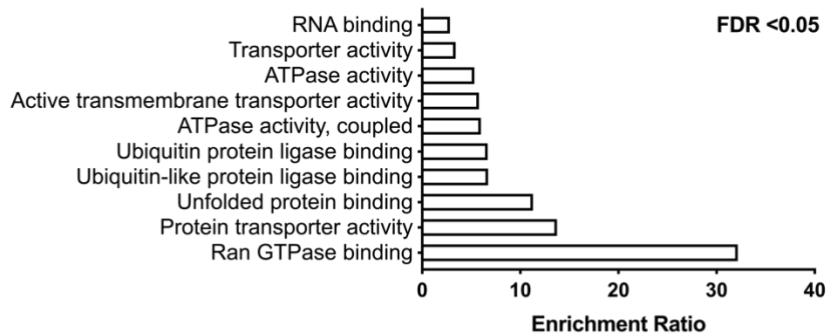
**Figure 5.31 – Cellular localisation of putative Sirt2 interactors.** Proteins were assigned to subcellular compartments based on immunofluorescence data from the Human Protein Atlas and show that lysine acetylation modification occurs in almost all cellular compartments.

Next, we performed a gene set enrichment analysis to determine enriched functions and pathways in the set of Sirt2 interactors. First, a Gene Ontology (Wang et al., 2017b) functional annotation analysis was performed to identify enriched gene ontology terms at  $p < 0.05$  for biological processes, molecular function, and cellular components associated with the set of potential Sirt2 interactors. Interestingly, 22 identified proteins, including Sirt2, were significantly enriched in myelin sheath (SLC25A5, SLC25A3, and PHB), which agrees with gene ontology analysis results identified from Sirt2KO acetylome profile and Sirt2 functions (Werner et al., 2007, Beirowski et al., 2011). Although we stated in the previous figure that most of the interactors are localised to the cytoplasm and nucleus, from gene ontology annotation, we found that most of those proteins are significantly enriched to mitochondria, plasma membrane and endoplasmic reticulum. Thus, we noticed that most biological process annotation results were related to protein transport and import between different cellular compartments. Interestingly, for molecular function annotation, 11 proteins were significantly enriched to Ran GTPase, including (IPO9, IPO7, XPO5, XPO7 and KPNB1), which is involved in the regulation of nuclear import and export and involved in the nucleocytoplasmic shuttle of Sirt2 (North and Verdin, 2007, Eldridge et al., 2020). Figure 5.33 shows those annotation results found using the human genome as a reference dataset.

## Cellular Components



## Molecular Functions



## Biological Process

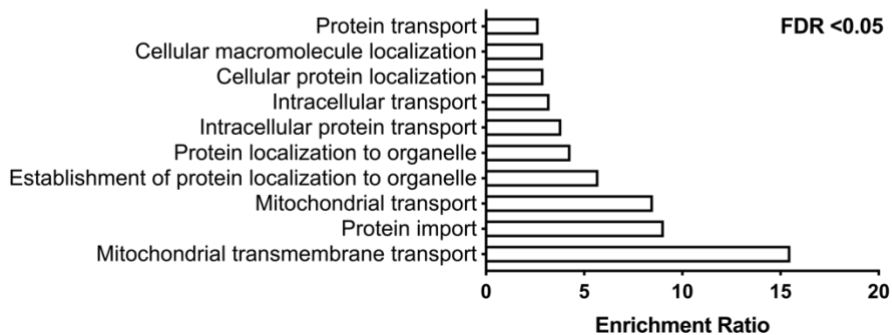


**Figure 5.32 – Significantly enriched proteins grouped into cellular component molecular pathways and biological processes.** Gene ontology enrichment analysis of the total dataset of identified acetylated proteins at FDR < 0.05 was generated using WebGestalt gene toolkit (53) human genome used as a background.

Next, to further investigate pathways enriched in the set of putative Sirt2 interactors, we used the PANTHER pathways library Table 5.7 (Thomas et al., 2003). In agreement with what we identified previously from the Sirt2 KO/WT acetylome, Sirt2 interactors are involved in Parkinson disease and Huntington disease (Wang et al., 2020b, Bhattacharjee et al., 2019, Donmez and Outeiro, 2013). In addition, the Sirt2 interactors were involved in the apoptosis pathway, DNA replication and energy productions via ATP synthesis. Identified pathways are consistent with Sirt2 functions (Piracha et al., 2020, Lin et al., 2013, Gomes et al., 2015, He et al., 2012). Although most of the identified interactors were unknown previously, pathways enrichment analysis showed very familiar pathways known for Sirt2.

The same analysis was repeated to identify the protein classes of the identified Sirt2 interactors, which included transporter, metabolite interconversion enzyme and cytoskeletal proteins (Table 5.8). This list is similar to protein classes identified previously from the Sirt2 KO/WT acetylome profile.

<b>Panther pathways</b>	<b>Protein number</b>
Apoptosis signalling pathway (P00006)	5
Huntington disease (P00029)	4
Parkinson disease (P00049)	4
Gonadotropin-releasing hormone receptor pathway (P06664)	4
ATP synthesis (P02721)	3
Angiogenesis (P00005)	2
Interleukin signalling pathway (P00036)	2
5-Hydroxytryptamine degradation (P04372)	2
Heterotrimeric G-protein signalling pathway-Gq alpha and Go alpha mediated pathway (P00027)	2
Heterotrimeric G-protein signalling pathway-Gi alpha and Gs alpha mediated pathway (P00026)	2
DNA replication (P00017)	2
Cytoskeletal regulation by Rho GTPase (P00016)	2
PDGF signalling pathway (P00047)	2

**Table 5.7 –Panther pathways significantly enriched in Sirt2 interactors.**

*Enrichment analysis of the identified proteins from Sirt2-Flag AP-MS using panther analysis tools (Thomas et al., 2003).*

Protein classes	Protein number
Transporter (PC00227)	38
Metabolite interconversion enzyme (PC00262)	26
Nucleic acid metabolism protein (PC00171)	9
Cytoskeletal protein (PC00085)	9
Chaperone (PC00072)	8
Translational protein (PC00263)	8
Protein modifying enzyme (PC00260)	7
Protein-binding activity modulator (PC00095)	6
Scaffold/adaptor protein (PC00226)	5
Membrane traffic protein (PC00150)	4
Transfer/carrier protein (PC00219)	4
Chromatin/chromatin-binding, or -regulatory protein (PC00077)	4
Transmembrane signal receptor (PC00197)	2
Defense/immunity protein (PC00090)	1
Calcium-binding protein (PC00060)	1
Gene-specific transcriptional regulator (PC00264)	1

**Table 5.8 – Putative Sirt2 interactors grouped into protein classes.**

*Enrichment analysis of the identified proteins from Sirt2-Flag AP-MS using panther analysis tools (Thomas et al., 2003).*

### **5.3.9 BioPlex data analysis**

Finally, our dataset of putative Sirt2 interactors was compared to a large-scale AP-MS Protein-Protein interaction data (BioPlex) (Schweppe et al., 2018), which contains two biological replicates only for each bait expressed in HEK cells. We downloaded raw data for all available sirtuins (Sirt2, 3, 4, 5, and 6) and reanalysed them with MaxQuant. This analysis identified 2,293 proteins, of which 740 proteins were found in Sirt2 pulldowns. To provide an interactors list more specific to Sirt2, the LFQ intensities average of those 740 proteins were calculated from SIRT3, 4, 5, and 6 pulldowns, and the ratio LFQ intensities Sirt2 and other sirtuins were compared. All proteins at a ratio above 1 were considered as a possible Sirt2 interactor. The result contained 500 proteins mapped to the potential Sirt2 interactors identified from Sirt2 pulldowns and found 69 proteins that are primarily Sirt2 interactors (Table 5.9).

Gene name	Intensity	Gene name	Intensity
Sirt2	8.16E+11	TRIP13	1.11E+08
SSR1	3.14E+08	DDOST	5.18E+08
HSPA6	1.82E+08	HSD17B12	1.52E+08
SLC3A2	4.88E+08	RPL11	1.33E+08
SSR4	2.05E+08	ALDH1B1	8.28E+07
HSPA4	3.35E+08	SLC25A1	2.48E+08
HSPA1B	6.21E+10	C1QBP	2.77E+08
RPN2	6.19E+08	TIMM50	9.61E+07
KPNA2	1.02E+09	HAX1	1.05E+08
ATP2A2	5.43E+08	HSP90AA1	4.44E+08
FAR1	1.57E+08	EEF1G	1.28E+09
STT3A	3.54E+08	NUP205	3.89E+07
SLC1A5	1.50E+08	SFXN4	7.26E+07
NUP93	1.03E+08	VDAC2	2.69E+08
SLC25A13	1.07E+09	HSP90AB1	4.38E+09
ATP1A1	2.28E+09	DPM1	1.15E+08
ABCD3	1.28E+08	SLC25A11	1.24E+09
SRPRB	9.80E+07	HSPA8	1.16E+10
PCNA	2.48E+08	TUBB2A	6.74E+08
AIFM1	3.24E+08	YTHDF2	8.30E+07
SLC16A1	8.56E+08	IRS4	1.05E+09
SLC25A6	4.86E+09	CCT3	1.89E+08

SLC25A22	1.54E+08	HSPB1	2.77E+08
SLC25A3	2.82E+09	TUBB	4.98E+09
HACD3	3.10E+08	COPB1	7.96E+07
MSH6	1.14E+08	PRKDC	1.63E+09
RPN1	7.01E+08	DNAJA1	2.56E+08
IMMT	2.04E+08	RAB3GAP1	3.45E+07
PHGDH	2.08E+09	PCBP2	7.20E+07
SLC25A5	2.87E+09	RAB3GAP2	9.60E+07
BSG	1.21E+08	TUBA1B	1.75E+10
KPNB1	3.76E+08	COPA	3.45E+08
CANX	6.22E+07	CAD	7.25E+08
TCP1	3.56E+08	AGK	1.66E+08
		TUBB4B	1.59E+10

**Table 5.9 – List of significantly enriched protein in Sirt2 pulldowns and those previously identified from the BioPlex dataset.**

### ***5.3.10 Does protein interaction are required for Sirt2 deacetylase functions***

Several studies have shown that Sirt2 interact with deacetylase substrates, such as CDK9 (Zhang et al., 2013), Tubulin (North et al., 2003), AMPAR (Wang et al., 2017a), ACLY (Guo et al., 2019) and others. However, only five putative Sirt2 substrates were found as Sirt2 interactors in our dataset, which was lower than expected based on the evidence in the literature. We compared the Sirt2 interactors dataset and Phosphosite ac(K) sites datasets (Signling, 2017) to identify the overlaps between ac(K) and Sirt2 interactors. The results found that 122 proteins out of 171 are known as ac(K) proteins, showing that most Sirt2 interactors are subject to acetylation. However, it is unclear what portion of these may be deacetylated by Sirt2. Furthermore, we reanalysed Sirt2 interactor results with Maxquant and allowed the search for ac(K) and UB peptides, and 47 ac(K) peptides and 170 UB peptides were identified. None of the ac(K) peptides were related to any Sirt2 known or putative substrates. On the other hand, VAMP3 (K42) and HIST1H2BB (K13) sites significantly increased in acetylation with sirt2KO were identified as UB sites. This might indicate that overexpression Sirt2 deacetylates its substrates and make the lysine residue subject for ubiquitination and degradation as suggested previously (Wang et al., 2017a, Lalonde et al., 2017). In other words, overexpression of Sirt2 may alter protein stability and remove protein-protein interaction.

## **5.4 Discussion**

### **5.4.1 VAMP2/3 acetylation**

In Sirt2 KO/WT brain acetylome, we found that VAMP2/3 is acetylated on more than one site (K35, K42, K66). These sites were identified in old vs young brain tissue, rat brain tissues and HeLa cells (Bogi Karbech et al., 2019, Lundby et al., 2012b). However, VAMP2/3 (K42 and K66) were significantly acetylated in the Sirt2 KO brain, and old vs young acetylome VAMP2/3, these sites were only detected in some replicates that were not shown a significant change during ageing (Lundby et al., 2012b). In a HeLa cell acetylome profile, VAMP2/3 ac(K) sites were identified, but the stoichiometry was determined to be very low (Bogi Karbech et al., 2019). Those finding emphasis that Vamp2/3 acK are normally acetylated, but it showed a significant increase under the regulation of Sirt2.

This chapter aimed to validate the results above *in vitro* and investigate how Sirt2 regulates the function and stability of VAMP2/3. However, the results showed unexpected outcomes, as we could not detect any evidence of VAMP2/3 acetylation *in vitro*. This was also the case with known Sirt2 substrates, used as positive controls such as CDK9, AMPAR and NRF2 (Zhang et al., 2013, Wang et al., 2017a, QING-QUAN LIU1\*, 2019, Carbon et al., 2021, Liu et al., 2019a). We attempted to detect acetylation using many approaches used in previous studies. KDAC inhibitor concentrations were chosen as suggested in the literature, although we showed that treating cells with high concentrations of combined inhibitors caused cell death. For example, the recommended TSA concentrations to successfully inhibit acetylation are in the nanomolar range; TSA inhibits deacetylase activity at IC50= 0.11µM with an efficiency of 99% (Hsu et al., 2016). Higher concentration for extended treatment time induced apoptosis and cell death (Schnichels et al., 2012, Yamashita et al., 2003, You and Park, 2013). Treating HeLa cells with 2.5-5µM of AGK2 for 24 hours inhibited cell growth, increasing with dose and

time (Kim et al., 2016). On the other hand, studies showed that NAM did not affect cell proliferation and cell growth at different concentrations up to 5mM on HeLa cells, and it promotes cell survival (Kim et al., 2016, Meng et al., 2018). Previous studies investigating acetylation of Sirt2 substrates used much higher concentrations than recommended, and none of those studies reported a cell death that we faced (Wang et al., 2020a, Zhang et al., 2013, Wang et al., 2017a, Bogi Karbech et al., 2019). Overall, we optimised inhibitor concentrations to demonstrate a change in global acetylation and tubulin acetylation levels. Protein abundance is an important factor in detecting lysine acetylation, as increasing protein levels increase both modified and unmodified peptides (Bogi Karbech et al., 2019). Thus, acetylation detection depends on protein copy number in a cell. For example, histones are very abundant proteins that are also highly acetylated and readily detected by immunoblotting from a cell lysate, as proven previously. Histone acetylation was responsible for 74% of the acetylation in cells, compared to 26% of non-histone proteins. Therefore, VAMP2/3 were overexpressed and immunoprecipitated for immunoblotting and LC-MS/MS. All protein pulldown experiments were successful, but a larger immunoprecipitation was carried out to provide and increase the protein concentration of interest. Nevertheless, VAMP2/3 acetylation was not detectable in the cell lines tested. The stoichiometry level for ac(K) peptides corresponding to the ac(K) sites were (~0.03%) as reported previously (Bogi Karbech et al., 2019). Studies showed that most ac(K) sites have a stoichiometry level less than 1%, which indicates that the mechanism by which acetylation regulates protein function should be consistent with low-modification stoichiometry (Bogi Karbech et al., 2019). Therefore, the inability to detect VAMP2/3 acetylation in vitro does not imply a lack of function.

In the literature, most studies used site specific ac(K) antibodies, acetylation of specific proteins or sites has been detected either by the generation and use of acetylation-site specific antibodies or through pan acetyl-lysine antibodies in combination with pulldowns of proteins of interest. For example, CDK9 is deacetylated by HDAC1/3, and its acetylation was detected by overexpression of CDK9 and inhibition of KDACs enzymes by TSA and NAM inhibitors. Pan anti-acetyl-lysine and anti-ac-CDK9 antibodies were used to detect acetylation (Sabò et al., 2008, Zhang et al., 2013). This approach was repeated in many studies, such as IDH1 (Wang et al., 2020a), ACLY (Guo et al., 2019, Lin et al., 2013), tubulin (North et al., 2003), and others. Techniques like in vitro acetylation/ deacetylation assays and enzymatic or chemical induce for acetylation has been used in many studies during functional investigating of ac(K) sites (Yang et al., 2017, Zhang et al., 2013).

#### ***5.4.2 Sirt2 interactors from HEK239 cells***

In this study, we found 486 proteins were quantified across a minimum of three replicates in either group Sirt2-FLAG and control pulldowns. 171 proteins were significantly enriched in FLAG pulldowns versus control pulldowns and considered putative Sirt2 interactors. Known Sirt2 interactors such as VAMP7, XPO1 and RAB3GAP2 were in our Sirt2 enriched set (Stark et al., 2006).

On the other hand, around 55 interactors were previously reported as Sirt2 interactors from a Sirt2 pulldown study on HeLa cells (Eldridge et al., 2020) and 69 proteins were previously identified from Sirtuins large scale AP-MS study on HEK239 cells (Schweppe et al., 2018).

Our data suggested that Sirt2 interact with proteins distributed in all cellular compartments. Putative Sirt2 interactors were majorly found in cytoplasm and nucleus with 32% and 35%, respectively. . These data are consistent with Sirt2 localisation and the localisation of putative Sirt2 substrates found from Sirt2 KO Acetylome (North and Verdin, 2007).

According to this data, 48 putative Sirt2 interactors were significantly localised to mitochondria and involved in mitochondrial transport and ATPase activity. This finding is consistent with other research indicating that Sirt2 can localise to mitochondria and interact with mitochondrial proteins (Liu et al., 2017c). Deletion of Sirt2 in the mouse brain and MEFs increased oxidative stress indicators while decreasing ATP generation and affecting autophagic/mitophagic processes. Our data add to the evidence that Sirt2 may play a role in mitochondrial biology (Liu et al., 2017c, Coates et al., 2001, Bertholet et al., 2019).

As discussed before, Sirt2 is linked strongly with the myelination process; this data found that Sirt2 interact with 20 proteins localised to the myelin sheath (Li et al., 2007, Fourcade et al., 2017).

Overall, while providing a Sirt2 interactors dataset was quite helpful, this study did not find many putative Sirt2 (deacetylase) substrates. Previous research has found an interaction between Sirt2 and deacetylase substrates such AMPA, CDK9, and ACLY. These findings were identified using a co-immunoprecipitation for tagged proteins in HEK239 cells and immunoblotting (O'Connor et al., 2020, Wang et al., 2017a). It's also important to note that AMPA and CDK9 were not detected as deacetylase substrates in Sirt2 KO acetylome data. ACLY was not significantly acetylated in the Sirt2 KO acetylome, suggesting that other KDACs deacetylate ACLY and that Sirt2 overexpression/knockout alters protein stability (Guo et al., 2019). Since acetylation is a common PTM modification, 70% of putative Sirt2 interactors contains at least one known ac(K) site (Signling, 2017). Many of those proteins were not known as substrates or linked to Sirt2 before, such as PHB.

In conclusion, acetylation signals of VAMP2/3 were extremely difficult to detect, despite having previously been reported in three acetylome datasets. This was due to a combination of very low stoichiometry and poor performance of immunoblotting with a pan anti-acK site

antibody. We conclude that knowledge of acetylation stoichiometry information is an important aspect of this modification and should be considered carefully when investigating the function of acetylation sites.

Sirt2 AP-MS from HEK239 cells revealed very little overlap between Sirt2 interaction and deacetylation functions. We suggest that the main reason for this is that they were generated using mouse brain tissue and HEK cells, respectively. Characterisation of Sirt2 interactors by viral transduction of tagged Sirt2 would likely generate an interactome that would better align with the set of putative substrates that we identified.

## **CHAPTER 6**

### ***Discussion and Future Prospects***

## **6.1 Summary of significant findings and discussion**

### **6.1.1 Chapter 3 - Characterisation of the Sirt2-regulated mouse brain acetylome**

Our acetylome analysis of Sirt2 KO mouse brain tissue characterised 2,054 ac(K) sites corresponding to 818 different mouse proteins, with 266 ac(K) sites showing a significant increase in acetylation in Sirt2 KO versus wild type brain tissue. This is the first study to use an MS-based quantitative acetylome analysis to identify potential Sirt2 substrates in the brain. It is also the first whole mouse brain acetylome so far. Interestingly, 197 of the 226 Sirt2-regulated ac(K) sites mapped to known synaptic proteins, with some of them significantly enriched in pre-or postsynaptic fractions (Bayés et al., 2017). The possibility that Sirt2 regulates the acetylation status of many synaptic proteins supports our hypothesis that Sirt2 is a key synaptic KDAC.

A comparison with a previous dataset of global lysine acetylation in rat brain reveals a 56% overlap of acetylated proteins (Lundby et al., 2012b). Another comparison to the Phosphosite acetylation dataset revealed that most of the identified acetylation sites were novel (Signling, 2017). These findings suggested that the Sirt2 KO brains brought to light new acetylation sites that had not previously been reported and that Sirt2 could play a more significant role in the regulation acetylation and acetylation functions in the brain.

Analysis of the subcellular localisation of putative Sirt2 substrates in Sirt2 KO mouse brains revealed that most acetylated proteins are found in the cytoplasm, consistent with Sirt2's primary location. According to our findings, more than half of those substrates are distributed in other compartments. This finding reinforces previous studies that suggest Sirt2 deacetylase activity isn't restricted to cytoplasmic proteins (Wang et al., 2019b, Liu et al., 2017c, Ji et al., 2011, North and Verdin, 2007, 2021, Vaquero et al., 2006, Chamberlain et al., 2021).

In contrast, proteins from the total mouse brain acetylome were located in all cellular compartments, with the highest proportion in the nucleus. According to the literature, many acetylated proteins that localised in cytoplasm and mitochondria are associated with essential pathways and functions, such as autophagic/mitophagic processes and others (Liu et al., 2017a, 2021, Silva et al., 2017, Lundby et al., 2012b, Choudhary et al., 2014, Chamberlain et al., 2021). The acetylated proteins identified are involved in various pathways, mostly related to glycolysis, synaptic vesicle trafficking, the TCA cycle, Parkinson's disease, and others. The acetylation enrichment in metabolic pathways confirms previous studies in the rat brain acetylome (Lundby et al., 2012b). Our data support the conclusion of studies that suggest lysine acetylation is a primary PTM modification (Wang et al., 2020b) to regulate synaptic and brain proteins (Tyagi et al., 2018, Wang et al., 2017a, Saha and Sen, 2019, Bogi Karbech et al., 2019, Lalonde et al., 2017, Carbon et al., 2021).

In this study, we found that putative Sirt2 substrates are involved in various functions and are enriched in critical cellular components. For example, it has been shown that Sirt2 increase axonal mitochondrial ATP production by deacetylating mitochondrial proteins via oligodendrocyte to axon delivery of Sirt2. Thus, Sirt2 is considered a positive regulator of axonal metabolism required for distal axons and synapses (Wang et al., 2017a, Fourcade et al., 2017, 2021, Chamberlain et al., 2021). In our dataset of putative Sirt2 substrates, many ac(K) proteins are localised to the myelin sheath, axons, and synapses such as Plp1, Slc25a5, and Slc25a4. This indicates that our results are consistent with previous research showing that Sirt2 KO mice have locomotor dysfunction and impaired cognitive function (Fourcade et al., 2017, Werner et al., 2007, Wang et al., 2019b).

In addition, our data revealed that Sirt2 is a potential regulator of the acetylation of proteins involved in neurodegenerative diseases such as Mapt, Snca, Ywhah, and others. These findings are consistent with numerous studies that have proposed Sirtuins in general and Sirt2 in particular as a therapeutic target for those diseases. (Cacabelos et al., 2019, Biella et al., 2016, Chen et al., 2015, Outeiro et al., 2007). Thus, Sirt2 absence cause acetylation at specific sites to accumulate, which may contribute much more than what has previously been reported in the Sirt2 KO phenotype of these mice.

As a result, the lysine acetylome profile of the Sirt2 KO mouse brain will likely be a helpful resource for future research into the function of Sirt2 and its therapeutic implications in neurodegenerative disease, as well as understanding the potential for tissue-specific acetylation regulation.

### **6.1.2 Chapter 4 - Acetylome profiling of young versus old mouse brain tissue**

Our acetylome analysis of aged mouse brain tissues identified 2,496 ac(K) sites corresponding to 1,091 different mouse proteins, with 60 of these sites indicating a significant change in acetylation in aged (old) brain tissues. We found that acetylation increased in 24 sites and decreased in 36 sites with age. This is the first study to measure global changes in lysine acetylation in the mouse brain during ageing.

Comparison of this the whole young/old brain acetylome dataset with previous acetylome profile of rat brain (Lundby et al., 2012b), and Sirt2 KO brain showed an overlap of 37% and 52% respectively. Another comparison to the Phosphosite acetylation dataset revealed that most of the identified acetylation sites were novel, with ubiquitination also modifying 40% of those sites (Signling, 2017). These results are consistent with previous studies and show that novel sites identified might be related to ageing. Furthermore, these results confirm the importance of the crosstalk between acetylation and ubiquitination (Kozuka-Hata et al., 2020, O'Connor et al., 2020). Thus, protein aggregation caused by acetylation is considered a hallmark of age-related disease, are mediated by different acetylation functions including preventing ubiquitination modification (Wang et al., 2020b, Yakhine-Diop et al., 2018, Lee et al., 2011, Min et al., 2010).

The set of 60 ac(K) sites regulated by ageing map to proteins localised mainly to the cytoplasm; however, most downregulated ac(K) sites map to proteins found in the nucleus and the mitochondri (Carbon et al., 2021). These findings are consistent with the mitochondrial dysfunction during ageing, and most mitochondrial proteins are non-enzymatically acetylated. The loss in acetyl-CoA production causes a decrease in acetylation levels during ageing (Pougovkina et al., 2014, Wagner and Payne, 2011). The acetylated

proteins regulated by ageing are significantly enriched in GO terms related to NAD binding, metabolic process and cellular component terms, including the mitochondria and myelin sheath. These findings suggest a correlation between NAD binding functions and ageing, which many studies previously reported (Camacho-Pereira et al., 2016, Mouchiroud et al., 2013, Imai and Guarente, 2014).

From pathway enrichment analyses, Ac(K) sites regulated by ageing are also involved in glycolysis, Parkinson disease, Pyruvate metabolism pathways, and others. This confirmed a previous study of the rat brain acetylome (Lundby et al., 2012b) and Sirt2 KO acetylome that acetylation is involved in neurodegenerative and metabolic pathways (Kim et al., 2006a, Choudhary et al., 2009b). Our data support the hypothesis that lysine acetylation is affected by age and vice versa (Satoh et al., 2017) and that acetylation may play a greater role in the pathogenesis of many age-related diseases in the brain and other tissues.

### **6.1.3 Chapter 5 - Validation of putative Sirt2 substrates**

Vamp2/3 is one of the putative Sirt2 substrates identified from the Sirt2 KO acetylome profile. Vamp2/3 was chosen for validation as its identified ac(K) sites fit a specific set of shortlisting criteria. Acetylation sites of Vamp2/3 were previously identified in rat brain tissues, HeLa cells, and in our young/old mouse brain acetylome. Yet, those sites showed a significant change in acetylation in Sirt2 KO brain acetylome only (Lundby et al., 2012b, Bogi Karbech et al., 2019). Furthermore, the identified Vamp2/3 ac(K) sites were previously reported as ubiquitinated sites indicating a potential role in regulating protein stability (Signling, 2017, Akimov et al., 2018). Although those acetylation sites were detected in many studies, no research has investigated the impact of acetylation by Sirt2 on Vamp2/3 function or stability.

Unfortunately, in this chapter, we could not detect Vamp2/3 acetylation using in vitro studies. Although global acetylation signals were detected in HEK239, HeLa and NSC34 cell lines, detecting acetylation of specific proteins was very challenging.

Studies that successfully investigated the Sirt2 deacetylase role on a specific protein, such as AMPA receptor, CDK9, and others, have used acetylation detection methods such as tagged or endogenous immunoprecipitation, inhibition of KDAC enzymes and acetylation site-specific antibodies for detection (Zhang et al., 2013, Sabò et al., 2008, Wang et al., 2020a).

Immunoblotting and mass-spectrometry detection approaches were tested on VAMP2/3 and other known Sirt2 substrates. The optimisation was performed many times by changing factors such as (i) concentrations of inhibitors, antibodies, and proteins. (ii) time of transfection, treatment, or incubation of pulldowns and (iii) type, the density of cells.

The pulldowns were successfully performed; we detected target pulldown proteins observed a change in acetylation levels with different KDAC inhibitors in cell lysates with detection using pan-acetylation antibodies and peptides with target lysines were detected by mass

spectrometry but only in their unmodified form. Nevertheless, acetylation of VAMP2/3 was not detected. This was a surprising result, especially as the acetylation of known Sirt2 substrates used as controls was also not detected.

In this chapter, we also investigated the interactome of Sirt2, which identified 171 putative interactors in HEK239 cells using FLAG-tagged pulldown and LC-MS/MS analysis. Among those proteins, 55 proteins were previously reported as Sirt2 interactors in HeLa cells (Eldridge et al., 2020), three proteins are known Sirt2 interactors in BioGRID dataset (Stark et al., 2006), and 69 proteins are previously identified from BioPlex Sirtuin pulldowns (Schweppe et al., 2018). This data also revealed various proteins which have not been previously reported to associate with Sirt2. Although Sirt2 is mainly localised in the cytoplasm (Wang et al., 2019b, Wang et al., 2017a), subcellular localisation of putative Sirt2 interactors was found in the nucleus, mitochondria, and cytoplasm agreement with the many studies (North and Verdin, 2007, Eldridge et al., 2020, 2021, Liu et al., 2017b).

Our findings contribute to understanding Sirt2-regulated processes; Gene ontology analysis revealed that Sirt2-interacting partners are involved in a wide range of functional processes. Such as Ran GTPase, protein transporter activity, ATPase activity, protein binding and transport, proteins localisation. These functions and processes were among the Sirt2 interactome's most significantly enriched terms (Wang et al., 2017b, 2019, The Gene Ontology Consortium, 2019).

Many of the identified putative Sirt2 interactors are significantly enriched to mitochondria and mitochondrial parts, myelin sheath such as SLC25A5, PHB, SLC25A3 and others. Identification of such proteins is consistent with many studies suggesting that Sirt2 localises to mitochondria and regulates myelin production (Liu et al., 2017c, 2021, Chamberlain et al., 2021) and with our data from Sirt2 KO mouse brain and old mouse brain acetylome profiles.

The results shows that Sirt2 interacts with many proteins in different subcellular compartments which may is suggested the association of Sirt2 with important cellular processes. It increases the probability that the Sirt2 deacetylase function is active in nearly all cellular compartments, expanding the range of potential Sirt2 substrates further than what is now known.

## **6.2 Overview and future work**

### **6.2.1 Synaptic proteins are regulated by acetylation and Sirt2 deacetylase enzyme**

As proposed in this study hypothesis, evidence has linked lysine acetylation to many important brain proteins (4,264 acetylation sites on rat brain tissue) and specifically synaptic proteins (Bayes et al., 2017, Wang et al., 2017a, Lalonde et al., 2017, Lundby et al., 2012b). Based on data available at the time, we suggested that acetylation of synaptic proteins was widespread, with 64% of mouse synaptic proteins potentially acetylated (Signling, 2017, Bayes et al., 2017).

We confirmed this by detecting 2,054 ac(K) sites in the Sirt2 KO/wild type mouse brain tissue dataset and 2,496 ac(K) sites in the old/young brain mouse tissue dataset. We found 81% and 77% of ac(K) sites were acetylated on synaptic proteins from those datasets. In both datasets, acetylation was more abundant in the synaptosome fraction than in the PSD portion. Thus, lysine acetylation modification is a potentially important regulator of synapses and a very common PTM of synaptic proteins.

According to gene ontology functional analysis, putative Sirt2 substrates identified are significantly enriched in pre-and post-synapses, consistent with previous studies (Wang et al., 2017a, Saha and Sen, 2019, Sun et al., 2021, Outeiro et al., 2007). Some of those sites were reported for the first time as acetylated and Sirt2 substrates such as Pclo, Vamp2/3, Ank3 and others. This finding is supported by the fact that Sirt2 is found in both synaptosome and PSD portions of mouse synapse proteome, which shows that Sirt2 deacetylase is a possible regulator of synaptic protein acetylation (Signling, 2017, Bayes et al., 2017).

Although we have presented significant proof for Sirt2's role in regulating brain acetylome, more validation of those potential substrates and acetylation sites is necessary to evaluate

whether Sirt2 and acetylation influence the functions of those proteins and impacts brain and synaptic functions during ageing.

### **6.2.2 Non-enzymatic and enzymatic acetylation of brain proteins**

Protein acetylation is linked directly to acetyl-CoA concentrations; studies suggest that acetylation occurs enzymatically by KATs or potentially non-enzymatically via acetyl-CoA. Is it possible that lysine residues on proteins are directly modified by acetyl-CoA? Do KATs influence the acetylation level of synapse proteins at the synapse? Bioinformatic analysis of mouse synapse proteome has failed to identify KATs enzymes that mediate enzymatic acetylation. Similar results were found in Sirt2 KO and old brain tissue proteome profiles, as Crebbp was the only enzyme identified from both data. In the Sirt2 KO brain acetylome, Ep300 was acetylated, but not in the old brain acetylome. An overlap of 9% of ac(K) sites was found between CBP/EP300 knockout mouse embryonic fibroblasts and Sirt2 KO mouse brain acetylome profile (Weinert et al., 2018).

KAT2A and KAT2B are potentially significant KATs for the brain acetylome sites identified. Most identified acetylated proteins from mouse brain tissue were predicted to be acetylated by KAT2A and KAT2B. KAT2A and KAT2B are highly expressed in the cerebral cortex, prefrontal cortex, and brain but are both found in the nucleus (Stilling et al., 2014, Drazic et al., 2016). However, a growing number of studies showed that they translocate to the cytoplasm (Drazic et al., 2016, Sadoul et al., 2010). For example, acetylation regulates KAT2B localisation, KAT2B is autoacetylated in the nucleus which then deacetylates on the NLS domain in the cytoplasm which leads to its accumulation in the cytoplasm (Blanco-García et al., 2009, Wang et al., 2019a).

This finding indicates a significant overlap between KATs and KDAC in the brain (Wankun et al., 2016, Stilling et al., 2014). Many identified ac(K) sites are found in mitochondria; however, we know from the literature that there is only 2 KATs enzyme found in mitochondria. Acetylation modifications in mitochondria are mostly non-enzymatic and reliable on high PH and high acetyl-CoA concentrations, unlike other cellular compartments where KATs enzymes are required (Drazic et al., 2016). These findings are only a prediction; more research is needed to investigate the role of KAT enzymes in brain acetylome.

### ***6.2.3 Ubiquitination and acetylation crosstalk***

Lysine acetylation of synaptic proteins has been shown to regulate protein stability and degradation (5, 19). This is mediated by the occurrence of PTM switches on lysine residues; ubiquitination at these sites promotes degradation whilst acetylation prevents ubiquitination. Preventing protein ubiquitination and inhibiting proteasome-dependent degradation is a common mechanism of acetylation-dependent protein stability. This might be because of direct competition for lysine residue modification between acetylation and ubiquitination (Narita et al., 2018, Wang et al., 2017a). For example, acetylation of AMPA K813, K819, K822 and K868 prevents their ubiquitination by E3 ligases such as Nedd4, thereby preventing degradation of AMPAR (Wang et al., 2017a).

On the other hand, studies showed that acetylation could also induce protein degradation by promoting ubiquitination. For example, acetylation of PCK1 and DNMT1 recruits E3 ubiquitin-protein ligase to induce protein ubiquitination and degradation (Du et al., 2010, Jiang et al., 2011). As mentioned before, a bioinformatic analysis demonstrates that 36% (6,032) out of (13,635) ac(K) sites that were predicted to be acetylated on synaptic proteins can also be ubiquitinated according to the Phosphosite dataset (Signling, 2017). A comparison of ac(K)

sites identified from Sirt2 KO and old mouse brain acetylomes to ubiquitination dataset (Signling, 2017) revealed ~ 40% overlap, which means more than 1,000 lysine sites are shared between both PTMs.

These results show another evidence to support the previous studies, which suggest that Sirt2 regulate acetylation and ubiquitination switches (Lalonde et al., 2017). For example, studies showed the identified VAMP3 ac(K) sites are ubiquitinated by Goliath ubiquitin ligases which regulate the recycling endosome trafficking of SNARE protein (Yamazaki et al., 2013). Despite the role of Sirt2, there is a general interest in how this type of PTM crosstalk balance protein turnover rates and contribute to physiological functions (Kozuka-Hata et al., 2020).

### ***6.3 Clinical implications of Sirt2 and acetylation in the brain***

This study and previous studies have shown that lysine acetylation is implicated in several neurodegenerative diseases by a dysregulation of the acetylation mechanism, protein stability and aggregation (Ali et al., 2018, Wang et al., 2020b, Sun et al., 2021). Moreover, Sirt2 plays an important role in neurological diseases, making Sirt2 modulators is promising avenue of research for those diseases (Donmez and Outeiro, 2013).

#### ***6.3.1 Parkinson's disease***

One of our findings was the strong relationship between acetylation, Sirt2 and Parkinson's disease pathways, observed from Sirt2 KO and aged mouse brain acetylome profiles and Sirt2 interactors dataset (Thomas et al., 2003). Studies showed that SNCA is acetylated on K6 and K10 and that Sirt2 deacetylates these residues (Rita Machado de et al., 2017, Bhattacharjee et al., 2019). Our data confirmed what was previously suggested about acetylation and Sirt2 role in regulating SNCA, and additionally, we identified the K96 ac(K) site that was not reported before. Blocking ubiquitination via acetylation worsens SNCA toxicity and increases

the formation of lewy bodies in the substantia nigra. As suggested, inhibition of Sirt2 prevents neurotoxicity by suppressing SNCA aggregation (Wang et al., 2020b, Rita Machado de et al., 2017).

Many studies have proposed that Sirt2 inhibitors might be helpful to treat various synucleinopathies (Rita Machado de et al., 2017, Singh et al., 2017b). Furthermore, we found that Sirt2 either deacetylated or interacted with many other proteins involved in Parkinson's disease pathways such as Aldoc, Uchl1, Gapdh, TUBA1C, and Ywah. Some of those proteins were previously identified in acetylomes of human fibroblasts from Parkinson's disease patients (Yakhine-Diop et al., 2018). This result could provide further evidence that regulating acetylation via Sirt2 is a possible therapeutic target for this disease.

### ***6.3.2 Alzheimer's disease***

Tau (MAPT) protein hyperphosphorylation is one of the hallmarks of Alzheimer's disease. Hyperphosphorylated Tau forms fibrils, a significant factor in the aetiology of Alzheimer's and related tauopathies. Tau is also hyperacetylated; lysine that might ordinarily be ubiquitinated are not when tau is acetylated, and this causes protein accumulation and leads to Alzheimer's disease development (Drazic et al., 2016, Donmez and Outeiro, 2013, Saha and Sen, 2019). Studies show that acetylation of MAPT is regulated by Ep300, KAT2B, SIRT1 and Sirt2. In addition, SIRT1 levels are negatively linked to tau fibril formation and the duration of Alzheimer's symptoms (Donmez and Outeiro, 2013, Wątroba and Szukiewicz, 2016).

Our data found that MAPT is acetylated on more than ten sites in Sirt2 KO and aged brain acetylome profiles. Interestingly, two acetylated peptides were significantly increased with Sirt2 KO but not with the old brain. Those MAPT acetylated peptides were among the few acetylated peptides significantly increased in the human brain acetylome of AD patients (Sun

et al., 2021). Our data also supported the idea that these increases were primarily caused by decreased Sirt2 levels no change in Ep300 or SIRT1 levels, which was previously declined significantly in AD patients (Sun et al., 2021).

In conclusion, Sirt2 is important in the pathophysiology of several neurodegenerative diseases. Most recent research suggests that modulators of Sirt2 have clear neuroprotective benefits in patients with pathological neuropathy. To determine the viability of Sirt2 as a therapeutic target for neurological disorders, more in vivo work such as Sirt2 activators or inhibitors administration in different disease animal model and clinical data for validating proposed drugs are needed.

### **6.3.3 Myelination**

Studies that Sirt2 is abundant in oligodendrocytes. Our data suggest that Sirt2 putatively deacetylates several myelin proteins, and other myelin proteins such as (Plp1, Slc25a5, Mbp and Slc25a4) have been linked to Sirt2 in previous studies (2021, Wang et al., 2019b, Fourcade et al., 2017, Chamberlain et al., 2021). For example, PLP is essential for axonal Sirt2 transport; thus, both proteins are abundant in the myelin of the CNS (Werner et al., 2007). In addition, aberrant PLP decreases Sirt2 levels and causes axonal degeneration (Werner et al., 2007, Zhu et al., 2012, 2021). These data agree with the Sirt2 KO mice phenotype that included locomotor dysfunction caused by axonal degeneration (Fourcade et al., 2017, Wang et al., 2019b). The myelin sheath appeared as a significantly enriched cellular compartment in the Sirt2 KO brain, old brain acetylomes and Sirt2 AP-MS datasets, further supporting the link between Sirt2 and myelination via acetylation.

#### 6.4 Do low stoichiometry acetylation sites have a biological function?

The stoichiometry of a PTM, also known as PTM site occupancy or fractional PTM occupancy, refers to the percentage of a protein that a PTM modifies at a given site. As demonstrated in figure 6.1, acetylation stoichiometry is defined as the percentage of acetylated proteins divided by the total abundance.

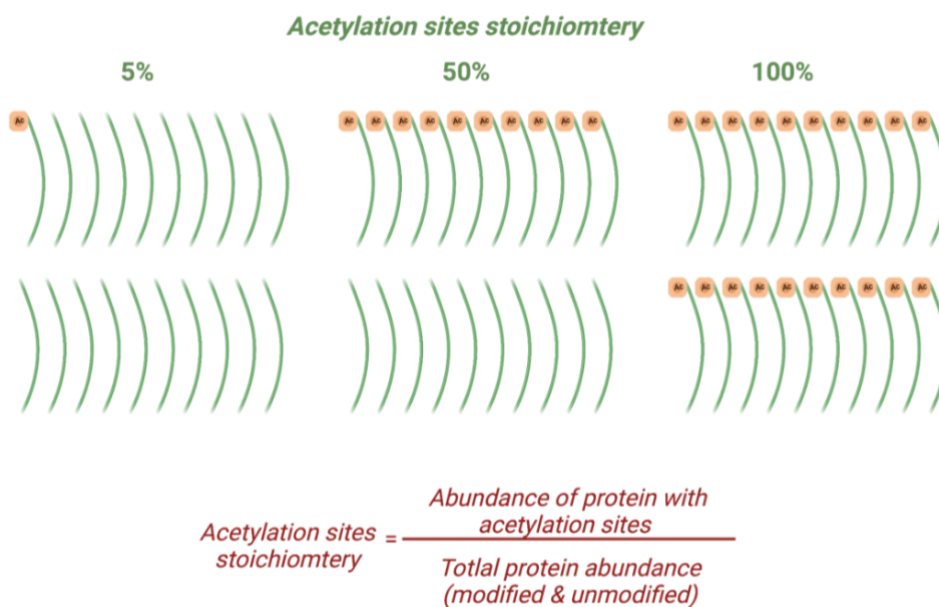


**Figure 6.1 – Acetylation site stoichiometry.** Acetylated peptides are marked, indicating the percentage of total proteins stoichiometry.

A critical step in acetylome analysis is the acetylation-enrichment step to allow for in-depth LC-MS/MS analysis in which thousands of ac(K) sites are identified in single experiments, including many low stoichiometry ac(K) sites. This contrasts with proteomics studies without acetylation enrichment steps which will mainly allow identification of high stoichiometry acetylation sites that occur on highly abundant proteins such as histones (Lundby et al., 2012b, Svinkina et al., 2015, Drazic et al., 2016). Therefore, identifying thousands of

acetylated peptides without acetyl-lysine antibody enrichments is challenging (Svinkina et al., 2015, Bogi Karbech et al., 2019, Lundby et al., 2012b). For example, in our data, only 0.98% and 0.46% of total identified peptides in Sirt2 KO and old mouse brain tissue were acetylated without enrichment, respectively. Our findings agree with the deep proteome study performed on HeLa cells showed 0.17% of the total identified acetylated peptides were detected without antibody enrichment (Bekker-Jensen et al., 2017, Bogi Karbech et al., 2019).

It could be assumed that low stoichiometry acetylation might indicate that this site is not likely to have a function, but there is no evidence to support this claim (Bogi Karbech et al., 2019). Studies have revealed that the mechanism of action of those sites is what determines their ability to regulate protein function (Bogi Karbech et al., 2019, Prus et al., 2019). Low stoichiometry acetylation could regulate acetylation that confers a gain-of-function or regulates protein activity at a specific time and/or location. For example, if acetylation of one particular site causes enzyme inactivation, the degree of inactivation should be reflected in the acetylation stoichiometry (Narita et al., 2018, Bogi Karbech et al., 2019).

For example, acetylation of MAPT and SNCA is known to impact protein functions and stability and contribute highly to the mechanisms of the pathology of AD and PD, respectively (Rita Machado de et al., 2017, Wang et al., 2020b, Saha and Sen, 2019, Sun et al., 2021). The hyperacetylated MAPT is acetylated on more than ten sites. However, the stoichiometry of those sites is less than 0.1% (Bogi Karbech et al., 2019). Similarly, the stoichiometry levels of SNCA sites did not exceed 1% (Bogi Karbech et al., 2019). Moreover, known Sirt2 substrates that contribute to many biological functions have similar levels CDK9, 0.025% (Sabò et al., 2008, Bogi Karbech et al., 2019), alpha-tubulin, 0.085% (Eshun-Wilson et al., 2019, Janke and Montagnac, 2017) and others (Bogi Karbech et al., 2019).

One of the common methods used to assess the impact of acetylation on protein activity is to use acetylation mimicking glutamine substitution mutations to protect acetylation modification and provide 100% stoichiometry level of the desired sites (Guo et al., 2019). However, because the great majority of acetylation happens at a stoichiometry of less than 1%, a loss-of-function mechanism at a single acetylation site is unlikely to have an influence on protein activity (Bogi Karbech et al., 2019).

Understanding the acetylation stoichiometry contributes to understanding the functional significance of a modification site and how it affects the protein function (Bogi Karbech et al., 2019).

### **6.5 Future prospects**

This research was done *in vivo* (brain tissue) and *in vitro* (HEK239 cells). In an ideal world, the continuation of this study, particularly the validation of identified substrates and interactors, would involve comparative investigations but in more neuronal settings. For example, neuronal cell lines (SH-SY5Y cells), primary neurons, and isolated synaptosomes would be good candidates to investigate brain acetylome. It will allow both Sirt2 and acetylation modification functions to be reflected and help assess how this affects the various brain functions and pathways identified.

We identified 226 ac(K) with increased acetylation in Sirt2 KO mice and around 60 ac(K) sites that changed acetylation during ageing. Those sites were challenging to validate (VAMP2/3 sites); other substrates might be better candidates for validation. Moreover, more optimisations might be required considering stoichiometry levels, protein turnover and how different PTMs could influence the detection of ac(K) sites such as phosphorylation and ubiquitination (van Noort et al., 2012).

Further testing will be performed to particularly investigate substrates after validation, e.g., VAMP2/3 that will allow us to make a precise observation of the change in their stability, turnover, activity, and the accumulation levels using drugs that inhibits protein synthesis and degradation, and immunofluorescence microscopy.

We generated a Sirt2 interactome dataset from HEK239 cells to validate putative Sirt2 substrates and identify the protein-protein interaction with Sirt2. Further work involving similar approaches using neuronal cell lines will provide more relevant Sirt2 interactors in the CNS system compatible with the Sirt2 KO acetylome profile.

A pilot experiment of AP-MS of endogenous Sirt2 from mouse brain tissue was performed (data not shown). This experiment will provide a Sirt2 interactome network from the brain tissue and better understand the protein-protein interaction changes from HeLa, HEK239 and brain tissue (Eldridge et al., 2020, Budayeva and Cristea, 2016).

Initial work was carried out on isolated synaptosomes from cultured primary neurons transfected with Flag-tagged Sirt2 and treated with AGK2 compared to non-treated neuronal cultures (data not shown). To assess the involvement of Sirt2 in synaptic functions, immunoblotting and mass spectrometry will be used to measure changes in protein levels and expression, as well as immunofluorescence to measure changes in localisations. These experiments will also be performed using the Sirt2 siRNA gene knockdown (Wang et al., 2017a, Lalonde et al., 2017).

Regulation of protein stability and turnover are important functions of acetylation and Sirt2 (Narita et al., 2018, Bogi Karbech et al., 2019). Acetylation mimic constructs of several interesting proteins identified from the Sirt2 KO and aged brain acetylomes have been made by mutating the lysines (K) to glutamines (Q). A preliminary project is currently being carried out to determine if acetylation stabilises proteins and if Sirt2 overexpression or inhibition affects the unmodified version of the protein. Protein stability will be modulated by treating cells with CHX and mg132 after overexpression of those proteins. The investigating will be carried out via immunoblotting to determine changes in protein levels or immunofluorescence to observe proteins accumulation. Generating a stable cell line of WT and KQ versions of the substrates or Sirt2 WT or KD will be useful for further functional investigation and understanding the impact of the phenotype of Sirt2 deletion (Wang et al.,

2017a, Lin et al., 2013, Wang et al., 2019b). However, due to the lack of time and culturing difficulties alongside this data were not included here.

The acetylome datasets presented in this study contains many sites which are potentially acetylation/ubiquitination switches. As suggested for the Sirt2 KO mouse, increased acetylation levels should reduce ubiquitination at acetylation sites regulated by Sirt2. To determine which Sirt2 dependent acetylation sites form acetylation/ubiquitination switches, a proteomics-based analysis of ubiquitination could be performed. Samples would be prepared similarly to that described for the acetylome analysis except that an antibody that recognises the ubiquitin remnant (Lysine-Glycine-Glycine) will be used to purify ubiquitinated peptides. This will identify which ubiquitination sites are altered by Sirt2 deletion and will identify those that form acetylation/ubiquitination switches. In addition, in vitro inhibition or overexpression of Sirt2 could be a valuable indicator to study the competing process between ubiquitination and acetylation on identical lysine residues.

Research has shown that protein acetylation levels in synapses are affected by neuronal activity (Wang et al., 2017a). To validate this evidence, primary neuron cultures could be treated with glycine/bicuculline that selectively activates synaptic N-methyl-D-aspartate receptors and induces long-term chemical potentiation (cLTP). Additionally, long-term chemical depression (LTD) could be induced by treating cells with glycine/NMDA and then returned to basal media, which will result in AMPAR internalisation and synaptic depression (O'Connor et al., 2020). Western blotting with anti-acetyl-lysine antibodies could be performed to determine if global acetylation levels are altered upon induction of LTP or LTD. Additionally, acetylome analysis of these treatments may be performed to determine which proteins exhibit activity-dependent changes in acetylation.

Sirt2 KO mice showed a reduction in LTP and LTD compared to wild-type controls, suggesting that the absence of Sirt2 and increased acetylation levels may compromise synaptic plasticity. The combination of LTP/LTD protocols with specific inhibition of Sirt2 could be used to investigate how Sirt2 and acetylation impact the activity of synapses.

## 6.7 Conclusion

In this work, I provided insight into lysine acetylation and Sirt2 role in the brain, by generating acetylome profiles of mouse brain tissue under two important conditions that are believed to affect brain/synaptic functions through altered protein acetylation: i) loss of function/reduction of function of Sirt2 and ii) ageing

First, acetylome analysis of Sirt2<sup>-/-</sup> mouse brain tissue revealed a significant increase in 226 acetylation sites *in vivo*. These results advance the knowledge of Sirt2 involvement in brain proteins and associated functions and emphasise the potential critical role of lysine acetylation in regulating synaptic proteins. This work showed a significant change in lysine acetylation in brain tissue and highlighted the importance of tissue-specific mapping of PTM of proteins. This dataset of Sirt2 substrates and sites will be an important resource for initiating functional studies to understand mechanisms of regulation for specific proteins including those involved in human brain diseases and targets for drug development.

Second, our acetylome analysis of ageing revealed a significant change in 60 acetylation sites in aged mice *in vivo*. This work highlighted that lysine acetylation changes during ageing occur on many crucial proteins. Given that age-related disease require additional research and development of treatment options, any knowledge gained about the causes of those diseases can aid in the exploration of potential targets for therapeutic strategies. Indeed, many discussions of Sirt2 and other Sirtuins focused on inhibiting or activating their deacetylase activity to control acetylation. However, more research is needed to understand the functions behind Sirt2-mediated lysine deacetylation in relation to each disease.

Hopefully, this work will be helpful to other researchers in the future in understanding the role of lysine acetylation in the aged brain and via the function of Sirt2.

## Bibliography

- The Human Protein Atlas* [Online]. Available: <http://www.proteinatlas.org> [Accessed].
- AKIMOV, V., BARRIO-HERNANDEZ, I., HANSEN, S. V. F., HALLENBORG, P., PEDERSEN, A.-K., BEKKER-JENSEN, D. B., PUGLIA, M., CHRISTENSEN, S. D. K., VANSELOW, J. T., NIELSEN, M. M., KRATCHMAROVA, I., KELSTRUP, C. D., OLSEN, J. V. & BLAGOEV, B. 2018. Ubisite approach for comprehensive mapping of lysine and n-terminal ubiquitination sites. *Nat Struct Mol Biol*, 25, 631-640.
- ALARCÓN, J. M., MALLERET, G., TOUZANI, K., VRONSKAYA, S., ISHII, S., KANDEL, E. R. & BARCO, A. 2004. Chromatin Acetylation, Memory, and LTP Are Impaired in CBP +/- Mice : A Model for the Cognitive Deficit in Rubinstein-Taybi Syndrome and Its Amelioration. *Neuron*, 42, 947-959.
- ALI, I., CONRAD, R., VERDIN, E. & OTT, M. 2018. Lysine Acetylation Goes Global: From Epigenetics to Metabolism and Therapeutics. *Chem. Rev.*
- ALLFREY, V. G., FAULKNER, R. & MIRSKY, A. E. 1964. ACETYLATION + METHYLATION OF HISTONES + THEIR POSSIBLE ROLE IN REGULATION OF RNA SYNTHESIS. *Proceedings of the National Academy of Sciences of the United States of America*, 51, 786-+.
- ANDERSON, G. & MAES, M. 2013. Neurodegeneration in Parkinson's Disease: Interactions of Oxidative Stress, Tryptophan Catabolites and Depression with Mitochondria and Sirtuins. *Mol Neurobiol*, 49, 771-783.
- ANDERSON, K. A., HUYNH, F. K., FISHER-WELLMAN, K., STUART, J. D., PETERSON, B. S., DOUROS, J. D., WAGNER, G. R., THOMPSON, J. W., MADSEN, A. S., GREEN, M. F., SIVLEY, R. M., ILKAYEVA, O. R., STEVENS, R. D., BACKOS, D. S., CAPRA, J. A., OLSEN, C. A., CAMPBELL, J. E., MUOIO, D. M., GRIMSRUD, P. A. & HIRSCHHEY, M. D. 2017. SIRT4 Is a Lysine Deacylase that Controls Leucine Metabolism and Insulin Secretion. *Cell Metab*, 25, 838-855.e15.
- ANWAR, T., KHOSLA, S. & RAMAKRISHNA, G. 2016. Increased expression of SIRT2 is a novel marker of cellular senescence and is dependent on wild type p53 status. *Cell Cycle*, 15, 1883-1897.
- ARNESSEN, T., VAN DAMME, P., POLEVODA, B., HELSENS, K., EVJENTH, R., COLAERT, N., VARHAUG, J. E., VANDEKERCKHOVE, J., LILLEHAUG, J. R., SHERMAN, F. & GEVAERT, K. 2009. Proteomics Analyses Reveal the Evolutionary Conservation and Divergence of N-Terminal Acetyltransferases from Yeast and Humans. *Proc Natl Acad Sci U S A*, 106, 8157-8162.
- BALTUS, G. A., KOWALSKI, M. P., ZHAI, H., TUTTER, A. V., QUINN, D., WALL, D. & KADAM, S. 2009. Acetylation of Sox2 Induces its Nuclear Export in Embryonic Stem Cells: Sox2 Acetylation Promotes Nuclear Export. *Stem cells (Dayton, Ohio)*, 27, 2175-2184.
- BATEMAN, A., MARTIN, M.-J., ORCHARD, S., AGIVETOVA, R., BOWLER-BARNETT, E. H., BRITTO, R., BYE-A-JEE, H., COETZEE, R., CUKURA, A., SILVA, A. D., DENNY, P., EBENEZER, T., GARMIRI, P., GEORGHIOU, G., HATTON-ELLIS, E., HUSSEIN, A., IGNATCHENKO, A., ISHTIAQ, R., JOKINEN, P., JOSHI, V., JYOTHI, D., LOPEZ, R., LUCIANI, A., LUSSI, Y., MACDOUGALL, A., MADEIRA, F., MAHMOUDY, M., MENCHI, M., MISHRA, A., MOULANG, K., OLIVEIRA, C. S., PUNDIR, S., QI, G., RAJ, S., RICE, D., SAMPSON, J., SAWFORD, T., SPERETTA, E., TURNER, E., VASUDEV, P., VOLYNKIN, V., WARNER, K., WATKINS, X., ZELLNER, H., POUX, S., REDASCHI, N., AIMO, L., ARGOU-DU, G., AUCHINCLOSS, A., AXELSEN, K., BANSAL, P., BARATIN, D., BLATTER, M.-C., BOUTET, E., BREUZA, L., DE CASTRO, E., COUDERT, E., CUCHE, B., DOCHE, M., DORNEVIL, D., ESTREICHER, A., FAMILIETTI, M. L., FEUERMANN, M., GASTEIGER, E., GERRITSEN, V., HINZ, U., HULO, C., HYKA-NOUSPIKEL, N., KELLER, G., KERHORNOU, A., LARA, V., LE MERCIER, P., LIEBERHERR, D., LOMBARDOT, T., MARTIN, X., MASSON, P., MORGAT, A., PAESANO, S., PILBOUT, S., POURCEL, L., PRUESS, M., RIVOIRE, C., SIGRIST, C., SONESSON, K., STUTZ, A., TOGNOLLI, M., VERBREGUE, L., WU, C. H., ARMINSKI, L., CHEN, C., CHEN, Y., HUANG, H., LAIHO, K., MCGARVEY, P., NATALE, D. A., ROSS, K., VINAYAKA, C. R., WANG, Q., WANG, Y. & ZHANG, J. 2021. UniProt: the universal protein knowledgebase in 2021. *Nucleic Acids Res*, 49, D480-D489.

- BAYES, A., COLLINS, M. O., CRONING, M. D. R., VAN DE LAGEMAAT, L. N., CHOUDHARY, J. S. & GRANT, S. G. N. 2012. Comparative Study of Human and Mouse Postsynaptic Proteomes Finds High Compositional Conservation and Abundance Differences for Key Synaptic Proteins. *Plos One*, 7, 13.
- BAYES, A., COLLINS, M. O., GALTREY, C. M., SIMONNET, C., ROY, M., CRONING, M. D. R., GOU, G., VAN DE LAGEMAAT, L. N., MILWARD, D., WHITTLE, I. R., SMITH, C., CHOUDHARY, J. S. & GRANT, S. G. N. 2014. Human post-mortem synapse proteome integrity screening for proteomic studies of postsynaptic complexes. *Molecular Brain*, 7.
- BAYES, A., COLLINS, M. O., REIG-VIADER, R., GOU, G., GOULDING, D., IZQUIERDO, A., CHOUDHARY, J. S., EMES, R. D. & GRANT, S. G. N. 2017. Evolution of complexity in the zebrafish synapse proteome. *Nature Communications*, 8, 15.
- BAYÉS, À., COLLINS, M. O., REIG-VIADER, R., GOU, G., GOULDING, D., IZQUIERDO, A., CHOUDHARY, J. S., EMES, R. D. & GRANT, S. G. N. 2017. Evolution of complexity in the zebrafish synapse proteome. *Nature Communications*, 8.
- BEIROWSKI, B., GUSTIN, J., ARMOUR, S. M., YAMAMOTO, H., VIADER, A., NORTH, B. J., MICHAN, S., BALOH, R. H., GOLDEN, J. P., SCHMIDT, R. E., SINCLAIR, D. A., AUWERX, J. & MILBRANDT, J. 2011. Sir-two-homolog 2 (Sirt2) modulates peripheral myelination through polarity protein Par-3/atypical protein kinase C (aPKC) signaling. *Proc Natl Acad Sci U S A*, 108, E952-E961.
- BEKKER-JENSEN, D. B., KELSTRUP, C. D., BATTH, T. S., LARSEN, S. C., HALDRUP, C., BRAMSEN, J. B., SØRENSEN, K. D., HØYER, S., ØRNTTOFT, T. F., ANDERSEN, C. L., NIELSEN, M. L. & OLSEN, J. V. 2017. An Optimized Shotgun Strategy for the Rapid Generation of Comprehensive Human Proteomes. *Cell Syst*, 4, 587-599.e4.
- BELMAN, J. P., BIAN, R. R., HABTEMICHAEL, E. N., LI, D. T., JURCZAK, M. J., ALCÁZAR-ROMÁN, A., MCNALLY, L. J., SHULMAN, G. I. & BOGAN, J. S. 2015. Acetylation of TUG Protein Promotes the Accumulation of GLUT4 Glucose Transporters in an Insulin-responsive Intracellular Compartment. *J Biol Chem*, 290, 4447-4463.
- BERTHOLET, A. M., CHOUCANI, E. T., KAZAK, L., ANGELIN, A., FEDORENKO, A., LONG, J. Z., VIDONI, S., GARRITY, R., CHO, J., TERADA, N., WALLACE, D. C., SPIEGELMAN, B. M. & KIRICHOK, Y. 2019. H<sup>+</sup> transport is an integral function of the mitochondrial ADP/ATP carrier. *Nature*, 571, 515-520.
- BHATTACHARJEE, P., ÖHRFELT, A., LASHLEY, T., BLENNOW, K., BRINKMALM, A. & ZETTERBERG, H. 2019. Mass Spectrometric Analysis of Lewy Body-Enriched  $\alpha$ -Synuclein in Parkinson's Disease. *J. Proteome Res*, 18, 2109-2120.
- BIELLA, G., FUSCO, F., NARDO, E., BERNOCCHI, O., COLOMBO, A., LICHTENTHALER, S. F., FORLONI, G. & ALBANI, D. 2016. Sirtuin 2 Inhibition Improves Cognitive Performance and Acts on Amyloid- $\beta$  Protein Precursor Processing in Two Alzheimer's Disease Mouse Models. *J Alzheimers Dis*, 53, 1193-1207.
- BLACK, J. C., MOSLEY, A., KITADA, T., WASHBURN, M. & CAREY, M. 2008. The SIRT2 Deacetylase Regulates Autoacetylation of p300. *Mol Cell*, 32, 449-455.
- BLANCO-GARCÍA, N., ASENSIO-JUAN, E., DE LA CRUZ, X. & MARTÍNEZ-BALBÁS, M. A. 2009. Autoacetylation Regulates P/CAF Nuclear Localization. *J Biol Chem*, 284, 1343-1352.
- BLISS, T. V. P., COLLINGRIDGE, G. L. & MORRIS, R. G. M. 2014. Synaptic plasticity in health and disease: introduction and overview. *Phil. Trans. R. Soc. B*, 369, 20130129-20130129.
- BOBROWSKA, A., DONMEZ, G., WEISS, A., GUARENTE, L. & BATES, G. 2012. SIRT2 ablation has no effect on tubulin acetylation in brain, cholesterol biosynthesis or the progression of Huntington's disease phenotypes in vivo. *PLoS One*, 7, e34805-e34805.
- BOGI KARBECH, H., RAJAT, G., LINDA, B., DAVID, L., TAKEO, N., MICHAEL, L., CHUNARAM, C. & BRIAN, T. W. 2019. Analysis of human acetylation stoichiometry defines mechanistic constraints on protein regulation. *Nature Communications*, 10, 1-11.
- BORDONE, L., MOTTA, M. C., PICARD, F., ROBINSON, A., JHALA, U. S., APFELD, J., MCDONAGH, T., LEMIEUX, M., MCBURNEY, M., SZILVASI, A., EASLON, E. J., LIN, S.-J. & GUARENTE, L. 2006.

- Sirt1 regulates insulin secretion by repressing UCP2 in pancreatic  $\beta$  cells. *PLoS Biol*, 4, 210-220.
- BRAIDY, N., POLJAK, A., GRANT, R., JAYASENA, T., MANSOUR, H., CHAN-LING, T., SMYTHE, G., SACHDEV, P. & GUILLEMIN, G. J. 2015. Differential expression of sirtuins in the aging rat brain. *Front Cell Neurosci*, 9, 167-167.
- BROWNELL, J. E., ZHOU, J. X., RANALLI, T., KOBAYASHI, R., EDMONDSON, D. G., ROTH, S. Y. & ALLIS, C. D. 1996. Tetrahymena histone acetyltransferase A: A homolog to yeast Gcn5p linking histone acetylation to gene activation. *Cell*, 84, 843-851.
- BUDAYEVA, H. G. & CRISTEA, I. M. 2016. Human Sirtuin 2 Localization, Transient Interactions, and Impact on the Proteome Point to Its Role in Intracellular Trafficking. *Mol Cell Proteomics*, 15, 3107-3125.
- CACABELOS, R., CARRIL, J. C., CACABELOS, N., KAZANTSEV, A. G., VOSTROV, A. V., CORZO, L., CACABELOS, P. & GOLDGABER, D. 2019. Sirtuins in alzheimer's disease: SIRT2-related genophenotypes and implications for pharmacoeugenetics. *Int J Mol Sci*, 20, 1249.
- CAMACHO-PEREIRA, J., TARRAGÓ, M. G., CHINI, C. C. S., NIN, V., ESCANDE, C., WARNER, G. M., PURANIK, A. S., SCHOON, R. A., REID, J. M., GALINA, A. & CHINI, E. N. 2016. CD38 Dictates Age-Related NAD Decline and Mitochondrial Dysfunction through an SIRT3-Dependent Mechanism. *Cell Metab*, 23, 1127-1139.
- CAO, W., LIU, N., TANG, S., BAO, L., SHEN, L., YUAN, H., ZHAO, X. & LU, H. 2008. Acetyl-Coenzyme A acyltransferase 2 attenuates the apoptotic effects of BNIP3 in two human cell lines. *Biochimica et biophysica acta. General subjects*, 1780, 873-880.
- CARBON, S., HARRIS, N. L., BASU, S., HARTLINE, E., EBERT, D., KESLING, M. J., MUSHAYAHAMA, T., LABONTE, S. A., SIEGELE, D. A., BROWN, N. H., TROVISCO, V., DOS SANTOS, G., FALLS, K., TABONE, C., ZHOU, P., STRELETS, V. B., RODRÍGUEZ-LÓPEZ, M., KUIPER, M., LOVERING, R. C., KRAMARZ, B., SAVERIMUTTU, S. C. C., PINHEIRO, S. M., GUNN, H., CHIBUCOS, M., MUNRO, J., DUESBURY, M. J., ORCHARD, S., SHRIVASTAVA, A., CHANG, H.-Y., RICHARDSON, L., DOLAN, M. E., DRABKIN, H. J., NI, L., SITNIKOV, D. M., HARRIS, M. A., OLIVER, S. G., RUTHERFORD, K., HAYLES, J., BÄHLER, J., BOLTON, E. R., DE PONS, J. L., DWINELL, M. R., HAYMAN, G. T., KALDUNSKI, M. L., LAULEDERKIND, S. J. F., PLASTERER, C., TUTAJ, M. A., VEDI, M., WANG, S.-J., MATTHEWS, L., ALEKSANDER, S. A., ALEXANDER, M. J., CHERRY, J. M., ENGEL, S. R., SIMISON, M., SKRZYPEK, M. S., WONG, E. D., FEUERMANN, M., GAUDET, P., MORGAT, A., BERARDINI, T. Z., REISER, L., HUALA, E., AUCHINCLOSS, A., ARGOUUD-PUY, G., BATEMAN, A., BLATTER, M.-C., BOUTET, E., BOWLER, E., BREUZA, L., BRITTO, R., BYE-A-JEE, H., GEORGHIOU, G., GOS, A.-N., GRUAZ-GUMOWSKI, N., HULO, C., IGNATCHENKO, A., JUNGO, F., LAIHO, K., LE MERCIER, P., MA-GRANE, M., MARTIN, M. J., MASSON, P., HYKA-NOUSPIKEL, N., POURCEL, L., SPERETTA, E., WU, C. H., CHAN, J. N., GROVE, C., VAN AUKEN, K., STERNBERG, P. W., BERRIMAN, M., HOWE, K., WRIGHT, A., HOWE, D. G., WESTERFIELD, M., JAISWAL, P., COOPER, L. & ELSER, J. 2021. The Gene Ontology resource: Enriching a Gold mine. *Nucleic Acids Res*, 49, D325-D334.
- CARLOMAGNO, Y., CHUNG, D.-E. C., YUE, M., CASTANEDES-CASEY, M., MADDEN, B. J., DUNMORE, J., TONG, J., DETURE, M., DICKSON, D. W., PETRUCCELLI, L. & COOK, C. 2017. An acetylation–phosphorylation switch that regulates tau aggregation propensity and function. *J Biol Chem*, 292, 15277-15286.
- CARON, C., BOYAULT, C. & KHOCHBIN, S. 2005. Regulatory cross-talk between lysine acetylation and ubiquitination: role in the control of protein stability. *BioEssays*, 27, 408-415.
- CHAMBERLAIN, K. A., HUANG, N., XIE, Y., LICAUSI, F., LI, S., LI, Y. & SHENG, Z.-H. 2021. Oligodendrocytes enhance axonal energy metabolism by deacetylation of mitochondrial proteins through transcellular delivery of SIRT2. *Neuron*, 109, 3456-3472.e8.
- CHEN, X. Q., WALES, P., QUINTI, L., ZUO, F. X., MONIOT, S., HERISSON, F., RAUF, N. A., WANG, H., SILVERMAN, R. B., AYATA, C., MAXWELL, M. M., STEEGBORN, C., SCHWARZSCHILD, M. A., OUTEIRO, T. F. & KAZANTSEV, A. G. 2015. The Sirtuin-2 Inhibitor AK7 Is Neuroprotective in

- Models of Parkinson's Disease but Not Amyotrophic Lateral Sclerosis and Cerebral Ischemia. *Plos One*, 10.
- CHOI, J., LEVEY, A. I., WEINTRAUB, S. T., REES, H. D., GEARING, M., CHIN, L.-S. & LI, L. 2004. Oxidative Modifications and Down-regulation of Ubiquitin Carboxyl-terminal Hydrolase L1 Associated with Idiopathic Parkinson's and Alzheimer's Diseases. *J Biol Chem*, 279, 13256-13264.
- CHOPRA, V., QUINTI, L., KIM, J., VOLLOR, L., NARAYANAN, K. L., EDGERLY, C., CIPICCHIO, P. M., LAUVER, M. A., CHOI, S. H., SILVERMAN, R. B., FERRANTE, R. J., HERSCH, S. & KAZANTSEV, A. G. 2012. The Sirtuin 2 Inhibitor AK-7 Is Neuroprotective in Huntington's Disease Mouse Models. *Cell Reports*, 2, 1492-1497.
- CHOUDHARY, C., KUMAR, C., GNAD, F., NIELSEN, M. L., REHMAN, M., WALTHER, T. C., OLSEN, J. V. & MANN, M. 2009a. Lysine acetylation targets protein complexes and co-regulates major cellular functions. *Science*, 325, 834-40.
- CHOUDHARY, C., KUMAR, C., GNAD, F., NIELSEN, M. L., REHMAN, M., WALTHER, T. C., OLSEN, J. V. & MANN, M. 2009b. Lysine Acetylation Targets Protein Complexes and Co-Regulates Major Cellular Functions. *Science*, 325, 834-840.
- CHOUDHARY, C., WEINERT, B. T., NISHIDA, Y., VERDIN, E. & MANN, M. 2014. The growing landscape of lysine acetylation links metabolism and cell signalling. *Nature Reviews Molecular Cell Biology*, 15, 536-550.
- CHRISTIAN, S., BRIAN, T. W., SEBASTIAN, A. W., PETRA, B., YASUYUKI, M., JUN, Q., LARS, J. J., WERNER, S., ANNA, R. M., NICHOLAS, J. W., SONIA, L., JÜRGEN, C., PATRICK, M., MATTHIAS, M., JAMES, E. B. & CHUNARAM, C. 2015. Acetylation site specificities of lysine deacetylase inhibitors in human cells. *Nature Biotechnology*, 33.
- COATES, P. J., NENUTIL, R., MCGREGOR, A., PICKSLEY, S. M., CROUCH, D. H., HALL, P. A. & WRIGHT, E. G. 2001. Mammalian Prohibitin Proteins Respond to Mitochondrial Stress and Decrease during Cellular Senescence. *Exp Cell Res*, 265, 262-273.
- COOK, C., STANKOWSKI, J. N., CARLOMAGNO, Y., STETLER, C. & PETRUCELLI, L. 2014. Acetylation: a new key to unlock tau's role in neurodegeneration. *Alzheimers Research & Therapy*, 6, 8.
- COULOMBE, J., GAMAGE, P., GRAY, M. T., ZHANG, M., TANG, M. Y., WOULFE, J., SAFFREY, M. J. & GRAY, D. A. 2014. Loss of UCHL1 promotes age-related degenerative changes in the enteric nervous system. *Front Aging Neurosci*, 6, 129-129.
- COX, J. & MANN, M. 2008. MaxQuant enables high peptide identification rates, individualized p.p.b.-range mass accuracies and proteome-wide protein quantification. *Nature Biotechnology*, 26, 1367-1372.
- DE OLIVEIRA, R. M., SARKANDER, J., KAZANTSEV, A. G. & OUTEIRO, T. F. 2012. SIRT2 as a therapeutic target for age-related disorders. *Front Pharmacol*, 3, 82-82.
- DIAZ-PERDIGON, T., BELLOCH, F. B., RICOBARAZA, A., ELBORAY, E. E., SUZUKI, T., TORDERA, R. M. & PUERTA, E. 2020. Early sirtuin 2 inhibition prevents age-related cognitive decline in a senescence-accelerated mouse model. *Neuropsychopharmacology*, 45, 347-357.
- DONMEZ, G. & OUTEIRO, T. F. 2013. SIRT1 and SIRT2: emerging targets in neurodegeneration. Weinheim.
- DRAZIC, A., MYKLEBUST, L. M., REE, R. & ARNESEN, T. 2016. The world of protein acetylation. *Biochimica Et Biophysica Acta-Proteins and Proteomics*, 1864, 1372-1401.
- DU, J., ZHOU, Y., SU, X., YU, J. J., KHAN, S., JIANG, H., KIM, J., WOO, J., KIM, J. H., CHOI, B. H., HE, B., CHEN, W., ZHANG, S., CERIONE, R. A., AUWERX, J., HAO, Q. & LIN, H. 2011. Sirt5 Is a NAD-Dependent Protein Lysine Demalonylase and Desuccinylase. *Science*, 334, 806-809.
- DU, Z., SONG, J., WANG, Y., ZHAO, Y., GUDA, K., YANG, S., KAO, H.-Y., XU, Y., WILLIS, J., MARKOWITZ, S. D., SEDWICK, D., EWING, R. M. & WANG, Z. 2010. DNMT1 stability is regulated by proteins coordinating deubiquitination and acetylation-driven ubiquitination. *Sci Signal*, 3, ra80-ra80.
- DUGAS, J. C., TAI, Y. C., SPEED, T. P., NGAI, J. & BARRES, B. A. 2006. Functional Genomic Analysis of Oligodendrocyte Differentiation. *J Neurosci*, 26, 10967-10983.

- ELDRIDGE, M. J. G., PEREIRA, J. M., IMPENS, F. & HAMON, M. A. 2020. Active nuclear import of the deacetylase Sirtuin-2 is controlled by its C-terminus and importins. *Sci Rep*, 10, 2034-2034.
- ERBURU, M., MUÑOZ-COBO, I., DIAZ-PERDIGON, T., MELLINI, P., SUZUKI, T., PUERTA, E. & TORDERA, R. M. 2017. SIRT2 inhibition modulate glutamate and serotonin systems in the prefrontal cortex and induces antidepressant-like action. *Neuropharmacology*, 117, 195-208.
- ESHUN-WILSON, L., ZHANG, R., PORTRAN, D., NACHURY, M. V., TOSO, D. B., LÖHR, T., VENDRUSCOLO, M., BONOMI, M., FRASER, J. S. & NOGALES, E. 2019. Effects of  $\alpha$ -tubulin acetylation on microtubule structure and stability. *Proc Natl Acad Sci U S A*, 116, 10366-10371.
- ESTEVEES, A. R., ARDUINO, D. M., SILVA, D. F., VIANA, S. D., PEREIRA, F. C. & CARDOSO, S. M. 2017. Mitochondrial Metabolism Regulates Microtubule Acetylation and Autophagy Through Sirtuin-2: Impact for Parkinson's Disease. *Molecular neurobiology*.
- ESTEVEES, A. R., ARDUÍNO, D. M., SILVA, D. F., VIANA, S. D., PEREIRA, F. C. & CARDOSO, S. M. 2018. Mitochondrial Metabolism Regulates Microtubule Acetylation and Autophagy Through Sirtuin-2: Impact for Parkinson's Disease. *Mol Neurobiol*, 55, 1440-1462.
- FERNANDEZ, E., COLLINS, M. O., FRANK, R. A. W., ZHU, F., KOPANITSA, M. V., NITHIANANTHARAJAH, J., LEMPRIERE, S. A., FRICKER, D., ELSEGOOD, K. A., MCLAUGHLIN, C. L., CRONING, M. D. R., MCLEAN, C., ARMSTRONG, J. D., HILL, W. D., DEARY, I. J., CENCELLI, G., BAGNI, C., FROMER, M., PURCELL, S. M., POCKLINGTON, A. J., CHOUDHARY, J. S., KOMIYAMA, N. H. & GRANT, S. G. N. 2017. Arc Requires PSD95 for Assembly into Postsynaptic Complexes Involved with Neural Dysfunction and Intelligence. *Cell Reports*, 21, 679-691.
- FISCHER, A., MÜHLHÄUSER, W. W. D., WARSCHIED, B. & RADZIWIŁŁ, G. 2017. Membrane localization of acetylated CNK1 mediates a positive feedback on RAF/ERK signaling. *Sci Adv*, 3, e1700475-e1700475.
- FOURCADE, S., MORATÓ, L., PARAMESWARAN, J., RUIZ, M., RUIZ-CORTÉS, T., JOVÉ, M., NAUDÍ, A., MARTÍNEZ-REDONDO, P., DIERSSEN, M., FERRER, I., VILLARROYA, F., PAMPLONA, R., VAQUERO, A., PORTERO-OTÍN, M. & PUJOL, A. 2017. Loss of SIRT2 leads to axonal degeneration and locomotor disability associated with redox and energy imbalance. *Aging Cell*, 16, 1404-1413.
- FOX, J. G. 2006. *The Mouse in Biomedical Research [electronic resource] : Immunology*, Burlington, Burlington : Elsevier Science, 2006.
- FRANKEL, S., ZIAFAZELI, T. & ROGINA, B. 2011. dSir2 and longevity in Drosophila. *Exp Gerontol*, 46, 391-396.
- FUJISAWA, T. & FILIPPAKOPOULOS, P. 2017. Functions of bromodomain-containing proteins and their roles in homeostasis and cancer. *Nat Rev Mol Cell Biol*, 18, 246-262.
- FULCO, M., SCHILTZ, R. L., IEZZI, S., KING, M. T., ZHAO, P., KASHIWAYA, Y., HOFFMAN, E., VEECH, R. L. & SARTORELLI, V. 2003. Sir2 Regulates Skeletal Muscle Differentiation as a Potential Sensor of the Redox State. *Mol Cell*, 12, 51-62.
- GAL, J., BANG, Y. & CHOI, H. J. 2012. SIRT2 interferes with autophagy-mediated degradation of protein aggregates in neuronal cells under proteasome inhibition. *Neurochem Int*, 61, 992-1000.
- GIL, J., RAMIREZ-TORRES, A. & ENCARNACION-GUEVARA, S. 2017. Lysine acetylation and cancer: A proteomics perspective. *Journal of Proteomics*, 150, 297-309.
- GLEAVE, J. A., ARATHOON, L. R., TRINH, D., LIZAL, K. E., GIGUÈRE, N., BARBER, J. H. M., NAJARALI, Z., KHAN, M. H., THIELE, S. L., SEMMEN, M. S., KOPRICH, J. B., BROTCHE, J. M., EUBANKS, J. H., TRUDEAU, L.-E. & NASH, J. E. 2017. Sirtuin 3 rescues neurons through the stabilisation of mitochondrial biogenetics in the virally-expressing mutant  $\alpha$ -synuclein rat model of parkinsonism. *Neurobiol Dis*, 106, 133-146.
- GLOZAK, M. A., SENGUPTA, N., ZHANG, X. & SETO, E. 2005. Acetylation and deacetylation of non-histone proteins. *Gene*, 363, 15-23.

- GOMES, P., OUTEIRO, T. F. & CAVADAS, C. 2015. Emerging Role of Sirtuin 2 in the Regulation of Mammalian Metabolism. *Trends in Pharmacological Sciences*, 36, 756-768.
- GRAY, B., CADD, V., ELLIOTT, M. & BEARD, M. 2018. The in vitro detection of botulinum neurotoxin-cleaved endogenous VAMP is epitope-dependent. *Toxicology in Vitro*, 48, 255-261.
- GRAY, L. R., TOMPKINS, S. C. & TAYLOR, E. B. 2013. Regulation of pyruvate metabolism and human disease. *Cell Mol Life Sci*, 71, 2577-2604.
- GUAN, J.-S., HAGGARTY, S. J., GIACOMETTI, E., DANNENBERG, J.-H., JOSEPH, N., GAO, J., NIELAND, T. J. F., ZHOU, Y., WANG, X., MAZITSCHKEK, R., BRADNER, J. E., DEPINHO, R. A., JAENISCH, R. & TSAI, L.-H. 2009. HDAC2 negatively regulates memory formation and synaptic plasticity. *Nature*, 459, 55-60.
- GUO, L., GUO, Y. Y., LI, B. Y., PENG, W. Q., CHANG, X. X., GAO, X. & TANG, Q. Q. 2019. Enhanced acetylation of ATP-citrate lyase promotes the progression of nonalcoholic fatty liver disease. *Journal of Biological Chemistry*, 294, 11805-11816.
- GUO, Y.-J., DONG, S.-Y., CUI, X.-X., FENG, Y., LIU, T., YIN, M., KUO, S.-H., TAN, E.-K., ZHAO, W.-J. & WU, Y.-C. 2016. Resveratrol alleviates MPTP-induced motor impairments and pathological changes by autophagic degradation of  $\alpha$ -synuclein via SIRT1-deacetylated LC3. *Mol. Nutr. Food Res*, 60, 2161-2175.
- HAMAIDI, I., ZHANG, L., KIM, N., WANG, M.-H., ICLOZAN, C., FANG, B., LIU, M., KOOMEN, J. M., BERGLUND, A. E., YODER, S. J., YAO, J., ENGELMAN, R. W., CREELAN, B. C., CONEJO-GARCIA, J. R., ANTONIA, S. J., MULÉ, J. J. & KIM, S. 2020. Sirt2 Inhibition Enhances Metabolic Fitness and Effector Functions of Tumor-Reactive T Cells. *Cell Metab*, 32, 420-436.e12.
- HAN, Y., JIN, Y., KIM, Y., KANG, B., CHOI, H., KIM, D., YEO, C. & LEE, K. 2008. Acetylation of Sirt2 by p300 attenuates its deacetylase activity. *Biochem. Biophys. Res. Commun.*, 375, 576-580.
- HARRIS, R. A., TINDALE, L. & CUMMING, R. C. 2014. Age-dependent metabolic dysregulation in cancer and Alzheimer's disease. *Biogerontology*, 15, 559-577.
- HE, X., NIE, H., HONG, Y., SHENG, C., XIA, W. & YING, W. 2012. SIRT2 activity is required for the survival of C6 glioma cells. *Biochemical and Biophysical Research Communications*, 417, 468-472.
- HELSENS, K., VAN DAMME, P., DEGROEVE, S., MARTENS, L., ARNESEN, T., VANDEKERCKHOVE, J. & GEVAERT, K. 2011. Bioinformatics Analysis of a *Saccharomyces cerevisiae* N-Terminal Proteome Provides Evidence of Alternative Translation Initiation and Post-Translational N-Terminal Acetylation. *J. Proteome Res*, 10, 3578-3589.
- HERSKOVITS, A. Z. & GUARENTE, L. 2013. Sirtuin deacetylases in neurodegenerative diseases of aging. *Cell Research*, 23, 746-758.
- HSU, C.-W., SHOU, D., HUANG, R., KHUC, T., DAI, S., ZHENG, W., KLUMPP-THOMAS, C. & XIA, M. 2016. Identification of HDAC Inhibitors Using a Cell-Based HDAC I/II Assay. *J Biomol Screen*, 21, 643-652.
- HU, H., ZHU, W., QIN, J., CHEN, M., GONG, L., LI, L., LIU, X., TAO, Y., YIN, H., ZHOU, H., ZHOU, L., YE, D., YE, Q. & GAO, D. 2017. Acetylation of PGK1 promotes liver cancer cell proliferation and tumorigenesis. *Hepatology*, 65, 515-528.
- IMAI, S.-I. & GUARENTE, L. 2014. NAD<sup>+</sup> and sirtuins in aging and disease. *Trends Cell Biol*, 24, 464-471.
- IMAI, S.-I. & GUARENTE, L. 2016. It takes two to tango: Nad<sup>+</sup> and sirtuins in aging/longevity control. *NPJ Aging Mech Dis*, 2, 16017-16017.
- INCONTRO, S., DÍAZ-ALONSO, J., IAFRATI, J., VIEIRA, M., ASENSIO, C. S., SOHAL, V. S., ROCHE, K. W., BENDER, K. J. & NICOLL, R. A. 2018. The CaMKII/NMDA receptor complex controls hippocampal synaptic transmission by kinase-dependent and independent mechanisms. *Nat Commun*, 9, 2069-2069.
- ITZHAK, D. N., DAVIES, C., TYANOVA, S., MISHRA, A., WILLIAMSON, J., ANTROBUS, R., COX, J., WEEKES, M. P. & BORNER, G. H. H. 2017. A Mass Spectrometry-Based Approach for Mapping

- Protein Subcellular Localization Reveals the Spatial Proteome of Mouse Primary Neurons. *Cell Reports*, 20, 2706-2718.
- IVANOVA, D., DIRKS, A., MONTENEGRO-VENEGAS, C., SCHÖNE, C., ALTROCK, W. D., MARINI, C., FRISCHKNECHT, R., SCHANZE, D., ZENKER, M., GUNDELFINGER, E. D. & FEJTOVA, A. 2015. Synaptic activity controls localization and function of CtBP1 via binding to Bassoon and Piccolo. *EMBO J*, 34, 1056-1077.
- JAMES, A. M., SMITH, C. L., SMITH, A. C., ROBINSON, A. J., HOOGEWIJS, K. & MURPHY, M. P. 2018. The Causes and Consequences of Nonenzymatic Protein Acylation. *Trends in Biochemical Sciences*, 43, 921-932.
- JANKE, C. & MONTAGNAC, G. 2017. Causes and Consequences of Microtubule Acetylation. *Curr Biol*, 27, R1287-R1292.
- JAYASENA, T., POLJAK, A., BRAIDY, N., ZHONG, L., ROWLANDS, B., MUENCHHOFF, J., GRANT, R., SMYTHE, G., TEO, C., RAFTERY, M. & SACHDEV, P. 2016. Application of Targeted Mass Spectrometry for the Quantification of Sirtuins in the Central Nervous System. *Scientific Reports*, 6.
- Jl, S., DOUCETTE, J. R. & NAZARALI, A. J. 2011. Sirt2 is a novel in vivo downstream target of Nkx2.2 and enhances oligodendroglial cell differentiation. *J Mol Cell Biol*, 3, 351-359.
- JIANG, H., KHAN, S., WANG, Y., CHARRON, G., HE, B., SEBASTIAN, C., DU, J., KIM, R., GE, E., MOSTOSLAVSKY, R., HANG, H. C., HAO, Q. & LIN, H. 2013. SIRT6 regulates TNF-[alpha] secretion through hydrolysis of long-chain fatty acyl lysine.(tumor necrosis factor and sirtuin 6). *Nature (London)*, 496, 110.
- JIANG, W., WANG, S., XIAO, M., LIN, Y., ZHOU, L., LEI, Q., XIONG, Y., GUAN, K.-L. & ZHAO, S. 2011. Acetylation Regulates Gluconeogenesis by Promoting PEPCK1 Degradation via Recruiting the UBR5 Ubiquitin Ligase. *Mol Cell*, 43, 33-44.
- JIN, Y.-H., JEON, E.-J., LI, Q.-L., LEE, Y. H., CHOI, J.-K., KIM, W.-J., LEE, K.-Y. & BAE, S.-C. 2004. Transforming growth factor- $\beta$  stimulates p300-dependent RUNX3 acetylation, which inhibits ubiquitination-mediated degradation. *J Biol Chem*, 279, 29409-29417.
- JING, E., GESTA, S. & KAHN, C. R. 2007. SIRT2 regulates adipocyte differentiation through FoxO1 acetylation/deacetylation. *Cell metabolism*, 6, 105.
- JONES, D. P. 2015. Redox theory of aging. *Redox Biol*, 5, 71-79.
- JOSEPH, P. O. S., MICHAEL, F. C., SAAD, A. Q., JAMES, K. R., GEORGE, M. C. & DANIEL, S. 2013. pLogo: a probabilistic approach to visualizing sequence motifs. *Nature Methods*, 10, 1211.
- JULIEN, C., TREMBLAY, C., ÉMOND, V., LEBBADI, M., SALEM, N., BENNETT, D. A. & CALON, F. 2009. Sirtuin 1 Reduction Parallels the Accumulation of Tau in Alzheimer Disease. *J Neuropathol Exp Neurol*, 68, 48-58.
- JUNG, Y. J., LEE, A. S., NGUYEN-THANH, T., KIM, D., KANG, K. P., LEE, S., PARK, S. K. & KIM, W. 2015. SIRT2 Regulates LPS-Induced Renal Tubular CXCL2 and CCL2 Expression. *Journal of the American Society of Nephrology : JASN*, 26, 1549.
- JURI, R., MATTHIAS, M. & YASUSHI, I. 2007. Protocol for micro- purification, enrichment, pre-fractionation and storage of peptides for proteomics using StageTips. *Nature Protocols*, 2, 1896.
- JÜRGEN, C. & MATTHIAS, M. 2008. MaxQuant enables high peptide identification rates, individualized p.p.b.- range mass accuracies and proteome- wide protein quantification. *Nature Biotechnology*, 26, 1367.
- JĘŚKO, H., WENCEL, P., STROSZNAJDER, R. P. & STROSZNAJDER, J. B. 2016. Sirtuins and Their Roles in Brain Aging and Neurodegenerative Disorders. *Neurochem Res*, 42, 876-890.
- KIM, G. W. & YANG, X. J. 2011. Comprehensive lysine acetylomes emerging from bacteria to humans. *Trends in Biochemical Sciences*, 36, 211-218.
- KIM, H.-S., VASSILOPOULOS, A., WANG, R.-H., LAHUSEN, T., XIAO, Z., XU, X., LI, C., VEENSTRA, TIMOTHY D., LI, B., YU, H., JI, J., WANG, XIN W., PARK, S.-H., CHA, YONG I., GIUS, D. & DENG,

- C.-X. 2011. SIRT2 Maintains Genome Integrity and Suppresses Tumorigenesis through Regulating APC/C Activity. *Cancer Cell*, 20, 487-499.
- KIM, H.-W., KIM, S.-A. & AHN, S.-G. 2016. Sirtuin inhibitors, EX527 and AGK2, suppress cell migration by inhibiting HSF1 protein stability. *Oncol Rep*, 35, 235-242.
- KIM, S. C., SPRUNG, R., CHEN, Y., XU, Y., BALL, H., PEI, J., CHENG, T., KHO, Y., XIAO, H., XIAO, L., GRISHIN, N. V., WHITE, M., YANG, X.-J. & ZHAO, Y. 2006a. Substrate and functional diversity of lysine acetylation revealed by a proteomics survey. *Molecular Cell*, 23, 607-618.
- KIM, S. C., SPRUNG, R., CHEN, Y., XU, Y., BALL, H., PEI, J., CHENG, T., KHO, Y., XIAO, H., XIAO, L., GRISHIN, N. V., WHITE, M., YANG, X.-J. & ZHAO, Y. 2006b. Substrate and Functional Diversity of Lysine Acetylation Revealed by a Proteomics Survey. *Mol Cell*, 23, 607-618.
- KIRTI, S., SEBASTIAN, S., CAROLINE, G. B., STEFKA, T., NIRMAL, K., NATALIA, M.-H., KARINA, K., LUDOVICO, C., UWE-KARSTEN, H., MARI-ANNE, P., MORITZ, J. R., MATTHIAS, M. & MIKAEL, S. 2015. Cell type- and brain region- resolved mouse brain proteome. *Nature Neuroscience*, 18.
- KOSCIUCZUK, E. M., MEHROTRA, S., SALEIRO, D., KROCZYNSKA, B., MAJCHRZAK-KITA, B., LISOWSKI, P., DRIEHAUS, C., ROGALSKA, A., TURNER, A., LIENHOOP, T., GIUS, D., FISH, E. N., VASSILOPOULOS, A. & PLATANIAS, L. C. 2018. Sirtuin 2- mediated deacetylation of cyclin-dependent kinase 9 promotes STAT1 signaling in type I interferon responses. *The Journal of biological chemistry*.
- KOZUKA-HATA, H., KITAMURA, A., HIROKI, T., AIZAWA, A., TSUMOTO, K., INOUE, J.-I. & OYAMA, M. 2020. System-wide analysis of protein acetylation and ubiquitination reveals a diversified regulation in human cancer cells. *Biomolecules*, 10, 411.
- KUTIL, Z., NOVAKOVA, Z., MELESHIN, M., MIKESOVA, J., SCHUTKOWSKI, M. & BARINKA, C. 2018. Histone Deacetylase 11 Is a Fatty-Acid Deacylase. *ACS chemical biology*, 13, 685-693.
- LALONDE, J., REIS, S. A., SIVAKUMARAN, S., HOLLAND, C. S., WESELING, H., SAULD, J. F., ALURAL, B., ZHAO, W.-N., STEEN, J. A. & HAGGARTY, S. J. 2017. Chemogenomic analysis reveals key role for lysine acetylation in regulating Arc stability. *Nature communications*, 8, 1659.
- LEAL, S. L. & YASSA, M. A. 2015. Neurocognitive Aging and the Hippocampus across Species. *Trends Neurosci*, 38, 800-812.
- LEE, S.-H., LEE, J.-H., LEE, H.-Y. & MIN, K.-J. 2019. Sirtuin signaling in cellular senescence and aging. *BMB reports*, 52, 24-34.
- LEE, V. M. Y., COHEN, T. J., GUO, J. L., HURTADO, D. E., KWONG, L. K., MILLS, I. P. & TROJANOWSKI, J. Q. 2011. The acetylation of tau inhibits its function and promotes pathological tau aggregation. *Nat Commun*, 2, 252-252.
- LI, W., ZHANG, B., TANG, J., CAO, Q., WU, Y., WU, C., GUO, J., LING, E.-A. & LIANG, F. 2007. Sirtuin 2, a mammalian homolog of yeast silent information regulator-2 longevity regulator, is an oligodendroglial protein that decelerates cell differentiation through deacetylating  $\alpha$ -tubulin. *J Neurosci*, 27, 2606-2616.
- LI, Y., KOKURA, K. & INOUE, T. 2019. Stabilization of P/CAF, as a ubiquitin ligase toward MDM2, suppresses mitotic cell death through p53-p21 activation in HCT116 cells with SIRT2 suppression. *Biochem Biophys Res Commun*, 508, 230-236.
- LIN, R., TAO, R., GAO, X., LI, T., ZHOU, X., GUAN, K.-L., XIONG, Y. & LEI, Q.-Y. 2013. Acetylation Stabilizes ATP-Citrate Lyase to Promote Lipid Biosynthesis and Tumor Growth. *Molecular Cell*, 51, 506-518.
- LIU, D., LIU, C., LI, J., AZADZOI, K., YANG, Y., ZHOU, F., DOU, K., KOWALL, N., VIEIRA, F. & JING-HUA, Y. 2013a. Proteomic Analysis Reveals Differentially Regulated Protein Acetylation in Human Amyotrophic Lateral Sclerosis Spinal Cord. *PLoS One*, 8, e80779.
- LIU, G., PARK, S.-H., IMBESI, M., NATHAN, W. J., ZOU, X., ZHU, Y., JIANG, H., PARISIADOU, L. & GIUS, D. 2017a. Loss of NAD-Dependent Protein Deacetylase Sirtuin-2 Alters Mitochondrial Protein Acetylation and Dysregulates Mitophagy. *Antioxid Redox Signal*, 26, 849-863.

- LIU, G., PARK, S. H., IMBESI, M., NATHAN, W. J., ZOU, X., ZHU, Y., JIANG, H., PARISIADOU, L. & GIUS, D. 2017b. Loss of NAD-Dependent Protein Deacetylase Sirtuin-2 Alters Mitochondrial Protein Acetylation and Dysregulates Mitophagy. *Antioxid Redox Signal*, 26, 849-863.
- LIU, G. X., PARK, S. H., IMBESI, M., NATHAN, W. J., ZOU, X. H., ZHU, Y. M., JIANG, H. Y., PARISIADOU, L. & GIUS, D. 2017c. Loss of NAD-Dependent Protein Deacetylase Sirtuin-2 Alters Mitochondrial Protein Acetylation and Dysregulates Mitophagy. *Antioxidants & Redox Signaling*, 26, 849-+.
- LIU, P. Y., XU, N., MALYUKOVA, A., SCARLETT, C. J., SUN, Y. T., ZHANG, X. D., LING, D., SU, S. P., NELSON, C., CHANG, D. K., KOACH, J., TEE, A. E., HABER, M., NORRIS, M. D., TOON, C., ROOMAN, I., XUE, C., CHEUNG, B. B., KUMAR, S., MARSHALL, G. M., BIANKIN, A. V. & LIU, T. 2013b. The histone deacetylase SIRT2 stabilizes Myc oncoproteins. *Cell death and differentiation*, 20, 503.
- LIU, Q.-Q., REN, K., LIU, S.-H., LI, W.-M., HUANG, C.-J. & YANG, X.-H. 2019a. MicroRNA-140-5p aggravates hypertension and oxidative stress of atherosclerosis via targeting Nrf2 and Sirt2. *International journal of molecular medicine*, 43, 839-849.
- LIU, S., ZHOU, Z., ZHANG, L., MENG, S., LI, S. & WANG, X. 2019b. Inhibition of SIRT2 by targeting GSK3 $\beta$ -mediated phosphorylation alleviates SIRT2 toxicity in SH-SY5Y cells. *Front Cell Neurosci*, 13, 148-148.
- LUDWIG, K. R., SCHROLL, M. M. & HUMMON, A. B. 2018. Comparison of In- Solution, FASP, and S-Trap Based Digestion Methods for Bottom- Up Proteomic Studies. *Journal of Proteome Research*, 17, 2480-2490.
- LUNDBY, A., LAGE, K., WEINERT, BRIAN T., BEKKER-JENSEN, DORTE B., SECHER, A., SKOVGAARD, T., KELSTRUP, CHRISTIAN D., DMYTRIYEV, A., CHOUDHARY, C., LUNDBY, C. & OLSEN, JESPER V. 2012a. Proteomic Analysis of Lysine Acetylation Sites in Rat Tissues Reveals Organ Specificity and Subcellular Patterns. *Cell reports (Cambridge)*, 2, 419-431.
- LUNDBY, A., NOVO NORDISK FOUNDATION CENTER FOR PROTEIN RESEARCH, D. F. P., FACULTY OF HEALTH SCIENCES, UNIVERSITY OF COPENHAGEN, BLEGDAMSVEJ 3B, 2200 COPENHAGEN N, DENMARK, THE DANISH NATIONAL RESEARCH FOUNDATION CENTRE FOR CARDIAC ARRHYTHMIA, C. N., DENMARK, THE BROAD INSTITUTE OF MASSACHUSETTS INSTITUTE OF TECHNOLOGY AND HARVARD, C., MA 02142, USA, LAGE, K., NOVO NORDISK FOUNDATION CENTER FOR PROTEIN RESEARCH, D. F. P., FACULTY OF HEALTH SCIENCES, UNIVERSITY OF COPENHAGEN, BLEGDAMSVEJ 3B, 2200 COPENHAGEN N, DENMARK, THE BROAD INSTITUTE OF MASSACHUSETTS INSTITUTE OF TECHNOLOGY AND HARVARD, C., MA 02142, USA, PEDIATRIC SURGICAL RESEARCH LABORATORY, M. G. H., BOSTON, MA 02114, USA, DEPARTMENT OF SURGERY, H. M. S., BOSTON, MA 02115, USA, WEINERT, B. T., NOVO NORDISK FOUNDATION CENTER FOR PROTEIN RESEARCH, D. F. P., FACULTY OF HEALTH SCIENCES, UNIVERSITY OF COPENHAGEN, BLEGDAMSVEJ 3B, 2200 COPENHAGEN N, DENMARK, BEKKER-JENSEN, D. B., NOVO NORDISK FOUNDATION CENTER FOR PROTEIN RESEARCH, D. F. P., FACULTY OF HEALTH SCIENCES, UNIVERSITY OF COPENHAGEN, BLEGDAMSVEJ 3B, 2200 COPENHAGEN N, DENMARK, SECHER, A., NOVO NORDISK FOUNDATION CENTER FOR PROTEIN RESEARCH, D. F. P., FACULTY OF HEALTH SCIENCES, UNIVERSITY OF COPENHAGEN, BLEGDAMSVEJ 3B, 2200 COPENHAGEN N, DENMARK, NOVO NORDISK A/S, N. N. P., 2760 MÅLØV, DENMARK, SKOVGAARD, T., NOVO NORDISK FOUNDATION CENTER FOR PROTEIN RESEARCH, D. F. P., FACULTY OF HEALTH SCIENCES, UNIVERSITY OF COPENHAGEN, BLEGDAMSVEJ 3B, 2200 COPENHAGEN N, DENMARK, KELSTRUP, C. D., NOVO NORDISK FOUNDATION CENTER FOR PROTEIN RESEARCH, D. F. P., FACULTY OF HEALTH SCIENCES, UNIVERSITY OF COPENHAGEN, BLEGDAMSVEJ 3B, 2200 COPENHAGEN N, DENMARK, DMYTRIYEV, A., NOVO NORDISK FOUNDATION CENTER FOR PROTEIN RESEARCH, D. F. P., FACULTY OF HEALTH SCIENCES, UNIVERSITY OF COPENHAGEN, BLEGDAMSVEJ 3B, 2200 COPENHAGEN N, DENMARK, CHOUDHARY, C., NOVO NORDISK FOUNDATION CENTER FOR PROTEIN RESEARCH, D. F. P., FACULTY OF HEALTH SCIENCES,

- UNIVERSITY OF COPENHAGEN, BLEGDAMSVEJ 3B, 2200 COPENHAGEN N, DENMARK, LUNDBY, C., ZÜRICH CENTRE FOR INTEGRATIVE HUMAN PHYSIOLOGY, D. O. P., UNIVERSITY OF ZÜRICH, 8057 ZÜRICH, SWITZERLAND, OLSEN, J. V., JESPER.OLSEN@CPR.KU.DK & NOVO NORDISK FOUNDATION CENTER FOR PROTEIN RESEARCH, D. F. P., FACULTY OF HEALTH SCIENCES, UNIVERSITY OF COPENHAGEN, BLEGDAMSVEJ 3B, 2200 COPENHAGEN N, DENMARK 2012b. Proteomic Analysis of Lysine Acetylation Sites in Rat Tissues Reveals Organ Specificity and Subcellular Patterns. *Cell Reports*, 2, 419-431.
- LUTHI-CARTER, R., TAYLOR, D. M., PALLOS, J., LAMBERT, E., AMORE, A., PARKER, A., MOFFITT, H., SMITH, D. L., RUNNE, H., GOKCE, O., KUHN, A., XIANG, Z., MAXWELL, M. M., REEVES, S. A., BATES, G. P., NERI, C., THOMPSON, L. M., MARSH, J. L. & KAZANTSEV, A. G. 2010a. SIRT2 inhibition achieves neuroprotection by decreasing sterol biosynthesis. *Proceedings of the National Academy of Sciences of the United States of America*, 107, 7927.
- LUTHI-CARTER, R., TAYLOR, D. M., PALLOS, J., LAMBERT, E., AMORE, A., PARKER, A., MOFFITT, H., SMITH, D. L., RUNNE, H., GOKCE, O., KUHN, A., XIANG, Z., MAXWELL, M. M., REEVES, S. A., BATES, G. P., NERI, C., THOMPSON, L. M., MARSH, J. L. & KAZANTSEV, A. G. 2010b. SIRT2 inhibition achieves neuroprotection by decreasing sterol biosynthesis. *Proc Natl Acad Sci U S A*, 107, 7927-7932.
- LÓPEZ-OTÍN, C., BLASCO, M. A., PARTRIDGE, L., SERRANO, M. & KROEMER, G. 2013. The Hallmarks of Aging. *Cell*, 153, 1194-1217.
- MA, L., GAO, J.-S., GUAN, Y., SHI, X., ZHANG, H., AYRAPETOV, M. K., ZHANG, Z., XU, L., HYUN, Y.-M., KIM, M., ZHUANG, S. & CHIN, Y. E. 2010. Acetylation modulates prolactin receptor dimerization. *Proceedings of the National Academy of Sciences of the United States of America*, 107, 19314.
- MARMORSTEIN, R. & ZHOU, M.-M. 2014. Writers and readers of histone acetylation: Structure, mechanism, and inhibition. *Cold Spring Harb Perspect Biol*, 6, a018762-a018762.
- MARTENS, C. R., DENMAN, B. A., MAZZO, M. R., ARMSTRONG, M. L., REISDORPH, N., MCQUEEN, M. B., CHONCHOL, M. & SEALS, D. R. 2018. Chronic nicotinamide riboside supplementation is well-Tolerated and elevates NAD<sup>+</sup> in healthy middle-Aged and older adults. *Nat Commun*, 9, 1286-1286.
- MAXWELL, M. M., TOMKINSON, E. M., NOBLES, J., WIZEMAN, J. W., AMORE, A. M., QUINTI, L., CHOPRA, V., HERSCH, S. M. & KAZANTSEV, A. G. 2011a. The Sirtuin 2 microtubule deacetylase is an abundant neuronal protein that accumulates in the aging CNS. *Human Molecular Genetics*, 20, 3986-3996.
- MAXWELL, M. M., TOMKINSON, E. M., NOBLES, J., WIZEMAN, J. W., AMORE, A. M., QUINTI, L., CHOPRA, V., HERSCH, S. M. & KAZANTSEV, A. G. 2011b. The Sirtuin 2 microtubule deacetylase is an abundant neuronal protein that accumulates in the aging CNS. *Hum Mol Genet*, 20, 3986-3996.
- MCCULLOUGH, C. E. & MARMORSTEIN, R. 2016. Molecular Basis for Histone Acetyltransferase Regulation by Binding Partners, Associated Domains, and Autoacetylation. *ACS Chem. Biol*, 11, 632-642.
- MCQUAIL, J. A., BAÑUELOS, C., LASARGE, C. L., NICOLLE, M. M. & BIZON, J. L. 2012. GABAB receptor GTP-binding is decreased in the prefrontal cortex but not the hippocampus of aged rats. *Neurobiology of aging*, 33, 1124.e1-1124.e12.
- MENG, Y., REN, Z., XU, F., ZHOU, X., SONG, C., WANG, V. Y.-F., LIU, W., LU, L., THOMSON, J. A. & CHEN, G. 2018. Nicotinamide Promotes Cell Survival and Differentiation as Kinase Inhibitor in Human Pluripotent Stem Cells. *Stem Cell Reports*, 11, 1347-1356.
- MERCURIO, V., CUOMO, A., DESSALVI, C. C., DEIDDA, M., DI LISI, D., NOVO, G., MANGANARO, R., ZITO, C., SANTORO, C., AMERI, P., SPALLAROSSA, P., ARBOSCELLO, E., TOCCHETTI, C. G. & PENNA, C. 2020. Redox imbalances in ageing and metabolic alterations: Implications in cancer and cardiac diseases. An overview from the working group of cardiotoxicity and cardioprotection of the Italian society of cardiology (SIC). *Antioxidants*, 9, 1-20.

- MICHAEL, A., CATHERINE, A. B., JUDITH, A. B., DAVID, B., HEATHER, B., CHERRY, J. M., ALLAN, P. D., KARA, D., SELINA, S. D., JANAN, T. E., MIDORI, A. H., DAVID, P. H., LAURIE, I.-T., ANDREW, K., SUZANNA, L., JOHN, C. M., JOEL, E. R., MARTIN, R., GERALD, M. R. & GAVIN, S. 2000. Gene Ontology: tool for the unification of biology. *Nature Genetics*, 25, 25.
- MICHAEL, A. H. & RAYMOND, C. S. 2000. Cocrystal structure of synaptobrevin-II bound to botulinum neurotoxin type B at 2.0 Å resolution. *Nature Structural Biology*, 7, 687.
- MICHAN, S. & SINCLAIR, D. 2007. Sirtuins in mammals: insights into their biological function. *Biochemical Journal*, 404, 1-13.
- MIN, J. S., KIM, J. C., KIM, J. A., KANG, I. & AHN, J. K. 2018a. SIRT2 reduces actin polymerization and cell migration through deacetylation and degradation of HSP90. *Biochim Biophys Acta Mol Cell Res*, 1865, 1230-1238.
- MIN, S.-W., CHO, S.-H., ZHOU, Y., SCHROEDER, S., HAROUTUNIAN, V., SEELEY, W. W., HUANG, E. J., SHEN, Y., MASLIAH, E., MUKHERJEE, C., MEYERS, D., COLE, P. A., OTT, M. & GAN, L. 2010. Acetylation of Tau Inhibits Its Degradation and Contributes to Tauopathy. *Neuron*, 67, 953-966.
- MIN, S.-W., SOHN, P. D., LI, Y., DEVIDZE, N., JOHNSON, J. R., KROGAN, N. J., MASLIAH, E., MOK, S.-A., GESTWICKI, J. E. & GAN, L. 2018b. SIRT1 deacetylates tau and reduces pathogenic tau spread in a mouse model of tauopathy. *J Neurosci*, 38, 3680-3688.
- MORRISON, J. H. & BAXTER, M. G. 2012. The ageing cortical synapse: Hallmarks and implications for cognitive decline. *Nat Rev Neurosci*, 13, 240-250.
- MOUCHIROUD, L., HOUTKOOPER, RIEKELT H., MOULLAN, N., KATSYUBA, E., RYU, D., CANTÓ, C., MOTTIS, A., JO, Y.-S., VISWANATHAN, M., SCHOONJANS, K., GUARENTE, L. & AUWERX, J. 2013. The NAD<sup>+</sup>/Sirtuin Pathway Modulates Longevity through Activation of Mitochondrial UPR and FOXO Signaling. *Cell*, 154, 430-441.
- MOYNIHAN, K. A., GRIMM, A. A., PLUEGER, M. M., BERNAL-MIZRACHI, E., FORD, E., CRAS-MÉNEUR, C., PERMUTT, M. A. & IMAI, S.-I. 2005. Increased dosage of mammalian Sir2 in pancreatic β cells enhances glucose-stimulated insulin secretion in mice. *Cell Metab*, 2, 105-117.
- NAGARAJ, N., LU, A. P., MANN, M. & WISNIEWSKI, JR. 2008. Detergent-Based but Gel-Free Method Allows Identification of Several Hundred Membrane Proteins in Single LC-MS Runs. *J. Proteome Res.*, 7, 5028-5032.
- NAHHAS, F., DRYDEN, S. C., ABRAMS, J. & TAINSKY, M. A. 2007. Mutations in SIRT2 deacetylase which regulate enzymatic activity but not its interaction with HDAC6 and tubulin. *Mol Cell Biochem*, 303, 221-230.
- NAKAO, L. S., KADIISKA, M. B., MASON, R. P., GRIJALBA, M. T. & AUGUSTO, O. 2000. Metabolism of acetaldehyde to methyl and acetyl radicals: in vitro and in vivo electron paramagnetic resonance spin-trapping studies. *Free Radic Biol Med*, 29, 721-729.
- NARITA, T., WEINERT, B. T. & CHOUDHARY, C. 2018. Functions and mechanisms of non-histone protein acetylation. *Nature Reviews Molecular Cell Biology*.
- NORTH, B. & VERDIN, E. 2007. Interphase Nucleo- Cytoplasmic Shuttling and Localization of SIRT2 during Mitosis. *PLoS One*, 2, e784.
- NORTH, B. J., MARSHALL, B. L., BORRA, M. T., DENU, J. M. & VERDIN, E. 2003. The human Sir2 ortholog, SIRT2, is an NAD(+)-dependent tubulin deacetylase. *Molecular Cell*, 11, 437-444.
- NORTH, B. J., ROSENBERG, M. A., JEGANATHAN, K. B., HAFNER, A. V., MICHAN, S., DAI, J., BAKER, D. J., CEN, Y., WU, L. E., SAUVE, A. A., VAN DEURSEN, J. M., ROSENZWEIG, A. & SINCLAIR, D. A. 2014. SIRT2 induces the checkpoint kinase BubR1 to increase lifespan. *EMBO J*, 33, 1438-1453.
- O'CONNOR, M., SHENTU, Y.-P., WANG, G., HU, W.-T., XU, Z.-D., WANG, X.-C., LIU, R. & MAN, H.-Y. 2020. Acetylation of AMPA Receptors Regulates Receptor Trafficking and Rescues Memory Deficits in Alzheimer's Disease. *iScience*, 23, 101465-101465.
- OUTEIRO, T. F., KONTOPOULOS, E., ALTMANN, S. M., KUFAREVA, I., STRATHEARN, K. E., AMORE, A. M., VOLK, C. B., MAXWELL, M. M., ROCHET, J.-C., MCLEAN, P. J., YOUNG, A. B., ABAGYAN, R.,

- FEANY, M. B., HYMAN, B. T. & KAZANTSEV, A. G. 2007. Sirtuin 2 inhibitors rescue [alpha]-synuclein--mediated toxicity in models of Parkinson's disease. *Science (American Association for the Advancement of Science)*, 317, 516.
- PAIS, T. F., SZEGŐ, É. M., MARQUES, O., MILLER-FLEMING, L., ANTAS, P., GUERREIRO, P., DE OLIVEIRA, R. M., KASAPOGLU, B. & OUTEIRO, T. F. 2013. The NAD- dependent deacetylase sirtuin 2 is a suppressor of microglial activation and brain inflammation. *EMBO Journal*, 32, 2603-2616.
- PANDITHAGE, R., LILISCHKIS, R., HARTING, K., WOLF, A., JEDAMZIK, B., LUSCHER-FIRZLAFF, J., VERVOORTS, J., LASONDER, E., KREMMER, E., KNOLL, B. & LUSCHER, B. 2008. The Regulation of SIRT2 Function by Cyclin-Dependent Kinases Affects Cell Motility. *J Cell Biol*, 180, 915-929.
- PANZA, F., LOZUPONE, M., LOGROSCINO, G. & IMBIMBO, B. P. 2019. A critical appraisal of amyloid- $\beta$ -targeting therapies for Alzheimer disease. *Nat Rev Neurol*, 15, 73-88.
- PARK, G., TAN, J., GARCIA, G., KANG, Y., SALVESEN, G. & ZHANG, Z. 2016a. Regulation of Histone Acetylation by Autophagy in Parkinson Disease. *J Biol Chem*, 291, 3531-3540.
- PARK, S.-H., OZDEN, O., LIU, G., SONG, H. Y., ZHU, Y., YAN, Y., ZOU, X., KANG, H.-J., JIANG, H., PRINCIPE, D. R., CHA, Y.-I., ROH, M., VASSILOPOULOS, A. & GIUS, D. 2016b. SIRT2-mediated deacetylation and tetramerization of pyruvate kinase directs glycolysis and tumor growth. *Cancer Res*, 76, 3802-3812.
- PARODI-RULLÁN, R. M., CHAPA-DUBOCQ, X. R. & JAVADOV, S. 2018. Acetylation of mitochondrial proteins in the heart: The role of SIRT3. *Front Physiol*, 9, 1094-1094.
- PAVLETICH, N. P., FINNIN, M. S. & DONIGIAN, J. R. 2001. Structure of the histone deacetylase SIRT2. *Nat Struct Biol*, 8, 621-625.
- PELEG, S., FELLER, C., LADURNER, A. G. & IMHOF, A. 2016. The Metabolic Impact on Histone Acetylation and Transcription in Ageing. *Trends Biochem Sci*, 41, 700-711.
- PEREIRA, C. V., LEBIEDZINSKA, M., WIECKOWSKI, M. R. & OLIVEIRA, P. J. 2012. Regulation and protection of mitochondrial physiology by sirtuins. *Mitochondrion*, 12, 66-76.
- PIETROCOLA, F., GALLUZZI, L., BRAVO-SAN PEDRO, J. M., MADEO, F. & KROEMER, G. 2015. Acetyl Coenzyme A: A Central Metabolite and Second Messenger. *Cell Metabolism*, 21, 805-821.
- PIRACHA, Z. Z., SAEED, U., KIM, J., KWON, H., CHWAE, Y.-J., LEE, H. W., LIM, J. H., PARK, S., SHIN, H.-J. & KIM, K. 2020. An Alternatively Spliced Sirtuin 2 Isoform 5 Inhibits Hepatitis B Virus Replication from cccDNA by Repressing Epigenetic Modifications Made by Histone Lysine Methyltransferases. *J Virol*, 94.
- POUGOVKINA, O., TE BRINKE, H., OFMAN, R., VAN CRUCHTEN, A. G., KULIK, W., WANDERS, R. J. A., HOUTEN, S. M. & DE BOER, V. C. J. 2014. Mitochondrial protein acetylation is driven by acetyl-CoA from fatty acid oxidation. *Human Molecular Genetics*, 23, 3513-3522.
- PROTEOMICSDB 2017. NAD-dependent protein deacetylase sirtuin-2 (Q8IXJ6).
- PROTEOMICSDB 2017
- NAD-dependent protein deacetylase sirtuin-2 (Q8IXJ6).
- PRUS, G., HOEGL, A., WEINERT, B. T. & CHOUDHARY, C. 2019. Analysis and Interpretation of Protein Post-Translational Modification Site Stoichiometry. *Trends Biochem Sci*, 44, 943-960.
- PUKAß, K. & RICHTER-LANDSBERG, C. 2015. Inhibition of UCH-L1 in oligodendroglial cells results in microtubule stabilization and prevents  $\alpha$ -synuclein aggregate formation by activating the autophagic pathway: Implications for multiple system atrophy. *Front Cell Neurosci*, 9, 163-163.
- QING-QUAN LIU1\*, K. R., SU-HONG LIU1, WEI-MIN LI2, CHANG-JUN HUANG1 AND XIU-HUI YANG1 2019. MicroRNA-140-5p aggravates hypertension and oxidative stress of atherosclerosis via targeting Nrf2 and Sirt2. INTERNATIONAL JOURNAL OF MOLECULAR MEDICINE.
- QIU, D., HOU, X., HAN, L., LI, X., GE, J. & WANG, Q. 2018. Sirt2- BubR1 acetylation pathway mediates the effects of advanced maternal age on oocyte quality. *Aging Cell*, 17, n/a-n/a.

- REVOLLO, J. R., GRIMM, A. A. & IMAI, S.-I. 2004. The NAD Biosynthesis Pathway Mediated by Nicotinamide Phosphoribosyltransferase Regulates Sir2 Activity in Mammalian Cells. *J Biol Chem*, 279, 50754-50763.
- RITA MACHADO DE, O., HUGO VICENTE, M., LAETITIA, F., RAQUEL, P., ÉVA, M. S., RENATO, M., FRANCESCA, M., DIANA, F. L., SÉBASTIEN, M., PATRÍCIA, G., LUIS, F.-O., ZRINKA, M., PEDRO, A., ELLEN, G., FRANCISCO JAVIER, E., BRUNO, F., DEBORAH, P., TERESA FARIA, P., QIANG, T., STEFAN, B., SEBASTIAN, K., HILAL AHMED, L., CLEMENS, S., MARKUS, Z. & TIAGO FLEMING, O. 2017. The mechanism of sirtuin 2- mediated exacerbation of alpha- synuclein toxicity in models of Parkinson disease. *PLoS Biology*, 15, e2000374.
- ROGINA, B. & HELFAND, S. L. 2004. Sir2 Mediates Longevity in the Fly through a Pathway Related to Calorie Restriction. *Proc Natl Acad Sci U S A*, 101, 15998-16003.
- ROTHGIESSER, K. M., ERENER, S., WAIBEL, S., LÜSCHER, B. & HOTTIGER, M. O. 2010. SIRT2 regulates NF- $\kappa$ B dependent gene expression through deacetylation of p65 Lys310. *Journal of cell science*, 123, 4251.
- RUMPF, T., SCHIEDEL, M., KARAMAN, B., ROESSLER, C., NORTH, B. J., LEHOTZKY, A., OLAH, J., LADWEIN, K. I., SCHMIDTKUNZ, K., GAJER, M., PANNEK, M., STEEGBORN, C., SINCLAIR, D. A., GERHARDT, S., OVADI, J., SCHUTKOWSKI, M., SIPPL, W., EINSLE, O. & JUNG, M. 2015. Selective Sirt2 inhibition by ligand-induced rearrangement of the active site. *Nature Communications*, 6, 13.
- SABÒ, A., LUSIC, M., CERESETO, A. & GIACCA, M. 2008. Acetylation of conserved lysines in the catalytic core of cyclin- dependent kinase 9 inhibits kinase activity and regulates transcription. *Molecular and cellular biology*, 28, 2201-2212.
- SADOUL, K., WANG, J., DIAGOURAGA, B. & KHOCHBIN, S. 2010. The Tale of Protein Lysine Acetylation in the Cytoplasm. *J Biomed Biotechnol*, 2011, 970382-15.
- SAHA, P. & SEN, N. 2019. Tauopathy: A common mechanism for neurodegeneration and brain aging. *Mech Ageing Dev*, 178, 72-79.
- SANTOS-BARRIOPEDRO, I., BOSCH-PRESEGUÉ, L., MARAZUELA-DUQUE, A., DE LA TORRE, C., COLOMER, C., VAZQUEZ, B. N., FUHRMANN, T., MARTÍNEZ-PASTOR, B., LU, W., BRAUN, T., BOBER, E., JENUWEIN, T., SERRANO, L., ESTELLER, M., CHEN, Z., BARCELÓ-BATLLORI, S., MOSTOSLAVSKY, R., ESPINOSA, L. & VAQUERO, A. 2018. SIRT6- dependent cysteine monoubiquitination in the PRE- SET domain of Suv39h1 regulates the NF-  $\kappa$ B pathway. *Nature Communications*, 9.
- SANTOS-ROSA, H., VALLS, E., KOUZARIDES, T. & MARTÍNEZ-BALBÁS, M. 2003. Mechanisms of P/CAF auto-acetylation. *Nucl. Acids Res*, 31, 4285-4292.
- SARIKHANI, M., MAITY, S., MISHRA, S., JAIN, A., TAMTA, A. K., RAVI, V., KONDAPALLI, M. S., DESINGU, P. A., KHAN, D., KUMAR, S., RAO, S., INBARAJ, M., PANDIT, A. S. & SUNDARESAN, N. R. 2018a. SIRT2 deacetylase represses NFAT transcription factor to maintain cardiac homeostasis. *The Journal of biological chemistry*, 293, 5281.
- SARIKHANI, M., MISHRA, S., DESINGU, P. A., KOTYADA, C., WOLFGEHER, D., GUPTA, M. P., SINGH, M. & SUNDARESAN, N. R. 2018b. SIRT2 regulates oxidative stress-induced cell death through deacetylation of c-Jun NH-terminal kinase. *Cell death and differentiation*.
- SARIKHANI, M., MISHRA, S., MAITY, S., KOTYADA, C., WOLFGEHER, D., GUPTA, M. P., SINGH, M. & SUNDARESAN, N. R. 2018c. SIRT2 deacetylase regulates the activity of GSK3 isoforms independent of inhibitory phosphorylation. *eLife*, 7.
- SATOH, A., IMAI, S.-I. & GUARENTE, L. 2017. The brain, sirtuins, and ageing. *Nat Rev Neurosci*, 18, 362-374.
- SCHIEDEL, M., RUMPF, T., KARAMAN, B., LEHOTZKY, A., OLÁH, J., GERHARDT, S., OVÁDI, J., SIPPL, W., EINSLE, O. & JUNG, M. 2016. Aminothiazoles as Potent and Selective Sirt2 Inhibitors: A Structure- Activity Relationship Study. *Journal of medicinal chemistry*, 59, 1599.
- SCHINDELIN, J., ARGANDA-CARRERAS, I., FRISE, E., KAYNIG, V., LONGAIR, M., PIETZSCH, T., PREIBISCH, S., RUEDEN, C., SAALFELD, S., SCHMID, B., TINEVEZ, J.-Y., WHITE, D. J.,

- HARTENSTEIN, V., ELICEIRI, K., TOMANCAK, P. & CARDONA, A. 2012. Fiji: An open-source platform for biological-image analysis. *Nat Methods*, 9, 676-682.
- SCHMIDT, T., SAMARAS, P., FREJNO, M., GESSULAT, S., BARNERT, M., KIENEGGER, H., KRCDMAR, H., SCHLEGL, J., EHRLICH, H.-C., AICHE, S., KUSTER, B. & WILHELM, M. 2018. ProteomicsDB. *Nucleic Acids Res*, 46, D1271-D1281.
- SCHNICHELS, S., SCHULTHEIß, M., HOFMANN, J., SZURMAN, P., BARTZ-SCHMIDT, K. U. & SPITZER, M. S. 2012. Trichostatin A induces cell death at the concentration recommended to differentiate the RGC-5 cell line. *Neurochem Int*, 60, 581-591.
- SCHWEPPE, D. K., HUTTLIN, E. L., HARPER, J. W. & GYGI, S. P. 2018. BioPlex Display: An Interactive Suite for Large-Scale AP-MS Protein-Protein Interaction Data. *J. Proteome Res*, 17, 722-726.
- SCHWER, B., BUNKENBORG, J., VERDIN, R. O., ANDERSEN, J. S. & VERDIN, E. 2006. Reversible Lysine Acetylation Controls the Activity of the Mitochondrial Enzyme Acetyl-CoA Synthetase 2. *Proc Natl Acad Sci U S A*, 103, 10224-10229.
- SEO, J. & LEE, K. J. 2004. Post-translational modifications and their biological functions: Proteomic analysis and systematic approaches. *Journal of Biochemistry and Molecular Biology*, 37, 35-44.
- SEO, K. S., PARK, J. H., HEO, J. Y., JING, K., HAN, J., MIN, K. N., KIM, C., KOH, G. Y., LIM, K., KANG, G. Y., UEE LEE, J., YIM, Y. H., SHONG, M., KWAK, T. H. & KWEON, G. R. 2015. SIRT2 regulates tumour hypoxia response by promoting HIF-1 $\alpha$  hydroxylation. *Oncogene*, 34, 1354.
- SERRANO, L., MARTÍNEZ-REDONDO, P., MARAZUELA-DUQUE, A., VAZQUEZ, B. N., DOOLEY, S. J., VOIGT, P., BECK, D. B., KANE-GOLDSMITH, N., TONG, Q., RABANAL, R. M., FONDEVILA, D., MUÑOZ, P., KRÜGER, M., TISCHFIELD, J. A. & VAQUERO, A. 2013. The tumor suppressor SirT2 regulates cell cycle progression and genome stability by modulating the mitotic deposition of H4K20 methylation. *Genes Dev*, 27, 639-653.
- SERRANO, M., HERRANZ, D., MUÑOZ-MARTIN, M., CAÑAMERO, M., MULERO, F., MARTINEZ-PASTOR, B. & FERNANDEZ-CAPETILLO, O. 2010. Sirt1 improves healthy ageing and protects from metabolic syndrome-associated cancer. *Nat Commun*, 1, 1-8.
- SHARMA, K., SCHMITT, S., BERGNER, C. G., TYANOVA, S., KANNAIYAN, N., MANRIQUE-HOYOS, N., KONGI, K., CANTUTI, L., HANISCH, U. K., PHILIPS, M. A., ROSSNER, M. J., MANN, M. & SIMONS, M. 2015. Cell type- and brain region-resolved mouse brain proteome. *Nature Neuroscience*, 18, 1819-1831.
- SHEPHERD, J. D., RUMBAUGH, G., WU, J., CHOWDHURY, S., PLATH, N., KUHL, D., HUGANIR, R. L. & WORLEY, P. F. 2006. Arc/Arg3.1 mediates homeostatic synaptic scaling of AMPA receptors. *Neuron*, 52, 475-484.
- SIDOROVA-DARMOS, E., WITHER, R. G., SHULYAKOVA, N., FISHER, C., RATNAM, M., AARTS, M., LILGE, L., MONNIER, P. P. & EUBANKS, J. H. 2014. Differential expression of sirtuin family members in the developing, adult, and aged rat brain. *Frontiers in Aging Neuroscience*, 6, 20.
- SIGNLING, P. P. B. C. 2017. Phosphosite.
- SILVA, D., ESTEVES, A., OLIVEIRA, C. & CARDOSO, S. 2017. Mitochondrial Metabolism Power SIRT2-Dependent Deficient Traffic Causing Alzheimer's- Disease Related Pathology. *Molecular Neurobiology*, 54, 4021-4040.
- SINGH, P., HANSON, P. S. & MORRIS, C. M. 2017a. SIRT1 ameliorates oxidative stress induced neural cell death and is down-regulated in Parkinson's disease. *BMC Neurosci*, 18, 46-46.
- SINGH, P., HANSON, P. S. & MORRIS, C. M. 2017b. Sirtuin- 2 Protects Neural Cells from Oxidative Stress and Is Elevated in Neurodegeneration. *Parkinson's Disease*, 2017.
- SNIDER, N. T., LEONARD, J. M., KWAN, R., GRIGGS, N. W., RUI, L. & BISHR OMARY, M. 2013. Glucose and SIRT2 reciprocally mediate the regulation of keratin 8 by lysine acetylation. *J Cell Biol*, 200, 241-247.
- SON, S. M., PARK, S. J., FERNANDEZ-ESTEVEZ, M. & RUBINSZTEIN, D. C. 2021. Autophagy regulation by acetylation—implications for neurodegenerative diseases. *Exp Mol Med*, 53, 30-41.

- SON, S. M., PARK, S. J., STAMATAKOU, E., VICINANZA, M., MENZIES, F. M. & RUBINSZTEIN, D. C. 2020. Leucine regulates autophagy via acetylation of the mTORC1 component raptor. *Nat Commun*, 11, 3148-3148.
- SONG, H. Y., BIANCUCCI, M., KANG, H.-J., O'CALLAGHAN, C., PARK, S.-H., PRINCIPE, D. R., JIANG, H., YAN, Y., SATCHELL, K. F., RAPARIA, K., GIUS, D. & VASSILOPOULOS, A. 2016. SIRT2 deletion enhances KRAS-induced tumorigenesis in vivo by regulating K147 acetylation status. *Oncotarget*, 7, 80336-80349.
- SOPPA, J. 2010. Protein Acetylation in Archaea, Bacteria, and Eukaryotes. *Archaea*, 2010, 1-9.
- SOUTOGLU, E., KATRAKILI, N. & TALIANIDIS, I. 2000. Acetylation Regulates Transcription Factor Activity at Multiple Levels. *Mol Cell*, 5, 745-751.
- SPINELLI, K. J., TAYLOR, J. K., OSTERBERG, V. R., CHURCHILL, M. J., POLLOCK, E., MOORE, C., MESHUL, C. K. & UNNI, V. K. 2014. Presynaptic alpha-synuclein aggregation in a mouse model of Parkinson's disease. *The Journal of neuroscience : the official journal of the Society for Neuroscience*, 34, 2037-2050.
- STARK, C., BREITKREUTZ, B., REGULY, T., BOUCHER, L., BREITKREUTZ, A. & TYERS, M. 2006. BioGRID: a general repository for interaction datasets. *Nucleic Acids Res.*, 34, D535-D539.
- STEFKA, T., TIKIRA, T., PAVEL, S., ARTHUR, C., MARCO, Y. H., TAMAR, G., MATTHIAS, M. & JÜRGEN, C. 2016. The Perseus computational platform for comprehensive analysis of (prote)omics data. *Nature Methods*, 13.
- STILLING, R. M., RÖNICKE, R., BENITO, E., URBANKE, H., CAPECE, V., BURKHARDT, S., BAHARI-JAVAN, S., BARTH, J., SANANBENESI, F., SCHÜTZ, A. L., DYCZKOWSKI, J., MARTINEZ-HERNANDEZ, A., KERIMOGLU, C., DENT, S. Y., BONN, S., REYMANN, K. G. & FISCHER, A. 2014. K-Lysine acetyltransferase 2a regulates a hippocampal gene expression network linked to memory formation. *EMBO Journal*, 33, 1912-1927.
- STORM, D. R. & XIA, Z. 2005. The role of calmodulin as a signal integrator for synaptic plasticity. *Nat Rev Neurosci*, 6, 267-276.
- SUN, L., BHAWAL, R., XU, H., CHEN, H., ANDERSON, E. T., HAROUTUNIAN, V., CROSS, A. C., ZHANG, S. & GIBSON, G. E. 2021. The human brain acetylome reveals that decreased acetylation of mitochondrial proteins associates with Alzheimer's disease. *J Neurochem*, 158, 282-296.
- SVINKINA, T., GU, H. B., SILVA, J. C., MERTINS, P., QIAO, J., FERESHETIAN, S., JAFFE, J. D., KUHN, E., UDESHI, N. D. & CARR, S. A. 2015. Deep, Quantitative Coverage of the Lysine Acetylome Using Novel Anti-acetyl-lysine Antibodies and an Optimized Proteomic Workflow. *Molecular & Cellular Proteomics*, 14, 2429-2440.
- SZEGŐ, É. M., GERHARDT, E. & OUTEIRO, T. F. 2017. Sirtuin 2 enhances dopaminergic differentiation via the AKT/GSK-3 $\beta$ / $\beta$ -catenin pathway. *Neurobiol Aging*, 56, 7-16.
- TAN, J., CANG, S. D., MA, Y., PETRILLO, R. & LIU, D. L. 2010. Novel histone deacetylase inhibitors in clinical trials as anti-cancer agents. *J. Hematol. Oncol.*
- TANG, X., CHEN, X.-F., WANG, N.-Y., WANG, X.-M., LIANG, S.-T., ZHENG, W., LU, Y.-B., ZHAO, X., HAO, D.-L., ZHANG, Z.-Q., ZOU, M.-H., LIU, D.-P. & CHEN, H.-Z. 2017. SIRT2 Acts as a Cardioprotective Deacetylase in Pathological Cardiac Hypertrophy. *Circulation*, 136, 2051.
- TAPIAS, A. & WANG, Z.-Q. 2017. Lysine Acetylation and Deacetylation in Brain Development and Neuropathies. *Genomics Proteomics & Bioinformatics*, 15, 19-36.
- TAUNTON, J., HASSIG, C. A. & SCHREIBER, S. L. 1996. A mammalian histone deacetylase related to the yeast transcriptional regulator Rpd3p. *Science*, 272, 408-411.
- THE GENE ONTOLOGY CONSORTIUM 2019. The Gene Ontology Resource: 20 years and still GOing strong. *Nucleic Acids Res*, 47, D330.
- THOMAS, P. & SMART, T. G. 2005. HEK293 cell line: A vehicle for the expression of recombinant proteins. *J Pharmacol Toxicol Methods*, 51, 187-200.
- THOMAS, P. D., CAMPBELL, M. J., KEJARIWAL, A., MI, H., KARLAK, B., DAVERMAN, R., DIEMER, K., MURUGANUJAN, A. & NARECHANIA, A. 2003. PANTHER: A library of protein families and subfamilies indexed by function. *Genome Res*, 13, 2129-2141.

- TODD, J. C., ANDREW, W. H., CLARK, R. R., CHAO-XING, Y., JOHN, Q. T. & VIRGINIA, M. Y. L. 2015. An acetylation switch controls TDP- 43 function and aggregation propensity. *Nature Communications*, 6.
- TYAGI, A., NGUYEN, C. U., CHONG, T., MICHEL, C. R., FRITZ, K. S., REISDORPH, N., KNAUB, L., REUSCH, J. E. B. & PUGAZHENTHI, S. 2018. SIRT3 deficiency-induced mitochondrial dysfunction and inflammasome formation in the brain. *Sci Rep*, 8, 17547-16.
- TYANOVA, S., TEMU, T., SINITYCYN, P., CARLSON, A., HEIN, M. Y., GEIGER, T., MANN, M. & COX, J. 2016. The Perseus computational platform for comprehensive analysis of (prote)omics data. *Nature Methods*, 13, 731-740.
- TÓKÉSI, N., LEHOTZKY, A., HORVÁTH, I., SZABÓ, B., OLÁH, J., LAU, P. & OVÁDI, J. 2010. TPPP/p25 Promotes Tubulin Acetylation by Inhibiting Histone Deacetylase 6. *J Biol Chem*, 285, 17896-17906.
- UDESHI, N. D., SVINKINA, T., MERTINS, P., KUHN, E., MANI, D. R., QIAO, J. W. & CARR, S. A. 2013. Refined Preparation and Use of Anti-diglycine Remnant (K-ε-GG) Antibody Enables Routine Quantification of 10,000s of Ubiquitination Sites in Single Proteomics Experiments. *Mol Cell Proteomics*, 12, 825-831.
- UHLÉN, M., FAGERBERG, L., HALLSTRÖM, B. M., LINDSKOG, C., OKSVOLD, P., MARDINOGLU, A., SIVERTSSON, Å., KAMPF, C., SJÖSTEDT, E., ASPLUND, A., OLSSON, I., EDLUND, K., LUNDBERG, E., NAVANI, S., SZIGYARTO, C. A.-K., ODEBERG, J., DJUREINOVIC, D., TAKANEN, J. O., HOBER, S., ALM, T., EDQVIST, P.-H., BERLING, H., TEGEL, H., MULDER, J., ROCKBERG, J., NILSSON, P., SCHWENK, J. M., HAMSTEN, M., VON FEILITZEN, K., FORSBERG, M., PERSSON, L., JOHANSSON, F., ZWAHLEN, M., VON HEIJNE, G., NIELSEN, J. & PONTÉN, F. 2015. Tissue-based map of the human proteome. *Science (American Association for the Advancement of Science)*, 347, 394-394.
- VAN NOORT, V., SEEBACHER, J., BADER, S., MOHAMMED, S., VONKOVA, I., BETTS, M. J., KÜHNER, S., KUMAR, R., MAIER, T., O'FLAHERTY, M., RYBIN, V., SCHMEISKY, A., YUS, E., STÜLKE, J., SERRANO, L., RUSSELL, R. B., HECK, A. J. R., BORK, P. & GAVIN, A. C. 2012. Cross-talk between phosphorylation and lysine acetylation in a genome-reduced bacterium. *Mol Syst Biol*, 8, 571-n/a.
- VAQUERO, A., SCHER, M. B., DONG, H. L., SUTTON, A., CHENG, H.-L., ALT, F. W., SERRANO, L., STERNGLANZ, R. & REINBERG, D. 2006. Sir2 is a histone deacetylase with preference for histone H4 Lys 16 during mitosis. *Genes Dev*, 20, 1256-1261.
- VERDIN, E. & OTT, M. 2015. 50 years of protein acetylation: from gene regulation to epigenetics, metabolism and beyond. *Nature Reviews Molecular Cell Biology*, 16, 258-264.
- WAGNER, G. R. & PAYNE, R. M. 2011. Mitochondrial Acetylation and Diseases of Aging. *J Aging Res*, 2011, 234875-13.
- WAGNER, S. A., BELI, P., WEINERT, B. T., SCHÖLZ, C., KELSTRUP, C. D., YOUNG, C., NIELSEN, M. L., OLSEN, J. V., BRAKEBUSCH, C. & CHOUDHARY, C. 2012. Proteomic Analyses Reveal Divergent Ubiquitylation Site Patterns in Murine Tissues. *Mol Cell Proteomics*, 11, 1578-1585.
- WANG, B., YE, Y., YANG, X., LIU, B., WANG, Z., CHEN, S., JIANG, K., ZHANG, W., JIANG, H., MUSTONEN, H., PUOLAKKAINEN, P., WANG, S., LUO, J. & SHEN, Z. 2020a. SIRT 2-dependent IDH 1 deacetylation inhibits colorectal cancer and liver metastases. *EMBO reports*, 21.
- WANG, D., KON, N., LASSO, G., JIANG, L., LENG, W., ZHU, W.-G., QIN, J., HONIG, B. & GU, W. 2016. Acetylation-regulated interaction between p53 and SET reveals a widespread regulatory mode. *Nature*, 538, 118-122.
- WANG, F., CHAN, C. H., CHEN, K., GUAN, X., LIN, H. K. & TONG, Q. 2012. Deacetylation of FOXO3 by SIRT1 or SIRT2 leads to Skp2-mediated FOXO3 ubiquitination and degradation. *Oncogene*, 31, 1546-1557.
- WANG, F., NGUYEN, M., QIN, F. X. F. & TONG, Q. 2007. SIRT2 deacetylates FOXO3a in response to oxidative stress and caloric restriction. *Aging Cell*, 6, 505-514.

- WANG, G., LI, S., GILBERT, J., GRITTON, H. J., WANG, Z., LI, Z., HAN, X., SELKOE, D. J. & MAN, H.-Y. 2017a. Crucial Roles for SIRT2 and AMPA Receptor Acetylation in Synaptic Plasticity and Memory. *Cell Reports*, 20, 1335-1347.
- WANG, J., VASAIKAR, S., SHI, Z., GREER, M. & ZHANG, B. 2017b. WebGestalt 2017: a more comprehensive, powerful, flexible and interactive gene set enrichment analysis toolkit. *Nucleic Acids Research*, 45, W130-W137.
- WANG, M. M., YOU, D. & YE, B. C. 2017c. Site-specific and kinetic characterization of enzymatic and nonenzymatic protein acetylation in bacteria. *Scientific Reports*, 7, 12.
- WANG, R., SUN, H., WANG, G. & REN, H. 2020b. Imbalance of lysine acetylation contributes to the pathogenesis of parkinson's disease. *Int J Mol Sci*, 21, 1-22.
- WANG, Y., TU, K., LIU, D., GUO, L., CHEN, Y., LI, Q., MAIERS, J. L., LIU, Z., SHAH, V. H., DOU, C., TSCHUMPERLIN, D., VONESCHEN, L., YANG, R. & KANG, N. 2019a. p300 Acetyltransferase Is a Cytoplasm-to-Nucleus Shuttle for SMAD2/3 and TAZ Nuclear Transport in Transforming Growth Factor  $\beta$ -Stimulated Hepatic Stellate Cells. *Hepatology*, 70, 1409-1423.
- WANG, Y., YANG, J., HONG, T., CHEN, X. & CUI, L. 2019b. SIRT2: Controversy and multiple roles in disease and physiology. *Ageing Res Rev*, 55, 100961-100961.
- WANG, Y. P., ZHOU, L. S., ZHAO, Y. Z., WANG, S. W., CHEN, L. L., LIU, L. X., LING, Z. Q., HU, F. J., SUN, Y. P., ZHANG, J. Y., YANG, C., YANG, Y., XIONG, Y., GUAN, K. L. & YE, D. 2014. Regulation of G6PD acetylation by SIRT2 and KAT9 modulates NADPH homeostasis and cell survival during oxidative stress. *EMBO J*, 33, 1304-1320.
- WANKUN, D., CHENWEI, W., YING, Z., YANG, X., SHUANG, Z., ZEXIAN, L. & YU, X. 2016. GPS-PAIL: prediction of lysine acetyltransferase-specific modification sites from protein sequences. *Scientific Reports*, 6.
- WATANABE, H., INABA, Y., KIMURA, K., MATSUMOTO, M., KANEKO, S., KASUGA, M. & INOUE, H. 2018. Sirt2 facilitates hepatic glucose uptake by deacetylating glucokinase regulatory protein. *Nature communications*, 9, 30.
- WEINERT, B. T., IESMANTAVICIUS, V., WAGNER, S. A., SCHOLZ, C., GUMMESSON, B., BELI, P., NYSTROM, T. & CHOUDHARY, C. 2013. Acetyl-Phosphate Is a Critical Determinant of Lysine Acetylation in *E. coli*. *Molecular Cell*, 51, 265-272.
- WEINERT, B. T., NARITA, T., SATPATHY, S., SRINIVASAN, B., HANSEN, B. K., SCHÖLZ, C., HAMILTON, W. B., ZUCCONI, B. E., WANG, W. W., LIU, W. R., BRICKMAN, J. M., KESICKI, E. A., LAI, A., BROMBERG, K. D., COLE, P. A. & CHOUDHARY, C. 2018. Time-Resolved Analysis Reveals Rapid Dynamics and Broad Scope of the CBP/p300 Acetylome. *Cell*, 174, 231-244.e12.
- WEINERT, B. T., WAGNER, S. A., HORN, H., HENRIKSEN, P., LIU, W. S. R., OLSEN, J. V., JENSEN, L. J. & CHOUDHARY, C. 2011. Proteome-Wide Mapping of the *Drosophila* Acetylome Demonstrates a High Degree of Conservation of Lysine Acetylation. *Science Signaling*, 4, 11.
- WELLEN, K. E. & THOMPSON, C. B. 2012. A two-way street: reciprocal regulation of metabolism and signalling. *Nature Reviews Molecular Cell Biology*, 13, 270-U1.
- WERNER, H. B., KUHLMANN, K., SHEN, S., UECKER, M., SCHARDT, A., DIMOVA, K., ORFANIOTOU, F., DHAUNCHAK, A., BRINKMANN, B. G., MOBIUS, W., GUARENTE, L., CASACCIA-BONNEFIL, P., JAHN, O. & NAVE, K.-A. 2007. Proteolipid Protein Is Required for Transport of Sirtuin 2 into CNS Myelin. *J Neurosci*, 27, 7717-7730.
- WISNIEWSKI, J. R., ZOUGMAN, A., NAGARAJ, N. & MANN, M. 2009. Universal sample preparation method for proteome analysis. *Nature Methods*, 6, 359-U60.
- [WWW.ALLENINSTITUTE.ORG](http://WWW.ALLENINSTITUTE.ORG) Allen institute.
- WĄTROBA, M. & SZUKIEWICZ, D. 2016. The role of sirtuins in aging and age-related diseases. *Adv Med Sci*, 61, 52-62.
- XIAO, Q., ZHANG, F., NACEV, B. A., LIU, J. O. & PEI, D. 2010. Protein N-Terminal Processing: Substrate Specificity of *Escherichia coli* and Human Methionine Aminopeptidases. *Biochemistry*, 49, 5588-5599.

- XU, Y., LI, F., LV, L., LI, T., ZHOU, X., DENG, C.-X., GUAN, K.-L., LEI, Q.-Y. & XIONG, Y. 2014. Oxidative stress activates SIRT2 to deacetylate and stimulate phosphoglycerate mutase. *Cancer research*, 74, 3630.
- YAKHINE-DIOP, S. M. S., ROÍGUEZ-ARRIBAS, M., MARTÍNEZ-CHACÓN, G., URIBE-CARRETERO, E., GÓMEZ-SÁNCHEZ, R., AIASTUI, A., LÓPEZ DE MUNAIN, A., BRAVO-SAN PEO, J. M., NISO-SANTANO, M., GONZÁLEZ-POLO, R. A. & FUENTES, J. M. 2018. Acetylome in Human Fibroblasts From Parkinson's Disease Patients. *Front Cell Neurosci*, 12, 97-97.
- YAMAMOTO, H., IDA, T., TSUTSUKI, H., MORI, M., MATSUMOTO, T., KOHDA, T., MUKAMOTO, M., GOSHIMA, N., KOZAKI, S. & IHARA, H. 2012. Specificity of botulinum protease for human VAMP family proteins. *Microbiology and Immunology*, 56, 245-253.
- YAMASHITA, Y. I., SHIMADA, M., HARIMOTO, N., RIKIMARU, T., SHIRABE, K., TANAKA, S. & SUGIMACHI, K. 2003. Histone deacetylase inhibitor trichostatin a induces cell-cycle arrest/apoptosis and hepatocyte differentiation in human hepatoma cells. *Int J Cancer*, 103, 572-576.
- YAMAZAKI, Y., SCHÖNHERR, C., VARSHNEY, G. K., DOGRU, M., HALLBERG, B. & PALMER, R. H. 2013. Goliath family E3 ligases regulate the recycling endosome pathway via VAMP3 ubiquitylation. *EMBO Journal*, 32, 524-537.
- YANG, M. H., LAURENT, G., BAUSE, A. S., SPANG, R., GERMAN, N., HAIGIS, M. C. & HAIGIS, K. M. 2013. HDAC6 and SIRT2 regulate the acetylation state and oncogenic activity of mutant K-RAS. *Mol Cancer Res*, 11, 1072-1077.
- YANG, X., PARK, S.-H., CHANG, H.-C., SHAPIRO, J. S., VASSILOPOULOS, A., SAWICKI, K. T., CHEN, C., SHANG, M., BURRIDGE, P. W., EPTING, C. L., WILSBACHER, L. D., JENKITKASEMWONG, S., KNUTSON, M., GIUS, D. & ARDEHALI, H. 2017. Sirtuin 2 regulates cellular iron homeostasis via deacetylation of transcription factor NRF2. *The Journal of clinical investigation*, 127, 1505.
- YANG, X. J. & SETO, E. 2008. Lysine acetylation: Codified crosstalk with other posttranslational modifications. *Molecular Cell*, 31, 449-461.
- YEUNG, F., RAMSEY, C. S., POPKO-SCIBOR, A. E., ALLISON, D. F., GRAY, L. G., SHIN, M., KUMAR, M., LI, D., MCCUBREY, J. A. & MAYO, M. W. 2015. Regulation of the mitogen-activated protein kinase kinase (MEK)-1 by NAD<sup>+</sup>-dependent deacetylases. *Oncogene*, 34, 798-804.
- YOON, T.-Y. & MUNSON, M. 2018. SNARE complex assembly and disassembly. *Current Biology*, 28, R397-R401.
- YOU, B. R. & PARK, W. H. 2013. Trichostatin A induces apoptotic cell death of HeLa cells in a Bcl-2 and oxidative stress-dependent manner. *International journal of oncology*, 42, 359-366.
- YU, M., ZHANG, H., WANG, B., ZHANG, Y., ZHENG, X., SHAO, B., ZHUGE, Q. & JIN, K. 2021. Key Signaling Pathways in Aging and Potential Interventions for Healthy Aging. *Cells*, 10, 1-26.
- ZHANG, H., HEAD, PAMELASARA E., DADDACHA, W., PARK, S.-H., LI, X., PAN, Y., MADDEN, MATTHEW Z., DUONG, DUC M., XIE, M., YU, B., WARREN, MATTHEW D., LIU, ELAINE A., DHERE, VISHAL R., LI, C., PRADILLA, I., TORRES, MYLIN A., WANG, Y., DYNAN, WILLIAM S., DOETSCH, PAUL W., DENG, X., SEYFRIED, NICHOLAS T., GIUS, D. & YU, DAVID S. 2016. ATRIP Deacetylation by SIRT2 Drives ATR Checkpoint Activation by Promoting Binding to RPA-ssDNA. *Cell Rep*, 14, 1435-1447.
- ZHANG, H., PARK, S.-H., PANTAZIDES, B. G., KARPIUK, O., WARREN, M. D., HARDY, C. W., DUONG, D. M., PARK, S.-J., KIM, H.-S., VASSILOPOULOS, A., SEYFRIED, N. T., JOHNSEN, S. A., GIUS, D. & YU, D. S. 2013. SIRT2 directs the replication stress response through CDK9 deacetylation. *Proceedings of the National Academy of Sciences of the United States of America*, 110, 13546.
- ZHANG, H.-L., ZHAO, B., HAN, W., SUN, Y.-B., YANG, P., CHEN, Y., NI, D., ZHANG, J. & YIN, D.-M. 2021. Acetylation of calmodulin regulates synaptic plasticity and fear learning. *The Journal of biological chemistry*, 297, 101034-101034.

- ZHANG, J. M., SPRUNG, R., PEI, J. M., TAN, X. H., KIM, S., ZHU, H., LIU, C. F., GRISHIN, N. V. & ZHAO, Y. M. 2009. Lysine Acetylation Is a Highly Abundant and Evolutionarily Conserved Modification in Escherichia Coli. *Molecular & Cellular Proteomics*, 8, 215-225.
- ZHANG, T., WANG, S., LIN, Y., XU, W., YE, D., XIONG, Y., ZHAO, S. & GUAN, K.-L. 2012. Acetylation Negatively Regulates Glycogen Phosphorylase by Recruiting Protein Phosphatase 1. *Cell Metab*, 15, 75-87.
- ZHANG, X., NING, Z., MAYNE, J., YANG, Y., DEEKE, S. A., WALKER, K., FARNSWORTH, C. L., STOKES, M. P., COUTURE, J.-F., MACK, D., STINTZI, A. & FIGEYS, D. 2020. Widespread protein lysine acetylation in gut microbiome and its alterations in patients with Crohn's disease. *Nature communications*, 11, 4120-4120.
- ZHAO, D., MO, Y., LI, M.-T., ZOU, S.-W., CHENG, Z.-L., SUN, Y.-P., XIONG, Y., GUAN, K.-L. & LEI, Q.-Y. 2014. NOTCH-induced aldehyde dehydrogenase 1A1 deacetylation promotes breast cancer stem cells. *J Clin Invest*, 124, 5453-5465.
- ZHAO, D., ZOU, S.-W., LIU, Y., ZHOU, X., MO, Y., WANG, P., XU, Y.-H., DONG, B., XIONG, Y., LEI, Q.-Y. & GUAN, K.-L. 2013. Lysine-5 Acetylation Negatively Regulates Lactate Dehydrogenase A and Is Decreased in Pancreatic Cancer. *Cancer Cell*, 23, 464-476.
- ZHAO, L.-J., SUBRAMANIAN, T., ZHOU, Y. & CHINNADURAI, G. 2006. Acetylation by p300 Regulates Nuclear Localization and Function of the Transcriptional Corepressor CtBP2. *J Biol Chem*, 281, 4183-4189.
- ZHOU, T., CHUNG, Y.-H., CHEN, J. & CHEN, Y. 2016a. Site-Specific Identification of Lysine Acetylation Stoichiometries in Mammalian Cells. *Journal of proteome research*, 15, 1103-1113.
- ZHOU, T., CHUNG, Y. H., CHEN, J. J. & CHEN, Y. 2016b. Site-Specific Identification of Lysine Acetylation Stoichiometries in Mammalian Cells. *Journal of Proteome Research*, 15, 1103-1113.
- ZHOU, W., NI, T. K., WRONSKI, A., GLASS, B., SKIBINSKI, A., BECK, A. & KUPERWASSER, C. 2016c. The SIRT2 Deacetylase Stabilizes Slug to Control Malignancy of Basal-like Breast Cancer. *Cell reports*, 17, 1302.
- ZHOU, Z., CHEN, Y., JIN, M., HE, J., GULI, A., YAN, C. & DING, S. 2019. Comprehensive Analysis of Lysine Acetylome Reveals a Site-Specific Pattern in Rapamycin-Induced Autophagy. *Journal of proteome research*, 18, 865-877.
- ZHU, H., ZHAO, L., WANG, E., DIMOVA, N., LIU, G., FENG, Y. & CAMBI, F. 2012. The QKI-PLP pathway controls SIRT2 abundance in CNS myelin. *Glia*, 60, 69-82.
- ZHU, X.-H., LU, M., LEE, B.-Y., UGURBIL, K. & CHEN, W. 2015. In vivo NAD assay reveals the intracellular NAD contents and redox state in healthy human brain and their age dependences. *Proc Natl Acad Sci U S A*, 112, 2876-2881.
- ZOUGMAN, A., SELBY, P. J. & BANKS, R. E. 2014. Suspension trapping (STrap) sample preparation method for bottom-up proteomics analysis. *PROTEOMICS*, 14, 1006-1000.
- ZU, Y., LIU, L., LEE, M. Y. K., XU, C., LIANG, Y., MAN, R. Y., VANHOUTTE, P. M. & WANG, Y. 2010. SIRT1 Promotes Proliferation and Prevents Senescence Through Targeting LKB1 in Primary Porcine Aortic Endothelial Cells. *Circ Res*, 106, 1384-1393.